EXPERIMENTALLY DETERMINE THE IMPACT OF JACKING-OIL POCKETS ON THE ROTORDYNAMIC CHARACTERISTICS OF A FOUR-PAD, LBP, TILTING-PAD JOURNAL BEARING

A Thesis

by

MATTHEW PHILIP KLUITENBERG

Submitted to the Office of Graduate and Professional Studies of
Texas A&M University
in partial fulfillment of the requirements for the degree of

MASTER OF SCIENCE

Chair of Committee,	Dara W. Childs
Committee Members,	Luis San Andres
	Lynn Beason
Head of Department,	Andreas A. Polycarpou

May 2015

Major Subject: Mechanical Engineering

ABSTRACT

Test results that examine the influence of jacking-oil ports on a tilting pad journal (TPJ) bearing are presented. The static and dynamic characteristics before and after adding jacking-oil ports are compared. The test bearing is a four-pad, rocker-pivot, 57% pivot offset TPJ bearing in load between pad configuration. This original bearing was modified to include jacking-oil ports on the two loaded pads and retested at the same operating conditions. The ports occupy 5% of the pad's surface area and have an approximate depth of 25 times the radial clearance. Pressurized jacking-oil was not used during testing; however, oil supply lines complete with check valves were added to emulate a typical industrial bearing assembly. This thesis compares both the static and dynamic bearing characteristics to determine the effects jacking-oil ports had.

Rotordynamic coefficients are presented as dimensionless values, using a frequency-independent [*K*][*C*][*M*] model. The added jacking-oil ports caused a decrease in direct damping and increase in virtual-mass. Direct damping coefficients were reduced by an average of -26% in the loaded *y*-direction, and -9% in the orthogonal *x*-direction. The original bearing had all negative direct virtual-mass coefficients (stiffening with increasing frequency). The modified bearing had negative coefficients that were smaller in magnitude, and some virtual-mass coefficients that were positive. No significant changes were observed in any of the cross-coupled coefficients or the direct stiffness coefficients.

The added jacking-oil ports has no significant impact on the static characteristics of the TPJ bearing. Static characteristics included the steady-state journal eccentricity, attitude angle, minimum film-thickens, and pad temperature.

A predictive bearing code was modified to account for the jacking-oil port geometry but was unable to produce predictions matching the measured change in dynamic performance. Contrary to measurements, the code predicted frequency-dependent direct

rotordynamic coefficients and no reduction in direct stiffness or damping for the bearing with jacking-oil ports.

The influence of jacking-oil ports on a simple rotor-bearing system is presented. Rotordynamic predictions were made for a rigid rotor symmetrically supported by two TPJ bearings. Predictions showed that jacking-oil ports can significantly lower the first critical speed. This was attributed to the change in virtual-mass coefficients. There was only a small reduction in damping ratio predicted.

DEDICATION

To my family for their continued support throughout my prolonged scholastic journey.

ACKNOWLEDGEMENTS

I would like to specially thank Dr. Dara Childs for awarding me the opportunity to study at the Texas A&M Turbomachinery Laboratory, and for the knowledge he has shared with me during this project.

I thank Dr. San Andrés and Yingkun Li for their work with the *XLTPJB* bearing code and for their advice. I thank the faculty and staff at the Turbomachinery Laboratory, and my fellow students for their guidance and for making my time at Texas A&M very enjoyable.

TABLE OF CONTENTS

Page

ABSTRACT ii

DEDICATION iv

ACKNOWLEDGEMENTS v

LIST OF FIGURES viii

LIST OF TABLES xii

NOMENCLATURE xvi

INTRODUCTION 1

DESCRIPTION OF THE TEST RIG 11

- Testing Apparatus 11
- Instrumentation 15
- Bearing Description 17
  - Modifications 18

EXPERIMENTAL PROCEDURE 21

- Procedure Overview 21
- Operating Conditions 21
- Static Characteristics 22
  - Clearance Measurement 24
- Dynamic Characteristics 25
  - Parameter Identification Model 26
  - Curve Fit Procedure 27
  - Baseline 29
  - Uncertainty Analysis 29
  - Dimensionless Coefficients 31

STATIC CHARACTERISTICS 33

- Clearance 33
- Bearing Center 35

Eccentricity and Attitude Angle 36
Pad Temperatures 39
Closure 42

DYNAMIC CHARACTERISTICS 43

[*K*][*C*][*M*] Model 43
Baseline Dynamic-Stiffness 45
Stiffness Coefficients 47
Damping Coefficients 50
Virtual-Mass Coefficients 53
Closure 57

BEARING PREDICTIONS 58

Bearing Code 58
Input Parameters 59
Results 60

ROTORDYNAMIC MODEL STUDY 65

SUMMARY, DISCUSSION, AND CONCLUSION 68

Static 68
Dynamic 69
Bearing Predictions 70
Rotordynamic Study 70

REFERENCES 72

APPENDIX A: XLTPJB PARAMETERS 76

APPENDIX B: STATIC CONDITIONS 79

APPENDIX C: STATIC DATA 80

APPENDIX D: DYNAMIC CONDITIONS 82

APPENDIX E: DYNAMIC DATA 84

APPENDIX F: DYNAMIC-STIFFNESS DATA 90

APPENDIX G: R-SQUARED VALUES 105

LIST OF FIGURES

Page

Figure 1. Fluid-film modelled as stiffness and damping coefficients, K_{ij} and C_{ij} 1

Figure 2. Pivot type and load orientation, (a) rocker-pivot (LBP), (b) spherical-seat (LOP), (c) flexure-pivot (LBP) 3

Figure 3. TPJ bearing parameters illustrated with a single pad 4

Figure 4. Low pressure (LP) and high pressure (HP) oil flows for (a) hydrodynamic TPJ bearing (b) jacking-oil TPJ bearing 6

Figure 5. Test rig cross-section view, figure from [19] 11

Figure 6. Exploded view of stator assembly 12

Figure 7. NDE view of the static loader assembly, figure from [19] 14

Figure 8. DE view of the shaker assembly with static load F_s 15

Figure 9. DE view of stator assembly with instrumentation, figure adapted from [20] 16

Figure 10. DE view of thermocouple locations and pad orientation for (a) original bearing (b) modified bearing 18

Figure 11. Jacking-oil ports added to pad #1 18

Figure 12. Test bearing with attached jacking-oil supply lines 19

Figure 13. Static displacement coordinate system 23

Figure 14. Average clearance fit 24

Figure 15. Repeatability and curve fit uncertainties for two data sets 30

Figure 16. Original bearing measured pad profiles and bearing center 33

Figure 17. Modified bearing measured pad profiles and bearing center 34

Figure 18. Comparison of measurement methods for bearing center, figure from [26] 36

Figure 19. Static eccentricity (a) original bearing (b) modified bearing 36

Figure 20. Attitude angle plot (a) original bearing (b) modified bearing 37

Figure 21. Bearing loci and clearance at shaft speed: (a) 6,800 rpm (b) 9,000 rpm (c) 10,800 rpm (d) 13,200 rpm 38

Figure 22. Temperature data coordinate system 40

Figure 23. Pad temperature rise at 6,800 rpm and 0.725 MPa (105.3 psi) 41

Figure 24. Pad temperature rise at 10,800 rpm and 2.903 MPa (421.1 psi) 41

Figure 25. Im(H_{ij}) with and without ports at 6,800 rpm and 1.452 MPa (210.5 psi) 44

Figure 26. Re(H_{ij}) with and without ports at 6,800 rpm and 1.452 MPa (210.5 psi) 44

Figure 27. Baseline dynamic-stiffness Im(H_{ij}) for the original bearing 45

Figure 28. Baseline dynamic-stiffness Re(H_{ij}) for the original bearing 46

Figure 29. Baseline dynamic-stiffness Im(H_{ij}) for the modified bearing 46

Figure 30. Baseline dynamic-stiffness Re(H_{ij}) for the modified bearing 47

Figure 31. Direct stiffness coefficients k_{yy} (load direction) 48

Figure 32. Direct stiffness coefficients k_{xx} 48

Figure 33. Cross-coupled stiffness ceofficients k_{xy} 49

Figure 34. Cross-coupled stiffness ceofficients k_{yx} 50

Figure 35. Direct damping coefficients c_{yy} (load direction) 51

Figure 36. Direct damping coefficients c_{xx} 51

Figure 37. Cross-coupled damping coefficients c_{xy} 52

Figure 38. Cross-coupled damping coefficients c_{yx} 53

Figure 39. Direct virtual-mass coefficients m_{yy} 54

Figure 40. Direct virtual-Mass coefficients m_{xx} 54

Figure 41. Re(H_{ij}) with and without ports at 6,800 rpm and 2.177 MPa (315.8 psi) 55

Figure 42. Cross-coupled virtual-mass coefficients m_{xy} 56

Figure 43. Cross-coupled virtual-mass coefficients m_{yx} 56

Figure 44. Jacking-oil port geometry in *XLTPJB* 59

Figure 45. Real part of dynamic-stiffness predicitons with and without jacking-oil ports at 6,800 rpm and 2.177 Mpa (315.8 psi) 61

Figure 46. Imaginary part of dynamic-stiffness predicitons with and without jacking-oil ports at 6,800 rpm and 2.177 Mpa (315.8 psi) 61

Figure 47. Re(H_{xx}) and Re(H_{yy}) with varying port depth at 6,800 rpm and 2.177 Mpa 62

Figure 48. Im(H_{xx}) and Im(H_{yy}) with varying port depth at 6,800 rpm and 2.177 Mpa 63

Figure 49. Model of rigid rotor supported by TPJ bearings 65

Figure 50. Rotor-bearing system predictions with and without jacking-oil ports (a) damped natural frequency (b) damping ratio 66

Figure 51. Rotor-bearing system predictions changing individual dynamic coefficients (a) damped natural frequency (b) damping ratio 67

Figure A. 1. Load-deflection curve [21].....77

Figure G. 1. Dynamic-stiffness Im(H_{xx}) at 10,800 rpm and 1.452 MPa (210.5 psi).....106

Figure G. 2. Dynamic-stiffness Im(H_{yy}) at 10,800 rpm and 1.452 MPa (210.5 psi).....107

Figure G. 3. Dynamic-stiffness Im(H_{xy}) at 10,800 rpm and 1.452 MPa (210.5 psi).....108

Figure G. 4. Dynamic-stiffness Im(H_{yx}) at 10,800 rpm and 1.452 MPa (210.5 psi).....108

LIST OF TABLES

Page

Table 1. TPJ bearing geometric parameters 3

Table 2. Nominal bearing properties 17

Table 3. Nominal operating conditions 21

Table 4. Measured bearing cold and hot clearances 34

Table 5. Estimated minimum film thickness 39

Table A. 1. XLTPJB bearing geometry 76

Table A. 2. XLTPJB fluid properties 76

Table A. 3. XLTPJB pad geometry 76

Table A. 4. XLTPJB pad properties 77

Table A. 5. XLTPJB Jacking-oil pocket options 77

Table B. 1. Average static operating conditions (modified bearing) 79

Table C. 1. Static location and eccentricity (original bearing) 80

Table C. 2. Static location and eccentricity (modified bearing) 81

Table D. 1. Dynamic operating conditions (original bearing) 82

Table D. 2. Dynamic operating conditions (modified bearing) 83

Table E. 1. Stiffness coefficients (original bearing) 84

Table E. 2. Stiffness coefficients (modified bearing) 84

Table E. 3. Damping coefficients (original bearing) 85

Table E. 4. Damping coefficients (modified bearing) 85

Table E. 5. Virtual-mass coefficients (original bearing) 86

Table E. 6. Virtual-mass coefficients (modified bearing) 86

Table E. 7. Dimensionless stiffness coefficients (original bearing) 87

Table E. 8. Dimensionless stiffness coefficients (modified bearing) 87

Table E. 9. Dimensionless damping coefficients (original bearing) 88

Table E. 10. Dimensionless damping coefficients (modified bearing) 88

Table E. 11. Dimensionless virtual-mass coefficients (original bearing) 89

Table E. 12. Dimensionless virtual-mass coefficients (modified bearing) 89

Table F. 1. Dynamic-stiffness 6,800 rpm 726 kPa (original bearing) 90

Table F. 2. Dynamic-stiffness 6,800 rpm 726 kPa (modified bearing) 90

Table F. 3. Dynamic-stiffness 6,800 rpm 1,452 kPa (original bearing) 91

Table F. 4. Dynamic-stiffness 6,800 rpm 1,452 kPa (modified bearing) 91

Table F. 5. Dynamic-stiffness 6,800 rpm 2,177 kPa (original bearing) 92

Table F. 6. Dynamic-stiffness 6,800 rpm 2,177 kPa (modified bearing) 92

Table F. 7. Dynamic-stiffness 6,800 rpm 2,903 kPa (original bearing) 93

Table F. 8. Dynamic-stiffness 6,800 rpm 2,903 kPa (modified bearing) 93

Table F. 9. Dynamic-stiffness 9,000 rpm 726 kPa (original bearing) 94

Table F. 10. Dynamic-stiffness 9,000 rpm 726 kPa (modified bearing) 94

Table F. 11. Dynamic-stiffness 9,000 rpm 1,452 kPa (original bearing).....95

Table F. 12. Dynamic-stiffness 9,000 rpm 1,452 kPa (modified bearing).....95

Table F. 13. Dynamic-stiffness 9,000 rpm 2,177 kPa (original bearing).....96

Table F. 14. Dynamic-stiffness 9,000 rpm 2,177 kPa (modified bearing).....96

Table F. 15. Dynamic-stiffness 9,000 rpm 2,903 kPa (original bearing).....97

Table F. 16. Dynamic-stiffness 9,000 rpm 2,903 kPa (modified bearing).....97

Table F. 17. Dynamic-stiffness 10,800 rpm 726 kPa (original bearing).....98

Table F. 18. Dynamic-stiffness 10,800 rpm 726 kPa (modified bearing).....98

Table F. 19. Dynamic-stiffness 10,800 rpm 1,452 kPa (original bearing).....99

Table F. 20. Dynamic-stiffness 10,800 rpm 1,452 kPa (modified bearing).....99

Table F. 21. Dynamic-stiffness 10,800 rpm 2,177 kPa (original bearing).....100

Table F. 22. Dynamic-stiffness 10,800 rpm 2,177 kPa (modified bearing).....100

Table F. 23. Dynamic-stiffness 10,800 rpm 2,903 kPa (original bearing).....101

Table F. 24. Dynamic-stiffness 10,800 rpm 2,903 kPa (modified bearing).....101

Table F. 25. Dynamic-stiffness 13,200 rpm 726 kPa (original bearing).....102

Table F. 26. Dynamic-stiffness 13,200 rpm 726 kPa (modified bearing).....102

Table F. 27. Dynamic-stiffness 13,200 rpm 1,452 kPa (original bearing).....103

Table F. 28. Dynamic-stiffness 13,200 rpm 1,452 kPa (modified bearing).....103

Table F. 29. Dynamic-stiffness 13,200 rpm 2,177 kPa (modified bearing).....104

Table F. 30. Dynamic-stiffness 13,200 rpm 2,903 kPa (modified bearing).....104

Table G. 1. R-squared values for Im(H_{ij}) curve fits 105

NOMENCLATURE

$\boldsymbol{A}_i$	Fourier Transform of stator accelerations [L/t^2]
C_b	Bearing clearance [L]
C_p	Pad clearance [L]
c_{ij}	Dimensionless damping coefficients [-]
C_{ij}	Direct and cross-coupled damping coefficients [F.t/L]
$\boldsymbol{D}_{ij}$	Fourier Transform of relative journal position [L]
e_o	Static displacement [L]
$f_{\mathrm{b}x}, f_{\mathrm{b}y}$	Fluid film reaction forces [F]
f_x, f_y	Bearing assembly applied forces [F]
$\boldsymbol{h}_{ij}$	Dimensionless dynamic-stiffness [-]
$\boldsymbol{H}_{ij}$	Dynamic-stiffness [F/L]
j	Imaginary unit, $\sqrt{-1}$ [-]
k_{ij}	Dimensionless stiffness coefficients [-]
K_{ij}	Direct and cross-coupled stiffness coefficients [F/L]
$\boldsymbol{L}$	Pad axial length [L]
m_{ij}	Dimensionless virtual-mass coefficients [-]
M_{ij}	Direct and cross-coupled virtual-mass coefficients [M]
M_s	Bearing assembly mass [M]
n	Number of data sets in curve fit [-]
N	Number of data sets for uncertainty calculations [-]
R_s	Shaft radius [L]

R_p	Pad radius [L]
R_b	Bearing radius [L]
t	Standard deviation constant for 95% confidence interval [-]
$U_{c,ij}$	Uncertainty of dimensionless damping coefficient [-]
$U_{k,ij}$	Uncertainty of dimensionless stiffness coefficient [-]
$U_{m,ij}$	Uncertainty of dimensionless virtual-mass coefficient [-]
x_o, y_o	Bearing center position [L]
x_r, y_r	Rotor center position [L]
$\ddot{x}_s, \ddot{y}_s$	Bearing assembly accelerations [L/t^2]
γ	Attitude angle [Angle]
ΔH_{ij}	Standard deviation uncertainty of dynamic-stiffness [F/L]
ΔT	Steady-state rise in pad temperature [°]
$\Delta x, \Delta y$	Change in journal positions relative to equilibrium [L]
$\Delta \dot{x}, \Delta \dot{y}$	Journal velocities relative to equilibrium [L/t]
$\Delta \ddot{x}, \Delta \ddot{y}$	Journal accelerations relative to equilibrium [L/t^2]
ε_o	Eccentricity [-]
θ	Angular coordinate [Angle]
ω	Journal angular velocity [Angle/t]
Ω	Excitation frequency [1/t]

Subscripts and Prefixes

Original	Bearing tested without jacking-oil ports
Modified	Bearing tested with jacking-oil ports
Test	Data from specific operating conditions (non-zero shaft speed)

Base	Baseline data (zero shaft speed)
x, y	x and y direction
xx, yy	Direct terms
xy, yx	Cross-coupled terms
ij	General notation for i-direction force and j-direction motion.
k	Individual dynamic-stiffness data point
Δ	Uncertainty
e	Error

Abbreviations

CC	Cold clearance
DE	Drive end
HC	Hot clearance
HP	High pressure
[*K*][*C*]	Reaction force model with stiffness and damping
[*K*][*C*][*M*]	Reaction force model with stiffness, damping, and virtual-mass
LBP	Load between pad
LOP	Load on pad
LP	Low pressure
NDE	Non-drive end
NPT	National pipe thread
OEM	Original equipment manufacturer
TPJ	Tilting-pad journal

INTRODUCTION

Fluid-film journal bearings are essential components in high-speed rotating machinery such as compressors and turbines. They provide support for the rotor and transfer lateral reaction forces to the stationary support structure by means of a lubricant such as oil. Hydrodynamic bearings are one of the two main categories of fluid-film bearings, the other being hydrostatic. Hydrodynamic bearings rely on shaft rotation and the lubricant's viscosity to create a pressure field in the thin film of lubricant. Lubricant is supplied to the bearing at a low pressure and then dragged between the rotor and bearing surfaces by shearing forces. The two surfaces form a converging wedge which causes a pressure rise large enough to support the weight of the rotor.

The journal, or section of the shaft within the bearing, has an equilibrium position that changes with the applied load and shaft rotating speed. Fluid-film reaction forces caused by vibrations about this equilibrium position are typically modeled by assuming small perturbations. The fluid-film can be modeled as a linear two degree-of-freedom system that includes both spring coefficients (K_{ij}) and damping coefficients (C_{ij}) as shown in Figure 1.

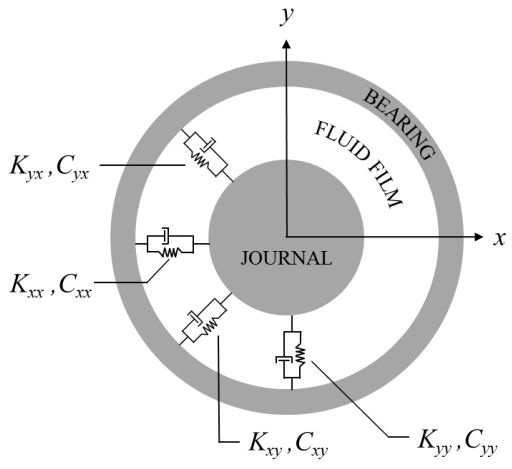

Figure 1. Fluid-film modelled as stiffness and damping coefficients, K_{ij} and C_{ij}

In this dynamic model, reactions forces (f_{bx}, f_{by}) are caused by both relative displacement and velocity between the journal and bearing. The displacements about the equilibrium position are denoted as Δx and Δy while the relative velocities are denoted as $\Delta \dot{x}$ and $\Delta \dot{y}$. The bearing reaction forces (f_{bx}, f_{by}) are

$$-\begin{Bmatrix} f_{bx} \\ f_{by} \end{Bmatrix} = \begin{bmatrix} K_{xx} & K_{xy} \\ K_{yx} & K_{yy} \end{bmatrix} \begin{Bmatrix} \Delta x \\ \Delta y \end{Bmatrix} + \begin{bmatrix} C_{xx} & C_{xy} \\ C_{yx} & C_{yy} \end{bmatrix} \begin{Bmatrix} \Delta \dot{x} \\ \Delta \dot{y} \end{Bmatrix} \tag{1}$$

The subscripts *xx*, and *yy* denote direct coefficients while subscripts *xy* and *yx* denote cross-coupled coefficients. A direct coefficient relates a displacement or velocity with a reaction force in the same direction. A cross-coupled coefficient relates displacement or velocity with a reaction force in the orthogonal direction. For example, the cross-coupled stiffness term K_{xy} quantifies the reaction force in the *x*-direction due to a displacement in the *y*-direction.

Tilting pad journal (TPJ) bearings are a type of hydrodynamic bearing often used in place of fixed arc bearings because of their improved stability characteristics. TPJ bearings support the rotor with four to six individual pads that are free to rotate about their own pivots. TPJ bearings are more stable because the pads cannot provide a reaction moment, leading to cross-coupled stiffness terms (K_{xy}, K_{yx}) that are very small in magnitude compared to fixed arc bearings. This attribute allows machinery to run at higher speeds and/or lighter loads without experiencing instabilities.

The rotordynamic characteristics of a TPJ bearing depend on many parameters including the load orientation and pivot type. The three common types of pivots are rocker-pivot, spherical-seat, and flexure-pivot. TPJ bearings are typically oriented in either load on pad (LOP) orientation where the load is directed through a pivot, or load between pad (LBP) orientation where the load is applied halfway between two pivots. The typical load orientations and pivot types are shown in Figure 2. All three pivot designs allow the pad to rotate about an axis parallel to the rotor. Spherical-seat pads use a ball-in-socket design allowing the pads to rotate along two axes (radial and axial), accommodating for axial

misalignment. Rocker-pivot pads are sometimes machined with a slight axial curvature to mimic this design. Flexure-pivot and most rocker-pivot pads (including the bearing discussed in this thesis) have only a single axis of rotation.

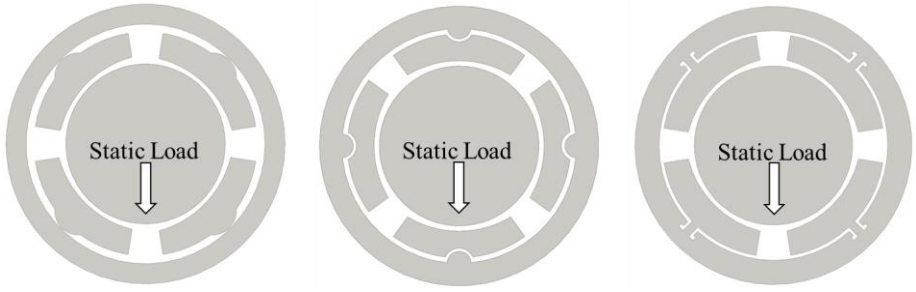

(a) **(b)** **(c)**

Figure 2. Pivot type and load orientation, (a) rocker-pivot (LBP), (b) spherical-seat (LOP), (c) flexure-pivot (LBP)

The rotordynamic characteristics of a TPJ bearing also depend on bearing geometry. The essential parameters for defining bearing geometry are listed in Table 1 and illustrated in Figure 3.

Table 1. TPJ bearing geometric parameters

Symbol	Definition
L	Pad axial length
R_s	Shaft radius
R_p	Pad radius
R_b	Bearing radius
θ_{pad}	Pad arc angle
θ_{pivot}	Pivot arc angle

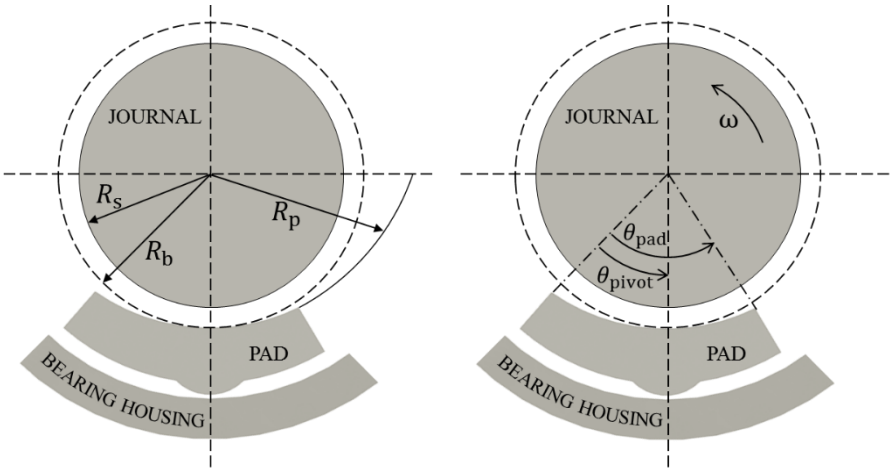

Figure 3. TPJ bearing parameters illustrated with a single pad

TPJ bearings are often characterized in terms of their clearances and non-dimensional parameters such as preload and pivot offset. The bearing clearance (C_b) is the difference between the rotor and bearing radius. It is a measure of the minimum clearance for a centered journal position.

$$C_b = R_b - R_s \tag{2}$$

The pad clearance (C_p) is defined as

$$C_p = R_p - R_s \tag{3}$$

The pad preload is a non-dimensional term that relates the radius of the bearing and rotor.

$$preload = 1 - \frac{C_b}{C_p} \tag{4}$$

A positive preload indicates that the pad radius is larger than the bearing radius as seen in Figure 3. With a positive preload, the pads form a converging wedge with the journal when

the journal is centered in the bearing. Typical preload values range from 0.3 to 0.6 [1]. These values ensure that all pads will form a converging wedge regardless of the journal position. Increasing preload is typically predicted to increase the bearing's stiffness and decrease direct damping [2].

Pivot offset ratio is defined as

$$offset = \frac{\theta_{\text{pivot}}}{\theta_{\text{pad}}} \tag{5}$$

A pivot offset of 0.5 indicates that the pad's geometric center is directly above the pivot. Typical values range from 0.5 to 0.6 [1]. Increasing the pivot offset is used to increase load capacity and decrease bearing operating temperature [3].

As stated before, hydrodynamic bearings rely on shaft rotation to create fluid pressure and lifting force. These bearings can experience rubbing between the rotor and bearing during start-up of machinery with large radial unit loads. One common method to avoid rubbing contact is to add jacking-oil capabilities (Figure 4b). Jacking-oil bearings combine the method of hydrodynamic lubrication with externally pressurized lubricant (hydrostatic) to provide additional lifting force at low speeds. High-pressure lubricant is supplied through an orifice into a recess to create lift and avoid rubbing during start-up. The high-pressure lubricant is only used during start-up and subsequently turned off when the rotor has reached an adequate speed for creating hydrodynamic lift.

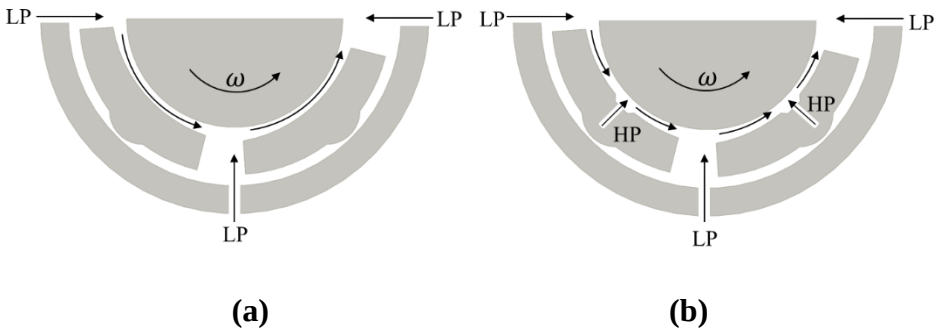

Figure 4. Low pressure (LP) and high pressure (HP) oil flows for (a) hydrodynamic TPJ bearing (b) jacking-oil TPJ bearing

The use of jacking-oil is most common in thrust bearings and fixed-geometry journal bearings because of the high loads associated with these bearing types. TPJ bearings are typically used for high-speed machinery with lighter loads [1], and do not usually require jacking-oil. As a result, the effects of adding jacking-oil ports to TPJ bearing have not been studied in detail. No documented work has directly compared the rotordynamic characteristics of a TPJ bearing with and without inactive jacking-oil ports.

The addition of jacking-oil ports to TPJ bearings can eliminate start-up rubbing but it is expected to change the rotordynamic characteristics of the bearing (G. Vannini, personal communication, May 2013). Understanding the changes in static and dynamic characteristics is important because they change the rotordynamic performance of the entire machine. A change in either stiffness or damping affects the system's natural frequency, mode shapes, and log decrement. A change in the journal's equilibrium position can affect the behavior of other components, such as seals, and impact the stability of the machine. A better understanding of the effects of jacking-oil ports is needed for accurately modeling the bearing and predicting the rotordynamic behavior of an assembled machine.

Modeling and prediction of TPJ bearings without jacking ports has been studied for many years. In 1964, Lund [4] introduced a method for calculating the dynamic coefficients of a TPJ bearing. His method was based on the Reynolds equation and

assumed that the fluid-film forces of a single pad can be modeled as spring and damping forces. He developed equations of motion for each individual pad and completed a summation of pad forces to determine spring and damping coefficients for the entire bearing. This has become known as the Lund's pad-assembly method, and has been used as a basis for subsequent research in TPJ bearings.

In 1978, Nicholas *et al.* completed a design optimization of five-pad TPJ bearings for a centrifugal compressor. They performed a stability analysis for the rotor-bearing system using the synchronous frequency to determine bearing coefficients. In response to this paper, Lund stated that the stability analysis should be completed using the damped natural frequency. This prompted the questions of whether or not the bearing coefficients (mainly damping) are frequency dependent [5]. Many subsequent computational studies predicted that TPJ bearing coefficients depend on frequency [6]-[8]. In 1983, Parsell *et al.* [6] presented predictions suggesting that both damping and stiffness are highly frequency dependent, and that damping coefficients tend to zero as the frequency ratio approaches 0.5. White and Chan (1992) [8] predicted that the effective damping is lower at the sub-synchronous frequencies than the synchronous frequency for bearings operating with small preloads and high Sommerfeld numbers.

These computational studies predicted that the vibration frequency can have a large impact on the dynamic coefficients and ultimately the rotor-bearing system response. Following this work, many experimental studies were conducted to measure these frequency effects. In 1999, Ha and Yang [9] measured a five-pad, TPJ bearing in LOP configuration and determined bearing coefficients using the traditional stiffness and damping reaction force model referred to as the [K][C] model. Tests were completed at five speeds ranging from 1,200 to 3,600 rpm with a range of single frequency excitations. Their tests concluded that the stiffness coefficients "slightly decrease or remain almost constant," and damping coefficients slightly increase with increased excitation frequency [9]. The measured frequency effects were not as prevalent at predicted by Parsell *et al.*

In 2006, Rodriguez and Childs [10] tested the frequency dependency for a four-pad, flexure-pivot, TPJ bearing in LOP configuration. Tests were completed at four speeds ranging from 6,000 to 16,000 rpm and unit load ranging from 172 to 1,034 kPa. The bearing was excited with a single waveform containing multiple frequencies ranging from 20 to 320 Hz in 10 Hz increments. Rotordynamic coefficients were determined using the method outlined in an earlier paper by Childs and Hale [11]. Their experimental results showed that this bearing could be modeled with a frequency-independent [*K*][*C*][*M*] reaction force model.

$$-\begin{Bmatrix} f_{bx} \\ f_{by} \end{Bmatrix} = \begin{bmatrix} K_{xx} & K_{xy} \\ K_{yx} & K_{yy} \end{bmatrix} \begin{Bmatrix} \Delta x \\ \Delta y \end{Bmatrix} + \begin{bmatrix} C_{xx} & C_{xy} \\ C_{yx} & C_{yy} \end{bmatrix} \begin{Bmatrix} \Delta \dot{x} \\ \Delta \dot{y} \end{Bmatrix} + \begin{bmatrix} M_{xx} & M_{xy} \\ M_{yx} & M_{yy} \end{bmatrix} \begin{Bmatrix} \Delta \ddot{x} \\ \Delta \ddot{y} \end{Bmatrix} \tag{6}$$

Many subsequent tests were completed which validated these results. Harris and Childs (2008) [12] used the same procedure while testing a spherical-seat bearing in LBP configuration. Delgado *et al*. (2010) [13] measured the frequency dependency of five-pad and four-pad rocker-pivot TPJ bearings with both 50% and 60% offsets. These tests and others showed that the frequency-independent [*K*][*C*][*M*] model is sufficient for modeling TPJ bearings regardless of pivot type and pivot offset.

There are a few recent studies that involve TPJ bearings with jacking ports but the focus of those studies was not the effect of the jacking ports. In 2009, Hattenbach and Sandberg [14] presented a case study investigating the source of super-synchronous vibrations in a motor that used jacking-oil. The original four-lobe fixed geometry bearing was replaced with a four-pad TPJ bearing to eliminate the vibration problems. This new bearing was used in LBP configuration and had a jacking-oil port in each loaded pad. The bearing change did not completely solve the vibration problem. Further testing revealed that the volume of oil trapped between the bearing and an external check valve was the cause of the super-synchronous vibrations problem. A new bearing design was implemented that included a check valve within the bearing housing. The super-synchronous vibrations in the motor were eliminated presumably by reducing the amount of trapped oil.

In 2013, Hagemann and Sebasian [15] compared measured and predicted static data for a large TPJ bearing with jacking-oil. The test bearing was a five-pad, TPJ bearing in LBP configuration with a jacking-oil port in the center of each loaded pad. The authors compared their measurements to multiple codes, which included pad deformation models that varied in complexity. They determined that a simple beam model is not sufficient for modeling pad flexibility. Good agreement between measurements and predictions required a 3D structural mechanics model. However, they stated in the conclusions that this complex model may not be necessary for smaller bearings. Although this study did not focus on the effects of jacking-oil ports, the ports were included in their predictive models. The authors present a plot of the measured and predicted film pressure along the center plane of the bearing. The model predicted a greater change in the pressure profile due to the jacking recesses than measurements showed. Also, the measured peak pressure was lower than predicted. The dimensions of the jacking-oil port were not provided.

There have been many studies aimed at accurately predicting, modeling, and measuring the performance of TPJ bearings without jacking ports. The frequency-independent $[K][C][M]$ model has been found sufficient for modeling TPJ bearings. The effects of most design parameters such as preload, L/D ratio, and pivot offset are known. Little work has been done to understand how jacking ports affect TPJ bearings. There is no documented work that directly compares a TPJ bearing with and without jacking ports.

This thesis determines the effects of jacking-oil ports by providing measured static and dynamic data for a TPJ bearing both with and without jacking ports. Dynamic coefficients for both bearings are compared using the $[K][C][M]$ model. This thesis also includes a predictive study showing how jacking-oil ports impact a simple rotor-bearing system, and a discussion of the efforts made to model the added ports.

The work of this thesis was initiated by turbomachinery original equipment manufacturer (OEM). They had recently been using a TPJ bearing with jacking-oil ports in one of their machines. The measured natural frequency and log decrement for this machine did not agree with predictions, and they attributed the inaccuracies to the presence

of jacking-oil ports. They were concerned with performance of the TPJ bearing at full shaft speed after the jacking-oil had been turned off. The OEM did not have the predictive codes required to model the added jacking-oil ports and proposed that experimental testing be completed.

Testing was completed using an existing bearing that was modified to include jacking-oil ports. The bearing is a four-pad, rocker-pivot, TPJ bearing in LBP configuration. It was selected because it had the closest resemblance to the bearing used by the OEM. A jacking-oil port was machined in each loaded pad according to scaled dimensions provided by the OEM. Because this study is aimed at determining the effects of inactive jacking ports, no externally pressured lubricant was supplied to the jacking ports during testing. The original (no jacking-oil ports) bearing was tested by Tschoepe in 2011 [16]. The measured data provided in his thesis were used for this comparison. The modified bearing was tested at the same operating conditions to complete a direct comparison of a TPJ bearing with and without jacking-oil ports.

DESCRIPTION OF THE TEST RIG

Testing Apparatus

The bearing test rig, located at the Texas A&M Turbomachinery laboratory, was designed by Kaul [17] to test laminar-flow oil seals and later modified to test hydrodynamic bearings. The rig is based on the floating-bearing design, introduced by Glienicke (1967) [18], in which the test bearing is free to move about a rigidly supported shaft. This test rig is used to measure both the static and dynamic characteristics of high-speed hydrodynamic bearings. A section view of this rig can is shown in Figure 5.

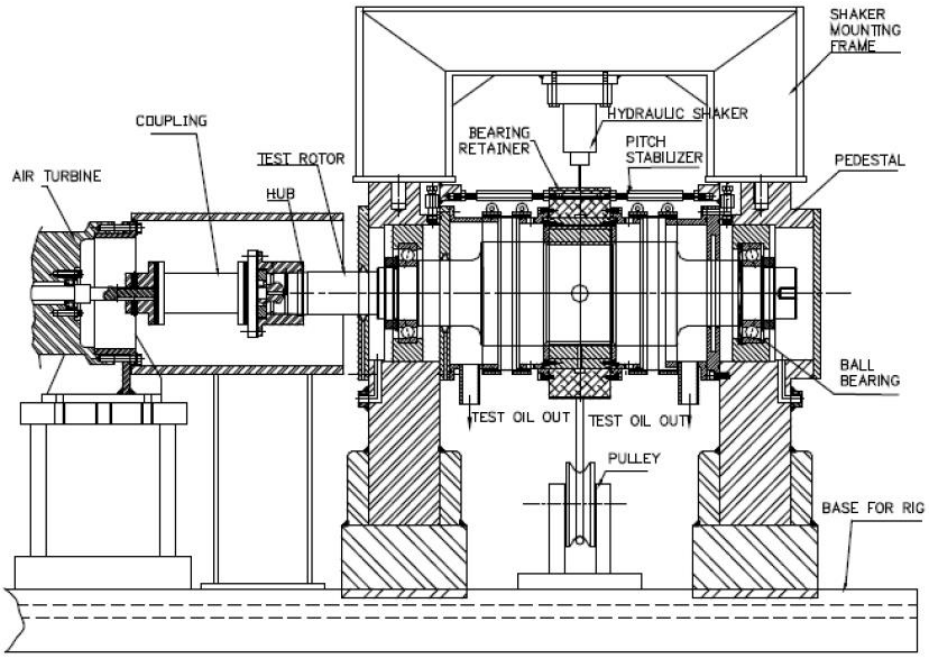

Figure 5. Test rig cross-section view, figure from [19]

The main test section consists of a test-bearing assembly, rotor, supporting pedestals, static loader, and two dynamic loaders. The rotor is driven by a 65 kW air turbine capable of driving the rotor up to 17,000 rpm. The main test section and air turbine are mounted

on a steel base. The rotor is precision machined to a diameter of 101.59 mm (3.9997 in) at the test bearing location. It is supported by angular-contact ball bearings on two pedestals spaced approximately 457 mm (18 in) apart. These ball bearings are preloaded to ensure contact between the balls and bearing race. The rotor and supporting pedestals were designed to be very rigid as suggested by Glienicke [18]. A nominally rigid rotor and support structure ensures that there is no significant deflection under the applied static and dynamic loads. This feature isolates the fluid-film properties from the support structure for measurement.

The test bearing is enclosed in a steel housing referred to as the stator. The stator connects the bearing to the pitch stabilizers, oil supply, static loader, two hydraulic shakers, and various instrumentation. Aluminum end-caps are attached on either side of the stator. Both the end-caps and stator are a split design and are bolted around the test bearing (Figure 6). The assembly consisting of the test bearing, end-seals, stator, and end-caps is referred to as the stator assembly.

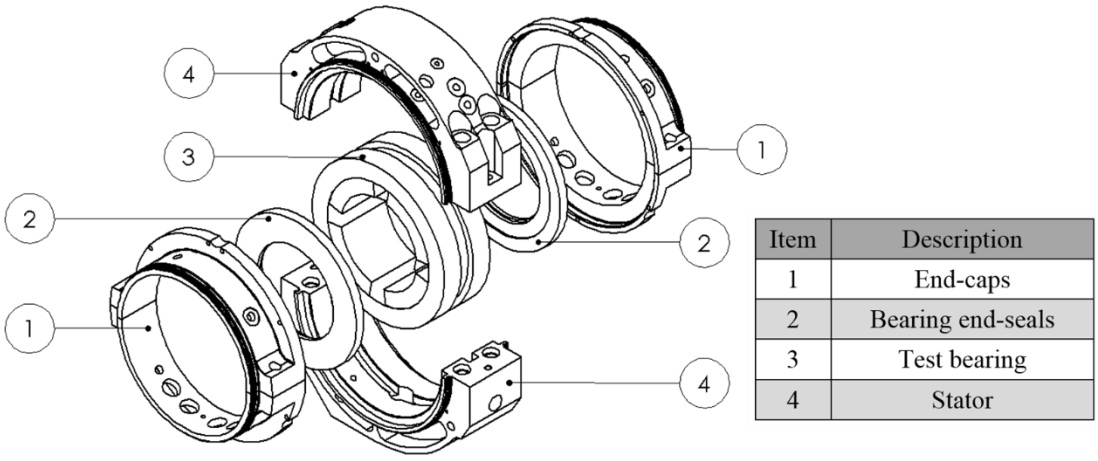

Item	Description
1	End-caps
2	Bearing end-seals
3	Test bearing
4	Stator

Figure 6. Exploded view of stator assembly

There are three pitch stabilizers on both the drive end (DE) and non-drive end (NDE) of the bearing. They are connected between the stator and pedestals and circumferentially spaced 120 degrees apart. The pitch stabilizers are all-thread steel rods used to axially align the bearing and rotor without restricting the radial movement of the bearing.

Oil is supplied to the bearing at a controlled flow rate and temperature by a separate system not shown in Figure 5. The inlet temperature is controlled by mixing hot and cold oil feeds, and flow rate is controlled with a pneumatically-actuated valve. Oil is supplied to the stator through a single hole and fills a cavity between the bearing housing and stator. Oil enters the bearing through multiple passages in the bearing housing, flows through the stator end-caps, and exits the stator assembly through the collection chambers on either side.

Bearing load conditions are simulated by applying a static load to the stator. The static loader assembly can be seen in Figure 7. The pneumatic actuator can generate static tension up to 22,240 N (5,000 lb). The actuator is connected to the stator housing through a spring, steel cable, and pulley wheel. This assembly allows for small movement of the stator while maintaining a constant load direction and magnitude. The stator is pulled in the positive *y*-direction simulating a rotor weight in the negative *y*-direction.

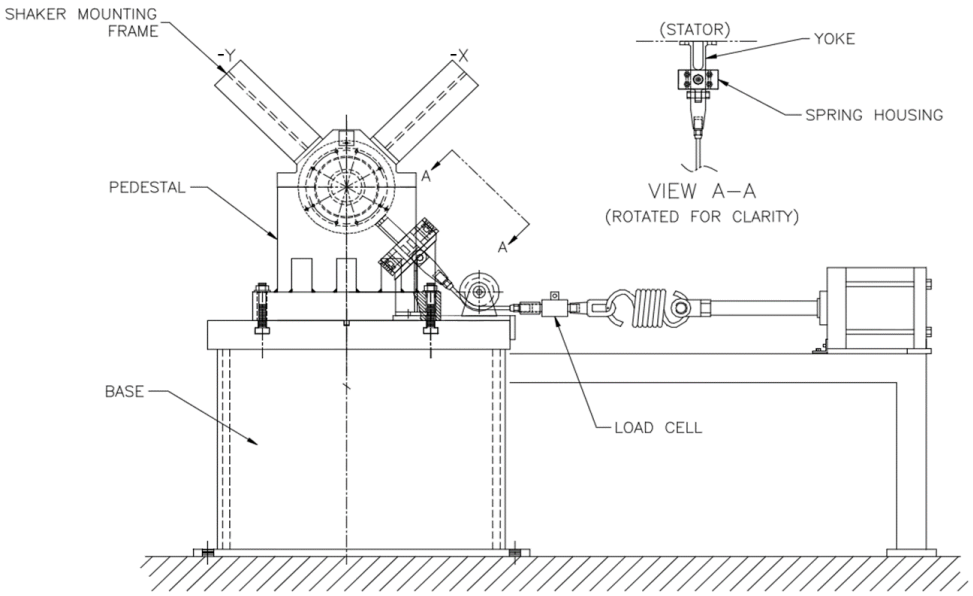

Figure 7. NDE view of the static loader assembly, figure from [19]

Dynamic loads are applied to the stator by two hydraulic shakers. The shaker assembly, as seen from the drive-end, is shown in Figure 8. The shakers are mounted in orthogonal directions with one shaker in-line with the static loading direction. Each shaker head is connected to the stator through a load cell and steel rod called a stinger. There is a separate hydraulic pump and control unit for each hydraulic shaker. Each shaker can produce static forces as well as dynamic loads with frequencies up to 1,000 Hz. The shaker static forces are adjusted before testing until the weight of the bearing assembly is supported by the shakers, and the bearing is centered about the rotor. This process allows gravity to be ignored, and measurements to be taken at a zero loading condition.

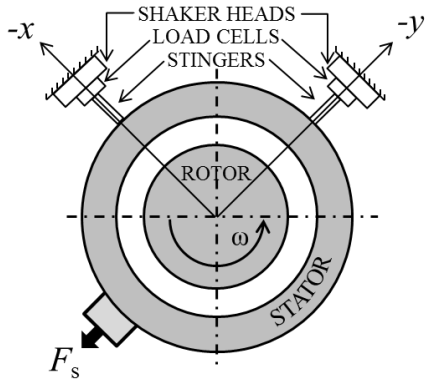

Figure 8. DE view of the shaker assembly with static load F_s

Instrumentation

The test variables, including speed, static load, oil flow rate, and inlet oil temperature, are controlled and measured during testing. Shaft speed ω is measured using a tachometer. The applied static load is measured with a force transducer (load cell) attached between the spring and cable (Figure 7). Oil flow rate is measured with a turbine flow meter, and inlet oil temperature is measured with a type J thermocouple located at the stator oil inlet (Figure 9).

The stator assembly contains instrumentation to measure the bearing's static and dynamic response. Figure 9 shows the stator assembly with instrumentation and additional hardware including stingers, pitch stabilizers (end view), static load connection, and the inlet oil connection. The DE bearing end-seal is removed to show the pads (shaded) and load orientation.

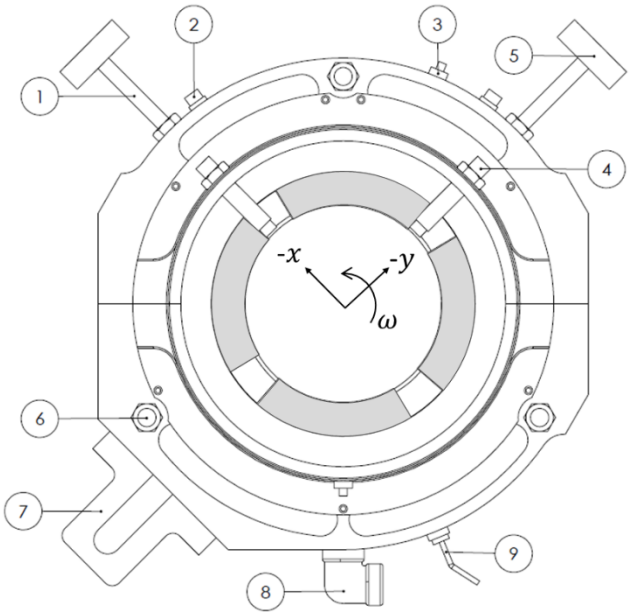

Item	Description	Quantity
1	Stinger	2
2	Accelerometer	2
3	Pressure transducer	3
4	Proximity probe	4
5	Load cell	2
6	Pitch stabilizer	6
7	Static load connection	1
8	Oil inlet connection	1
9	Oil inlet thermocouple	1

Figure 9. DE view of stator assembly with instrumentation, figure adapted from [20]

The relative displacement between the rotor and bearing is measured with proximity probes (eddy current sensors). There is a set of probes mounted in the stator end-cap on both the DE and NDE of the bearing. Each set has one proximity probe mounted in the *x*-direction and another in the *y*-direction. This configuration allows the measurement of both the radial displacement and tilt (angular misalignment) of the bearing. Pressure transducers are mounted in the stator and end-caps to measure inlet pressure and exit pressures respectively. Two piezoelectric accelerometers measure the absolute acceleration of the bearing in both the *x*-direction and *y*-direction. Load cells are attached between the hydraulic shakers and the stingers to measure the force applied by each shaker.

There is additional instrumentation not shown in Figure 9. Type J thermocouples are located in the collection chambers to measure the exit oil temperature on both sides of the bearing. The ambient temperature is measured with a type J thermocouple suspended above the stator assembly. Additionally, the test bearing contains a total of twenty-one

type K thermocouples embedded in the pads to measure operational pad temperatures. The location of these thermocouples is discussed in the *Bearing Description*.

Bearing Description

The test bearing is a four-pad, rocker-pivot, TPJ bearing originally tested by Tschoepe [21]. Jacking-oil ports and supply lines were added to the bearing to complete this comparative study. The nominal bearing properties are listed in Table 2.

Table 2. Nominal bearing properties

Property	Values
Bearing type	Four-pad, rocker-pivot
Configuration	LBP
Pivot offset	57%
Preload	0.3
Pad arc angle	72°
Rotor diameter	101.524 mm (3.9997 in)
Bearing (bore) diameter	101.758 mm (4.0062 in)
Radial pad clearance	0.118 mm (0.00465 in)
Radial bearing clearance	0.0826 mm (0.00325 in)
Pad axial length	60.33 mm (2.375 in)
Pad mass	0.96 kg (2.12 lbm)

This bearing features a flooded bearing design. Oil enters the bearing through four passages in the bearing housing and exits to the DE and NDE side of the bearing. Bearing end-seals restrict the exit flow and ensure the bearing is flooded.

There are twenty-one embedded thermocouples used to measure the operational pad temperatures. These thermocouples were used by Tschoepe [21] to measure the thermal gradients across the loaded pads, and estimate the thermal deflection in the pads. Temperature data are only presented for the inner ring of fifteen thermocouples. Figure 10 shows the thermocouple locations.

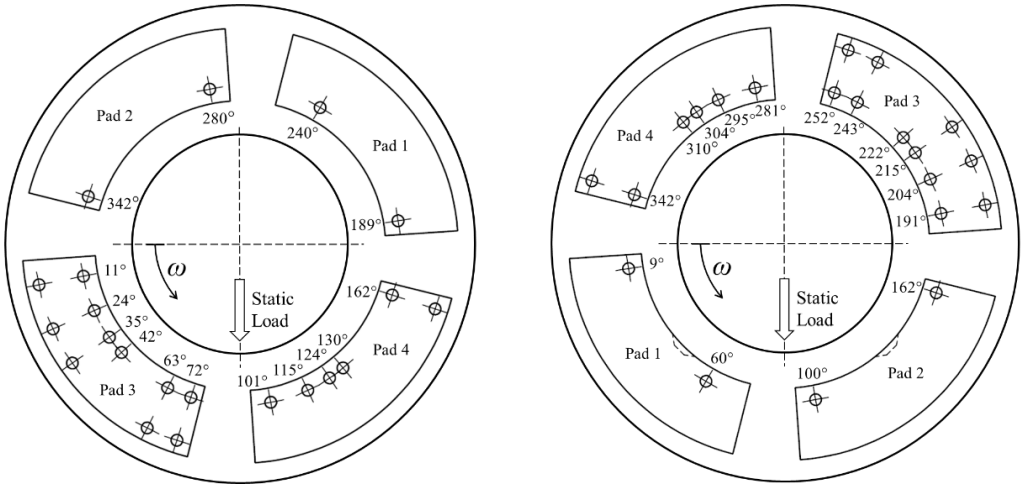

Figure 10. DE view of thermocouple locations and pad orientation for (a) original bearing (b) modified bearing

Modifications

Recesses (ports) were machined in the two loaded pads according to dimensions provided by the OEM. These ports reduce the surface area of the loaded pads by 5.2%, and the port depth is 2.11 mm (0.083 in), which is 25.5 times the nominal radial bearing clearance. They are located directly above the pad pivots. Jacking-oil supply channels were machined into the pads along with female NPT fittings on the side of each pad. The modifications to pad #1 are shown in Figure 11, and pad #2 modifications are identical.

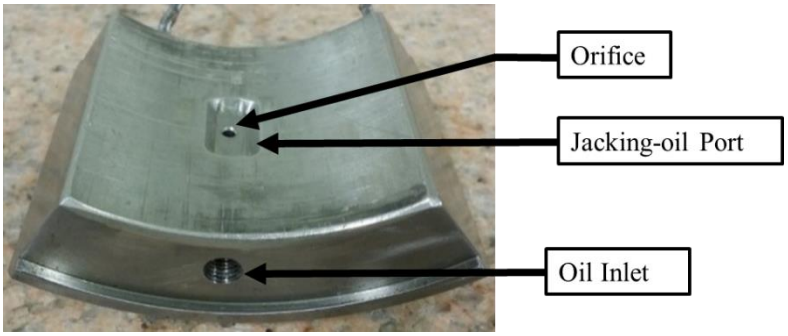

Figure 11. Jacking-oil ports added to pad #1

Tschoepe [21] tested the bearing with the load directed between pads 3 and 4. The pad locations were changed (Figure 10b) to allow for the jacking-oil modifications. Additionally, the Babbitt layer on pad #1 was damaged during previous testing and replaced during modification. Stainless-steel shims were placed behind pads #1 and #3 to replicate the bearing clearance measured by Tschoepe in 2011.

Jacking-oil supply lines were attached to both loaded pads. Prior to testing, the supply lines were used to purge the jacking-oil ports of air. No jacking-oil was used during testing. Each line contains a 1/8" NPT check valve to ensure that oil does not exit the bearing through the supply lines during testing. Check valves are typically mounted inside the pad pivot, but the rocker pivot pads used did not allow for this method. The check valves were added very close to the pad to minimize the volume of trapped oil.

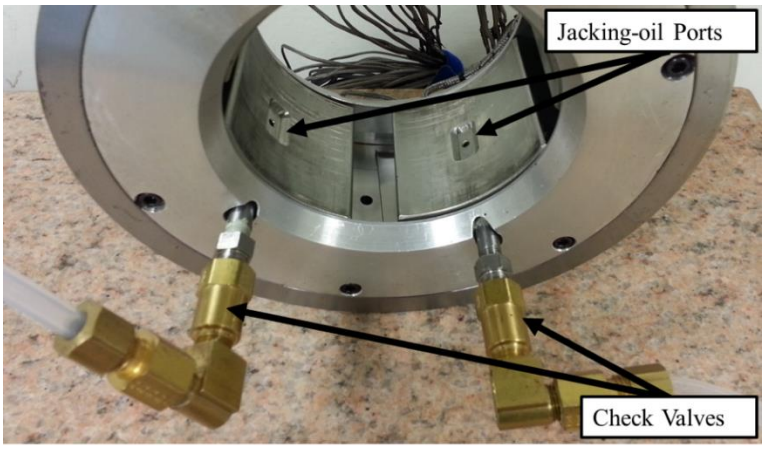

Figure 12. Test bearing with attached jacking-oil supply lines

Predictions were made to determine the added mass of the hardware would have an impact on the dynamic characteristics of the bearing. These modifications increased the pad mass from 0.932 kg to 0.996 kg. Additionally, the moment of inertia about the pivot axis was predicted to increase by 1.4%, based on a Solidworks model of the pad and attached hardware. The bearing was modelled using a TPJ bearing code *XLTRC*^{2}

(discussed in the *Bearing Predictions* Section). This code predicted that the change in mass and rotational inertia would have negligible impact on the dynamic characteristics of the bearing. Any additional stiffness or damping introduced by the added shims or flexible hoses is accounted for by taking "baseline" measurements (see *Baseline* section).

EXPERIMENTAL PROCEDURE

Procedure Overview

Tests are completed to measure the static and dynamic characteristics separately for each desired test condition. The test rig is brought to steady-state as close to the nominal test conditions as possible. The controlled test conditions include shaft speed, static load, oil flow rate, and inlet oil temperature. Once at steady-state near the desired operating conditions, static measurements are recorded over a 40 second interval. Immediately following static measurements, dynamic measurements are made by shaking the bearing in the *x* and *y*-directions separately, and recording the bearing response.

The bearing clearance is measured before testing and between each series of tests using the procedure developed by Wilkes [22]. A cold clearance refers to a clearance measurement taken at room temperature, and is taken before testing has started. A hot clearance is taken within 10 seconds after shutdown while the bearing rig is still at an elevated temperature.

Operating Conditions

Testing is completed at the same nominal conditions presented by Tschoepe [21] to allow for a direct comparison with and without jacking-oil ports. The bearing is tested at four speeds and four load as summarized in Table 3.

Table 3. Nominal operating conditions

Unit load [kPa (psi)]	Speed [RPM], (flow-rate [L/min])			
	6800, (22.7)	9000, (26.5)	10800, (30.3)	13200, (34.1)
725 (105.3)	X	X	X	X
1,452 (210.5)	X	X	X	X
2,177 (315.8)	X	X	X	□
2,903 (421.1)	X	X	X	□

X = results for both bearings presented □ = results presented only for modified bearing

Each shaft speed has a corresponding oil flow rate. The modified bearing is tested with ISO VG 46 oil and an inlet oil temperature of 54.7°C (130.5°F) for all test points. The original bearing was tested with ISO VG 32 and an inlet temperature of 43.3°C (110°F). The increased inlet oil temperature was selected such that the predicted oil viscosity was the same for both series of tests.

Results are not presented for the original bearing at the shaft speed of 13,200 rpm, for the unit loads of 2.177 and 2.903 MPa. The two operating conditions are designated by a square in Table 3. The only data available for the original bearing at these two operation conditions were tested at incorrect unit loads. This discrepancy was only realized after completing the jacking-oil modifications, and the original bearing could not be retested.

Static Characteristics

Static measurements are taken after the test rig reaches steady-state operation near the nominal test conditions. These measurements include the four test conditions as well as oil pressures, relative journal position, and temperatures at several locations. A total of 20 data samples are recorded over a span of 40 seconds. Static data for a single test condition are the average of these 20 samples. Confidence intervals are calculated for each measurement and used to verify that the test rig is at steady-state.

The four proximity probes measure the journal position in the x and y-directions relative to the bearing center (x_o, y_o). The DE and NDE measurements are averaged to provide a single position measurement located at the bearing center plane. The static displacement (e_o) is the distance between the bearing center (x_o, y_o) and the geometric rotor center (x_r, y_r).

$$e_o = \sqrt{(x_r - x_o) + (y_r - y_o)} \tag{7}$$

The journal's relative position can be expressed in terms of eccentricity ε_o and attitude angle γ (Figure 13).

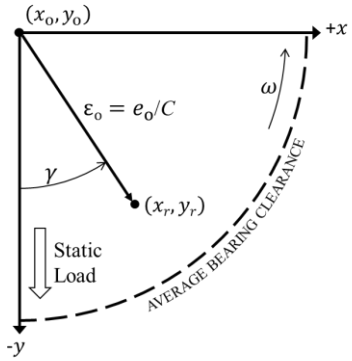

Figure 13. Static displacement coordinate system

The eccentricity (ε_o) is defined as the ratio of static displacement to the bearings radial clearance.

$$\varepsilon_o = \frac{e_o}{C_b} \tag{8}$$

The attitude angle (γ) is the angle between the load direction and the imaginary line connecting the bearing center and rotor center. A positive attitude angle is defined in the direction of rotation.

$$\gamma = \tan^{-1}\left(\frac{y_r - y_o}{x_r - x_o}\right) \tag{9}$$

The available measurement program used a left-handed coordinate system. The measured journal position in the *y*-direction was multiplied by negative one to convert the static data to the more traditional right-handed coordinated system. The remainder of this thesis will use a right handed coordinate system with the load in the downward or negative *y*-direction (Figure 13).

Clearance Measurement

The bearing clearance is measured by slowly precessing the bearing around the rotor with the hydraulic shakers. The applied force is large enough to maintain contact between the pads and rotor creating a "pad profile" as shown in Figure 14. The static displacement exceeds the bearing clearance when the load is directed between pads, because the pads are able to rotate. The four-pad geometry results in a measured pad profile that is rectangular in shape.

A cold clearance measurement is taken at room temperature before the test rig has been started. Hot clearance measurements are made for each shaft speed after testing the highest loading condition. These measured hot clearances provide the bearing centers (x_o, y_o) and the average bearing clearances used for calculating eccentricity, attitude angle, and dimensionless dynamic coefficients. The measured pad profile is fitted with a circle to estimate the average bearing clearance and bearing center. This procedure is illustrated in Figure 14 and described below.

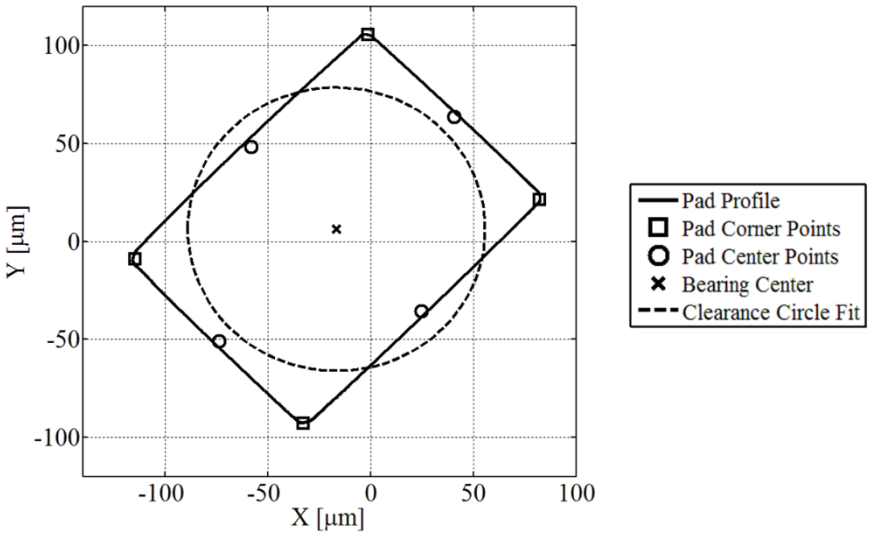

Figure 14. Average clearance fit

Pad corner points are selected on the largest pad outline. Pad center points are estimated by averaging the two surrounding corner points. The bearing center and average bearing clearance are estimated by fitting a circle to the four-pad center points.

Tschoepe [21] determined the bearing center by testing the bearing at zero static load and full shaft speed. All static data presented for the original bearing will use the "zero-load bearing center." This method was not used for the modified bearings. Preliminary predictions showed that the journal would not be located at the bearing center with zero static load. The bearing is no longer symmetric with the addition of jacking-oil ports. All static data for the modified bearing uses the measured clearance center as the bearing center. This will be discussed in detail in the *Eccentricity and Attitude Angle* section.

Dynamic Characteristics

Dynamic measurements are made after completing the static measurements for a given operating condition. The bearing is excited in the x and y-directions separately by the hydraulic shakers while maintaining the test conditions. The bearing response is measured in both orthogonal directions during each excitation. The bearing is excited with a designed waveform that contains multiple sinusoidal waveforms of varying frequency superimposed on each other. The frequencies vary from 10 to 350 Hz in 10 Hz increments and are offset to avoid shaking at multiples of 60 Hz. The designed waveform is repeated (without stopping) 320 times which takes 30 seconds to complete for each direction. The data are divided into 10 data sets each containing 32 shakes. Each data set is averaged separately and compared to determine the repeatability of the measurements.

The bearing test conditions are recorded four times during the 30 second dynamic shake test. These four data samples are averaged and referred to as the "dynamic conditions." These values are presented with confidence intervals in Appendix D.

Parameter Identification Model

The dynamic coefficients of the bearing are determined from the measured relative bearing position, stator acceleration, and input forces. The parameter identification method outlined by Rouvas and Childs [23] is used to estimate the coefficients based on the frequency-independent [*K*][*C*][*M*] reaction force model. This method begins by applying Newton's second law to the bearing assembly.

$$M_s \begin{Bmatrix} \ddot{x}_s \\ \ddot{y}_s \end{Bmatrix} = \begin{Bmatrix} f_x \\ f_y \end{Bmatrix} - \begin{Bmatrix} f_{bx} \\ f_{by} \end{Bmatrix} \tag{10}$$

The fluid-film reaction forces are denoted by f_{bx} and f_{by}, while the applied forces are denoted by f_x and f_y. The bearing assembly mass and accelerations are M_s and $\ddot{x}_s$, $\ddot{y}_s$ respectively. The force equations are combined with the [*K*][*C*][*M*] reaction force model.

$$\begin{Bmatrix} f_x - M_s\ddot{x}_s \\ f_y - M_s\ddot{y}_s \end{Bmatrix} = -\begin{bmatrix} K_{xx} & K_{xy} \\ K_{yx} & K_{yy} \end{bmatrix} \begin{Bmatrix} \Delta x \\ \Delta y \end{Bmatrix} - \begin{bmatrix} C_{xx} & C_{xy} \\ C_{yx} & C_{yy} \end{bmatrix} \begin{Bmatrix} \Delta \dot{x} \\ \Delta \dot{y} \end{Bmatrix} - \begin{bmatrix} M_{xx} & M_{xy} \\ M_{yx} & M_{yy} \end{bmatrix} \begin{Bmatrix} \Delta \ddot{x} \\ \Delta \ddot{y} \end{Bmatrix} \tag{11}$$

The equations are then converted to the frequency domain using a Fast Fourier Transform. This reduces the number of unknowns from twelve dynamic coefficients (K_{ij}, C_{ij}, and M_{ij}) to four complex dynamic-stiffness values ($\boldsymbol{H}_{ij}$).

$$\begin{Bmatrix} \boldsymbol{f}_x - M_s\boldsymbol{A}_x \\ \boldsymbol{f}_y - M_s\boldsymbol{A}_y \end{Bmatrix} = -\begin{bmatrix} \boldsymbol{H}_{xx} & \boldsymbol{H}_{xy} \\ \boldsymbol{H}_{yx} & \boldsymbol{H}_{yy} \end{bmatrix} \begin{Bmatrix} \boldsymbol{D}_x \\ \boldsymbol{D}_y \end{Bmatrix} \tag{12}$$

The coefficients $\boldsymbol{A}_i$ and $\boldsymbol{D}_i$ are the Fourier Transform of the measured acceleration and relative journal position respectively. The dynamic-stiffness values ($\boldsymbol{H}_{ij}$) are complex terms and functions of the excitation frequency Ω.

$$\boldsymbol{H}_{ij} = (K_{ij} - \Omega^2 M_{ij}) + \boldsymbol{j}(\Omega C_{ij}) \tag{13}$$

The subscript *ij* denotes the response in the *j*-direction due to an input force in the *i*-direction.

The frequency-domain force equations must be expanded to extract all four dynamic-stiffness terms. Position, force, and acceleration measurements are made in both orthogonal directions during the separate shakes in the *x* and *y*-directions. This method produces the following four equations.

$$\begin{bmatrix} \boldsymbol{f}_{xx} - M_s \boldsymbol{A}_{xx} & \boldsymbol{f}_{xy} - M_s \boldsymbol{A}_{xy} \\ \boldsymbol{f}_{yx} - M_s \boldsymbol{A}_{yx} & \boldsymbol{f}_{yy} - M_s \boldsymbol{A}_{yy} \end{bmatrix} = -\begin{bmatrix} \boldsymbol{H}_{xx} & \boldsymbol{H}_{xy} \\ \boldsymbol{H}_{yx} & \boldsymbol{H}_{yy} \end{bmatrix} \begin{bmatrix} \boldsymbol{D}_{xx} & \boldsymbol{D}_{xy} \\ \boldsymbol{D}_{yx} & \boldsymbol{D}_{yy} \end{bmatrix} \tag{14}$$

Each data set (32 shakes) is averaged in the frequency domain to determine values for the dynamic-stiffness at each of the 35 frequencies contained in the waveform. The dynamic-stiffness values of the 10 data sets are then averaged to provide a single measurement and corresponding uncertainty for each frequency.

Curve Fit Procedure

The rotordynamic coefficients (K_{ij}, C_{ij}, and M_{ij}) are estimated by curve fitting the frequency-dependent dynamic-stiffness values. The real and imaginary parts of $\boldsymbol{H}_{ij}$ are fitted separately. The imaginary part of $\boldsymbol{H}_{ij}$ is curve fitted as a linear function of excitation frequency. The slope of this line determines the frequency-independent damping coefficient C_{ij}.

$$\mathrm{Im}(\boldsymbol{H}_{ij}) = \Omega C_{ij} \tag{15}$$

The real part of $\boldsymbol{H}_{ij}$ is fitted with a quadratic function of excitation frequency. The intercept at $\Omega = 0$ estimates the stiffness coefficient, and the frequency dependency is captured by the virtual-mass coefficient.

$$\mathrm{Re}(\boldsymbol{H}_{ij}) = K_{ij} - \Omega^2 M_{ij} \tag{16}$$

The real and imaginary parts of $\boldsymbol{H}_{ij}$ are both fitted using a first-order least-squares regression if the general form of

$$\bar{y} = m\bar{x} + b \tag{17}$$

where $\bar{x}$ and $\bar{y}$ represent the independent and dependent variables respectively, and the slope and intercept are denoted by *m* and *b* respectively. The least-squares regression approach determines the values for *m* and *b* that minimizes the sum of the squares (*P*).

$$P = \sum_{k=1}^{n} \left(y_k{}^2 - \bar{y}_k{}^2 \right) \tag{18}$$

The term y_k represents the individual measured data points and $\bar{y}_k$ is the estimated value at each data point (y_k, x_k). The variable *n* is the number of frequencies or data points used for the curve fit. The corresponding equations for *m* and *b* are

$$m = \frac{\sum_{k=1}^{n} x_k \sum_{k=1}^{n} y_k - n \sum_{k=1}^{n} x_k y_k}{\left(\sum_{k=1}^{n} x_k \right)^2 - n \sum_{k=1}^{n} \left(x_k \right)^2} \tag{19}$$

$$b = \frac{\sum_{k=1}^{n} x_k \sum_{k=1}^{n} x_k y_k - \sum_{k=1}^{n} \left(x_k \right)^2 \sum_{k=1}^{n} y_k}{\left(\sum_{k=1}^{n} x_k \right)^2 - n \sum_{k=1}^{n} \left(x_k \right)^2} \tag{20}$$

When fitting the imaginary part of the dynamic-stiffness $\boldsymbol{H}_{ij}$, the intercept *b* is set to zero and the slope *m* estimates the damping coefficient. Applying the least-squares regression technique to the real part of $\boldsymbol{H}_{ij}$ requires a change in variables. The independent variable is defined as the excitation frequency squared, $\lambda = \Omega^2$, making $\mathrm{Re}(\boldsymbol{H}_{ij})$ a linear function of λ.

$$\mathrm{Re}(\boldsymbol{H}_{ij}) = K_{ij} + \lambda(-M_{ij}) \tag{21}$$

The slope estimates the virtual-mass coefficient (with a sign change), and the intercept estimates the stiffness coefficient.

Baseline

The dynamic response of the bearing is affected by the attached hardware including the pitch stabilizers, oil hose, and static loader assembly. This hardware affects the stiffness, damping, and the total mass of the bearing assembly. To isolate the properties of the fluid-film, these contributions must be accounted for by subtracting a "baseline." A baseline refers to the measured response while exciting the bearing assembly with absolutely no oil in the bearing and zero shaft speed. The same baseline measurement is used to adjust all dynamic tests. A static load of 1,112 N (250 lbf) is applied during the baseline measurement ensuring that the effects from the static loader assembly are included. The baseline is also used to determine the stator mass (M_s) for the force equation. The baseline dynamic-stiffness values are subtracted before the curve fit procedure ensuring that only the bearing (fluid-film) properties are estimated.

$$\boldsymbol{H}_{ij} = \boldsymbol{H}_{ij,\mathrm{TEST}} - \boldsymbol{H}_{ij,\mathrm{BASE}} \tag{22}$$

Uncertainty Analysis

Two types of uncertainty are used while discussing dynamic data. The first type quantifies the repeatability of the bearing response during a dynamic excitation. The average dynamic-stiffness value at each excitation frequency has an associated uncertainty. The second type of uncertainty quantifies how well the curve fit matches the dynamic-stiffness values. The estimated stiffness, damping, and virtual-mass coefficients each have an associated uncertainty derived from the curve fitting procedure. Figure 15 presents two separate data sets to illustrate these two types of uncertainty. The uncertainties from repeatability are denoted by error bars at each excitation frequency. The uncertainty from curve fitting the damping coefficients C_1 and C_2 are ±4.1 and ±23.7 kN·s/m respectively. The damping coefficient C_1 has a smaller uncertainty because the data points are described well by a linear curve fit. Dynamic coefficient uncertainties are presented as error bars in the *Dynamic Characteristics* section.

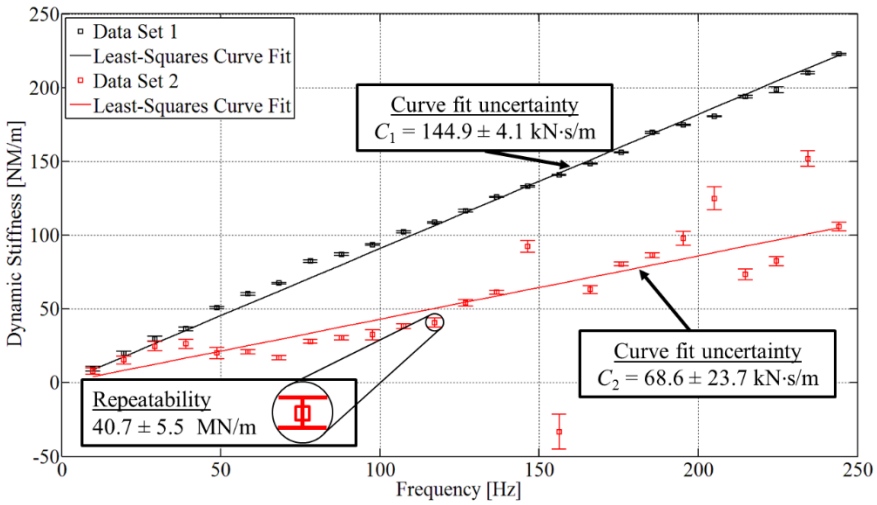

Figure 15. Repeatability and curve fit uncertainties for two data sets

The repeatability uncertainty at each frequency is found from the 10 data sets that were averaged. This uncertainty is defined to be twice the standard deviation

$$\Delta \boldsymbol{H}_{ij} = 2\sqrt{\frac{\sum_{k=1}^{N}\left[\left(\bar{\boldsymbol{H}}_{ij}\right)_k - \boldsymbol{H}_{ij}\right]^2}{N-1}} \tag{23}$$

where $(\bar{\boldsymbol{H}}_{ij})_k$ is the dynamic-stiffness for an individual data set, N is the number of data sets, and $\boldsymbol{H}_{ij}$ is the average of all N data sets. This equation is used to calculate uncertainty for the each dynamic test as well as the baseline. The uncertainty of the corrected dynamic-stiffness values is calculated using the root-sum-squares method.

$$\Delta \boldsymbol{H}_{ij} = \sqrt{(\Delta \boldsymbol{H}_{ij,TEST})^2 + (\Delta \boldsymbol{H}_{ij,BASE})^2} \tag{24}$$

For the remainder of this thesis, $\boldsymbol{H}_{ij}$ and $\Delta\boldsymbol{H}_{ij}$ will refer to the corrected (after subtracting baseline data) dynamic-stiffness and uncertainties respectively.

The uncertainties of the least-squares regression, Δm and Δb, provide the uncertainty of the stiffness, damping, and virtual-mass coefficients.

$$\Delta m = \pm t \frac{S_{yx}}{S_{xx}} \tag{25}$$

$$\Delta b = \pm (t) S_{yx} \sqrt{\frac{1}{n} + \frac{\left[\left(\frac{1}{n}\right)\sum_{k=1}^{n} x_k\right]^2}{S_{xx}^{\ 2}}} \tag{26}$$

The variable t is a constant based on the number of samples and the size of the confidence interval. The standard error, S_{yx}, and the value S_{xx} are defined as

$$S_{yx} = \sqrt{\frac{\sum_{k=1}^{n} (y_k - \bar{y}_k)^2}{n-2}} \tag{27}$$

$$S_{xx} = \sqrt{\sum_{k=1}^{n} x_k^2 - \frac{1}{n}\left(\sum_{k=1}^{n} x_k\right)^2} \tag{28}$$

where n is the total number of frequencies in the curve fit, y_k is a measured impedance value, and $\bar{y}_k$ is the impedance estimated from the curve fit at the frequency x_k [24]. The uncertainties presented here use t = 2.069 for a 95% confidence interval.

Dimensionless Coefficients

Dynamic coefficients will be presented as dimensionless quantities, denoted by lower case constants k_{ij}, c_{ij}, and m_{ij}.

$$k_{ij} = K_{ij}\left(\frac{C_b}{F_s}\right) \tag{29}$$

$$c_{ij} = C_{ij}\left(\frac{C_b \omega}{F_s}\right) \tag{30}$$

$$m_{ij} = M_{ij}\left(\frac{C_b \omega^2}{F_s}\right) \tag{31}$$

Measured values for the average radial hot bearing clearance C_b, the shaft speed ω, and the applied static load F_s will be used to calculate these dimensionless quantities. These values are included in the dynamic conditions presented in Appendix D.

Dynamic-stiffness will also be presented as dimensionless data, denoted as $\boldsymbol{h}_{ij}$, to compare the dynamic-stiffness with and without jacking-oil ports at a single excitation frequency.

$$\boldsymbol{h}_{ij} = \boldsymbol{H}_{ij}\left(\frac{C_b}{F_s}\right) \tag{32}$$

The dimensionless coefficients (c_{ij}, k_{ij}, and m_{ij}) contain uncertainty from both the dimensional coefficients (C_{ij}, K_{ij}, and M_{ij}) and the measured dynamic conditions F_s, C_b, and ω. These uncertainty values are combined using error propagation to find the uncertainty of the dimensionless stiffness, damping, and virtual-mass coefficients, $U_{k,ij}$ $U_{c,ij}$ and $U_{m,ij}$. The dynamic coefficients uncertainty from the linear regression is denoted by eK_{ij}, eC_{ij}, and eM_{ij}. The three dynamic conditions standard deviation denoted by σ_i where i denotes the respective dynamic condition.

$$U_{k,ij} = \sqrt{\left(\frac{C_b}{F_s}eK_{ij}\right)^2 + \left(\frac{K_{ij}}{F_s}\sigma_{c_b}\right)^2 + \left(\frac{K_{ij}C_b}{(F_s)^2}\sigma_{F_s}\right)^2} \tag{33}$$

$$U_{c,ij} = \sqrt{\left(\frac{C_b\omega}{F_s}eC_{ij}\right)^2 + \left(\frac{C_{ij}\omega}{F_s}\sigma_{c_b}\right)^2 + \left(\frac{C_{ij}C_b\omega}{(F_s)^2}\sigma_{F_s}\right)^2 + \left(\frac{C_{ij}C_b}{F_s}\sigma_{\omega}\right)^2} \tag{34}$$

$$U_{m,ij} = \sqrt{\left(\frac{C_b\omega^2}{F_s}eC_{ij}\right)^2 + \left(\frac{M_{ij}\omega^2}{F_s}\sigma_{c_b}\right)^2 + \left(\frac{M_{ij}C_b\omega^2}{(F_s)^2}\sigma_{F_s}\right)^2 + \left(\frac{2M_{ij}C_b\omega}{F_s}\sigma_{\omega}\right)^2} \tag{35}$$

STATIC CHARACTERISTICS

This section contains measured static data for the bearing both with and without jacking-oil ports. It contains measured cold and hot clearances, and a discussion of the methods used to estimate the bearing center location. Static equilibrium eccentricities and attitude angles are provided for all operating conditions including the four shaft speeds and four unit loads. The static equilibrium positions are also presented as bearing location plots to illustrate how the skewed clearance affects the static journal position. Pad temperatures are also presented for select operating conditions.

Clearance

Figure 16 and Figure 17 show the measured cold and hot clearance pad profiles for the original and modified bearing respectively. The circle fit method, described in the *Clearance Measurement* section, provides an average radial bearing clearance (C_b) for each measured pad profile.

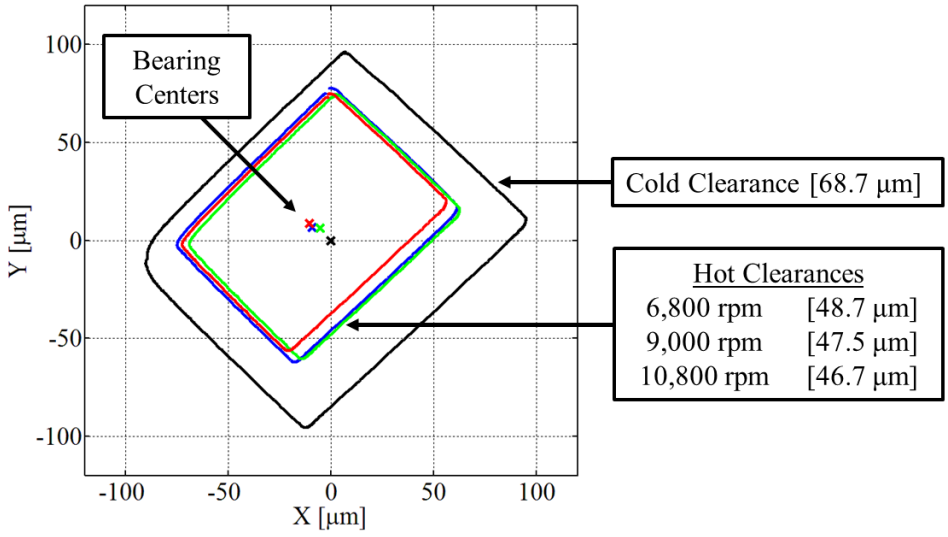

Figure 16. Original bearing measured pad profiles and bearing center

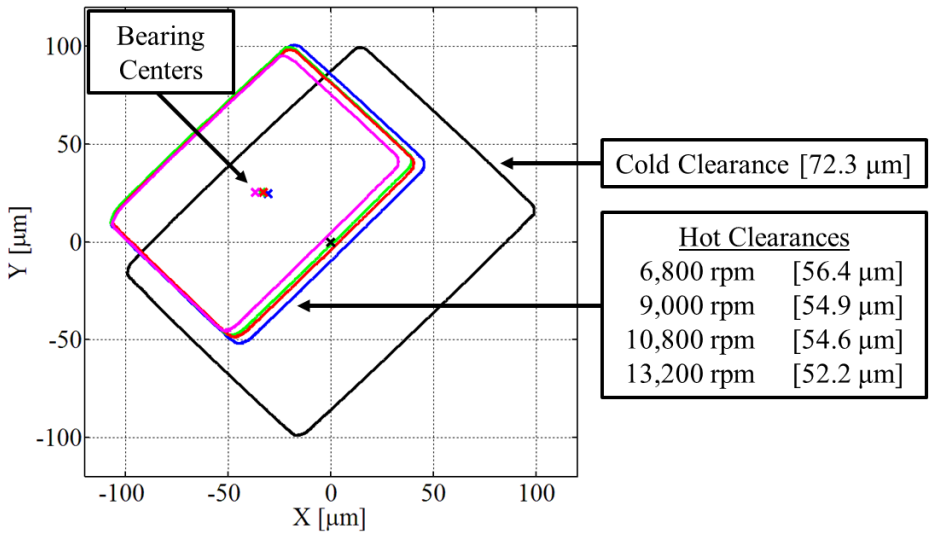

Figure 17. Modified bearing measured pad profiles and bearing center

Table 4 lists the average radial bearing clearances, along with the peak Babbitt temperature (T_{peak}) for the cold clearance and each hot clearance. The listed peak temperatures T_{peak} were recorded prior to taking the clearance and are the maximum of the inner-ring of fifteen embedded thermocouples.

Table 4. Measured bearing cold and hot clearances

Average radial bearing clearance (µm) and average temperature (°C)				
Speed [RPM]	Original bearing		Modified bearing	
	C_b	T_{peak}	C_b	T_{peak}
0 (CC)	68.7	26.6	72.3	26.6
6,800 (HC)	48.7	84.2	56.4	93.7
9,000 (HC)	47.5	95.0	54.9	103.0
10,800 (HC)	46.7	102.1	54.6	109.2
13,200 (HC)	-	-	52.2	114.0

Thermal expansion causes the observed reduction in bearing clearance. As the running speed increases, the operating temperature increases, causing the rotor and bearing to expand.

Bearing Center

The rotor position relative to the bearing is measured using the two sets of *x* and *y* proximity probes located in the stator end-caps. They are averaged to provide a single *x* and *y* measurement at the bearing's midplane. The bearing center location is required to determine static displacement, eccentricity, and attitude angle. It is measured while the test rig is at the operational temperature because thermal expansion shifts the bearing center position. The bearing-center is different for each shaft speed.

Previous work (including Tschoepe's thesis) used a zero-load test to determine the bearing center. The rotor position was measured while the test rig was at full speed and without any static load. This position was used as the bearing center for eccentricity and attitude angle calculations. Wygant [25] states that this method should be used because a truly unloaded case can never be achieved. In recent work, the bearing center has been determined by taking a hot clearance as described in the *Experimental Procedure* section. Coghlan [26] experimentally compared these two methods and, in agreement with Wygant's paper, concluded that the measured hot clearance center should be used. Figure 18 is reproduced from Coghlan's thesis. It shows the two bearing centers found using these two methods. Measured journal position for four non-zero loads are also shown. Coghlan's example shows that the zero-load method can cause significant errors in eccentricity and attitude angle. Based on the conclusions of Wygant and Coghlan, the hot clearance center was used to calculate eccentricity and attitude angle for the modified bearing.

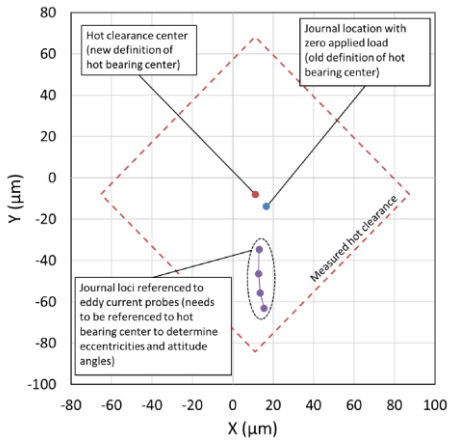

Figure 18. Comparison of measurement methods for bearing center, figure from [26]

Eccentricity and Attitude Angle

Figure 19 shows the static eccentricity for the bearing with and without jacking-oil ports. Each point represents the eccentricity (ε_o) for a given shaft speed and unit load. The line segments between points do not represent measured data.

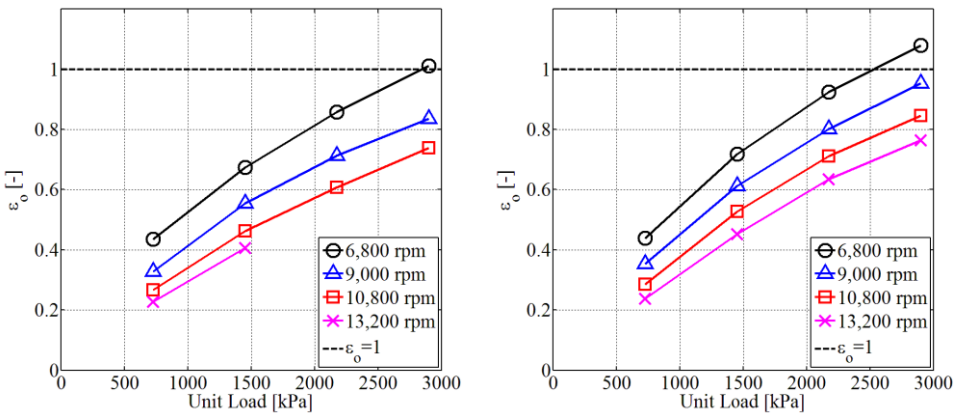

(a) **(b)**

Figure 19. Static eccentricity (a) original bearing (b) modified bearing

Eccentricity is calculated using the average hot bearing clearance corresponding to the respective shaft speed. As expected, the static displacement (e_o) increases as unit load increases and shaft speed decreases. For both bearings, the static displacement exceeds the average bearing clearance (ε_o=1) for the high unit load and low shaft speed testing condition. Figure 20 shows the attitude angles for the original and modified bearings.

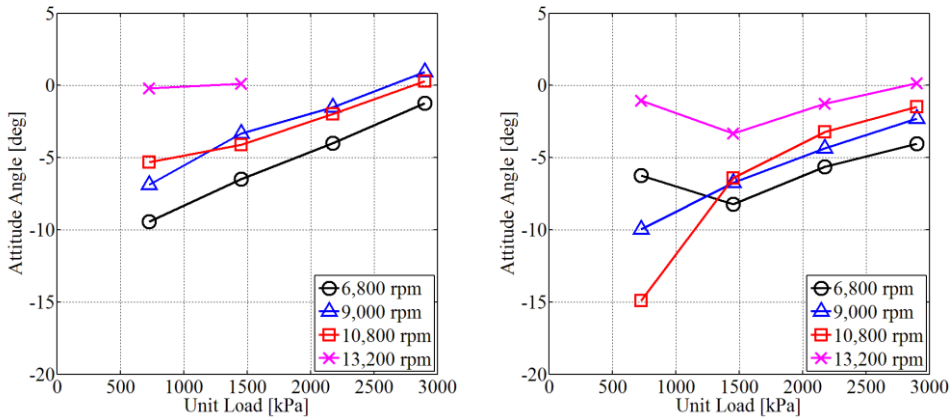

Figure 20. Attitude angle plot (a) original bearing (b) modified bearing

Non-zero attitude angles are caused by cross-coupled stiffness which arise in TPJ when pad rotation is impeded by pad inertia or pivot friction. The attitude angles for a rocker-pivot TPJ bearing are typically small in magnitude and positive (in the direction of journal rotation) [19],[20]. The negative attitude angles seen in Figure 20 were attributed to the non-symmetric or skewed clearance. Considering a centered journal position, the bearing clearance is larger at pad #1 than at pad #2. The increased clearance reduces the bearing stiffness, allowing larger displacement in the direction of pad #1.

Figure 21 shows the measured bearing loci, hot clearance profile, and average hot bearing clearance for both the original and modified bearing. The data points represent the bearing center and the journal location at each of the four unit loads (0.725, 1.452, 2.178,

and 2.903 MPa). All data for the original and modified bearing are shown in black and red respectively.

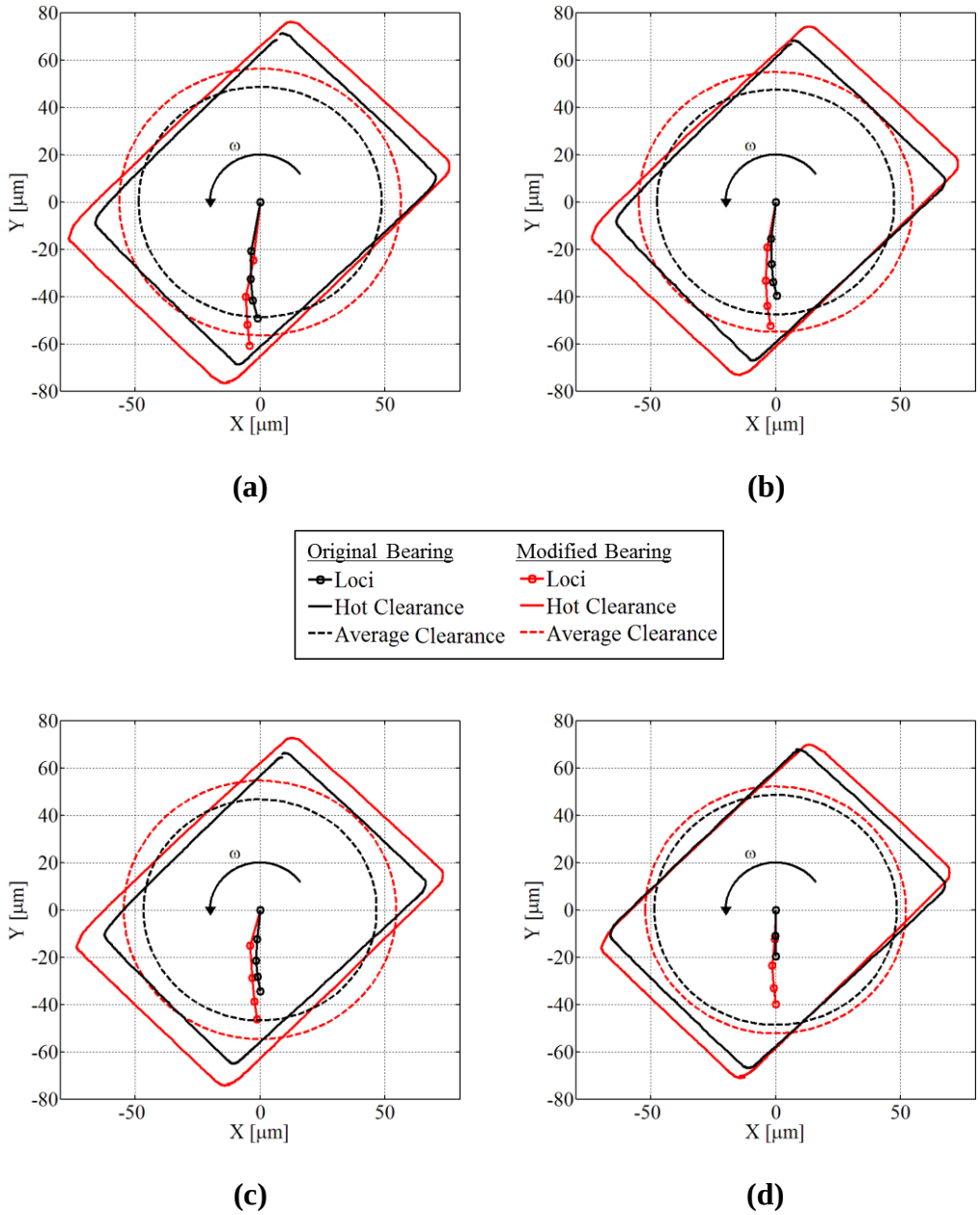

Figure 21. Bearing loci and clearance at shaft speed: (a) 6,800 rpm (b) 9,000 rpm (c) 10,800 rpm (d) 13,200 rpm

This representations of the static data shows that the increased clearance of the modified bearing affected the bearing loci. The static displacement is larger for the modified bearing regardless of shaft speed or unit load. Figure 21 also shows that the minimum film thickness is reduced for the modified bearing at high loads. Table 5 presents the minimum film thickness for each shaft speed at the load 2.903 MPa. These values are the minimum distance between the measured bearing loci and hot clearance pad profile at the respective speed.

Table 5. Estimated minimum film thickness

Minimum film-thickness [μm], at 2,903 kPa (421.1 psi)				
Speed [RPM]	6,800	9,000	10,800	13,200
Original bearing	9.7	13.9	15.8	-
Modified bearing	6.4	7.9	12.9	13.1

The data presented for the original and modified bearings used a different method for determining the bearing center. The potential error from this difference is enough to account for the reduction in minimum film thickness. Overall, adding jacking-oil ports did not cause any changes in eccentricity, attitude angle, or minimum film-thickness.

Pad Temperatures

The test bearing contains twenty-one thermocouples embedded in the pads. The locations are shown in Figure 10 in the *Bearing Description* section. The fifteen thermocouples in the inner ring are all located 5.08 mm (0.2 in) beneath the pad surface. These temperatures are considered approximations of the pad surface temperature (Babbitt temperature) during steady-state operation.

The original and modified bearings were tested with oil inlet temperatures of 43.3°C (110°F) and 54.7°C (130.5°F) respectively. The measured steady-state temperatures are compared by considering temperature rise ΔT,

$$\Delta T = T_{\text{pad}} - T_{\text{in}} \tag{36}$$

where T_{pad} is the pad temperature at a given location and T_{in} is the nominal oil inlet temperature. The pads were arranged differently to allow for the addition of jacking-oil ports (see *Bearing Description*). Pad temperatures will be presented using the coordinate system shown in Figure 22. With these coordinates, the static load is directed between pads #1 and #2 for both the original and modified bearing tests.

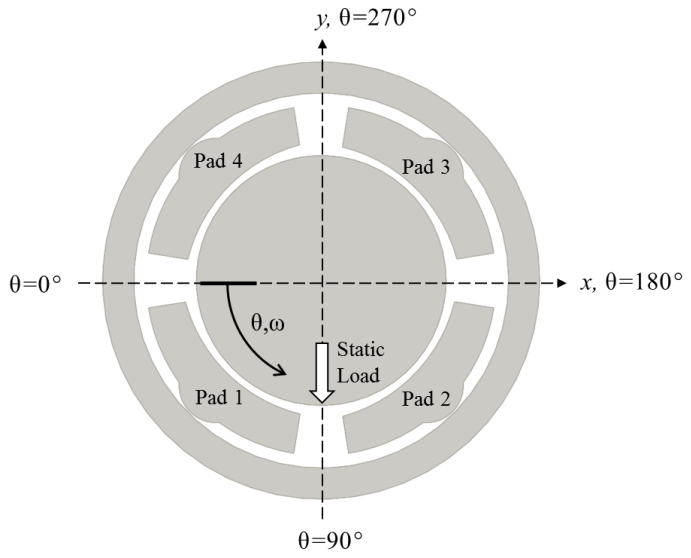

Figure 22. Temperature data coordinate system

Figure 23 shows the temperature rise (ΔT) for the operating condition of 6,800 rpm and 0.725 MPa (105.3 psi). Figure 24 shows the temperature rise (ΔT) for the operating condition of 10,800 rpm and 2.903 MPa (421.1 psi). Temperature data for the remaining fourteen operating conditions are located in Appendix C. The eight vertical lines denote

the leading and trailing edge of the pads. Data points connected by dashed lines represents the modified bearing. Data points connected by the solid lines represent the original bearing without jacking-oil ports.

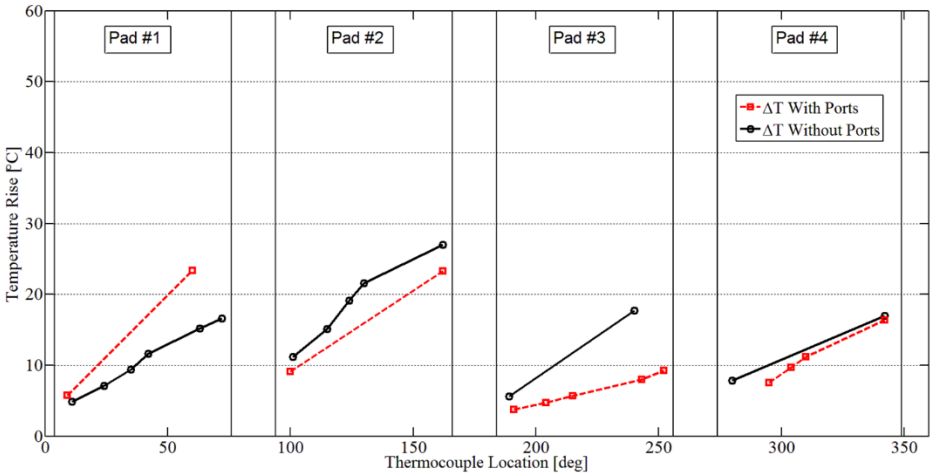

Figure 23. Pad temperature rise at 6,800 rpm and 0.725 MPa (105.3 psi)

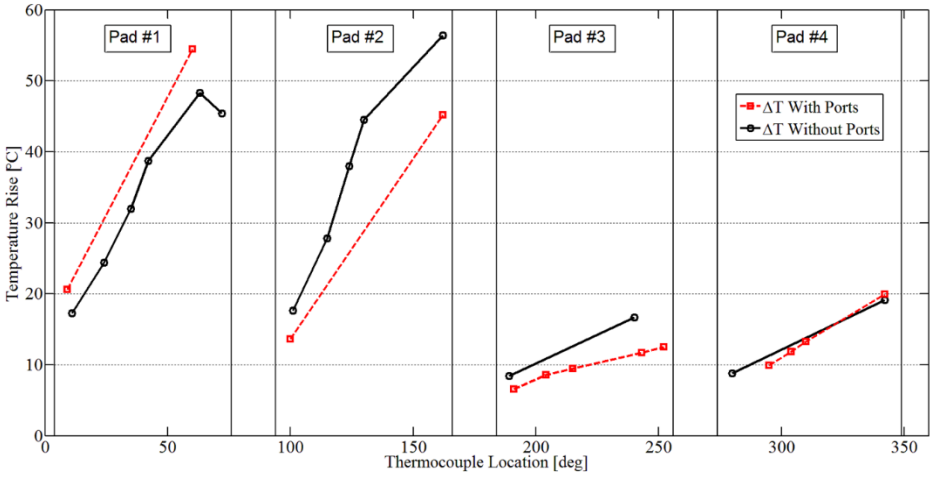

Figure 24. Pad temperature rise at 10,800 rpm and 2.903 MPa (421.1 psi)

Figure 23 and Figure 24 show the temperature rise at the minimum and maximum average bearing temperatures. Babbitt temperature increases with both the shaft speed and unit load. When comparing the bearing with and without jacking-oil, Pad #1 consistently showed an increase in ΔT while pads #2 and #3 showed a decrease in ΔT. Pad #4 showed very minimal changes in ΔT. The peak temperature rise (ΔT_{max}) was not greatly affected by the addition of jacking-oil ports. For all operating conditions, there was only a slight decrease in ΔT_{max}. However, this could be attributed to the change in bearing geometry and temperature distribution.

Closure

Hot clearance measurements showed that the original bearing clearance reduced between 29% and 32% at operational temperatures (compared to room temperature), and the modified bearing clearance was reduced between 22% and 28%. Negative attitude angle were measured and attributed to the skewed clearance. Adding jacking-oil ports caused only small changes in the static eccentricity, attitude angle, and minimum film thickness. These changes are attributed to the difference in bearing center measurement methods. Pad temperatures increased at pad #1 and decreased at pads #2 and #3. Overall, adding jacking-oil ports did not cause significant changes in the static journal positions. A slight decrease in peak metal temperature was observed across all operating conditions.

DYNAMIC CHARACTERISTICS

This section contains the measured dynamic results for the bearing with and without jacking-oil ports. Dynamic coefficients are presented as frequency-independent stiffness, damping, and virtual-mass coefficients. Dynamic-stiffness measurements will be shown for select test conditions to discuss the validity of the [*K*][*C*][*M*] model. As discussed in the *Uncertainty Analysis* section, the dynamic-stiffness plots have error bars showing twice the standard deviation, and the dynamic coefficient plots have error bars representing the coefficient uncertainty or goodness of the curve fit.

Dynamic coefficients of a TPJ bearing depend on the bearing clearance. They will be presented as dimensionless quantities (Eqs. (29)-(31)) to allow for a direct comparison between the bearing with and without jacking-oil ports without the effects of the increased clearance. Both dimensional and dimensionless dynamic coefficients are listed in Appendix E.

[*K*][*C*][*M*] Model

Dynamic-stiffness measurements for the bearing with and without jacking-oil ports are both fit reasonably well by the [*K*][*C*][*M*] model. Figure 25 shows the imaginary part of $\boldsymbol{H}_{xx}$ and $\boldsymbol{H}_{xy}$ and the linear curve fit for both bearings. The jacking-oil ports did not cause the damping to become frequency dependent regardless of shaft speed and unit load.

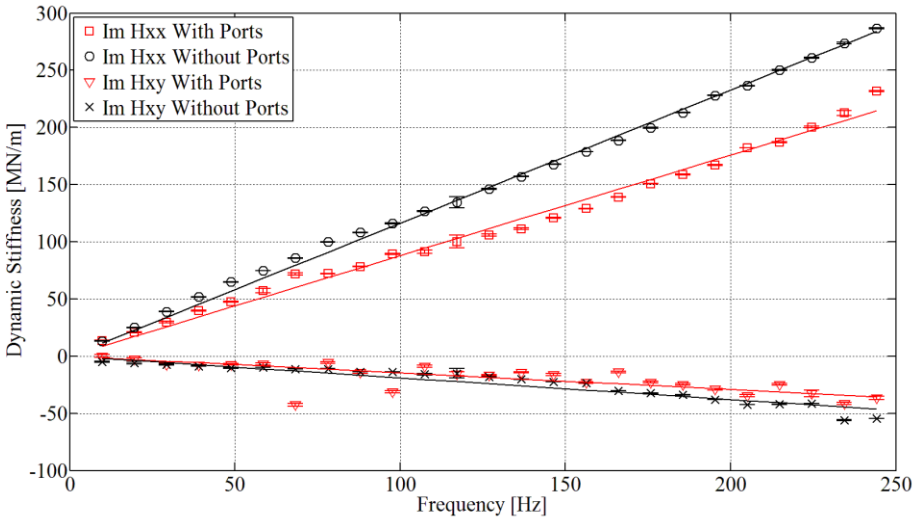

Figure 25. Im(H_{ij}) with and without ports at 6,800 rpm and 1.452 MPa (210.5 psi)

Figure 26 shows the real part of $\boldsymbol{H}_{xx}$ and $\boldsymbol{H}_{xy}$ and the respective curve fits with stiffness and virtual-mass for the bearing with and without jacking-oil ports.

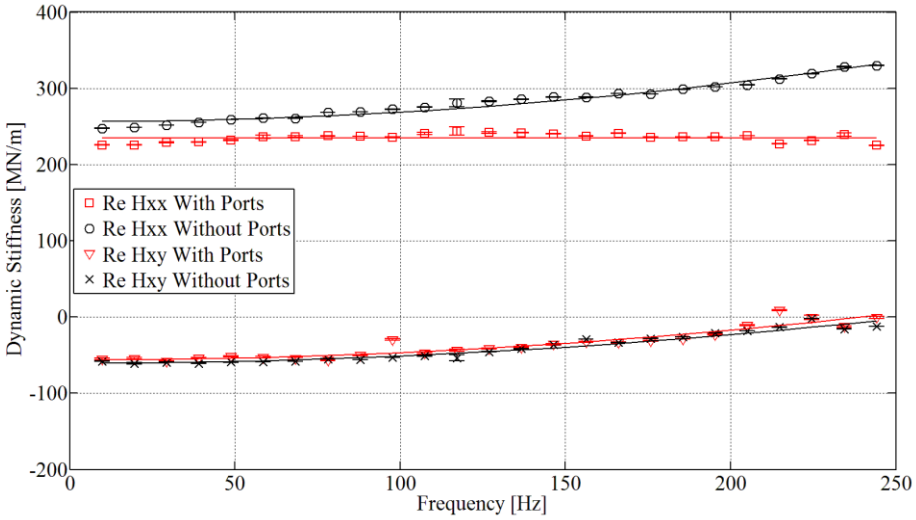

Figure 26. Re(H_{ij}) with and without ports at 6,800 rpm and 1.452 MPa (210.5 psi)

Adding jacking-oil ports changed the real part of dynamic-stiffness. The direct dynamic-stiffness terms, $\boldsymbol{H}_{xx}$ and $\boldsymbol{H}_{yy}$, are reduced at high excitation frequencies. This data can still be modeled well by constant stiffness and virtual-mass term. This is discussed further in the *Virtual-Mass Coefficients* section.

For certain operating conditions, including the data shown in Figure 26, the direct stiffness data could be accurately modelled with only a constant stiffness value. For consistency, the [*K*][*C*][*M*] model was still used in these cases with a negligible (nearly zero) virtual-mass coefficient.

Baseline Dynamic-Stiffness

Separate baseline tests were conducted for the original and modified bearing to account for any changes in the bearing assembly such as the added shims and jacking-oil hardware. The baseline for each bearing assembly is used to adjust the dynamic-stiffness values for all sixteen operating conditions. All dynamic-stiffness data in the remainder of this thesis have been adjusted with their respective baselines. Figure 27 and Figure 28 show the baseline data for the original bearing recorded by Tschoepe. Figure 29 and Figure 30 show the baseline data for the bearing after adding jacking-oil ports. These values and uncertainties are listed in Appendix F.

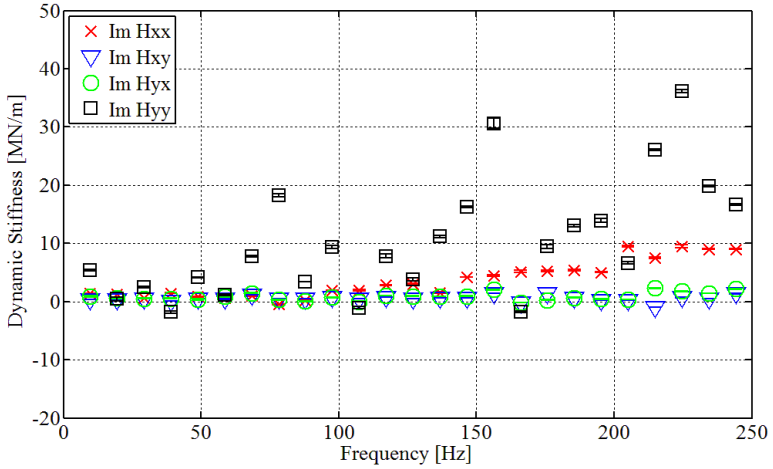

Figure 27. Baseline dynamic-stiffness Im($\boldsymbol{H}_{ij}$) for the original bearing

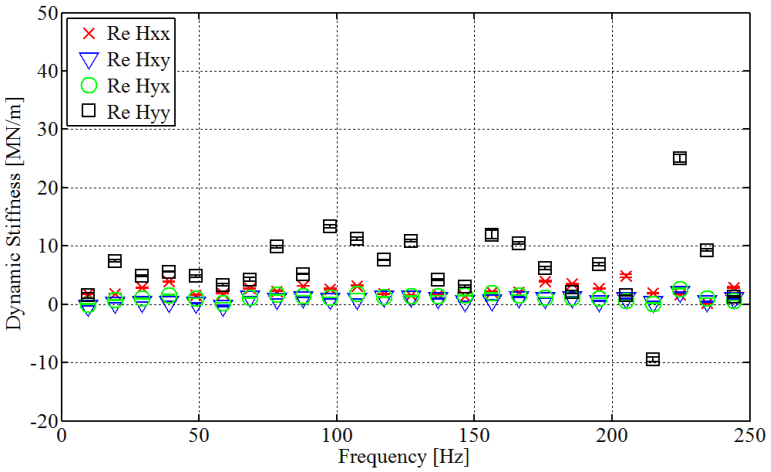

Figure 28. Baseline dynamic-stiffness Re(H_{ij}) for the original bearing

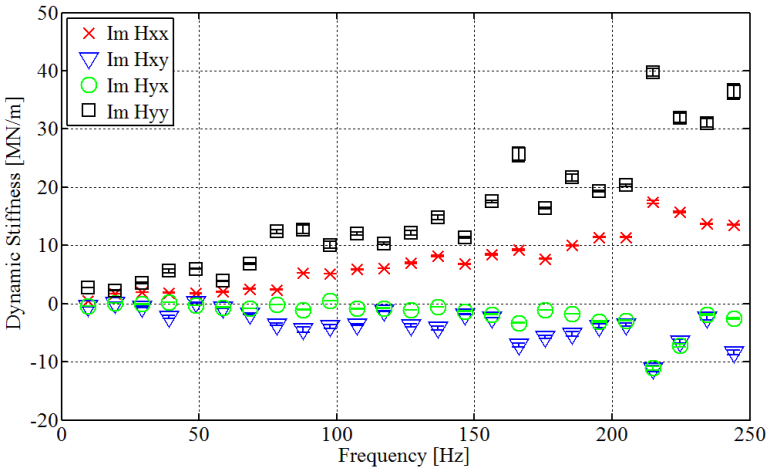

Figure 29. Baseline dynamic-stiffness Im(H_{ij}) for the modified bearing

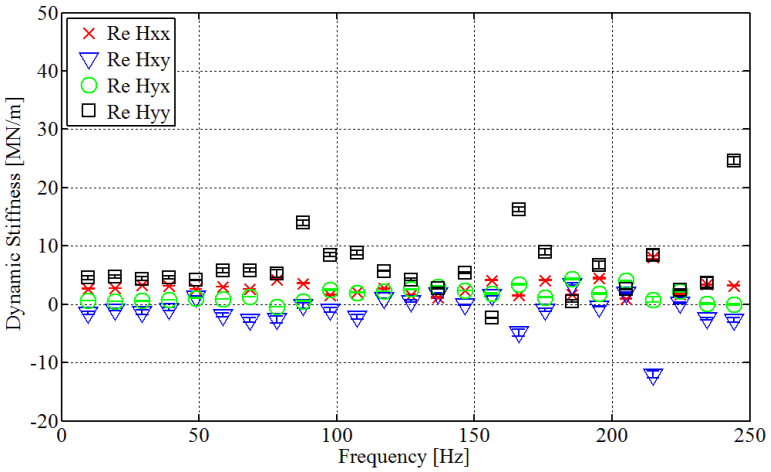

Figure 30. Baseline dynamic-stiffness Re(H_{ij}) for the modified bearing

Stiffness Coefficients

Dynamic coefficients are plotted versus unit load. Each figure contains four subplots which are labeled with the associated shaft speed. The error bars shown include the uncertainty from both the linear regression and the standard deviation of shaft speed, static load, and bearing clearance. The measured dynamic conditions and uncertainties are presented in Appendix D. For all measured dynamic results, circular data points connected by solid lines indicate the original bearing data taken from Tschoepe's thesis. Square data points connected by dashed lines indicate the modified bearing data.

Figure 31 and Figure 32 show direct stiffness in the *y*-direction and *x*-direction respectively. Figure 33 and Figure 34 show the cross-coupled stiffness, k_{xy} and k_{yx}, respectively. Stiffness coefficients and their uncertainties can also be found in Appendix E.

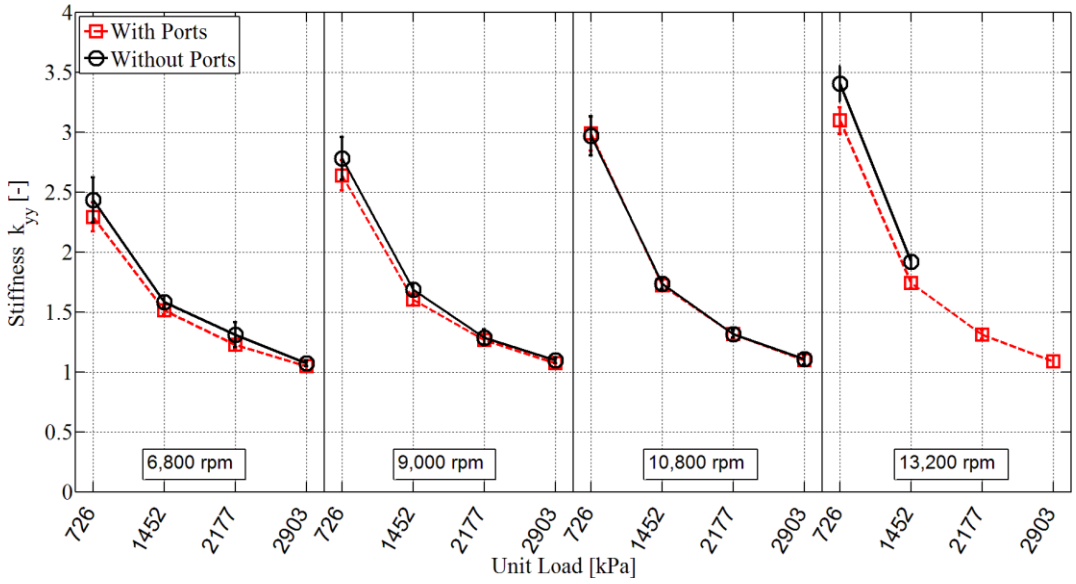

Figure 31. Direct stiffness coefficients k_{yy} (load direction)

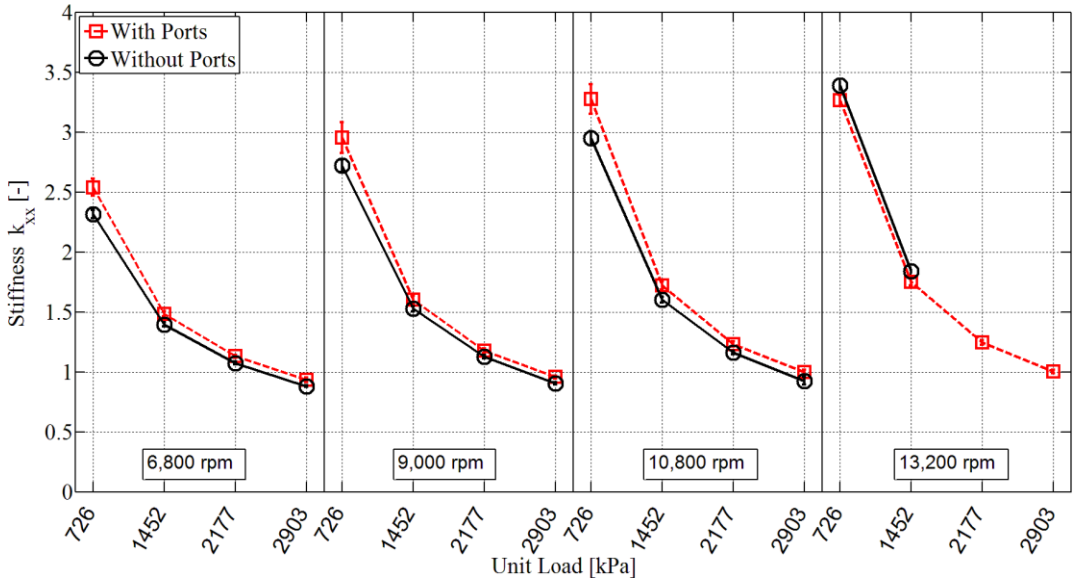

Figure 32. Direct stiffness coefficients k_{xx}

Adding jacking-oil ports had no significant effect on the direct stiffness coefficients regardless of shaft speed and unit load. The change in dimensionless stiffness range from

-9.1% to +0.6% in the *y*-direction, and from -4.8% to +11.1% in the *x*-direction. For both bearings, direct stiffness increased with increasing shaft speed and load, and the coefficients k_{yy} and k_{xx} were similar in magnitude.

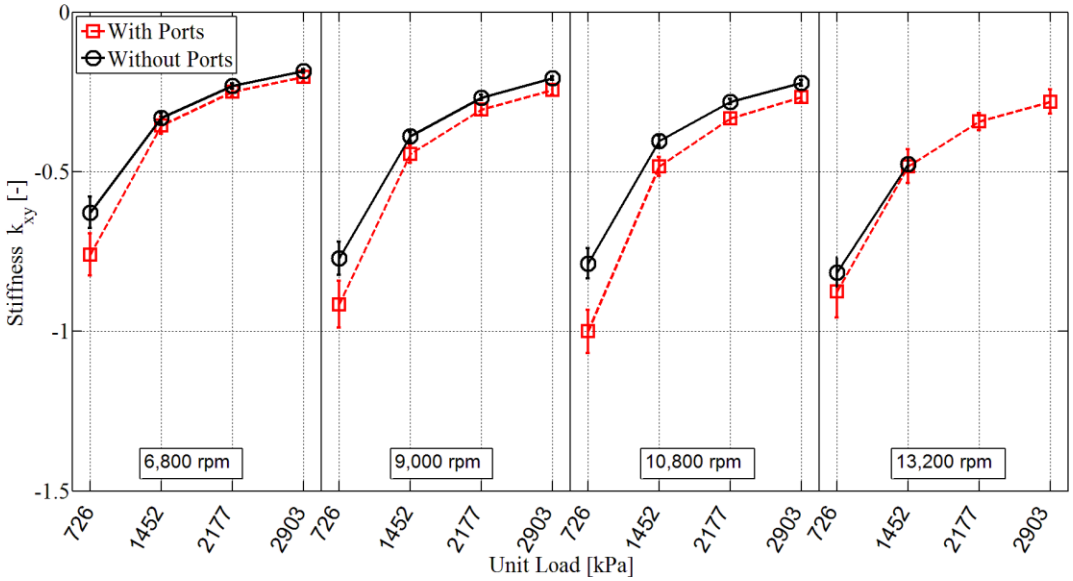

Figure 33. Cross-coupled stiffness ceofficients k_{xy}

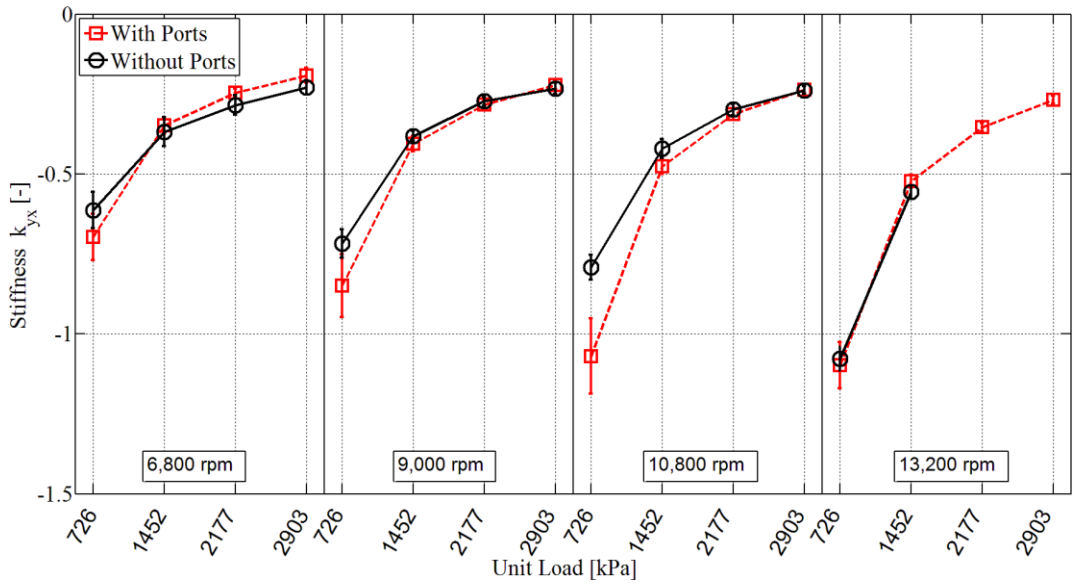

Figure 34. Cross-coupled stiffness ceofficients k_{yx}

The dimensionless cross-coupled stiffness coefficients, k_{xy} and k_{yx}, showed an increase in magnitude for most operating conditions. However, the large confidence intervals prevent any definite relation between the two bearing tests. These results show that adding jacking-oil ports to a TPJ bearing did not markedly change the magnitude or sign of the cross-coupled stiffness coefficients. For both bearings, k_{xy} and k_{yx} are both negative, similar in magnitude, and less than 35% of the magnitude of the direct stiffness k_{yy} and k_{xx}.

Damping Coefficients

Figure 35 and Figure 36 show the direct damping in the *y*-direction and *x*-direction respectively. Figure 37 and Figure 38 show the cross-coupled damping, c_{xy} and c_{yx}. The damping coefficients and their uncertainties can also be found in Appendix E.

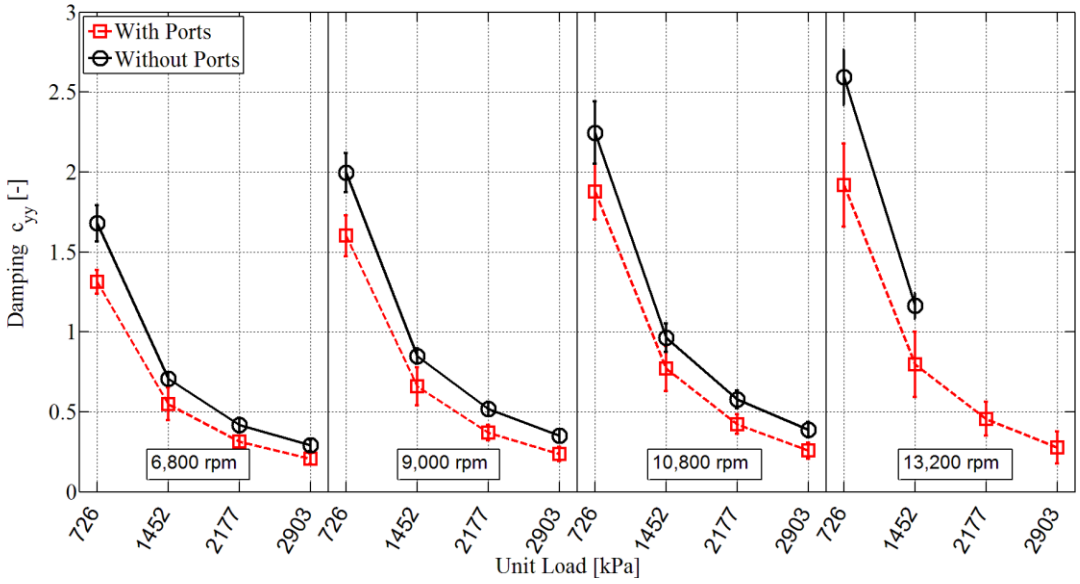

Figure 35. Direct damping coefficients c_{yy} (load direction)

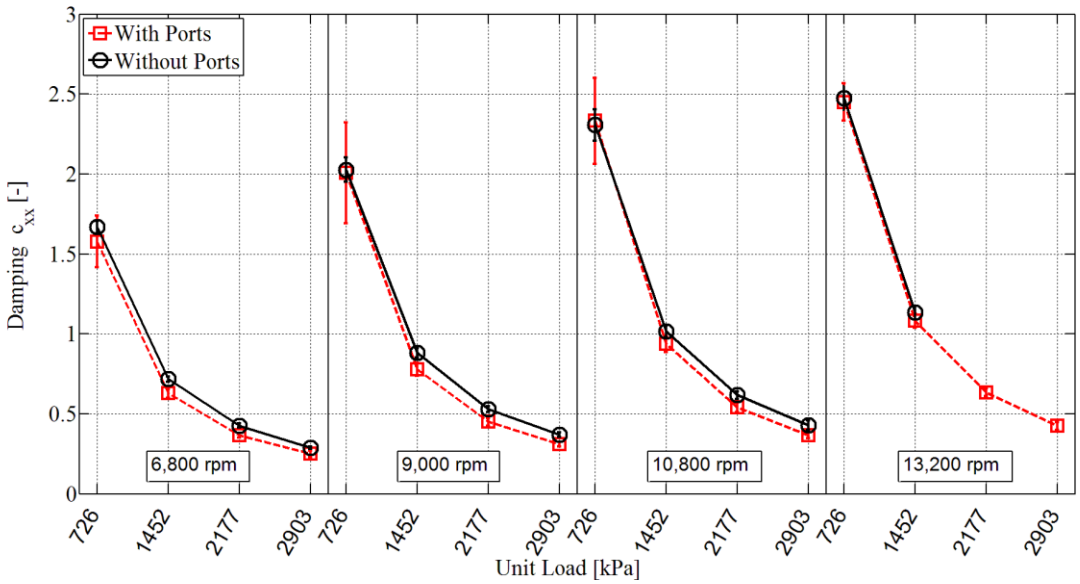

Figure 36. Direct damping coefficients c_{xx}

Direct damping decreased with the addition of jacking-oil ports in both the *x*-direction and *y*-direction. The load direction (*y*-direction) showed a larger decrease than the

orthogonal (x) direction. The change in the dimensionless direct damping coefficients c_{yy} ranged from -35% to -16%, with and average decrease of -25.5%. Dimensionless damping in the x-direction, c_{xx}, changed between +1% and -16%, with an average change of -9.2%. This decrease depended on unit load, with the largest changes occurring at the highest unit loads and smallest changes occurring at low loads.

Direct damping coefficients showed the same trends for both the original and modified bearing. Damping decreased with increasing shaft speed and load. Direct damping coefficients were very similar in magnitude for the original bearing, while the modified bearing had an average of 20% less damping in y-direction (c_{yy}) than the x-direction (c_{xx}).

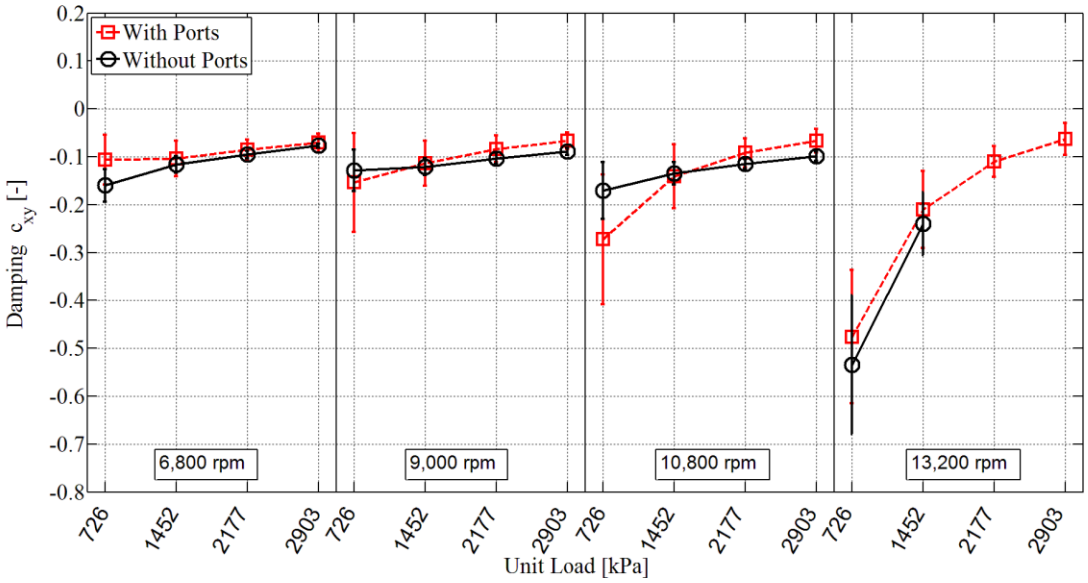

Figure 37. Cross-coupled damping coefficients c_{xy}

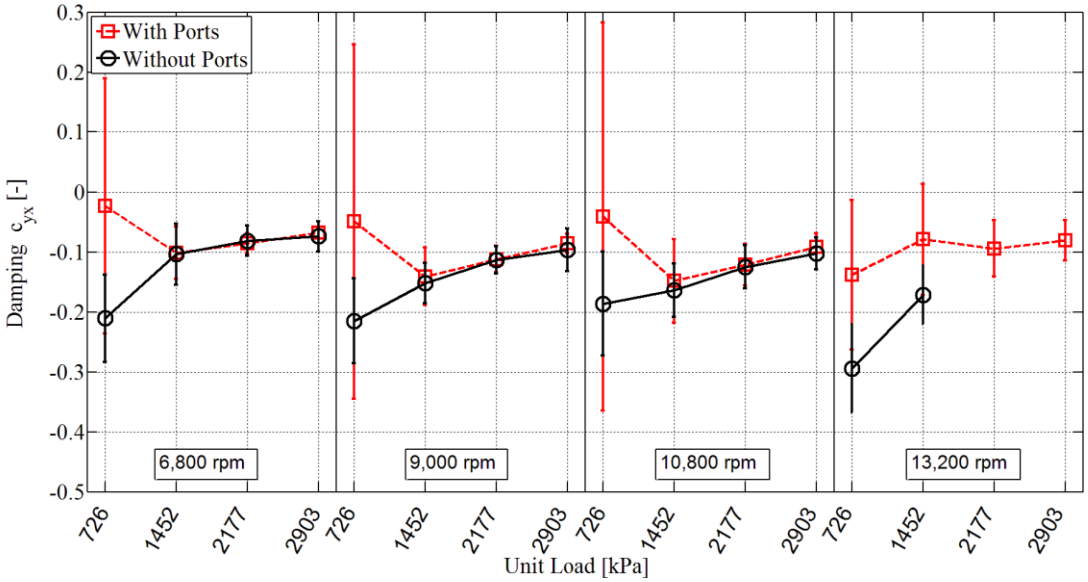

Figure 38. Cross-coupled damping coefficients c_{yx}

Adding jacking-oil ports caused no significant changes to the cross-coupled damping. All coefficients c_{xy} and c_{yx} are negative, providing dissipative damping, and small in magnitude compared to the direct damping.

Virtual-Mass Coefficients

Figure 39 and Figure 40 show the direct virtual-mass coefficients, m_{xx} and m_{yy}, in the *y*-direction and *x*-direction respectively. Figure 42 and Figure 43 show the cross-coupled virtual-mass, m_{xy} and m_{yx}. These dimensionless coefficients and their uncertainties, as well as the dimensional coefficients, are listed in Appendix E.

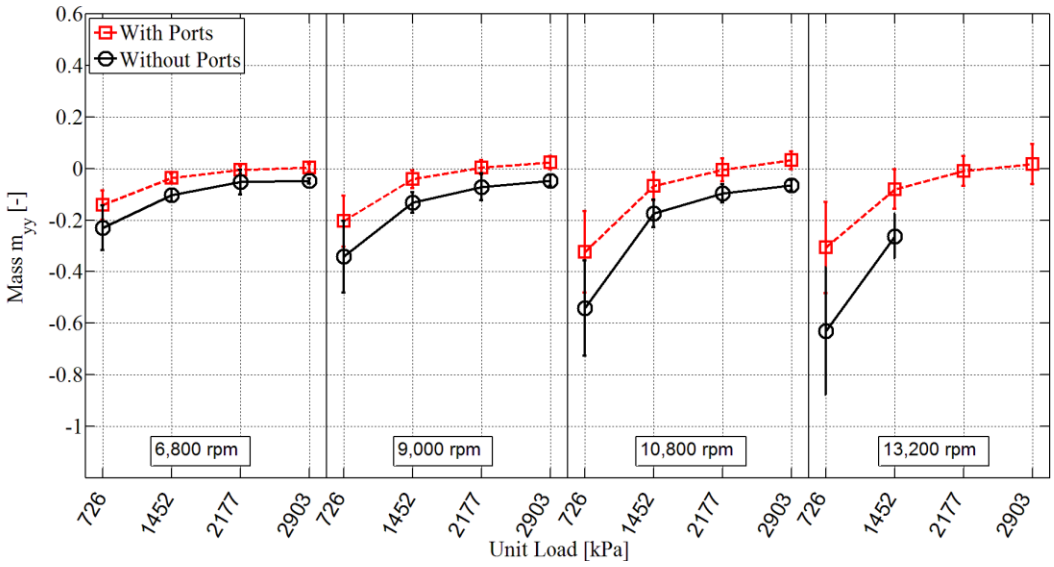

Figure 39. Direct virtual-mass coefficients m_{yy}

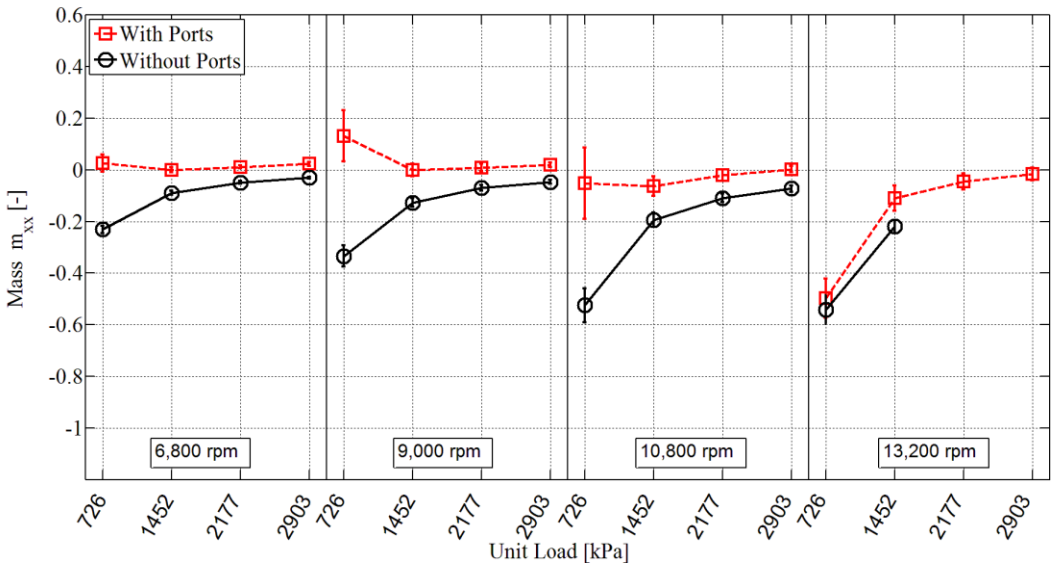

Figure 40. Direct virtual-Mass coefficients m_{xx}

The original bearing had negative direct virtual-mass coefficients. Adding jacking-oil ports caused an increase in m_{xx} and m_{yy} for all operating conditions (from negative towards

positive). The modified bearing had some positive virtual-mass terms, occurring mostly at high loads.

Recall that the virtual-mass coefficients were used to model the frequency-dependent dynamic-stiffness, Re($\boldsymbol{H}_{ij}$) = K_{ij} - $M_{ij}\Omega^2$. Positive coefficients describe a "softening" effect or reduced bearing stiffness at high excitation frequencies. Negative coefficients describe a "stiffening" of the bearing at high excitation frequencies. Figure 41 shows the dynamic-stiffness Re($\boldsymbol{H}_{ij}$) for both bearings at 6,800 rpm and 2.177 MPa (315.8 psi).

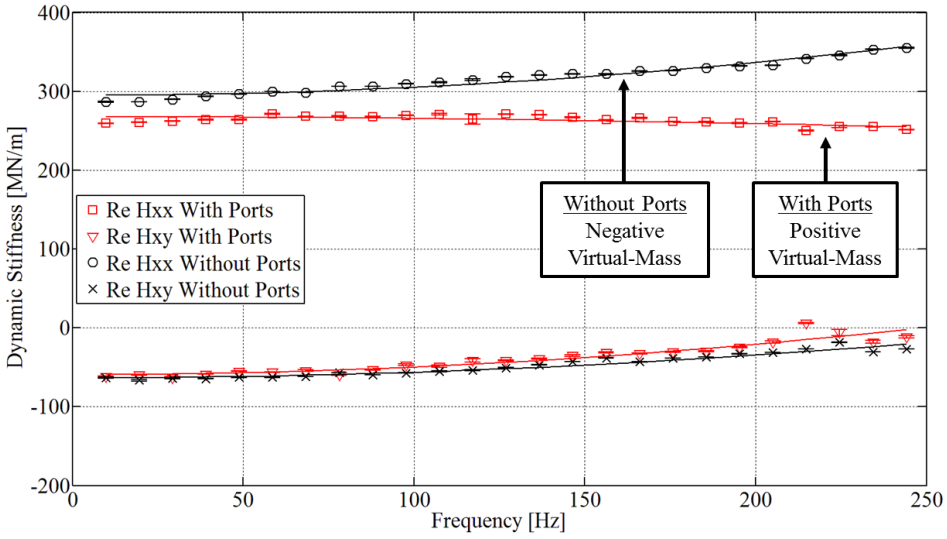

Figure 41. Re(H_{ij}) with and without ports at 6,800 rpm and 2.177 MPa (315.8 psi)

The addition of jacking-oil ports has the greatest effect on the bearing dynamic performance at high excitation frequencies. The dimensionless dynamic-stiffness Re($\boldsymbol{h}_{xx}$) at 244 Hz (14,640 rpm) is decreased by 18% by adding jacking-oil ports.

Figure 42 and Figure 43 show the cross-coupled virtual-mass, m_{xy} and m_{yx}.

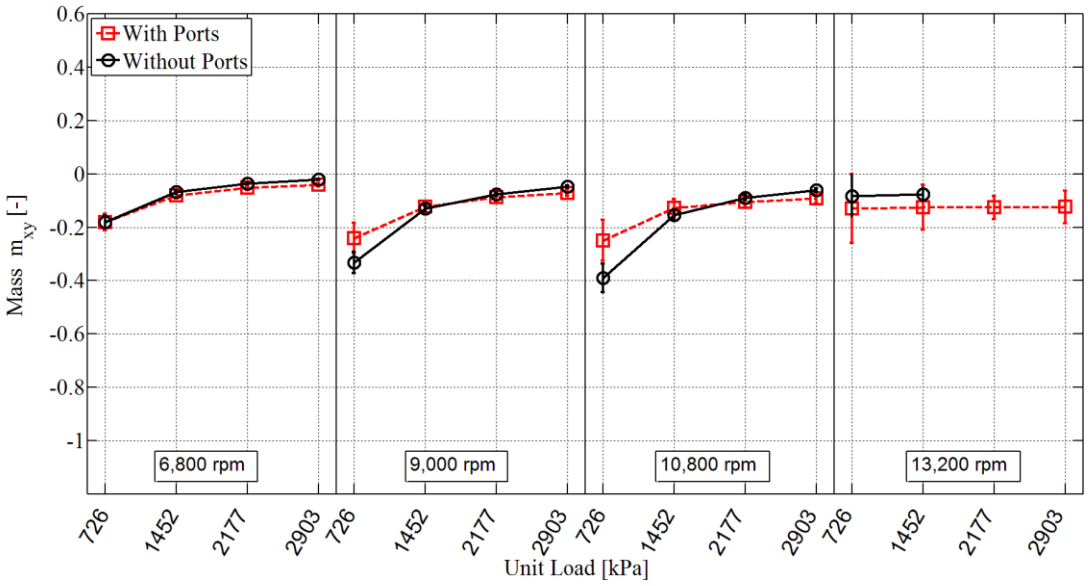

Figure 42. Cross-coupled virtual-mass coefficients m_{xy}

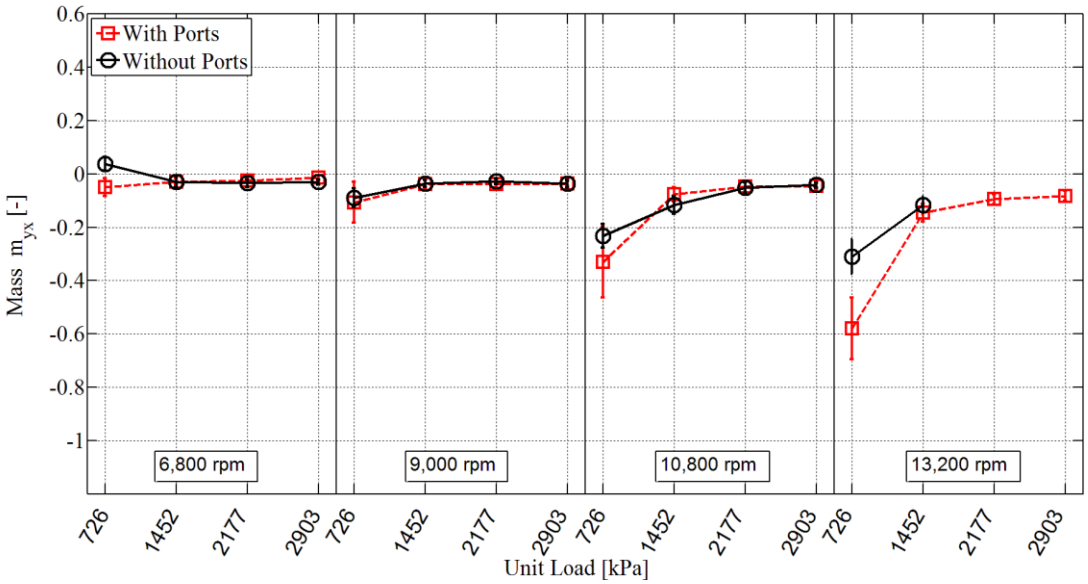

Figure 43. Cross-coupled virtual-mass coefficients m_{yx}

For both bearings (original and modified), the cross coupled virtual-mass coefficients are of equal magnitude and both negative, indicating that m_{xy} and m_{yx} are not destabilizing. The coefficients m_{xy} and m_{yx} were largely unaffected by the addition of jacking-oil ports.

Closure

This section compared the measured dynamic results for the bearing with and without jacking-oil ports. The [*K*][*C*][*M*] model was found sufficient to model both bearings. Data was presented as dimensionless dynamic coefficients (k_{ij}, c_{ij}, and m_{ij}) to account for the difference in bearing clearance.

The largest effect of adding jacking-oil ports to this TPJ bearing was on the direct damping and direct virtual-mass. Damping in the load direction (*y*-direction) showed a larger decrease than in the orthogonal (*x*) direction. Direct damping coefficients were reduced by an average of -25.5% in the load direction, c_{yy}, and as much an average of -9.2% in the orthogonal direction c_{xx}. Direct virtual-mass coefficient m_{xx} and m_{yy} of the original bearing were all negative. The bearing with jacking-oil ports showed an increase in m_{xx} and $m_{yy.}$ For many operating conditions, these coefficients were near zero, and some operating conditions had positive virtual-mass. Accounting for jacking-oil ports is of increased importance at increased excitation frequencies.

One concern that arise when adding large jacking-oil ports is the effects of fluid compressibility. Compressibility has been shown to significantly impact the dynamic coefficients of multi-recess hybrid journal bearings [27]. Ghosh showed that fluid compressibility causes a decrease in the direct damping coefficients for increasing excitation frequency. The test results show that direct damping decreased with the addition of the jacking-oil ports. However, damping does not become frequency dependent within the test range of 10 to 250 Hz. For this TPJ bearing, these frequency dependent fluid compressibility effects were not observed.

BEARING PREDICTIONS

This study began in part because there were no available bearing codes to predict the static and dynamic performance of a TPJ bearing with jacking-oil ports. In parallel with the presented experimental study, a predictive code was modified to include the port geometry and a turbulent flow model. Ultimately, this code was unable to predict the change in damping and virtual-mass as observed in measurements. This section provides a brief summary of the work done to improve this code, the lubricant and bearing properties used, and select predictions from the modified TPJ bearing code.

Bearing Code

The *XLTRC*^{2} suite contains the TPJ bearing code, *XLTPJB*, created by Tao and San Andrés [28]. This code predicts both static and dynamic performance of TPJ bearings. It is based on the laminar flow Reynolds equations and uses a Newton-Raphson method to iteratively solve for the journal static equilibrium position, which involves solving for the displacement and tilt angle of each pad. The code incorporates fluid flow thermal transport effects which are solved simultaneously to determine the fluid-film temperature and viscosity distribution across the pad surfaces. Temperature is assumed constant across the film thickness, and the fluid is assumed to be incompressible. Fluid inertia, pad mass, pad inertia, and pivot stiffness are also accounted for. Dynamic-stiffness values are predicted by considering small perturbations in the hydrodynamic pressure field [28].

The *XLTPJB* code was modified by Yingkun Li and San Andrés to include a jacking-oil port in the two loaded pads. This code includes four new input parameters that define the port geometry; start angle, extent angle, depth, and length as shown in Figure 44.

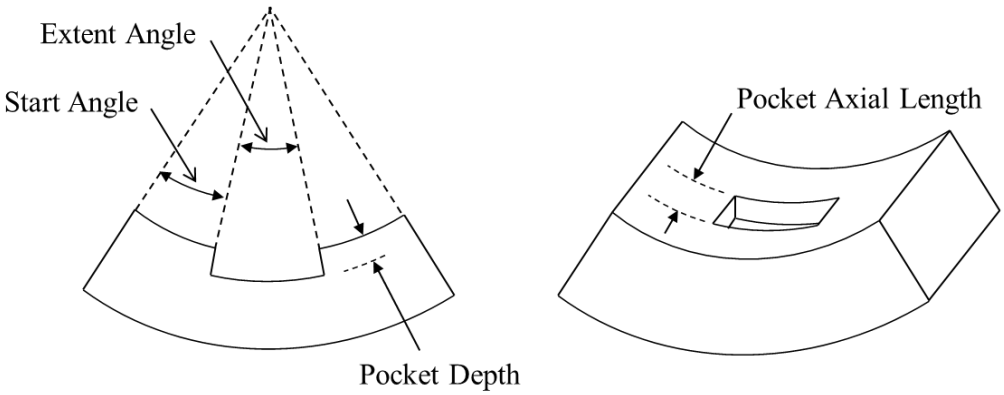

Figure 44. Jacking-oil port geometry in *XLTPJB*

The first and second pad include jacking-oil ports of equal geometry and location relative to the pad leading edge. Pressurized flow into the ports was not added to the bearing code. Only hydrodynamic pressure is considered because this study is concerned with inactive jacking-oil ports. The *XLTPJB* code uses finite-elements to model the fluid film. A symmetric boundary condition is assumed at the bearing's axial mid-plane such that only half of each pad is modeled. The fluid-film above each half pad is divided into 36 elements radially and 9 elements axially. The fluid-film thickness is not divided into separate elements, including the elements that define the jacking-oil ports. The Reynolds number is evaluated to determine the appropriate fluid model for each fluid element.

Input Parameters

Some *XLTPJB* inputs must be measured separately or estimated. This section offers a brief discussion of oil properties, bearing clearance, pivot stiffness, and pad flexibility. Simple parameters such as the bearing's geometry and shaft speed are presented in Appendix A, and will not be discussed.

The original bearing was tested with ISO VG 32, and the modified bearing was tested with ISO VG 46 oil. The ISO VG 46 oil inlet temperature was increased to 43.3°C (110°F) such that both oils had the same viscosity. A value of 23.24 cP was used for all predictions.

The slight variations in oil density, specific heat, thermal conductivity, and temperature reference coefficient were accounted for in the code input.

The operational clearance should be used as an input for *XLTPJB*. Use of either the cold clearance or nominal clearance does not accurately model the experimental study. The measured hot clearance cannot be directly entered into *XLTPJB*. Instead, the pad clearance and preload must be estimated from measured hot clearance. For predictions in this thesis, the pad clearance (C_p) was held constant at the nominal value of 118 μm. A "measured preload" is calculated using the preload equation, nominal C_p value, and measured hot clearance C_b.

Properly accounting for pivot stiffness can have a significant impact on predictions [29],[30]. The elastic support structure (pivot) acts as a spring in series with the fluid-film reducing both the equivalent stiffness and damping [31]. Tschoepe measured pivot stiffness by applying a static load to stator-housing and measuring the deflection as outlined by Harris [12]. Adding jacking-oil ports does not change the pivot stiffness. By definition, the pivot stiffness arises from the the Hertzian contact between back surface of the pad and the bearing housing. Tschoepe's measured values were used for all predictions. Appendix A contains a complete list of the oil properties, measured preload values, and the pivot stiffness function used.

Results

A series of predictions were made which only account for the added jacking-oil ports and not the change in bearing clearance. The jacking-oil pocket start and extent angle were rounded to a multiple of 2 degrees and the full pocket depth of 2.11 mm (0.083 in.) was used. The input parameters for the jacking-oil ports are listed in Appendix A.

Contrary to measured values, *XLTPJB* predicts strongly frequency-dependent dynamic-stiffness when jacking-oil ports are added. The [*K*][*C*][*M*] model is no longer sufficient to model these predictions. Figure 45 and Figure 46 show the predicted direct

dynamic-stiffness Re($\boldsymbol{H}_{ii}$) and Im($\boldsymbol{H}_{ii}$), respectively, for the bearing with and without jacking-oil ports at 6,800 rpm and 2.177 MPa (315.8 psi).

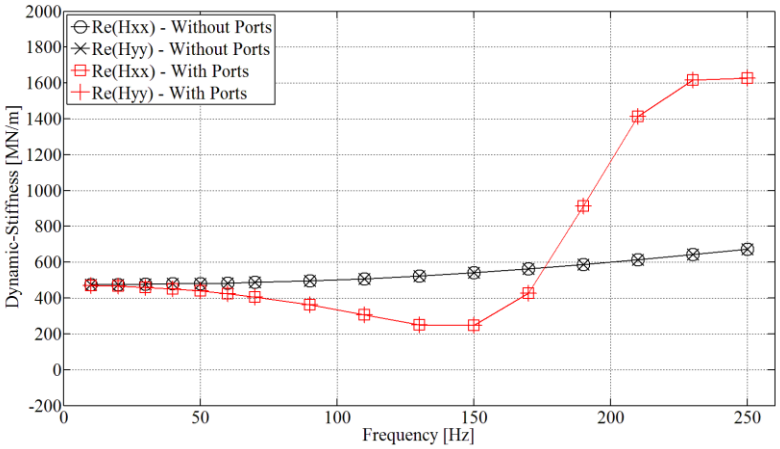

Figure 45. Real part of dynamic-stiffness predicitons with and without jacking-oil ports at 6,800 rpm and 2.177 Mpa (315.8 psi)

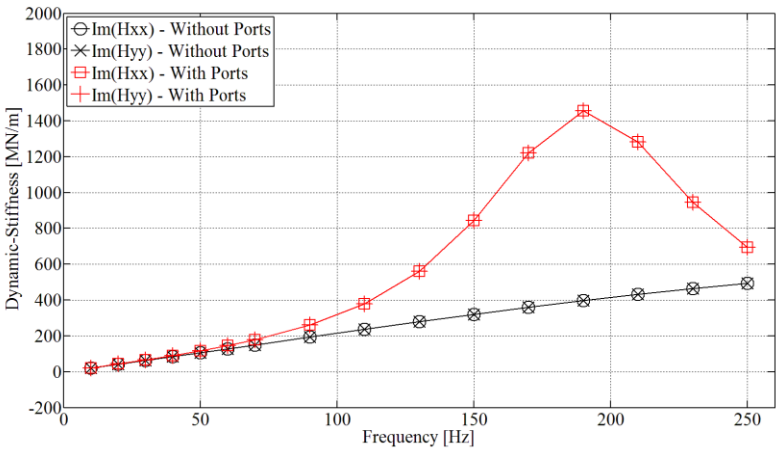

Figure 46. Imaginary part of dynamic-stiffness predicitons with and without jacking-oil ports at 6,800 rpm and 2.177 Mpa (315.8 psi)

The modified *XLTPJB* code predicts a large frequency dependence in both the real and imaginary part of the dynamic-stiffness. This behavior is seen at each shaft speed and unit load, and is a result of fluid inertia effects. The bearing code has the option to either include or neglect the effects of temporal fluid inertia. When excluded, the predicted dynamic-stiffness for the bearing with and without jacking-oil ports are nearly identical.

In 2010, Delgado and Andrés [32] found that predictions for a grooved seal could be improved by using an "effective depth" to model the groove rather than the full depth. A CFD study showed that recirculation occurs within the deep grooves creating two separate flow regions. Delgado and Andrés showed "good correlation with experimental data for groove effective depths smaller or equal to 50% of the actual groove depth" [32]. Their study does not directly correlate to the present work, as it dealt with pressurized flow and large radial grooves. However, a parametric study was completed to determine if changing the port depth could improve predications for a TPJ bearing with jacking-oil ports. Figure 47 and Figure 48 show dynamic-stiffness predictions with varying port depth (with fluid inertial included in the model).

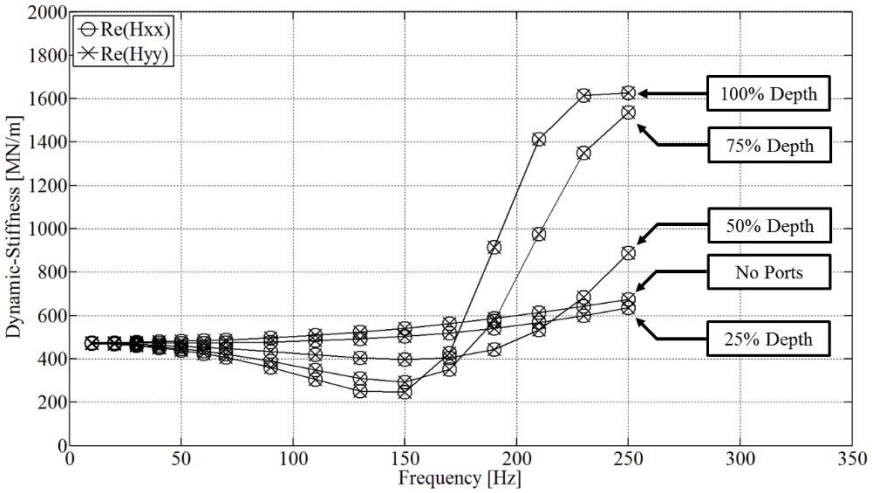

Figure 47. Re(H_{xx}) and Re(H_{yy}) with varying port depth at 6,800 rpm and 2.177 Mpa

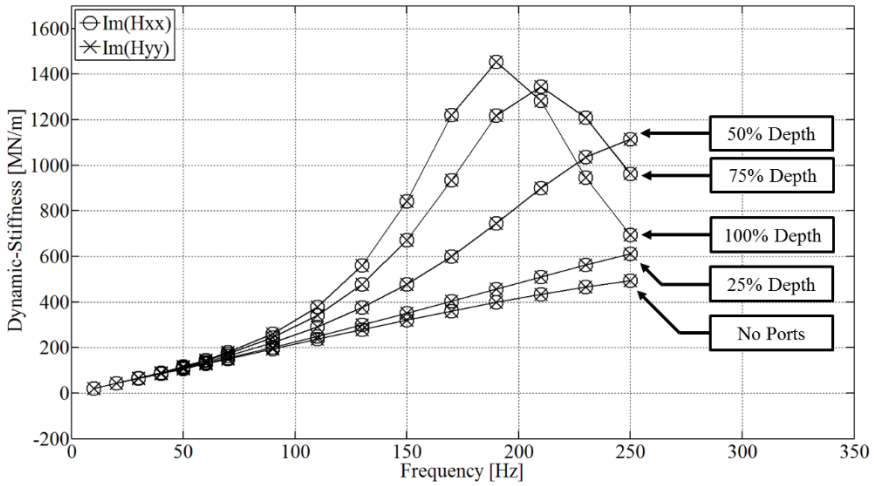

Figure 48. Im(H_{xx}) and Im(H_{yy}) with varying port depth at 6,800 rpm and 2.177 Mpa

Reducing the port depth shifts the frequency behavior to higher excitation frequencies and reduces the peak value of dynamic-stiffness. When the bearing is modeled with 25% of the actual port depth, the frequency dependent behavior is located mostly outside the test range. Dynamic-stiffness predictions converge to the "no ports" predictions as the port depth is reduced further.

Once again, this series of *XLTPJB* prediction only accounted for the added jacking-oil ports and ignores the change in clearance between the two tests. For this case, there were no significant changes in the predicted eccentricity ratio, attitude angle, and pad temperature distribution with the addition of jacking-oil ports. This is consistent with measured results. Any measured change in the static characteristics could be attributed to the difference in bearing clearance.

Overall, the modified *XLTPJB* code predictions and the measured trends in dynamic-stiffness values did not correspond well. The large frequency dependence was not observed in the measured data within the test range. Using an effective port depth only reduced the peak value and shifted the frequency-dependent behavior to higher

frequencies. Regardless of port depth, the code did not predict the observed reduction in direct damping and increase in virtual-mass.

ROTORDYNAMIC MODEL STUDY

The work of this thesis was initiated by a turbomachinery OEM to determine if adding jacking-oil ports to a TPJ bearing could affect the natural frequency and log decrement of their rotor-bearing system. To directly answer this question, this section presents an eigenvalue analysis for the simple system shown in Figure 49.

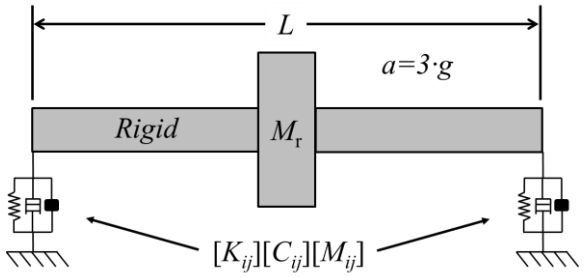

Figure 49. Model of rigid rotor supported by TPJ bearings

This system contains a rigid rotor with added mass M_r supported by two identical bearings. The system is modelled in *XLTRC*^{2} using the measured dynamic coefficients from the original and modified bearings tests. The total rotor mass and gravity constant were selected such that each bearing has a unit load of 0.725 MPa (105.3 psi), and the first damped natural frequency falls within the test range of 6,800 to 13,200 rpm. Stiffness, damping, and virtual-mass coefficients of the modified bearing were multiplied by the ratio of measured bearing clearance to account for the change in clearance.

$$\begin{Bmatrix} \tilde{K}_{ij} \\ \tilde{C}_{ij} \\ \tilde{M}_{ij} \end{Bmatrix}_{(Normalized)} = \left[\frac{C_{b,(Modified\ Bearing)}}{C_{b,(Original\ Bearing)}} \right] \begin{Bmatrix} K_{ij} \\ C_{ij} \\ M_{ij} \end{Bmatrix}_{(Modified\ Bearing)} \tag{37}$$

Figure 50 shows the calculated damped natural frequency and damping ratio for the simple rotor-bearing system supported by bearings with or without jacking-oil ports.

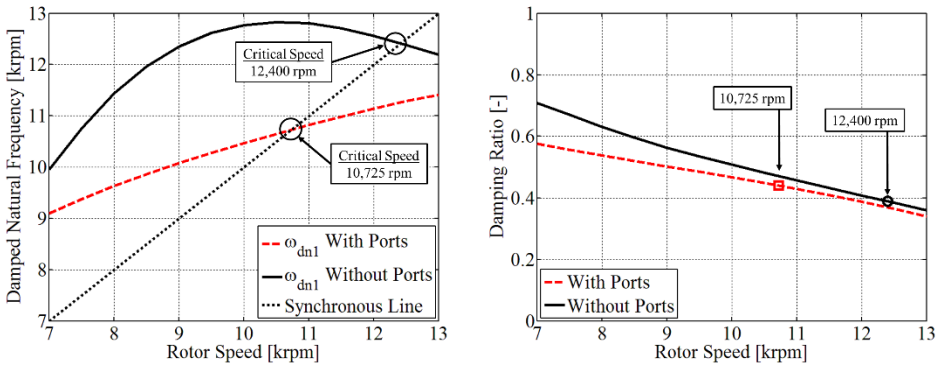

(a) **(b)**

Figure 50. Rotor-bearing system predictions with and without jacking-oil ports (a) damped natural frequency (b) damping ratio

When supported by the original bearing, the first critical speed occurs at ~12,400 rpm. Adding jacking-oil ports to the bearing is predicted to reduce the critical speed to ~10,725 rpm. At these critical speed locations, the damping ratio is predicted to change from 0.440 to 0.388 when adding jacking-oil ports.

To understand the change in natural frequency, predictions were made in which the stiffness, damping, and virtual-mass were changed individually. For example, one case used the damping and virtual-mass coefficients measured for the original bearing, but used the stiffness coefficients from the modified bearing. This case is referred to as "K only." Figure 51 compares these three cases with the predictions previously shown in Figure 50.

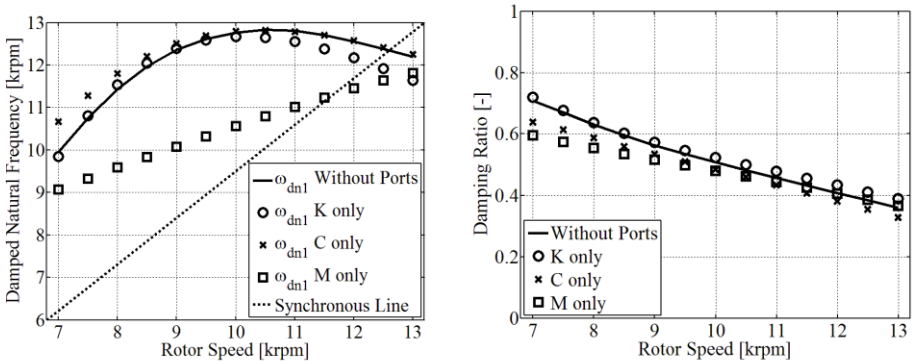

(a) **(b)**

Figure 51. Rotor-bearing system predictions changing individual dynamic coefficients (a) damped natural frequency (b) damping ratio

The measured change in virtual-mass coefficients had the largest effect on the damped natural frequency and damping ratio as shown by the "M only" case in Figure 51. This can explained by considering the undamped natural frequency, approximated by

$$\omega_{n1}(\Omega) = \sqrt{\frac{K_{\mathrm{b}}}{M_{\mathrm{r}}}} \approx \sqrt{\frac{K - M\Omega^2}{M_{\mathrm{r}}}} \tag{38}$$

The total bearing stiffness K_{b} changes with Ω^2. This simple approximation demonstrates that the smaller magnitude negative (and some positive) virtual-mass coefficient of the modified bearing decrease the natural frequency at high excitation frequencies. Ultimately, the change in dynamic characteristics caused by adding jacking-oil ports becomes increasingly important at high excitation frequencies.

SUMMARY, DISCUSSION, AND CONCLUSION

The static and dynamic characteristics of a TPJ bearing were measured before and after modifying the bearing to include jacking-oil ports. The test bearing was a four-pad, rocker-pivot, 57% offset, TPJ bearing originally tested by Tschoepe in 2011. This bearing was modified to include jacking-oil ports in the two loaded pads, and retested using the same test rig and operating conditions. Results were compared with the data provided in Tschoepe's thesis.

The bearing modifications included machining recesses (ports) in the two loaded pads, adding an oil supply line to both pads, and adding check valves to prevent oil from exiting through the supply lines during testing. The ports reduced the surface area of the loaded pads by 5.2%, and had a depth of 25.5 times the nominal radial clearance. Additionally, the Babbitt layer on pad #1 was replaced during modification. Stainless-steel shims were placed behind two of the pads to obtain the bearing clearance measured by Tschoepe.

The modified bearing was tested at four shaft speeds (6.8, 9.0, 10.8, and 13.2 krpm) and four unit loads (0.725, 1.452, 2.177, 2.903 MPa). Each shaft speed had an associated oil flow rate (Table 3). The original bearing was tested with ISO VG 32 and a constant inlet temperature of 43.3°C (110°F). The modified bearing was tested with ISO VG 46 oil and an inlet oil temperature of 54.7°C (130.5°F), such that the oil viscosity is the same for both series of tests. Tests were completed to measure the static and dynamic characteristics separately for each desired test condition.

Static

Static measurements were taken after the test rig had reached steady-state operation near the desired nominal test condition. Presented data were averages of 20 data samples over a span of 40 seconds. These measurements include the relative journal position, oil pressures, pad and oil temperatures, as well as the four test conditions. The bearing clearance was measured both at room temperature and the operating temperature within 10 seconds of shutdown.

Comparing the bearing with and without jacking-oil ports, only small changes were observed in eccentricity and attitude angle. Both bearings had negative attitude angles but they were larger in magnitude for the bearing with jacking-oil ports. This change was partly attributed to the change in clearance geometry caused by the bearing modification. At high loads, the modified bearing showed a reduced minimum film thickness. A difference in the method for finding the zero load center created additional uncertainty when comparing the two bearings. Overall, adding jacking-oil ports did not cause a significant change in the journal's static position.

Measured pad temperatures were compared for select operating conditions. There was a change in temperature rise when comparing the bearing with and without jacking-oil. Pad #1 (as shown in Figure 22) consistently showed an increase in ΔT while pads #2 and #3 showed a decrease in ΔT. Pad #4 showed very minimal changes. The peak temperature rise was not greatly affected.

Dynamic

Dynamic measurements were made, after completing static measurements, by shaking the bearing in the *x* and *y*-directions separately and recording the acceleration, position, and input forces. The bearing was excited with a designed waveform that contained multiple sinusoidal waveforms of superimposed frequencies varying from 10 to 350 Hz. Measurements were averaged and converted to the frequency domain to determine the dynamic-stiffness coefficients. This data was curve fitted to estimate the dynamic coefficients using the $[K][C][M]$ model.

Comparing the bearing with and without jacking-oil ports, the only significant changes were a decrease in direct damping and an increase in direct virtual-mass. Damping in the load direction (*y*-direction) showed a larger decrease than in the orthogonal (*x*) direction. Direct damping in the load direction, c_{yy}, was reduced between -35% to -16% with an average of -25.5%. In the orthogonal direction, damping changed between +1% and -16%, with an average of -9.2%. This decrease depended on unit load, with the largest changes occurring at the highest unit loads and smallest changes occurring at low loads.

The original bearing had negative virtual-mass coefficients at all unit loads and shaft speeds. The modified bearing showed an increase in direct virtual-mass (smaller negative or slightly positive value). Many coefficients m_{xx} and m_{yy} were near zero indicating that the direct dynamic-stiffness Re($\boldsymbol{H}_{xx}$) and Re($\boldsymbol{H}_{yy}$) were constant across the excitation frequency range.

There were only small changes in the dimensionless direct stiffness coefficients ranging between -9.1% to +0.6% in the *y*-direction and from -4.8% to 11.1% in the *x*-direction. No significant changes were observed in any of the cross-coupled coefficients (k_{ij}, c_{ij}, and m_{ij}).

Bearing Predictions

In parallel with the experimental study, a bearing code was used that had been modified to include the jacking-oil port geometry. The work by Li included user-defined recesses in the two loaded pads, and the addition of a turbulent flow model. This code was unable to match the measured dynamic results. It predicted strongly frequency-dependent dynamic-stiffness coefficients that was attributed to fluid inertia effects. Predictions were improved by using an effective port depth but could not match the decrease in damping or increase in virtual-mass observed in measurements. Predicted static characteristics showed no change when adding jacking-oil ports which was constant with measured results.

Rotordynamic Study

XLTRC^2 predictions were made for a simple rotor-bearing system to study how adding jacking-oil ports could affect the natural frequency and damping. Measured dynamic coefficients for both TPJ bearing were used, and the added mass was selected to match the tested bearing unit load. A rigid rotor case was presented with the first critical speed of 12,400 rpm. Predictions with jacking-oil ports reduced the critical speed to 10,500 rpm. There was only a small predicted reduction in damping ratio. The decrease in natural frequency was attributed mainly to the increase in direct virtual-mass coefficients. The

change in dynamic characteristics caused by adding jacking-oil ports were shown to becomes increasingly important at high excitation frequencies.

REFERENCES

[1] Childs, D., "Turbomachinery Rotordynamics with Case Studies," Wellborn: Minter Spring Publishing, 2013, Print.

[2] Zeidan, F., and Herbage, B., 1991, "Fluid Film Bearing Fundamentals and Failure Analysis," *Proceedings of 20th Texas A&M Turbo Symposium*, pp. 161-186.

[3] Vance, J., Zeidan, F., and Murphy, B., "Machinery Vibration and Rotordynamics," Hoboken: John Wiley & Sons, Inc., 2010, Print.

[4] Lund, J., 1964, "Spring and Damping Coefficients for the Tilting-Pad Journal Bearing," *ASLE Transactions*, **7**, pp. 342-352.

[5] Nicholas, J., 2003, "Lund's Tilting Pad Journal Bearing Pad Assembly Method," *Transactions of ASME*, **125**, pp. 448-454.

[6] Parsell, J., Allaire, P., and Barrett, L., 1983, "Frequency Effects in Tilting-Pad Journal Bearing Dynamic Coefficients," *ALSE Transactions*, **26**, pp. 222-227.

[7] Barrett, L., Allaire, P., and Wilson, B., 1988, "The Eigenvalue Dependence of Reduced Tilting Pad Bearing Stiffness and Damping Coefficients," *ASLE Transactions*, 3**1**, pp. 411-419.

[8] White, M., and Chan, S., 1992, "The Subsynchronous Dynamic Behavior of Tilting-Pad Journal Bearings," *ASME Journal of Tribology*, **114**, pp. 167-172.

[9] Ha, H., and Yang, S., 1999, "Excitation Frequency Effects on the Stiffness and Damping Coefficients of a Five-Pad Tilting Pad Journal Bearing," *ASME Journal of Tribology*, **121**, pp. 517-522.

[10] Rodriguez, L., and Childs, D., 2006, "Frequency Dependency of Measured and Predicted Rotordynamic Coefficients for a Load-on-Pad Flexible-Pivot Tilting-Pad Bearing," *ASME Transactions*, **128**, pp. 388-395

[11] Childs, D., and Hale, K., 1994, "A Test Apparatus and Facility to Identify the Rotordynamic Coefficients of High-Speed Hydrostatic Bearings," *ASME Journal of Tribology*, **116**, pp. 337-344.

[12] Harris, J., and Childs, D., 2008, "Static Performance Characteristics and Rotordynamic Coefficients for a Four-Pad Ball-In-Socket Tilting Pad Journal Bearing," *Proceedings of ASME Turbo Expo 2008*, Paper GT2008-50063, June 9-13, Berlin, Germany.

[13] Delgado, A., Ertas, B., Drexel, M., and Vannini, G., 2010, "Identification and Prediction of Force Coefficients in a Five-Pad and Four-Pad Tilting Pad Bearing for Load-On-Pad and Load-Between-Pad Configurations," *Proceedings of ASME Turbo Expo 2012*, Glasgow, UK, Paper GT2010-23802.

[14] Hattenbach, T., and Sandberg, M., 2009, "Influence of Jacking Oil Supply Configuration on Shaft Vibration of a Super-Synchronous Motor," PowerPoint, *Proceedings of 38th Texas A&M Turbo Symposium*. Case Study 06.

[15] Hagemann, T., Sebastian, K., and Schwarze, H., 2013, "Measurement and Prediction of the Static Operating Conditions of a Large Turbine Tilting-Pad Bearing Under High Circumferential Speeds and Heavy Loads," *Proceedings of ASME Turbo Expo 2013*, GT2013-95004, June 3-7, 2013, San Antonio, Texas.

[16] Tschoepe, D., 2012, "Measurement Versus Predictions for the Static and Dynamic Characteristics of a Four-Pad, Rocker-Pivot, Tilting-Pad Journal Bearing," M.S. thesis, Mechanical Engineering, Texas A&M University, College Station, TX.

[17] Kaul, A., 1999, "Design and Development of a Test Setup for the Experimental Determination of the Rotordynamic and Leakage Characteristics of Annular Bushing Oil Seals," M.S. thesis, Mechanical Engineering, Texas A&M University, College Station, TX.

[18] Glienicke, J., 1967, "Experimental Investigation of the Stiffness and Damping Coefficients of Turbine Bearings and their Application to Instability Predictions," *Proceedings of the International Mech. E.*, **181** (3B), pp. 116-129.

[19] Kulhanek, C., 2010, "Dynamic and Static Characteristics of a Rocker-Pivot, Tilting-Pad Bearing with 50% and 60% Offsets," M.S. thesis, Mechanical Engineering, Texas A&M University, College Station, TX.

[20] Gaines, J., 2015, "Examining the Impact of Pad Flexibility on the Rotordynamic Coefficients of Rocker-Pivot-Pad Tilting-Pad Journal Bearings," M.S. thesis, Mechanical Engineering, Texas A&M University, College Station, TX.

[21] Tschoepe, D., 2014, "Measurements Versus Predictions for the Static and Dynamic Characteristics of a Four-Pad, Rocker-Pivot, Tilting-Pad Journal Bearing," *ASME Journal of Engineering for Gas and Turbine Power*, **136**, 052501.

[22] Wilkes, J., 2011, "Measured and Predicted Rotor-Pad Transfer Functions for a Rocker-Pivot Tilting-Pad Journal Bearing," Doctoral dissertation, Mechanical Engineering, Texas A&M University, College Station, TX.

[23] Rouvas, L., and Childs, D., 1993, "A Parameter Identification Method for the Rotordynamic Coefficients of a High Reynolds Number Hydrostatic Bearing," *ASME Transactions*, **115**, pp. 264-270

[24] Beckwith, T., Marangoni, R., and Leinhard, J., 1995, "*Mechanical Measurements: Fifth Edition*," Addison-Wesley Publishing Company Inc., Reading, Massachusetts, pp. 857-859.

[25] Wygant, K.D., 2001, "The Influence of Negative Preload and Non-Synchronous Excitations on the Performance of Tilting Pad Journal Bearings," PhD Thesis, University of Virginia, Charlottesville, Virginia.

[26] Coghlan, D., 2014, "Static, Rotordynamic, and Thermal Characteristics of a Four Pad Spherical-Seat Tilting Pad Journal Bearing with Four Methods of Directed Lubrication," M.S. thesis, Mechanical Engineering, Texas A&M University, College Station, TX.

[27] Gosh, M., Guha, S., and Majumdar, B., 1988, "Rotordynamic Coefficients of Multirecess Hybrid Journal Bearings Part 1," *Wear*, Vol. 129, pp. 245-259

[28] Tao, Y., 2012, "A Novel Computational Model for Tilting Pad Journal Bearings with Soft Pivot Stiffness," M.S. thesis, Mechanical Engineering, Texas A&M University, College Station, TX.

[29] Wilkes, J., and Childs, D., 2012, "Tilting Pad Journal Bearings – A Discusstion on Stability Calculation, Frequency Dependence, and Pad and Pivot Flexibitity," *Proceedings of ASME Turbo Expo 2012*, Paper GT2012, June 11-15, 2012, Copenhagen, Denmark.

[30] San Andrès, L., and Tao, Y., 2013, "The Role of Pivot Stiffness on the Dynamic Force Coefficients of Tilting Pad Journal Bearings," *Proceedings of the ASME Turbo Expo 2013,* Paper GT2013-94403, June 3-7, 2013, San Antonio, Texas.

[31] Kirk, R., and Reedy, S., 1988, "Evaluation of Pivot Stiffness for Typical Tilting-Pad Journal Bearing Designs," *ASME Journal of Vibrations, Acoustics, Stress, and Reliability in Design*, **110**, pp. 165-171.

[32] Delgado, A., and Andrés, L. S., "A Model for Improved Prediction of Force Cofficients in Grooved Squeeze Film Dampers and Oil Seal Rings," *ASME Journal of Tribology*, **132** (3), 032202.

APPENDIX A: XLTPJB PARAMETERS

Table A. 1. XLTPJB bearing geometry

Input Parameter	Units	Value
Rotor Diameter	[m]	0.1016
Bearing Axial Length	[m]	0.0603
Number of Pads	[-]	4
Pad Leading Edge	[degrees]	3.96

Table A. 2. XLTPJB fluid properties

Input Parameter	Units	Value
Ambient Pressure	[bar]	0.00
Supply Pressure	[bar]	1.17
Cavitation Pressure	[bar]	0.00
Supply Temperature	[degC]	43.3
Viscosity at Tsupply	[centi-Poise]	23.2
Density	[kg/m^3]	854.6
Specific Heat	[J/(kg·degC)]	1959.6
Thermal Conductivity	[Watt/(m degC)]	0.1310
Viscosity Temp Coef.	[1/degC]	0.02930

Table A. 3. XLTPJB pad geometry

Speed [RPM]	Hot Preload				Pivot Offset	Pad Arc Length [deg]	C_p [μm]
	Pad #1	Pad #2	Pad #3	Pad #4			
6,800	0.547	0.645	0.547	0.645	0.57	72	118
9,000	0.557	0.656	0.55	0.656			
10,800	0.558	0.677	0.558	0.677			
13,200	0.541	0.662	0.541	0.662			

Table A. 4. XLTPJB pad properties

Input Parameter	Units	Value
Pad Mass	[kg]	0.96
Moment of Inertia	[kg·m^2]	1.81 x 10^{-4}
Mass Center Location	[m]	0.0127
Pad Surface to Pivot	[m]	0.0254

Table A. 5. XLTPJB Jacking-oil pocket options

Input Parameter	Units	Value	
		Without Ports	With Ports
Pocket Start Angle	[deg]	0	34
Pocket Extent Angle	[deg]	0	12
Pocket Depth	[m]	0	2.11 x 10^{-3}
Pocket Axial Length	[m]	0	1.675 x 10^{-2}

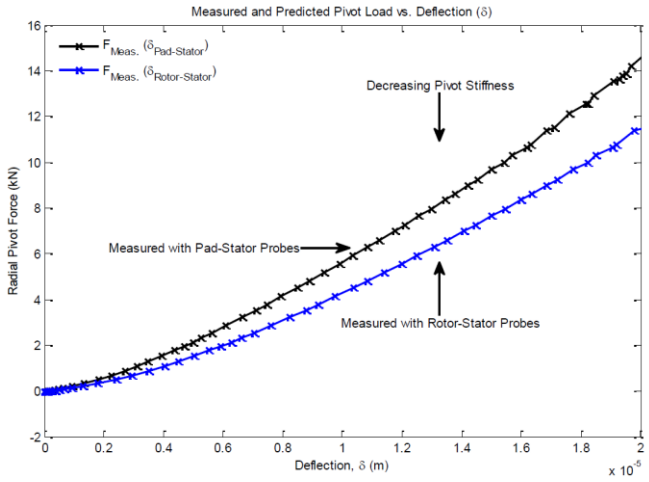

Figure A. 1. Load-deflection curve [21]

The measured pivot stiffness is included in *XLTPJB* by entering a user-defined load-deflection function. This equation defines the static force as a function of deflections (δ) with a fifth order polynomial.

$$f = 4.03 + \left(1.84 \times 10^{8}\right)\delta + \left(5.77 \times 10^{13}\right)\delta^{2} - \left(2.6 \times 10^{18}\right)\delta^{3} + \left(5.39 \times 10^{22}\right)\delta^{4} \qquad (39)$$

APPENDIX B: STATIC CONDITIONS

Table B. 1. Average static operating conditions (modified bearing)

Nominal Conditons				Measured Operating Conditions					
Inlet Temp [°C]	Speed [RPM]	Flow Rate [L/min]	Unit Load [kPa]	Inlet Temp [°C]	Speed [RPM]	Unit Load [kPa]	Flow Rate [L/min]	DE Outlet Temp [°C]	NDE Outlet Temp [°C]
54.72	6,800	22.7	725	54.54 ± 0.01	6,807.58 ± 2.53	731.61 ± 0.10	24.11 ± 0.00	59.05 ± 0.02	60.97 ± 0.04
			1,452	54.84 ± 0.01	6,825.39 ± 1.66	1,453.00 ± 0.22	23.16 ± 0.02	59.53 ± 0.01	61.71 ± 0.07
			2,178	54.90 ± 0.01	6,794.12 ± 3.00	2,183.00 ± 0.07	24.91 ± 0.18	59.47 ± 0.02	61.98 ± 0.05
			2,903	55.03 ± 0.01	6,818.41 ± 2.33	2,904.78 ± 0.05	23.02 ± 0.04	60.47 ± 0.01	63.03 ± 0.11
	9,000	26.5	725	54.65 ± 0.01	8,991.92 ± 2.72	728.84 ± 0.14	27.35 ± 0.18	61.63 ± 0.03	63.79 ± 0.05
			1,452	54.94 ± 0.01	8,983.38 ± 0.41	1,456.69 ± 0.05	26.84 ± 0.07	62.19 ± 0.02	64.03 ± 0.05
			2,178	55.00 ± 0.01	9,021.65 ± 4.29	2,183.12 ± 0.05	26.44 ± 0.08	62.60 ± 0.04	64.71 ± 0.04
			2,903	55.03 ± 0.01	8,982.53 ± 2.36	2,900.11 ± 0.08	26.84 ± 0.05	62.92 ± 0.01	65.24 ± 0.02
	10,800	30.3	725	54.73 ± 0.02	10,836.07 ± 0.58	724.28 ± 0.04	30.56 ± 0.02	63.69 ± 0.01	66.57 ± 0.03
			1,452	54.56 ± 0.02	10,825.19 ± 0.55	1,456.01 ± 0.05	30.64 ± 0.04	63.41 ± 0.01	66.58 ± 0.04
			2,178	54.60 ± 0.02	10,775.80 ± 1.75	2,181.97 ± 0.09	30.62 ± 0.04	63.49 ± 0.01	66.54 ± 0.04
			2,903	55.06 ± 0.02	10,821.62 ± 1.70	2,899.76 ± 0.03	30.70 ± 0.03	64.22 ± 0.02	66.68 ± 0.05
	13,200	34.1	725	54.59 ± 0.01	13,228.13 ± 2.15	727.89 ± 0.12	34.61 ± 0.04	64.99 ± 0.04	69.36 ± 0.05
			1,452	54.91 ± 0.00	13,211.38 ± 1.26	1,450.22 ± 0.05	34.41 ± 0.03	65.50 ± 0.03	69.13 ± 0.01
			2,178	54.63 ± 0.02	13,198.79 ± 5.21	2,177.91 ± 0.05	34.47 ± 0.10	65.70 ± 0.04	69.21 ± 0.03
			2,903	54.64 ± 0.02	13,186.51 ± 4.23	2,910.67 ± 0.05	34.31 ± 0.02	65.98 ± 0.02	69.63 ± 0.02

APPENDIX C: STATIC DATA

Table C. 1. Static location and eccentricity (original bearing)

Speed [RPM]	Radial Clearence [μm]	Load [lb]	X-NDE [μm]	Y-NDE [μm]	X-DE [μm]	Y-DE [μm]	X-AVG [μm]	Y-AVG*(-1) [μm]	ε_X - [μm]	ε_Y - [μm]	ε [-]	γ [deg]
6800	48.66	0	12.78	12.38	20.16	15.20	16.47	-13.79	0	0	0	-
		1000	9.46	34.85	16.54	34.47	13.00	-34.66	-0.07	-0.43	0.43	-9.45
		2000	9.26	46.11	16.25	46.70	12.76	-46.40	-0.08	-0.67	0.67	-6.50
		3000	10.47	54.76	16.67	56.16	13.57	-55.46	-0.06	-0.86	0.86	-3.99
		4000	12.84	62.13	18.01	63.88	15.42	-63.01	-0.02	-1.01	1.01	-1.22
9000	47.53	0	11.17	13.45	17.03	14.67	14.10	-14.06	0	0	0	-
		1000	8.98	30.21	15.47	28.97	12.23	-29.59	-0.04	-0.33	0.33	-6.87
		2000	9.60	40.74	15.53	39.97	12.56	-40.35	-0.03	-0.55	0.55	-3.34
		3000	10.30	47.94	16.10	48.02	13.20	-47.98	-0.02	-0.71	0.71	-1.52
		4000	11.95	53.81	17.53	53.76	14.74	-53.78	0.01	-0.84	0.84	0.92
10800	46.67	0	11.75	14.39	14.18	13.41	12.96	-13.90	0	0	0	-
		1000	9.14	27.80	14.47	24.78	11.81	-26.29	-0.02	-0.27	0.27	-5.33
		2000	8.85	36.48	13.99	34.42	11.42	-35.45	-0.03	-0.46	0.46	-4.09
		3000	9.47	42.82	14.50	41.68	11.98	-42.25	-0.02	-0.61	0.61	-1.98
		4000	10.82	48.60	15.47	48.10	13.14	-48.35	0.00	-0.74	0.74	0.30
13200	48.56	0	9.73	16.01	15.48	9.88	12.60	-12.94	0	0	0	-
		1000	8.84	28.01	16.28	19.93	12.56	-23.97	0.00	-0.23	0.23	-0.22
		2000	8.66	37.49	16.63	27.86	12.64	-32.68	0.00	-0.41	0.41	0.12

Table C. 2. Static location and eccentricity (modified bearing)

Speed [RPM]	Radial Clearence [μm]	Load [lb]	X-NDE [μm]	Y-NDE [μm]	X-DE [μm]	Y-DE [μm]	X-AVG [μm]	Y-AVG*(-1) [μm]	ε_X - [μm]	ε_Y - [μm]	ε [-]	γ [deg]
6800	56.38	0 (HC)	-	-	-	-	-46.93	30.85	0	0	0	-
		1000	-57.21	-8.91	-42.03	-3.58	-49.62	6.24	-0.05	-0.44	0.44	-6.23
		2000	-62.18	7.72	-43.28	10.80	-52.73	-9.26	-0.10	-0.71	0.72	-8.22
		3000	-61.68	20.83	-42.42	21.32	-52.05	-21.07	-0.09	-0.92	0.93	-5.63
		4000	-61.15	30.56	-41.26	29.22	-51.20	-29.89	-0.08	-1.08	1.08	-4.02
9000	54.91	0 (HC)	-	-	-	-	-50.17	31.64	0	0	0	-
		1000	-63.08	-14.65	-44.00	-10.37	-53.54	12.51	-0.06	-0.35	0.35	-9.97
		2000	-64.16	1.15	-44.08	2.31	-54.12	-1.73	-0.07	-0.61	0.61	-6.75
		3000	-64.35	13.04	-42.72	11.59	-53.53	-12.31	-0.06	-0.80	0.80	-4.37
		4000	-63.59	21.80	-40.98	19.55	-52.28	-20.68	-0.04	-0.95	0.95	-2.31
10800	54.63	0 (HC)	-	-	-	-	-49.36	31.81	0	0	0	-
		1000	-63.44	-19.72	-43.28	-13.83	-53.36	16.77	-0.07	-0.28	0.28	-14.92
		2000	-62.71	-4.39	-42.45	-1.91	-52.58	3.15	-0.06	-0.52	0.53	-6.42
		3000	-61.89	6.96	-41.22	7.06	-51.55	-7.01	-0.04	-0.71	0.71	-3.23
		4000	-60.97	15.16	-40.16	13.70	-50.56	-14.43	-0.02	-0.85	0.85	-1.49
13200	52.16	0 (HC)	-	-	-	-	-53.25	31.61	0	0	0	-
		1000	-66.90	-22.61	-40.07	-15.73	-53.48	19.17	0.00	-0.24	0.24	-1.07
		2000	-68.73	-10.49	-40.49	-5.62	-54.61	8.05	-0.03	-0.45	0.45	-3.31
		3000	-68.48	-1.16	-39.50	4.08	-53.99	-1.46	-0.01	-0.63	0.63	-1.28
		4000	-68.38	5.64	-37.93	10.82	-53.15	-8.23	0.00	-0.76	0.76	0.14

APPENDIX D: DYNAMIC CONDITIONS

Table D. 1. Dynamic operating conditions (original bearing)

Nominal Conditons				Measured Operating Conditions				
Inlet Temp [°C]	Speed [RPM]	Flow Rate [L/min]	Unit Load [kPa]	Speed [RPM]	Unit Load [kPa]	Flow Rate [L/min]	DE Outlet Temp [°C]	NDE Outlet Temp [°C]
43.3	6,800	22.7	725	6,816.45 ± 23.54	753.74 ± 3.16	23.44 ± 0.52	50.72 ± 0.14	46.44 ± 0.48
			1,452	6,979.62 ± 2.46	1459.06 ± 9.40	23.79 ± 0.09	51.71 ± 0.05	46.85 ± 0.36
			2,178	6,870.49 ± 60.69	2197.30 ± 5.34	23.80 ± 0.42	52.64 ± 0.17	47.14 ± 0.22
			2,903	6,929.07 ± 4.21	2921.56 ± 6.51	24.01 ± 0.04	53.24 ± 0.11	47.27 ± 0.24
	9,000	26.5	725	9,059.19 ± 3.10	734.62 ± 4.57	26.84 ± 0.03	56.16 ± 0.17	47.93 ± 0.11
			1,452	9,045.24 ± 43.67	1477.96 ± 7.26	26.86 ± 0.03	57.10 ± 0.11	47.80 ± 0.16
			2,178	9,014.63 ± 5.29	2200.89 ± 7.22	26.86 ± 0.01	57.73 ± 0.12	47.77 ± 0.04
			2,903	9,046.63 ± 6.50	2919.47 ± 4.51	26.84 ± 0.01	59.13 ± 0.17	48.23 ± 0.08
	10,800	30.3	725	10,882.69 ± 9.24	749.51 ± 3.56	30.02 ± 0.02	59.65 ± 0.05	49.93 ± 0.07
			1,452	10,848.45 ± 2.44	1462.54 ± 1.07	30.07 ± 0.02	60.10 ± 0.12	49.84 ± 0.04
			2,178	10,908.42 ± 18.53	2187.96 ± 8.42	30.07 ± 0.02	60.49 ± 0.10	50.02 ± 0.08
			2,903	10,745.23 ± 107.69	2976.70 ± 129.51	30.14 ± 0.02	60.95 ± 0.13	49.95 ± 0.20
	13,200	34.1	725	13,230.00 ± 21.61	741.34 ± 6.87	33.99 ± 0.02	62.27 ± 0.05	54.40 ± 0.50
			1,452	13,240.94 ± 33.69	1451.76 ± 1.82	33.97 ± 0.01	62.69 ± 0.11	54.28 ± 0.15

Table D. 2. Dynamic operating conditions (modified bearing)

Nominal Conditons				Measured Operating Conditions					
Inlet Temp [°C]	Speed [RPM]	Flow Rate [L/min]	Unit Load [kPa]	Inlet Temp [°C]	Speed [RPM]	Unit Load [kPa]	Flow Rate [L/min]	DE Outlet Temp [°C]	NDE Outlet Temp [°C]
54.72	6,800	22.7	725	54.73 ± 0.10	6,836.29 ± 8.52	731.22 ± 0.06	23.03 ± 0.21	59.45 ± 0.14	61.21 ± 0.19
			1,452	54.81 ± 0.04	6,798.91 ± 2.80	1,458.50 ± 0.71	22.80 ± 0.21	59.54 ± 0.09	61.61 ± 0.06
			2,178	54.97 ± 0.09	6,802.23 ± 14.23	2,182.08 ± 0.35	23.82 ± 0.73	59.75 ± 0.13	62.37 ± 0.05
			2,903	54.53 ± 0.02	6,758.76 ± 31.95	2,914.49 ± 2.28	23.25 ± 0.21	59.89 ± 0.01	62.65 ± 0.10
	9,000	26.5	725	54.45 ± 0.02	8,964.21 ± 4.46	718.38 ± 0.49	27.57 ± 0.18	61.35 ± 0.11	63.52 ± 0.17
			1,452	54.81 ± 0.00	8,986.59 ± 9.65	1,456.38 ± 0.10	27.69 ± 0.22	62.03 ± 0.05	63.71 ± 0.09
			2,178	55.03 ± 0.08	8,968.78 ± 15.58	2,182.34 ± 0.22	26.62 ± 0.08	62.43 ± 0.11	64.73 ± 0.16
			2,903	54.49 ± 0.01	9,034.84 ± 26.02	2,906.71 ± 1.78	27.45 ± 0.34	62.34 ± 0.03	64.91 ± 0.08
	10,800	30.3	725	54.53 ± 0.03	10,818.03 ± 31.51	719.93 ± 4.20	30.65 ± 0.04	63.49 ± 0.06	66.39 ± 0.03
			1,452	54.81 ± 0.14	10,842.95 ± 5.57	1,455.70 ± 0.13	30.71 ± 0.01	63.64 ± 0.10	66.85 ± 0.25
			2,178	54.77 ± 0.15	10,848.47 ± 63.69	2,180.66 ± 0.31	30.58 ± 0.04	63.75 ± 0.23	66.74 ± 0.22
			2,903	54.60 ± 0.11	10,793.11 ± 1.82	2,908.91 ± 0.11	30.76 ± 0.03	63.83 ± 0.07	66.45 ± 0.06
	13,200	34.1	725	54.98 ± 0.08	13,200.21 ± 18.89	724.57 ± 1.42	34.64 ± 0.40	65.29 ± 0.12	69.58 ± 0.24
			1,452	54.93 ± 0.05	13,208.72 ± 3.59	1,449.12 ± 6.59	34.13 ± 0.02	65.69 ± 0.02	69.22 ± 0.05
			2,178	55.05 ± 0.09	13,219.52 ± 15.67	2,177.65 ± 0.10	34.90 ± 0.30	66.01 ± 0.07	69.55 ± 0.08
			2,903	55.06 ± 0.07	13,184.73 ± 19.09	2,910.25 ± 0.22	34.69 ± 0.47	66.33 ± 0.08	69.89 ± 0.04

APPENDIX E: DYNAMIC DATA

Table E. 1. Stiffness coefficients (original bearing)

Speed [RPM]	Unit Load [kPa]	Kxx ± eKxx [MN/m]	Kxy ± eKxy [MN/m]	Kyx ± eKyx [MN/m]	Kyy ± eKyy [MN/m]
6,800	725	213.05 ± 2.88	-57.83 ± 4.47	-56.48 ± 5.23	223.92 ± 17.28
	1,452	256.33 ± 2.84	-60.76 ± 2.70	-67.54 ± 8.47	290.97 ± 9.62
	2,178	295.13 ± 2.85	-63.57 ± 2.30	-78.15 ± 8.33	359.33 ± 28.62
	2,903	323.19 ± 2.70	-67.64 ± 2.04	-84.08 ± 8.15	393.48 ± 8.75
9,000	725	251.86 ± 4.66	-71.50 ± 4.72	-66.47 ± 4.04	257.47 ± 16.23
	1,452	286.65 ± 4.00	-73.20 ± 2.45	-71.56 ± 2.91	316.62 ± 9.53
	2,178	316.52 ± 3.81	-75.27 ± 2.38	-76.74 ± 3.98	361.90 ± 18.54
	2,903	339.04 ± 3.60	-77.42 ± 2.04	-86.99 ± 6.52	411.15 ± 9.64
10,800	725	278.69 ± 5.35	-74.45 ± 4.28	-74.86 ± 3.58	280.58 ± 14.99
	1,452	306.32 ± 4.55	-77.03 ± 2.76	-80.29 ± 5.50	332.00 ± 8.71
	2,178	331.98 ± 4.07	-80.33 ± 2.37	-85.53 ± 4.67	376.75 ± 8.82
	2,903	353.07 ± 3.76	-84.79 ± 1.81	-90.91 ± 3.19	421.73 ± 6.69
13,200	725	310.09 ± 2.92	-74.56 ± 4.14	-98.55 ± 3.39	311.10 ± 13.10
	1,452	336.36 ± 2.62	-86.99 ± 2.68	-101.74 ± 3.19	350.66 ± 9.00

Table E. 2. Stiffness coefficients (modified bearing)

Speed [RPM]	Unit Load [kPa]	Kxx ± eKxx [MN/m]	Kxy ± eKxy [MN/m]	Kyx ± eKyx [MN/m]	Kyy ± eKyy [MN/m]
6,800	725	201.79 ± 5.75	-60.37 ± 5.30	-55.45 ± 5.77	182.20 ± 9.73
	1,452	235.21 ± 3.55	-56.33 ± 4.25	-55.29 ± 4.07	240.05 ± 5.37
	2,178	267.99 ± 2.81	-59.07 ± 3.83	-58.27 ± 3.18	291.19 ± 7.99
	2,903	295.71 ± 5.55	-64.35 ± 4.95	-60.62 ± 7.46	331.89 ± 10.15
9,000	725	236.89 ± 9.99	-73.41 ± 5.72	-68.06 ± 7.71	211.46 ± 9.91
	1,452	260.47 ± 4.92	-72.31 ± 4.33	-65.86 ± 3.81	260.12 ± 7.07
	2,178	286.35 ± 4.59	-74.22 ± 3.96	-68.95 ± 3.45	307.97 ± 8.31
	2,903	310.47 ± 3.78	-79.01 ± 4.81	-72.22 ± 3.56	347.90 ± 10.31
10,800	725	264.49 ± 9.65	-80.79 ± 5.32	-86.40 ± 9.24	241.14 ± 10.99
	1,452	280.94 ± 5.34	-79.00 ± 4.75	-77.85 ± 3.73	280.67 ± 7.60
	2,178	301.43 ± 4.66	-81.45 ± 4.31	-76.50 ± 4.26	321.05 ± 9.21
	2,903	325.56 ± 3.55	-86.68 ± 4.98	-77.23 ± 3.43	358.50 ± 9.85
13,200	725	277.85 ± 3.70	-74.55 ± 6.36	-93.54 ± 5.72	263.45 ± 8.73
	1,452	298.01 ± 4.78	-82.19 ± 8.32	-88.95 ± 3.27	296.71 ± 7.55
	2,178	318.68 ± 4.51	-87.87 ± 6.38	-90.44 ± 2.90	335.49 ± 8.54
	2,903	342.32 ± 4.77	-96.13 ± 12.08	-91.46 ± 3.88	371.35 ± 15.35

Table E. 3. Damping coefficients (original bearing)

Speed [RPM]	Unit Load [kPa]	Cxx ± eCxx [kN-s/m]	Cxy ± eCxy [kN-s/m]	Cyx ± eCyx [kN-s/m]	Cyy ± eCyy [kN-s/m]
6,800	725	214.52 ± 4.82	-20.59 ± 4.36	-27.12 ± 9.36	215.95 ± 14.51
	1,452	185.17 ± 4.05	-30.02 ± 4.36	-26.82 ± 13.15	182.13 ± 10.82
	2,178	164.57 ± 4.28	-36.95 ± 3.25	-31.39 ± 9.73	160.66 ± 17.39
	2,903	149.39 ± 4.39	-39.88 ± 2.28	-38.49 ± 12.86	150.55 ± 17.71
9,000	725	199.90 ± 7.34	-12.70 ± 4.29	-21.23 ± 6.97	197.07 ± 12.05
	1,452	175.89 ± 5.52	-24.08 ± 3.62	-30.40 ± 6.70	169.50 ± 9.40
	2,178	158.76 ± 5.81	-30.98 ± 3.60	-33.99 ± 6.92	155.12 ± 13.19
	2,903	145.96 ± 5.72	-35.18 ± 3.11	-38.22 ± 14.12	138.49 ± 16.43
10,800	725	192.48 ± 8.17	-14.26 ± 4.96	-15.54 ± 7.27	187.46 ± 16.37
	1,452	170.84 ± 6.37	-22.75 ± 3.97	-27.55 ± 7.46	162.15 ± 15.08
	2,178	155.46 ± 5.93	-29.02 ± 2.67	-31.45 ± 9.11	145.79 ± 14.08
	2,903	145.08 ± 6.17	-33.32 ± 2.75	-34.63 ± 8.90	131.48 ± 14.34
13,200	725	163.64 ± 4.58	-35.38 ± 9.55	-19.47 ± 4.87	171.47 ± 11.19
	1,452	150.14 ± 4.96	-31.75 ± 8.63	-22.65 ± 6.48	153.80 ± 10.57

Table E. 4. Damping coefficients (modified bearing)

Speed [RPM]	Unit Load [kPa]	Cxx ± eCxx [kN-s/m]	Cxy ± eCxy [kN-s/m]	Cyx ± eCyx [kN-s/m]	Cyy ± eCyy [kN-s/m]
6,800	725	175.17 ± 18.02	-11.84 ± 5.78	-02.58 ± 23.63	145.76 ± 8.06
	1,452	140.00 ± 6.21	-23.16 ± 8.18	-22.63 ± 9.66	122.00 ± 22.73
	2,178	121.75 ± 5.46	-28.55 ± 7.15	-28.63 ± 5.58	104.98 ± 12.42
	2,903	111.88 ± 9.26	-31.77 ± 8.78	-30.27 ± 4.04	91.82 ± 14.68
9,000	725	171.46 ± 26.93	-13.15 ± 8.81	-04.22 ± 25.26	136.68 ± 10.78
	1,452	134.48 ± 6.93	-19.71 ± 8.09	-24.32 ± 8.30	113.95 ± 20.62
	2,178	116.66 ± 6.36	-21.64 ± 7.08	-29.02 ± 5.87	95.44 ± 12.52
	2,903	105.94 ± 4.90	-22.99 ± 5.98	-29.33 ± 5.44	80.70 ± 15.00
10,800	725	166.30 ± 19.19	-19.44 ± 9.69	-02.93 ± 23.05	133.89 ± 12.41
	1,452	134.62 ± 7.39	-20.23 ± 9.57	-21.34 ± 10.02	110.70 ± 20.24
	2,178	116.34 ± 6.61	-19.80 ± 6.46	-26.08 ± 7.53	91.01 ± 13.01
	2,903	105.98 ± 5.25	-19.31 ± 7.24	-26.34 ± 6.52	73.99 ± 14.81
13,200	725	150.91 ± 7.21	-29.31 ± 8.60	-08.49 ± 7.68	118.12 ± 16.01
	1,452	133.45 ± 5.46	-25.89 ± 9.84	-09.73 ± 11.40	98.14 ± 25.16
	2,178	117.23 ± 4.24	-20.39 ± 6.00	-17.46 ± 8.71	84.12 ± 19.58
	2,903	105.14 ± 5.84	-15.61 ± 8.40	-20.05 ± 8.31	68.55 ± 25.13

Table E. 5. Virtual-mass coefficients (original bearing)

Speed [RPM]	Unit Load [kPa]	Mxx ± eMxx [kg]	Mxy ± eMxy [kg]	Myx ± eMyx [kg]	Myy ± eMyy [kg]
6,800	725	-41.39 ± 2.61	-32.33 ± 4.05	06.88 ± 4.74	-41.42 ± 15.64
	1,452	-32.08 ± 2.57	-24.66 ± 2.44	-10.38 ± 7.66	-37.48 ± 8.71
	2,178	-26.30 ± 2.58	-18.97 ± 2.08	-18.86 ± 7.54	-28.11 ± 25.90
	2,903	-21.97 ± 2.44	-14.59 ± 1.84	-21.83 ± 7.37	-35.19 ± 7.92
9,000	725	-35.05 ± 4.22	-34.93 ± 4.28	-09.39 ± 3.65	-35.97 ± 14.69
	1,452	-26.79 ± 3.62	-27.47 ± 2.21	-07.62 ± 2.63	-27.87 ± 8.62
	2,178	-22.27 ± 3.45	-23.94 ± 2.16	-08.59 ± 3.60	-22.78 ± 16.78
	2,903	-19.69 ± 3.26	-19.60 ± 1.84	-15.43 ± 5.90	-19.33 ± 8.73
10,800	725	-38.67 ± 4.85	-28.76 ± 3.87	-17.08 ± 3.24	-39.92 ± 13.56
	1,452	-28.76 ± 4.11	-22.99 ± 2.50	-17.27 ± 4.97	-25.81 ± 7.88
	2,178	-24.17 ± 3.68	-19.68 ± 2.14	-11.47 ± 4.22	-21.21 ± 7.98
	2,903	-21.68 ± 3.41	-18.27 ± 1.64	-12.38 ± 2.89	-19.55 ± 6.05
13,200	725	-25.95 ± 2.65	-03.93 ± 3.75	-14.86 ± 3.07	-30.20 ± 11.85
	1,452	-20.96 ± 2.37	-07.28 ± 2.42	-11.11 ± 2.89	-25.10 ± 8.14

Table E. 6. Virtual-mass coefficients (modified bearing)

Speed [RPM]	Unit Load [kPa]	Mxx ± eMxx [kg]	Mxy ± eMxy [kg]	Myx ± eMyx [kg]	Myy ± eMyy [kg]
6,800	725	04.20 ± 5.20	-28.12 ± 4.79	-07.65 ± 5.22	-21.86 ± 8.80
	1,452	-00.01 ± 3.21	-24.86 ± 3.84	-09.00 ± 3.68	-11.30 ± 4.86
	2,178	05.53 ± 2.54	-24.35 ± 3.47	-11.16 ± 2.87	-02.30 ± 7.23
	2,903	14.77 ± 5.02	-25.84 ± 4.48	-09.20 ± 6.75	02.47 ± 9.19
9,000	725	11.99 ± 9.04	-21.91 ± 5.18	-09.68 ± 6.98	-18.55 ± 8.97
	1,452	00.07 ± 4.45	-22.60 ± 3.92	-06.86 ± 3.45	-07.51 ± 6.40
	2,178	02.61 ± 4.15	-24.26 ± 3.59	-10.28 ± 3.12	01.37 ± 7.52
	2,903	07.10 ± 3.42	-25.76 ± 4.36	-13.20 ± 3.22	08.69 ± 9.33
10,800	725	-03.27 ± 8.74	-15.70 ± 4.81	-20.83 ± 8.36	-20.41 ± 9.94
	1,452	-08.02 ± 4.84	-16.18 ± 4.30	-09.71 ± 3.37	-08.62 ± 6.87
	2,178	-04.03 ± 4.22	-19.96 ± 3.90	-08.77 ± 3.86	-00.82 ± 8.33
	2,903	00.56 ± 3.21	-23.61 ± 4.51	-11.68 ± 3.11	08.34 ± 8.91
13,200	725	-22.14 ± 3.35	-05.79 ± 5.76	-25.85 ± 5.18	-13.64 ± 7.90
	1,452	-09.72 ± 4.32	-11.14 ± 7.53	-12.99 ± 2.96	-07.13 ± 6.83
	2,178	-06.02 ± 4.08	-16.75 ± 5.77	-12.67 ± 2.63	-01.11 ± 7.73
	2,903	-02.91 ± 4.31	-22.24 ± 10.93	-14.72 ± 3.51	03.22 ± 13.89

Table E. 7. Dimensionless stiffness coefficients (original bearing)

Speed [RPM]	Unit Load [kPa]	kxx ± ekxx [-]	kxy ± ekxy [-]	kyx ± ekyx [-]	kyy ± ekyy [-]
6,800	725	2.313 ± 0.034	-0.628 ± 0.049	-0.613 ± 0.057	2.431 ± 0.188
	1,452	1.395 ± 0.016	-0.331 ± 0.015	-0.368 ± 0.046	1.584 ± 0.053
	2,178	1.074 ± 0.011	-0.231 ± 0.008	-0.284 ± 0.030	1.307 ± 0.104
	2,903	0.880 ± 0.007	-0.184 ± 0.006	-0.229 ± 0.022	1.072 ± 0.024
9,000	725	2.719 ± 0.052	-0.772 ± 0.052	-0.718 ± 0.045	2.780 ± 0.179
	1,452	1.526 ± 0.022	-0.390 ± 0.013	-0.381 ± 0.016	1.686 ± 0.052
	2,178	1.125 ± 0.014	-0.267 ± 0.009	-0.273 ± 0.015	1.286 ± 0.068
	2,903	0.905 ± 0.010	-0.207 ± 0.006	-0.232 ± 0.018	1.097 ± 0.026
10,800	725	2.948 ± 0.060	-0.787 ± 0.047	-0.792 ± 0.040	2.968 ± 0.166
	1,452	1.602 ± 0.025	-0.403 ± 0.015	-0.420 ± 0.030	1.737 ± 0.048
	2,178	1.159 ± 0.015	-0.281 ± 0.009	-0.299 ± 0.017	1.316 ± 0.032
	2,903	0.924 ± 0.032	-0.222 ± 0.009	-0.238 ± 0.012	1.104 ± 0.040
13,200	725	3.391 ± 0.038	-0.815 ± 0.046	-1.078 ± 0.038	3.402 ± 0.145
	1,452	1.839 ± 0.019	-0.476 ± 0.015	-0.556 ± 0.018	1.917 ± 0.051

Table E. 8. Dimensionless stiffness coefficients (modified bearing)

Speed [RPM]	Unit Load [kPa]	kxx ± ekxx [-]	kxy ± ekxy [-]	kyx ± ekyx [-]	kyy ± ekyy [-]
6,800	725	2.538 ± 0.073	-0.759 ± 0.067	-0.698 ± 0.073	2.292 ± 0.123
	1,452	1.483 ± 0.023	-0.355 ± 0.027	-0.349 ± 0.026	1.514 ± 0.034
	2,178	1.130 ± 0.012	-0.249 ± 0.016	-0.246 ± 0.013	1.228 ± 0.034
	2,903	0.933 ± 0.019	-0.203 ± 0.016	-0.191 ± 0.024	1.048 ± 0.033
9,000	725	2.955 ± 0.128	-0.916 ± 0.073	-0.849 ± 0.099	2.637 ± 0.127
	1,452	1.602 ± 0.032	-0.445 ± 0.027	-0.405 ± 0.024	1.600 ± 0.045
	2,178	1.176 ± 0.020	-0.305 ± 0.017	-0.283 ± 0.015	1.264 ± 0.035
	2,903	0.957 ± 0.012	-0.244 ± 0.015	-0.223 ± 0.011	1.072 ± 0.033
10,800	725	3.275 ± 0.124	-1.000 ± 0.068	-1.070 ± 0.118	2.986 ± 0.141
	1,452	1.720 ± 0.034	-0.484 ± 0.030	-0.477 ± 0.024	1.719 ± 0.048
	2,178	1.232 ± 0.020	-0.333 ± 0.018	-0.313 ± 0.018	1.312 ± 0.039
	2,903	0.998 ± 0.018	-0.266 ± 0.016	-0.237 ± 0.011	1.099 ± 0.035
13,200	725	3.263 ± 0.048	-0.876 ± 0.081	-1.099 ± 0.073	3.094 ± 0.111
	1,452	1.750 ± 0.030	-0.483 ± 0.053	-0.522 ± 0.021	1.742 ± 0.048
	2,178	1.245 ± 0.020	-0.343 ± 0.027	-0.353 ± 0.012	1.311 ± 0.037
	2,903	1.001 ± 0.015	-0.281 ± 0.038	-0.267 ± 0.012	1.086 ± 0.049

Table E. 9. Dimensionless damping coefficients (original bearing)

Speed [RPM]	Unit Load [kPa]	cxx ± ecxx [-]	cxy ± ecxy [-]	cyx ± ecyx [-]	cyy ± ecyy [-]
6,800	725	1.667 ± 0.040	-0.160 ± 0.034	-0.211 ± 0.073	1.679 ± 0.114
	1,452	0.718 ± 0.017	-0.116 ± 0.017	-0.104 ± 0.051	0.706 ± 0.042
	2,178	0.426 ± 0.012	-0.096 ± 0.008	-0.081 ± 0.025	0.416 ± 0.045
	2,903	0.288 ± 0.009	-0.077 ± 0.004	-0.074 ± 0.025	0.290 ± 0.034
9,000	725	2.026 ± 0.076	-0.129 ± 0.043	-0.215 ± 0.071	1.997 ± 0.123
	1,452	0.881 ± 0.029	-0.121 ± 0.018	-0.152 ± 0.034	0.849 ± 0.048
	2,178	0.530 ± 0.020	-0.103 ± 0.012	-0.113 ± 0.023	0.518 ± 0.044
	2,903	0.368 ± 0.014	-0.089 ± 0.008	-0.096 ± 0.036	0.350 ± 0.041
10,800	725	2.306 ± 0.099	-0.171 ± 0.059	-0.186 ± 0.087	2.246 ± 0.197
	1,452	1.015 ± 0.038	-0.135 ± 0.024	-0.164 ± 0.044	0.963 ± 0.090
	2,178	0.617 ± 0.024	-0.115 ± 0.011	-0.125 ± 0.036	0.578 ± 0.056
	2,903	0.429 ± 0.030	-0.099 ± 0.010	-0.102 ± 0.027	0.389 ± 0.048
13,200	725	2.474 ± 0.075	-0.535 ± 0.145	-0.294 ± 0.074	2.592 ± 0.172
	1,452	1.135 ± 0.038	-0.240 ± 0.065	-0.171 ± 0.049	1.163 ± 0.080

Table E. 10. Dimensionless damping coefficients (modified bearing)

Speed [RPM]	Unit Load [kPa]	cxx ± ecxx [-]	cxy ± ecxy [-]	cyx ± ecyx [-]	cyy ± ecyy [-]
6,800	725	1.577 ± 0.162	-0.107 ± 0.052	-0.023 ± 0.213	1.313 ± 0.073
	1,452	0.629 ± 0.028	-0.104 ± 0.037	-0.102 ± 0.043	0.548 ± 0.102
	2,178	0.366 ± 0.016	-0.086 ± 0.021	-0.086 ± 0.017	0.315 ± 0.037
	2,903	0.250 ± 0.021	-0.071 ± 0.020	-0.068 ± 0.009	0.205 ± 0.033
9,000	725	2.007 ± 0.315	-0.154 ± 0.103	-0.049 ± 0.296	1.600 ± 0.126
	1,452	0.779 ± 0.040	-0.114 ± 0.047	-0.141 ± 0.048	0.660 ± 0.119
	2,178	0.450 ± 0.025	-0.083 ± 0.027	-0.112 ± 0.023	0.368 ± 0.048
	2,903	0.309 ± 0.014	-0.067 ± 0.017	-0.086 ± 0.016	0.235 ± 0.044
10,800	725	2.333 ± 0.270	-0.273 ± 0.136	-0.041 ± 0.323	1.878 ± 0.175
	1,452	0.936 ± 0.051	-0.141 ± 0.067	-0.148 ± 0.070	0.770 ± 0.141
	2,178	0.540 ± 0.031	-0.092 ± 0.030	-0.121 ± 0.035	0.423 ± 0.061
	2,903	0.367 ± 0.019	-0.067 ± 0.025	-0.091 ± 0.023	0.256 ± 0.051
13,200	725	2.450 ± 0.117	-0.476 ± 0.140	-0.138 ± 0.125	1.918 ± 0.260
	1,452	1.084 ± 0.045	-0.210 ± 0.080	-0.079 ± 0.093	0.797 ± 0.204
	2,178	0.634 ± 0.023	-0.110 ± 0.032	-0.094 ± 0.047	0.455 ± 0.106
	2,903	0.425 ± 0.024	-0.063 ± 0.034	-0.081 ± 0.034	0.277 ± 0.101

Table E. 11. Dimensionless virtual-mass coefficients (original bearing)

Speed [RPM]	Unit Load [kPa]	mxx ± emxx [-]	mxy ± emxy [-]	myx ± emyx [-]	myy ± emyy [-]
6,800	725	-0.230 ± 0.015	-0.180 ± 0.023	0.038 ± 0.026	-0.230 ± 0.087
	1,452	-0.089 ± 0.007	-0.068 ± 0.007	-0.029 ± 0.021	-0.103 ± 0.024
	2,178	-0.049 ± 0.005	-0.035 ± 0.004	-0.035 ± 0.014	-0.052 ± 0.048
	2,903	-0.030 ± 0.003	-0.020 ± 0.003	-0.030 ± 0.010	-0.048 ± 0.011
9,000	725	-0.333 ± 0.040	-0.332 ± 0.041	-0.089 ± 0.035	-0.342 ± 0.140
	1,452	-0.126 ± 0.017	-0.130 ± 0.011	-0.036 ± 0.012	-0.131 ± 0.041
	2,178	-0.070 ± 0.011	-0.075 ± 0.007	-0.027 ± 0.011	-0.071 ± 0.053
	2,903	-0.047 ± 0.008	-0.047 ± 0.004	-0.037 ± 0.014	-0.046 ± 0.021
10,800	725	-0.525 ± 0.066	-0.390 ± 0.053	-0.232 ± 0.044	-0.542 ± 0.184
	1,452	-0.194 ± 0.028	-0.155 ± 0.017	-0.116 ± 0.034	-0.174 ± 0.053
	2,178	-0.109 ± 0.017	-0.089 ± 0.010	-0.052 ± 0.019	-0.096 ± 0.036
	2,903	-0.072 ± 0.012	-0.061 ± 0.007	-0.041 ± 0.010	-0.065 ± 0.021
13,200	725	-0.542 ± 0.056	-0.082 ± 0.078	-0.311 ± 0.064	-0.631 ± 0.248
	1,452	-0.219 ± 0.025	-0.076 ± 0.025	-0.116 ± 0.030	-0.263 ± 0.085

Table E. 12. Dimensionless virtual-mass coefficients (modified bearing)

Speed [RPM]	Unit Load [kPa]	mxx ± emxx [-]	mxy ± emxy [-]	myx ± emyx [-]	myy ± emyy [-]
6,800	725	0.027 ± 0.034	-0.181 ± 0.031	-0.049 ± 0.034	-0.141 ± 0.057
	1,452	0.000 ± 0.010	-0.079 ± 0.012	-0.029 ± 0.012	-0.036 ± 0.016
	2,178	0.012 ± 0.005	-0.052 ± 0.007	-0.024 ± 0.006	-0.005 ± 0.015
	2,903	0.023 ± 0.008	-0.041 ± 0.007	-0.015 ± 0.011	0.004 ± 0.015
9,000	725	0.132 ± 0.099	-0.241 ± 0.057	-0.106 ± 0.077	-0.204 ± 0.099
	1,452	0.000 ± 0.024	-0.123 ± 0.021	-0.037 ± 0.019	-0.041 ± 0.035
	2,178	0.009 ± 0.015	-0.088 ± 0.013	-0.037 ± 0.011	0.005 ± 0.027
	2,903	0.020 ± 0.009	-0.071 ± 0.012	-0.036 ± 0.009	0.024 ± 0.026
10,800	725	-0.052 ± 0.139	-0.250 ± 0.077	-0.331 ± 0.133	-0.324 ± 0.158
	1,452	-0.063 ± 0.038	-0.128 ± 0.034	-0.077 ± 0.027	-0.068 ± 0.054
	2,178	-0.021 ± 0.022	-0.105 ± 0.021	-0.046 ± 0.020	-0.004 ± 0.044
	2,903	0.002 ± 0.013	-0.092 ± 0.018	-0.046 ± 0.012	0.033 ± 0.035
13,200	725	-0.497 ± 0.075	-0.130 ± 0.129	-0.580 ± 0.116	-0.306 ± 0.177
	1,452	-0.109 ± 0.049	-0.125 ± 0.085	-0.146 ± 0.033	-0.080 ± 0.077
	2,178	-0.045 ± 0.031	-0.125 ± 0.043	-0.095 ± 0.020	-0.008 ± 0.058
	2,903	-0.016 ± 0.024	-0.124 ± 0.061	-0.082 ± 0.020	0.018 ± 0.077

APPENDIX F: DYNAMIC-STIFFNESS DATA

Table F. 1. Dynamic-stiffness 6,800 rpm 726 kPa (original bearing)

Frequency [Hz]	Re (H_{xx}) [MN/m]	Re (H_{xy}) [MN/m]	Re (H_{yx}) [MN/m]	Re (H_{yy}) [MN/m]	Im (H_{xx}) [MN/m]	Im (H_{xy}) [MN/m]	Im (H_{yx}) [MN/m]	Im (H_{yy}) [MN/m]
9.77	202.89 ± 0.53	-50.76 ± 1.22	-59.19 ± 3.25	193.91 ± 9.41	15.12 ± 0.44	-4.36 ± 1.24	-17.52 ± 3.40	50.03 ± 5.15
19.53	206.83 ± 0.24	-57.96 ± 0.81	-61.11 ± 11.58	213.86 ± 9.29	30.91 ± 0.15	-4.69 ± 0.45	5.98 ± 6.33	-0.95 ± 8.47
29.30	207.67 ± 0.25	-55.70 ± 0.27	-68.56 ± 2.93	251.55 ± 3.99	44.58 ± 0.13	-6.39 ± 0.23	2.02 ± 2.89	11.59 ± 8.50
39.06	211.26 ± 0.31	-56.71 ± 0.20	-61.40 ± 7.87	206.96 ± 10.63	57.37 ± 0.33	-6.49 ± 0.38	1.77 ± 4.05	65.91 ± 3.75
48.83	216.24 ± 0.15	-55.20 ± 0.26	-63.91 ± 2.82	225.73 ± 5.08	73.57 ± 0.13	-8.62 ± 0.11	-6.04 ± 1.20	66.01 ± 4.18
58.59	218.32 ± 0.19	-54.37 ± 0.20	-52.86 ± 1.54	228.31 ± 1.80	85.16 ± 0.23	-6.68 ± 0.24	-13.70 ± 2.36	89.15 ± 2.57
68.36	219.90 ± 0.21	-55.42 ± 0.21	-67.43 ± 2.51	240.65 ± 3.32	104.60 ± 0.19	-4.84 ± 0.15	-0.30 ± 0.80	97.81 ± 1.47
78.13	227.52 ± 0.09	-50.25 ± 0.19	-48.32 ± 0.49	224.31 ± 2.83	112.26 ± 0.14	-6.75 ± 0.19	-8.41 ± 0.92	98.78 ± 1.40
87.89	228.80 ± 0.23	-50.47 ± 0.07	-58.01 ± 0.55	243.31 ± 1.98	123.42 ± 0.17	-9.17 ± 0.25	-21.31 ± 1.51	126.36 ± 0.97
97.66	233.27 ± 0.23	-47.87 ± 0.26	-55.08 ± 1.40	245.84 ± 3.48	133.48 ± 0.12	-8.42 ± 0.25	-25.06 ± 1.04	128.54 ± 2.23
107.42	236.45 ± 0.55	-46.50 ± 0.83	-58.26 ± 0.97	250.66 ± 2.30	144.61 ± 0.26	-9.91 ± 0.27	-22.21 ± 2.24	148.87 ± 3.76
117.19	241.72 ± 0.73	-43.19 ± 0.45	-52.86 ± 2.29	265.76 ± 0.53	155.13 ± 1.01	-11.52 ± 1.31	-28.25 ± 0.76	154.16 ± 2.01
126.95	245.89 ± 0.11	-40.14 ± 0.34	-55.24 ± 0.73	249.96 ± 0.40	168.46 ± 0.42	-11.86 ± 0.29	-28.08 ± 4.07	178.70 ± 2.00
136.72	248.74 ± 0.15	-35.02 ± 0.22	-53.01 ± 2.31	261.06 ± 1.54	180.66 ± 0.29	-13.44 ± 0.17	-32.42 ± 1.93	181.45 ± 1.37
146.48	252.27 ± 0.11	-28.42 ± 0.05	-66.83 ± 5.16	253.88 ± 1.96	192.29 ± 0.17	-14.01 ± 0.17	-44.55 ± 2.39	189.29 ± 3.26
156.25	256.07 ± 0.12	-17.89 ± 0.16	-75.58 ± 6.19	234.12 ± 2.08	205.41 ± 0.21	-13.78 ± 0.04	-23.05 ± 1.11	192.56 ± 0.32
166.02	260.03 ± 0.12	-21.77 ± 0.11	-65.98 ± 4.30	281.80 ± 0.82	218.51 ± 0.24	-22.92 ± 0.11	-9.49 ± 5.79	247.26 ± 1.44
175.78	260.83 ± 0.22	-16.92 ± 0.05	-51.81 ± 1.48	292.22 ± 2.60	233.22 ± 0.18	-24.77 ± 0.09	-29.86 ± 5.70	231.52 ± 1.80
185.55	268.84 ± 0.17	-12.55 ± 0.12	-51.36 ± 3.04	294.77 ± 4.56	246.08 ± 0.32	-25.68 ± 0.08	-38.89 ± 1.11	252.53 ± 1.04
195.31	274.70 ± 0.15	-9.04 ± 0.07	-55.65 ± 1.26	300.90 ± 1.47	260.86 ± 0.17	-27.67 ± 0.12	-28.36 ± 2.55	260.55 ± 4.71
205.08	278.26 ± 0.35	-7.08 ± 0.05	-62.95 ± 2.03	308.55 ± 2.31	273.15 ± 0.20	-30.58 ± 0.12	-33.79 ± 1.48	284.96 ± 1.97
214.84	286.81 ± 0.10	-1.43 ± 0.12	-68.05 ± 5.61	316.08 ± 3.81	291.58 ± 0.25	-27.73 ± 0.12	-36.78 ± 3.37	272.23 ± 4.42
224.61	293.78 ± 0.17	33.21 ± 0.11	-77.40 ± 6.11	200.43 ± 1.78	307.25 ± 0.47	-20.83 ± 0.19	-49.21 ± 2.82	330.22 ± 1.25
234.38	304.63 ± 0.27	1.03 ± 0.10	-80.45 ± 7.07	342.70 ± 1.69	317.08 ± 0.20	-42.88 ± 0.16	-39.43 ± 3.91	322.89 ± 3.65
244.14	305.48 ± 0.18	7.24 ± 0.19	-83.93 ± 8.09	332.16 ± 2.21	334.17 ± 0.24	-37.03 ± 0.15	-21.42 ± 2.21	325.31 ± 4.69

Table F. 2. Dynamic-stiffness 6,800 rpm 726 kPa (modified bearing)

Frequency [Hz]	Re (H_{xx}) [MN/m]	Re (H_{xy}) [MN/m]	Re (H_{yx}) [MN/m]	Re (H_{yy}) [MN/m]	Im (H_{xx}) [MN/m]	Im (H_{xy}) [MN/m]	Im (H_{yx}) [MN/m]	Im (H_{yy}) [MN/m]
9.77	189.86 ± 0.21	-50.36 ± 0.76	-50.78 ± 0.16	180.64 ± 0.73	13.17 ± 0.47	-2.12 ± 0.75	2.23 ± 0.34	7.64 ± 1.45
19.53	191.40 ± 0.18	-51.67 ± 0.74	-51.60 ± 0.23	183.64 ± 0.72	22.76 ± 0.17	-5.79 ± 0.54	-5.66 ± 0.21	22.19 ± 1.58
29.30	193.01 ± 0.39	-54.66 ± 0.63	-52.60 ± 0.14	185.17 ± 0.86	34.10 ± 0.24	-9.46 ± 0.78	-10.66 ± 0.18	33.17 ± 1.74
39.06	195.17 ± 0.45	-51.96 ± 0.95	-51.75 ± 0.20	183.61 ± 0.69	43.68 ± 0.17	-8.77 ± 0.59	-15.27 ± 0.15	45.48 ± 1.59
48.83	197.37 ± 0.15	-53.94 ± 0.68	-49.74 ± 0.13	180.16 ± 0.73	53.36 ± 0.25	-9.79 ± 0.51	-15.51 ± 0.26	52.81 ± 1.41
58.59	195.52 ± 1.73	-51.75 ± 0.88	-53.55 ± 0.98	187.79 ± 0.93	64.53 ± 1.34	-10.05 ± 0.85	2.42 ± 0.59	54.86 ± 1.54
68.36	207.39 ± 0.80	-79.88 ± 1.24	-40.28 ± 0.30	140.89 ± 0.94	72.83 ± 0.29	-12.81 ± 1.18	-7.31 ± 0.37	57.09 ± 1.92
78.13	201.27 ± 0.43	-56.42 ± 0.65	-49.61 ± 0.18	180.65 ± 0.83	81.45 ± 0.31	-7.57 ± 0.72	-13.83 ± 0.24	74.53 ± 1.61
87.89	201.94 ± 0.17	-52.82 ± 0.72	-59.44 ± 0.33	195.88 ± 0.77	88.59 ± 0.20	-11.53 ± 0.66	-16.80 ± 0.24	84.85 ± 1.51
97.66	200.88 ± 0.29	-36.51 ± 0.79	-65.75 ± 0.57	215.27 ± 1.87	101.25 ± 0.58	-24.78 ± 1.86	-18.81 ± 0.55	98.90 ± 2.22
107.42	204.61 ± 2.16	-49.76 ± 1.36	-60.34 ± 1.25	204.13 ± 0.88	105.04 ± 1.07	-9.95 ± 0.98	-16.06 ± 1.32	98.73 ± 2.00
117.19	207.61 ± 3.90	-48.31 ± 2.86	-47.01 ± 5.95	199.95 ± 1.96	119.95 ± 8.20	-9.57 ± 2.14	-18.69 ± 3.33	112.32 ± 3.40
126.95	204.69 ± 0.78	-46.22 ± 0.69	-59.06 ± 0.49	207.97 ± 0.95	122.48 ± 0.47	-10.11 ± 0.70	-21.05 ± 0.73	117.69 ± 1.51
136.72	205.07 ± 0.67	-44.46 ± 0.58	-58.18 ± 0.61	211.94 ± 0.76	131.29 ± 0.40	-7.36 ± 0.52	-24.00 ± 0.25	127.62 ± 1.45
146.48	205.87 ± 0.25	-41.52 ± 0.78	-47.67 ± 0.24	197.12 ± 0.98	141.98 ± 0.38	-7.92 ± 0.56	-26.03 ± 0.31	142.09 ± 1.52
156.25	201.51 ± 0.33	-34.15 ± 0.79	-44.31 ± 0.31	188.20 ± 1.00	151.58 ± 0.45	-9.53 ± 1.19	-29.14 ± 0.54	143.25 ± 2.24
166.02	205.45 ± 0.52	-38.59 ± 0.85	-49.61 ± 0.34	202.17 ± 1.04	165.91 ± 0.38	-5.87 ± 0.90	-19.13 ± 0.30	144.32 ± 1.69
175.78	201.95 ± 0.31	-32.72 ± 0.50	-50.03 ± 0.26	211.46 ± 0.87	179.79 ± 0.36	-10.89 ± 0.66	-21.86 ± 0.20	162.69 ± 1.47
185.55	202.77 ± 0.30	-30.19 ± 0.50	-55.44 ± 0.41	225.63 ± 0.77	189.66 ± 0.39	-12.24 ± 0.65	-22.88 ± 0.10	170.52 ± 1.43
195.31	201.06 ± 0.21	-22.76 ± 0.76	-40.01 ± 0.37	208.32 ± 0.82	204.82 ± 0.41	-13.98 ± 0.63	-13.38 ± 0.37	181.55 ± 1.51
205.08	201.31 ± 0.54	-10.31 ± 1.20	-47.71 ± 0.39	218.61 ± 1.06	219.17 ± 0.31	-9.89 ± 1.83	-8.28 ± 0.35	198.88 ± 1.60
214.84	197.51 ± 0.33	5.86 ± 0.67	-36.73 ± 0.48	227.61 ± 1.24	236.00 ± 0.40	-8.07 ± 0.74	10.57 ± 0.41	176.27 ± 1.56
224.61	195.74 ± 0.92	-1.83 ± 1.92	-32.79 ± 1.43	189.30 ± 2.68	262.30 ± 0.60	-9.84 ± 1.71	-6.61 ± 0.83	199.91 ± 4.02
234.38	161.40 ± 1.15	-0.82 ± 1.04	-58.93 ± 3.81	248.07 ± 3.29	281.61 ± 1.42	-26.32 ± 2.27	61.42 ± 1.66	230.57 ± 4.89
244.14	187.05 ± 0.56	11.61 ± 0.77	-14.21 ± 0.74	235.64 ± 1.57	339.98 ± 0.52	-21.80 ± 0.71	67.97 ± 0.64	205.07 ± 1.80

Table F. 3. Dynamic-stiffness 6,800 rpm 1,452 kPa (original bearing)

Frequency [Hz]	Re (H_{xx}) [MN/m]	Re (H_{xy}) [MN/m]	Re (H_{yx}) [MN/m]	Re (H_{yy}) [MN/m]	Im (H_{xx}) [MN/m]	Im (H_{xy}) [MN/m]	Im (H_{yx}) [MN/m]	Im (H_{yy}) [MN/m]
9.77	247.49 ± 0.38	-58.08 ± 0.37	-73.01 ± 1.04	285.66 ± 4.22	13.18 ± 0.38	-4.94 ± 0.46	-31.87 ± 8.21	36.62 ± 2.01
19.53	248.75 ± 0.24	-60.81 ± 0.87	-117.10 ± 8.93	314.84 ± 6.97	25.03 ± 0.20	-6.14 ± 0.60	-28.55 ± 10.81	-7.19 ± 3.90
29.30	251.53 ± 0.20	-59.45 ± 0.56	-60.92 ± 2.13	282.96 ± 1.21	38.85 ± 0.18	-7.40 ± 0.39	-14.02 ± 1.33	23.35 ± 1.58
39.06	255.15 ± 0.19	-60.85 ± 0.17	-42.06 ± 4.47	290.91 ± 1.69	51.66 ± 0.26	-8.73 ± 0.24	21.34 ± 8.07	43.70 ± 2.33
48.83	259.01 ± 0.18	-59.07 ± 0.32	-59.91 ± 2.56	289.30 ± 1.00	64.85 ± 0.13	-10.41 ± 0.21	-2.71 ± 3.45	58.71 ± 1.04
58.59	260.94 ± 0.08	-58.72 ± 0.10	-53.11 ± 3.56	295.36 ± 0.88	74.74 ± 0.25	-9.91 ± 0.23	-17.70 ± 1.16	74.65 ± 0.96
68.36	260.56 ± 0.25	-58.17 ± 0.29	-71.98 ± 1.97	303.60 ± 0.52	85.74 ± 0.17	-11.10 ± 0.14	-13.61 ± 2.63	70.44 ± 0.87
78.13	268.51 ± 0.23	-54.98 ± 0.20	-49.39 ± 2.96	290.47 ± 0.80	99.98 ± 0.21	-11.13 ± 0.14	-16.83 ± 2.82	81.41 ± 0.61
87.89	269.03 ± 0.19	-55.83 ± 0.13	-63.96 ± 1.29	311.93 ± 0.49	108.02 ± 0.22	-13.75 ± 0.25	-28.93 ± 1.01	116.20 ± 0.47
97.66	272.58 ± 0.48	-52.80 ± 0.19	-67.63 ± 2.86	303.42 ± 0.70	115.99 ± 0.27	-13.81 ± 0.23	-20.87 ± 1.39	107.96 ± 0.53
107.42	275.29 ± 0.50	-50.97 ± 0.59	-65.80 ± 1.24	313.81 ± 0.92	126.78 ± 0.43	-15.82 ± 0.18	-14.42 ± 1.36	126.65 ± 0.63
117.19	280.98 ± 4.93	-53.52 ± 4.24	-59.95 ± 8.15	322.15 ± 10.47	134.50 ± 5.83	-15.04 ± 8.07	-41.12 ± 4.84	140.69 ± 3.66
126.95	282.90 ± 0.48	-45.74 ± 0.35	-59.93 ± 1.14	310.54 ± 0.50	146.40 ± 0.50	-18.28 ± 0.48	-30.34 ± 0.83	151.25 ± 0.65
136.72	285.64 ± 0.31	-41.62 ± 0.27	-64.66 ± 2.04	313.23 ± 0.63	157.06 ± 0.31	-20.14 ± 0.09	-42.26 ± 1.41	159.84 ± 0.83
146.48	288.49 ± 0.07	-36.42 ± 0.08	-51.08 ± 1.29	316.29 ± 0.95	167.74 ± 0.19	-22.41 ± 0.24	-26.34 ± 1.55	166.52 ± 0.46
156.25	288.39 ± 0.13	-29.27 ± 0.13	-51.67 ± 3.71	307.40 ± 0.97	178.84 ± 0.24	-23.45 ± 0.08	-21.94 ± 1.93	157.69 ± 0.55
166.02	293.19 ± 0.22	-33.47 ± 0.11	-57.61 ± 0.70	338.58 ± 0.65	188.59 ± 0.21	-30.14 ± 0.13	-33.67 ± 2.15	200.41 ± 1.44
175.78	292.52 ± 0.28	-27.95 ± 0.10	-59.05 ± 1.29	340.76 ± 0.34	199.60 ± 0.21	-32.42 ± 0.13	-42.59 ± 2.36	208.57 ± 0.69
185.55	298.68 ± 0.19	-26.04 ± 0.14	-55.46 ± 1.65	345.37 ± 0.71	212.86 ± 0.36	-33.79 ± 0.08	-30.80 ± 0.88	212.46 ± 0.65
195.31	301.99 ± 0.25	-20.67 ± 0.08	-56.28 ± 2.70	344.50 ± 0.53	227.88 ± 0.27	-37.92 ± 0.09	-30.03 ± 2.80	222.91 ± 0.85
205.08	304.44 ± 0.39	-18.25 ± 0.12	-52.12 ± 1.88	365.09 ± 0.88	236.39 ± 0.21	-42.52 ± 0.15	-24.43 ± 2.80	246.09 ± 0.40
214.84	312.27 ± 0.31	-13.30 ± 0.15	-34.90 ± 1.21	368.64 ± 0.41	250.17 ± 0.31	-42.02 ± 0.10	-40.84 ± 2.87	235.56 ± 0.67
224.61	319.27 ± 0.35	-1.90 ± 0.07	-54.95 ± 1.98	312.24 ± 0.39	260.85 ± 0.38	-41.57 ± 0.15	-26.78 ± 2.00	250.66 ± 0.72
234.38	328.05 ± 0.71	-15.62 ± 0.40	-51.73 ± 2.24	395.38 ± 0.80	273.64 ± 0.21	-56.14 ± 0.28	-29.03 ± 2.83	269.88 ± 0.98
244.14	329.93 ± 0.49	-12.54 ± 0.07	-38.50 ± 2.93	391.47 ± 0.78	286.45 ± 0.17	-54.42 ± 0.10	-23.75 ± 5.19	276.44 ± 0.73

Table F. 4. Dynamic-stiffness 6,800 rpm 1,452 kPa (modified bearing)

Frequency [Hz]	Re (H_{xx}) [MN/m]	Re (H_{xy}) [MN/m]	Re (H_{yx}) [MN/m]	Re (H_{yy}) [MN/m]	Im (H_{xx}) [MN/m]	Im (H_{xy}) [MN/m]	Im (H_{yx}) [MN/m]	Im (H_{yy}) [MN/m]
9.77	225.58 ± 0.50	-55.19 ± 1.14	-51.54 ± 0.20	241.52 ± 1.06	13.27 ± 0.61	0.10 ± 1.04	3.38 ± 0.20	3.50 ± 1.48
19.53	225.63 ± 0.48	-54.20 ± 1.19	-52.16 ± 0.19	242.78 ± 1.15	20.65 ± 0.47	-2.72 ± 0.89	-5.56 ± 0.27	16.72 ± 1.75
29.30	229.14 ± 0.56	-58.53 ± 0.79	-52.08 ± 0.26	243.35 ± 1.20	29.72 ± 0.26	-7.26 ± 0.87	-11.32 ± 0.43	24.22 ± 1.64
39.06	229.45 ± 0.51	-53.51 ± 0.73	-50.14 ± 0.42	239.96 ± 0.76	39.64 ± 0.53	-8.02 ± 0.68	-14.75 ± 0.34	33.79 ± 1.66
48.83	231.86 ± 0.58	-51.70 ± 0.69	-49.04 ± 0.21	234.37 ± 0.90	47.58 ± 0.23	-7.24 ± 0.63	-14.13 ± 0.54	36.92 ± 1.60
58.59	236.24 ± 1.94	-52.85 ± 0.99	-49.68 ± 1.83	240.95 ± 0.97	57.41 ± 1.30	-7.00 ± 0.80	2.39 ± 1.66	37.65 ± 1.82
68.36	236.65 ± 0.81	-54.48 ± 1.18	-56.80 ± 0.45	253.27 ± 1.11	71.87 ± 0.45	-42.53 ± 1.66	11.68 ± 0.23	-57.31 ± 2.26
78.13	237.51 ± 0.29	-56.60 ± 0.56	-49.19 ± 0.14	229.86 ± 0.94	72.15 ± 0.42	-5.68 ± 0.64	-15.91 ± 0.15	58.47 ± 1.61
87.89	237.12 ± 0.24	-50.17 ± 0.67	-57.52 ± 0.37	240.55 ± 0.95	78.27 ± 0.36	-14.39 ± 0.66	-19.60 ± 0.32	64.43 ± 1.73
97.66	235.61 ± 0.44	-29.57 ± 1.16	-64.41 ± 0.68	262.40 ± 1.57	89.24 ± 0.54	-31.26 ± 0.91	-23.08 ± 0.70	82.07 ± 2.36
107.42	240.60 ± 1.63	-47.60 ± 0.91	-58.03 ± 1.38	244.54 ± 0.89	91.31 ± 1.09	-8.77 ± 0.74	-18.17 ± 1.34	76.94 ± 1.95
117.19	243.89 ± 5.49	-43.70 ± 1.69	-47.59 ± 3.73	246.34 ± 1.21	100.19 ± 5.28	-15.48 ± 1.28	-24.44 ± 5.80	96.71 ± 2.57
126.95	241.83 ± 0.85	-41.61 ± 0.56	-55.98 ± 0.48	252.81 ± 0.88	105.92 ± 0.59	-16.49 ± 0.66	-26.42 ± 0.60	97.02 ± 1.43
136.72	241.79 ± 0.60	-39.89 ± 0.59	-56.18 ± 0.67	252.18 ± 0.72	111.33 ± 0.62	-14.33 ± 0.62	-32.39 ± 0.52	107.83 ± 1.38
146.48	240.23 ± 0.33	-35.90 ± 0.89	-43.99 ± 0.11	239.64 ± 0.83	120.93 ± 0.21	-16.08 ± 0.61	-30.01 ± 0.49	120.65 ± 1.68
156.25	237.41 ± 0.25	-32.83 ± 0.77	-42.43 ± 0.38	234.75 ± 1.01	129.01 ± 0.54	-23.03 ± 0.88	-31.21 ± 0.27	117.12 ± 2.06
166.02	240.90 ± 0.19	-33.59 ± 0.69	-46.66 ± 0.33	246.06 ± 0.96	139.03 ± 0.24	-13.81 ± 1.06	-23.92 ± 0.37	120.31 ± 1.61
175.78	235.77 ± 0.24	-30.89 ± 0.74	-45.50 ± 0.20	253.44 ± 0.65	150.58 ± 0.28	-22.78 ± 0.66	-29.43 ± 0.23	139.42 ± 1.63
185.55	236.09 ± 0.30	-28.78 ± 0.62	-50.41 ± 0.21	262.90 ± 0.85	158.86 ± 0.23	-24.69 ± 0.56	-32.14 ± 0.20	146.35 ± 1.50
195.31	236.28 ± 0.39	-23.26 ± 0.59	-34.56 ± 0.42	247.64 ± 0.79	167.22 ± 0.49	-29.00 ± 1.05	-33.67 ± 0.43	156.30 ± 1.67
205.08	237.75 ± 0.15	-10.99 ± 0.87	-36.78 ± 0.34	256.18 ± 1.54	182.07 ± 0.39	-34.64 ± 1.81	-27.62 ± 0.32	172.65 ± 2.37
214.84	227.01 ± 0.41	8.91 ± 0.89	-41.62 ± 0.57	274.26 ± 1.04	186.92 ± 0.35	-24.73 ± 0.48	-16.20 ± 0.49	146.48 ± 1.64
224.61	231.54 ± 0.67	-0.76 ± 2.81	-42.09 ± 1.11	262.00 ± 1.57	200.35 ± 1.16	-32.63 ± 1.97	-21.51 ± 1.08	172.34 ± 5.11
234.38	239.14 ± 2.27	-12.64 ± 1.07	-19.34 ± 1.57	276.13 ± 1.56	212.59 ± 0.40	-41.49 ± 1.43	-38.33 ± 1.83	202.73 ± 1.85
244.14	225.33 ± 0.40	-0.79 ± 1.39	-41.23 ± 0.35	258.36 ± 1.20	231.86 ± 0.27	-36.46 ± 1.24	-10.10 ± 0.36	185.47 ± 2.14

Table F. 5. Dynamic-stiffness 6,800 rpm 2,177 kPa (original bearing)

Frequency [Hz]	Re (H_{xx}) [MN/m]	Re (H_{xy}) [MN/m]	Re (H_{yx}) [MN/m]	Re (H_{yy}) [MN/m]	Im (H_{xx}) [MN/m]	Im (H_{xy}) [MN/m]	Im (H_{yx}) [MN/m]	Im (H_{yy}) [MN/m]
9.77	286.30 ± 0.75	-63.34 ± 0.96	-114.02 ± 4.18	512.59 ± 17.95	11.98 ± 0.56	-4.07 ± 1.46	-5.68 ± 7.16	-7.83 ± 10.23
19.53	286.68 ± 0.25	-66.47 ± 0.91	-80.38 ± 8.06	235.39 ± 8.60	22.42 ± 0.27	-6.97 ± 0.68	-22.34 ± 16.44	85.02 ± 11.56
29.30	289.81 ± 0.18	-64.14 ± 0.38	-81.53 ± 4.57	410.65 ± 11.33	33.87 ± 0.35	-6.77 ± 0.37	-11.76 ± 3.45	2.60 ± 4.39
39.06	293.58 ± 0.31	-64.56 ± 0.42	-73.19 ± 6.41	376.02 ± 4.94	46.42 ± 0.19	-8.49 ± 0.28	-0.91 ± 12.41	11.86 ± 2.57
48.83	296.49 ± 0.09	-62.84 ± 0.15	-80.09 ± 1.13	334.59 ± 2.57	58.30 ± 0.13	-11.27 ± 0.24	-7.42 ± 2.63	47.70 ± 2.94
58.59	299.58 ± 0.15	-62.90 ± 0.34	-78.79 ± 4.55	367.77 ± 1.45	67.14 ± 0.22	-10.69 ± 0.30	-25.95 ± 1.69	52.02 ± 2.12
68.36	298.63 ± 0.16	-61.97 ± 0.20	-69.19 ± 3.76	350.98 ± 1.02	76.88 ± 0.25	-12.59 ± 0.18	-15.40 ± 6.11	53.84 ± 1.31
78.13	306.51 ± 0.10	-56.76 ± 0.23	-49.49 ± 1.57	340.65 ± 1.19	92.75 ± 0.16	-12.65 ± 0.15	-14.90 ± 2.06	62.04 ± 1.09
87.89	306.24 ± 0.17	-59.83 ± 0.15	-76.99 ± 2.59	365.28 ± 1.30	96.77 ± 0.30	-17.55 ± 0.32	-22.62 ± 1.46	91.14 ± 0.88
97.66	309.49 ± 0.42	-57.16 ± 0.37	-54.74 ± 2.63	347.18 ± 1.61	104.22 ± 0.21	-18.03 ± 0.32	-14.36 ± 1.91	92.70 ± 1.65
107.42	311.26 ± 0.68	-55.42 ± 0.95	-71.13 ± 1.42	374.81 ± 1.15	112.80 ± 0.35	-20.33 ± 0.45	-22.36 ± 1.94	113.62 ± 0.86
117.19	314.65 ± 0.88	-53.83 ± 0.45	-77.11 ± 8.17	363.56 ± 3.69	120.26 ± 1.67	-23.72 ± 1.78	-42.11 ± 1.48	126.64 ± 2.09
126.95	318.55 ± 0.22	-50.80 ± 0.37	-63.81 ± 1.68	365.39 ± 1.45	130.74 ± 0.57	-24.84 ± 0.34	-41.42 ± 0.57	128.73 ± 1.55
136.72	320.62 ± 0.20	-47.14 ± 0.31	-70.56 ± 1.62	376.68 ± 1.45	139.65 ± 0.35	-28.31 ± 0.21	-31.24 ± 1.47	141.34 ± 0.83
146.48	322.02 ± 0.16	-43.18 ± 0.06	-44.34 ± 3.21	388.90 ± 1.33	148.47 ± 0.13	-31.19 ± 0.24	-28.34 ± 1.77	155.15 ± 1.02
156.25	322.01 ± 0.14	-38.20 ± 0.14	-33.82 ± 3.75	363.96 ± 2.38	158.22 ± 0.23	-32.81 ± 0.08	-32.38 ± 2.80	153.48 ± 2.00
166.02	325.96 ± 0.33	-42.95 ± 0.05	-60.21 ± 2.55	399.13 ± 3.09	167.02 ± 0.24	-37.79 ± 0.07	-45.11 ± 2.35	191.61 ± 4.04
175.78	326.22 ± 0.32	-38.78 ± 0.10	-57.65 ± 2.57	394.18 ± 1.83	176.79 ± 0.22	-41.65 ± 0.14	-41.56 ± 4.81	192.06 ± 2.29
185.55	329.53 ± 0.20	-37.27 ± 0.12	-66.16 ± 2.47	412.75 ± 1.68	188.44 ± 0.26	-43.22 ± 0.06	-40.19 ± 2.02	182.30 ± 0.85
195.31	332.12 ± 0.27	-33.02 ± 0.05	-34.10 ± 7.80	395.18 ± 1.83	202.15 ± 0.17	-46.02 ± 0.08	-36.24 ± 1.37	193.79 ± 1.29
205.08	333.11 ± 0.49	-31.04 ± 0.09	-58.01 ± 1.22	414.31 ± 0.75	210.02 ± 0.20	-49.46 ± 0.07	-33.41 ± 0.91	217.48 ± 0.97
214.84	341.66 ± 0.34	-26.97 ± 0.12	-44.76 ± 1.91	432.39 ± 1.44	222.22 ± 0.28	-51.10 ± 0.10	-52.45 ± 2.89	211.62 ± 1.99
224.61	345.62 ± 0.47	-18.40 ± 0.07	-41.62 ± 2.93	373.77 ± 1.77	231.82 ± 0.41	-54.24 ± 0.13	-35.10 ± 1.80	223.61 ± 1.92
234.38	353.24 ± 0.50	-30.69 ± 0.07	-46.42 ± 3.54	439.28 ± 2.13	242.45 ± 0.18	-62.47 ± 0.16	-23.53 ± 4.58	228.03 ± 3.98
244.14	355.27 ± 0.48	-26.89 ± 0.07	-33.41 ± 4.19	432.42 ± 1.28	254.64 ± 0.14	-61.77 ± 0.06	-35.38 ± 0.63	239.16 ± 1.05

Table F. 6. Dynamic-stiffness 6,800 rpm 2,177 kPa (modified bearing)

Frequency [Hz]	Re (H_{xx}) [MN/m]	Re (H_{xy}) [MN/m]	Re (H_{yx}) [MN/m]	Re (H_{yy}) [MN/m]	Im (H_{xx}) [MN/m]	Im (H_{xy}) [MN/m]	Im (H_{yx}) [MN/m]	Im (H_{yy}) [MN/m]
9.77	259.31 ± 0.50	-61.53 ± 0.57	-56.37 ± 0.20	296.22 ± 0.87	11.40 ± 0.43	0.80 ± 0.91	3.52 ± 0.55	2.86 ± 1.55
19.53	260.47 ± 0.42	-59.47 ± 0.63	-57.40 ± 0.31	299.88 ± 0.87	18.42 ± 0.37	-2.69 ± 0.83	-4.72 ± 0.58	13.45 ± 1.66
29.30	262.07 ± 0.54	-63.01 ± 0.99	-56.65 ± 0.33	298.25 ± 1.03	26.07 ± 0.36	-6.15 ± 0.51	-8.92 ± 0.57	18.82 ± 1.77
39.06	263.80 ± 0.77	-58.60 ± 0.59	-54.27 ± 0.37	294.54 ± 0.87	34.22 ± 0.44	-6.29 ± 0.59	-12.38 ± 0.26	27.58 ± 1.38
48.83	264.06 ± 0.65	-55.06 ± 0.56	-54.11 ± 0.26	283.46 ± 0.69	40.41 ± 0.48	-5.19 ± 0.78	-13.70 ± 0.36	27.29 ± 1.59
58.59	271.20 ± 0.62	-56.34 ± 0.63	-55.41 ± 1.18	293.59 ± 0.89	48.32 ± 0.44	-4.48 ± 0.84	-2.92 ± 0.50	26.41 ± 1.48
68.36	268.44 ± 0.32	-54.30 ± 0.88	-61.54 ± 0.31	315.89 ± 0.88	55.56 ± 0.51	-9.53 ± 0.94	-5.21 ± 0.46	7.55 ± 1.82
78.13	268.11 ± 0.75	-59.55 ± 0.78	-50.76 ± 0.46	273.34 ± 0.81	62.57 ± 0.29	-2.98 ± 0.53	-14.98 ± 0.29	43.17 ± 1.65
87.89	267.96 ± 0.54	-52.81 ± 0.78	-58.41 ± 0.15	289.09 ± 0.72	66.66 ± 0.39	-13.42 ± 0.62	-20.32 ± 0.40	48.98 ± 1.71
97.66	269.31 ± 0.42	-46.99 ± 1.27	-64.58 ± 0.47	307.32 ± 1.45	78.61 ± 0.63	-39.67 ± 1.29	-24.12 ± 0.56	63.26 ± 2.30
107.42	270.94 ± 1.07	-48.50 ± 1.58	-57.70 ± 1.97	288.90 ± 1.67	78.89 ± 1.38	-9.62 ± 1.16	-18.22 ± 1.24	57.29 ± 2.20
117.19	264.72 ± 6.27	-41.31 ± 2.26	-51.28 ± 3.65	285.47 ± 3.16	84.25 ± 3.44	-15.86 ± 2.07	-21.65 ± 6.07	78.18 ± 2.98
126.95	270.98 ± 0.37	-41.72 ± 0.69	-54.12 ± 0.90	294.71 ± 0.84	91.71 ± 0.96	-17.20 ± 0.59	-26.33 ± 0.63	77.60 ± 1.60
136.72	270.45 ± 0.21	-39.53 ± 0.68	-55.04 ± 0.62	295.71 ± 0.84	96.43 ± 0.61	-18.02 ± 0.53	-32.34 ± 0.40	89.07 ± 1.51
146.48	267.04 ± 0.57	-35.18 ± 1.07	-41.99 ± 0.30	279.78 ± 0.78	103.83 ± 0.25	-19.84 ± 0.59	-31.32 ± 0.29	105.79 ± 1.47
156.25	263.89 ± 0.33	-31.26 ± 0.87	-40.89 ± 0.35	267.60 ± 1.53	112.23 ± 0.66	-31.10 ± 1.12	-30.28 ± 0.22	91.94 ± 2.16
166.02	266.25 ± 0.42	-32.65 ± 0.48	-46.96 ± 0.29	285.81 ± 0.74	119.71 ± 0.29	-16.79 ± 0.58	-27.89 ± 0.18	98.51 ± 1.58
175.78	261.65 ± 0.26	-30.45 ± 0.55	-43.97 ± 0.21	291.76 ± 0.80	131.06 ± 0.23	-28.63 ± 0.55	-33.55 ± 0.14	118.97 ± 1.39
185.55	261.34 ± 0.37	-29.69 ± 0.58	-48.55 ± 0.34	300.46 ± 0.86	138.33 ± 0.18	-31.49 ± 0.55	-37.65 ± 0.24	125.92 ± 1.47
195.31	259.75 ± 0.58	-24.81 ± 0.72	-32.47 ± 0.34	278.42 ± 1.11	146.96 ± 0.40	-37.86 ± 0.77	-39.01 ± 0.54	136.02 ± 1.51
205.08	261.40 ± 0.31	-18.17 ± 1.28	-33.68 ± 0.31	283.43 ± 1.11	160.27 ± 0.51	-47.06 ± 0.90	-36.47 ± 0.28	153.70 ± 1.89
214.84	250.11 ± 0.48	6.19 ± 0.62	-40.81 ± 0.60	312.12 ± 1.00	160.93 ± 0.40	-36.07 ± 0.81	-27.97 ± 0.40	126.33 ± 1.60
224.61	255.08 ± 1.34	-5.92 ± 4.20	-41.38 ± 0.57	299.07 ± 2.29	175.76 ± 0.88	-44.99 ± 3.05	-32.88 ± 1.36	143.15 ± 4.88
234.38	255.04 ± 0.54	-17.81 ± 2.08	-28.90 ± 0.89	320.47 ± 2.02	189.84 ± 1.64	-50.51 ± 2.17	-51.66 ± 1.50	187.41 ± 2.66
244.14	251.46 ± 0.46	-11.81 ± 1.47	-37.20 ± 0.45	292.28 ± 1.32	200.14 ± 0.28	-48.73 ± 1.24	-31.85 ± 0.34	160.77 ± 2.03

Table F. 7. Dynamic-stiffness 6,800 rpm 2,903 kPa (original bearing)

Frequency [Hz]	Re (H_{xx}) [MN/m]	Re (H_{xy}) [MN/m]	Re (H_{yx}) [MN/m]	Re (H_{yy}) [MN/m]	Im (H_{xx}) [MN/m]	Im (H_{xy}) [MN/m]	Im (H_{yx}) [MN/m]	Im (H_{yy}) [MN/m]
9.77	317.07 ± 0.41	-66.96 ± 1.47	-103.86 ± 3.25	402.03 ± 5.59	11.32 ± 0.45	-4.86 ± 1.36	-18.57 ± 8.68	86.42 ± 6.62
19.53	314.88 ± 0.32	-68.11 ± 1.00	-67.00 ± 8.39	366.94 ± 2.76	20.34 ± 0.47	-5.71 ± 0.72	25.28 ± 14.81	5.21 ± 4.02
29.30	318.50 ± 0.24	-67.75 ± 0.37	-80.12 ± 3.04	385.25 ± 1.91	30.29 ± 0.14	-7.06 ± 0.60	-29.59 ± 2.72	43.73 ± 3.19
39.06	322.18 ± 0.21	-68.53 ± 0.52	-90.34 ± 3.23	408.99 ± 4.26	42.69 ± 0.21	-9.79 ± 0.40	-7.47 ± 15.25	36.07 ± 3.78
48.83	324.58 ± 0.10	-67.78 ± 0.20	-83.86 ± 5.29	407.15 ± 1.96	52.60 ± 0.11	-11.96 ± 0.27	-8.11 ± 3.43	48.10 ± 1.33
58.59	328.25 ± 0.19	-68.13 ± 0.27	-83.30 ± 3.95	409.92 ± 1.51	60.87 ± 0.20	-13.31 ± 0.17	-29.21 ± 3.63	55.87 ± 1.92
68.36	326.18 ± 0.23	-66.88 ± 0.14	-67.12 ± 5.18	407.41 ± 1.25	69.26 ± 0.33	-15.74 ± 0.10	-31.68 ± 3.69	58.32 ± 1.17
78.13	324.55 ± 0.18	-64.77 ± 0.17	-79.27 ± 1.80	394.22 ± 0.70	87.93 ± 0.17	-13.45 ± 0.21	-12.99 ± 4.15	66.36 ± 1.14
87.89	333.67 ± 0.24	-65.47 ± 0.25	-83.10 ± 1.25	418.55 ± 0.80	88.38 ± 0.36	-20.98 ± 0.20	-27.06 ± 1.24	94.20 ± 0.81
97.66	336.34 ± 0.46	-62.68 ± 0.33	-65.64 ± 3.94	400.51 ± 0.93	94.97 ± 0.60	-21.81 ± 0.20	-23.05 ± 0.92	83.49 ± 0.73
107.42	337.24 ± 0.40	-61.49 ± 0.43	-69.70 ± 4.99	411.73 ± 2.05	102.54 ± 1.54	-24.17 ± 1.17	-17.73 ± 2.79	104.88 ± 0.64
117.19	341.28 ± 1.17	-60.37 ± 0.73	-96.65 ± 4.91	419.74 ± 1.35	110.19 ± 0.94	-27.39 ± 0.51	-35.87 ± 1.97	110.24 ± 1.01
126.95	343.54 ± 0.54	-58.22 ± 0.27	-64.31 ± 1.16	415.07 ± 0.89	118.84 ± 0.29	-28.88 ± 0.27	-41.98 ± 5.24	126.11 ± 1.10
136.72	345.01 ± 0.39	-53.77 ± 0.11	-71.82 ± 1.25	413.13 ± 0.66	128.38 ± 0.17	-32.73 ± 0.25	-29.69 ± 4.21	134.29 ± 0.90
146.48	346.33 ± 0.32	-47.04 ± 0.14	-47.00 ± 3.20	401.85 ± 1.04	134.66 ± 0.08	-36.22 ± 0.08	-43.06 ± 1.55	148.97 ± 0.93
156.25	346.59 ± 0.34	-48.76 ± 0.08	-43.20 ± 3.55	407.64 ± 1.27	143.29 ± 0.18	-38.14 ± 0.15	-45.67 ± 1.94	130.32 ± 0.76
166.02	349.63 ± 0.23	-53.46 ± 0.08	-63.69 ± 1.09	441.54 ± 1.17	151.31 ± 0.34	-41.71 ± 0.13	-47.69 ± 3.72	175.43 ± 1.00
175.78	349.72 ± 0.32	-49.53 ± 0.15	-69.84 ± 2.58	442.34 ± 0.63	160.68 ± 0.36	-45.76 ± 0.08	-49.96 ± 5.48	180.74 ± 1.64
185.55	351.68 ± 0.20	-47.32 ± 0.06	-77.77 ± 1.60	450.82 ± 0.58	171.49 ± 0.35	-46.71 ± 0.10	-44.03 ± 1.08	179.28 ± 0.86
195.31	353.59 ± 0.27	-42.32 ± 0.04	-32.27 ± 4.47	439.19 ± 1.34	182.97 ± 0.33	-49.10 ± 0.08	-50.71 ± 3.57	180.37 ± 1.50
205.08	353.67 ± 0.54	-42.12 ± 0.08	-55.06 ± 1.00	459.88 ± 1.20	190.11 ± 0.32	-52.18 ± 0.10	-42.29 ± 2.34	202.74 ± 0.76
214.84	361.96 ± 0.33	-36.94 ± 0.11	-56.98 ± 3.45	464.00 ± 1.03	202.19 ± 0.42	-51.35 ± 0.10	-77.00 ± 4.67	195.10 ± 1.38
224.61	365.51 ± 0.63	-37.27 ± 0.42	-29.93 ± 4.70	430.76 ± 1.20	207.55 ± 3.13	-56.94 ± 0.65	-42.75 ± 0.92	195.18 ± 1.06
234.38	372.35 ± 0.43	-43.88 ± 0.13	-34.12 ± 5.09	488.46 ± 1.03	220.22 ± 0.23	-64.91 ± 0.11	-33.90 ± 2.11	214.90 ± 1.49
244.14	372.48 ± 0.39	-37.83 ± 0.07	-31.92 ± 1.40	482.07 ± 1.03	231.36 ± 0.28	-64.06 ± 0.08	-41.78 ± 1.73	228.29 ± 0.73

Table F. 8. Dynamic-stiffness 6,800 rpm 2,903 kPa (modified bearing)

Frequency [Hz]	Re (H_{xx}) [MN/m]	Re (H_{xy}) [MN/m]	Re (H_{yx}) [MN/m]	Re (H_{yy}) [MN/m]	Im (H_{xx}) [MN/m]	Im (H_{xy}) [MN/m]	Im (H_{yx}) [MN/m]	Im (H_{yy}) [MN/m]
9.77	290.46 ± 0.63	-68.44 ± 0.64	-62.41 ± 0.52	340.72 ± 0.76	9.23 ± 0.52	1.87 ± 1.05	2.71 ± 0.59	4.26 ± 1.95
19.53	288.79 ± 0.42	-66.67 ± 0.60	-63.53 ± 0.30	344.98 ± 0.87	15.06 ± 0.22	-0.29 ± 1.05	-4.22 ± 0.27	12.85 ± 1.37
29.30	290.45 ± 0.71	-68.26 ± 0.95	-62.41 ± 0.31	345.94 ± 1.01	22.45 ± 0.53	-3.94 ± 0.67	-7.48 ± 0.14	17.08 ± 1.56
39.06	291.42 ± 0.44	-63.38 ± 0.59	-60.98 ± 0.61	341.14 ± 0.79	30.13 ± 0.54	-6.47 ± 0.70	-9.60 ± 0.19	21.31 ± 1.51
48.83	290.55 ± 0.59	-58.99 ± 1.16	-59.16 ± 0.50	326.54 ± 1.00	33.30 ± 0.46	-3.73 ± 0.60	-11.38 ± 0.55	20.52 ± 1.54
58.59	293.64 ± 1.10	-59.80 ± 0.72	-60.47 ± 1.10	338.09 ± 0.90	39.46 ± 1.26	-2.22 ± 0.67	-2.60 ± 0.46	18.06 ± 1.47
68.36	294.15 ± 0.46	-62.39 ± 0.56	-64.06 ± 0.16	351.47 ± 1.12	45.86 ± 0.28	-4.10 ± 0.99	-5.99 ± 0.24	12.22 ± 1.93
78.13	293.76 ± 0.37	-67.79 ± 0.65	-52.42 ± 0.14	306.67 ± 0.79	53.01 ± 0.41	-3.22 ± 0.58	-12.26 ± 0.20	30.46 ± 1.50
87.89	292.29 ± 0.49	-57.27 ± 0.70	-60.05 ± 0.24	330.01 ± 0.72	57.03 ± 0.23	-12.96 ± 0.64	-18.62 ± 0.17	35.11 ± 1.73
97.66	293.43 ± 0.47	-57.06 ± 1.88	-64.37 ± 0.77	341.63 ± 1.76	66.45 ± 0.48	-40.11 ± 0.77	-19.94 ± 0.41	43.85 ± 2.79
107.42	293.95 ± 1.43	-52.89 ± 2.21	-59.41 ± 1.16	326.78 ± 2.82	66.80 ± 0.56	-9.53 ± 1.64	-18.82 ± 1.99	44.71 ± 2.30
117.19	290.59 ± 1.93	-43.41 ± 2.25	-50.70 ± 3.89	320.94 ± 4.74	72.02 ± 4.26	-14.29 ± 3.81	-24.51 ± 3.84	58.96 ± 2.47
126.95	291.39 ± 0.86	-44.44 ± 0.90	-55.81 ± 0.52	331.46 ± 0.76	80.06 ± 0.68	-17.55 ± 0.71	-25.19 ± 0.36	63.79 ± 1.69
136.72	289.40 ± 0.48	-41.62 ± 0.54	-55.23 ± 0.64	331.33 ± 0.83	86.26 ± 0.64	-19.41 ± 0.71	-30.59 ± 0.48	72.74 ± 1.52
146.48	285.01 ± 0.42	-35.34 ± 1.15	-43.47 ± 0.37	305.31 ± 0.78	92.64 ± 0.52	-20.76 ± 0.72	-30.53 ± 0.26	91.93 ± 1.81
156.25	282.46 ± 0.64	-32.40 ± 1.38	-42.72 ± 0.56	300.76 ± 2.11	100.90 ± 0.46	-36.80 ± 1.63	-27.69 ± 0.40	67.25 ± 2.17
166.02	284.80 ± 0.34	-35.02 ± 0.76	-48.72 ± 0.43	320.62 ± 0.98	107.33 ± 0.33	-17.98 ± 0.64	-30.30 ± 0.46	84.55 ± 1.66
175.78	279.94 ± 0.25	-32.85 ± 0.66	-45.47 ± 0.22	324.08 ± 0.82	118.32 ± 0.22	-30.79 ± 0.46	-34.65 ± 0.31	104.38 ± 1.48
185.55	279.99 ± 0.29	-32.44 ± 0.59	-48.36 ± 0.24	332.17 ± 0.68	125.50 ± 0.31	-34.76 ± 0.51	-39.55 ± 0.27	110.52 ± 1.52
195.31	275.92 ± 0.40	-26.33 ± 1.15	-33.73 ± 0.46	308.44 ± 1.00	133.62 ± 0.43	-43.59 ± 0.86	-40.35 ± 0.41	122.13 ± 1.83
205.08	276.14 ± 0.54	-23.77 ± 1.30	-35.33 ± 0.37	310.45 ± 1.09	145.88 ± 0.42	-51.88 ± 1.65	-38.32 ± 0.36	133.57 ± 2.51
214.84	266.43 ± 0.42	5.37 ± 1.00	-40.46 ± 0.58	337.51 ± 1.05	146.14 ± 0.36	-41.83 ± 0.61	-32.81 ± 0.43	114.22 ± 1.75
224.61	229.56 ± 48.95	-3.76 ± 15.15	-91.56 ± 51.14	350.56 ± 9.73	192.67 ± 29.54	-59.80 ± 9.80	-41.89 ± 13.55	124.37 ± 14.49
234.38	271.23 ± 1.31	-25.13 ± 1.45	-28.38 ± 1.76	361.07 ± 2.14	175.10 ± 1.15	-56.43 ± 2.13	-53.33 ± 0.99	182.68 ± 2.46
244.14	269.67 ± 0.37	-17.29 ± 0.91	-35.01 ± 0.41	317.18 ± 0.71	183.95 ± 0.30	-52.86 ± 0.71	-39.64 ± 0.38	149.72 ± 1.92

Table F. 9. Dynamic-stiffness 9,000 rpm 726 kPa (original bearing)

Frequency [Hz]	Re (H_{xx}) [MN/m]	Re (H_{xy}) [MN/m]	Re (H_{yx}) [MN/m]	Re (H_{yy}) [MN/m]	Im (H_{xx}) [MN/m]	Im (H_{xy}) [MN/m]	Im (H_{yx}) [MN/m]	Im (H_{yy}) [MN/m]
9.77	237.96 ± 0.57	-61.89 ± 1.51	-75.09 ± 1.43	239.73 ± 4.69	14.38 ± 0.62	-4.39 ± 1.44	-12.00 ± 2.75	26.02 ± 8.18
19.53	241.78 ± 0.33	-67.65 ± 1.15	-53.86 ± 4.74	218.75 ± 5.38	31.74 ± 0.46	-8.75 ± 1.00	12.05 ± 6.30	15.96 ± 7.19
29.30	242.39 ± 0.34	-66.00 ± 1.12	-71.91 ± 2.94	259.23 ± 3.24	43.78 ± 0.29	-7.42 ± 0.17	-16.85 ± 2.74	34.33 ± 3.76
39.06	245.55 ± 0.25	-67.56 ± 0.73	-76.72 ± 1.64	256.35 ± 1.92	55.04 ± 0.21	-7.62 ± 0.46	-12.69 ± 3.88	65.32 ± 1.66
48.83	251.23 ± 0.25	-65.74 ± 0.19	-60.82 ± 0.54	249.04 ± 0.90	70.80 ± 0.23	-9.56 ± 0.35	2.09 ± 0.46	74.05 ± 1.15
58.59	253.57 ± 0.16	-65.87 ± 0.26	-73.51 ± 1.65	263.24 ± 1.20	83.48 ± 0.51	-8.22 ± 0.52	-12.03 ± 0.93	89.87 ± 1.19
68.36	258.48 ± 0.36	-66.52 ± 0.29	-67.07 ± 0.87	265.38 ± 0.78	102.03 ± 0.31	-6.69 ± 0.23	-3.56 ± 2.00	98.33 ± 1.07
78.13	263.54 ± 0.19	-62.02 ± 0.25	-59.31 ± 1.01	257.11 ± 0.70	108.50 ± 0.21	-7.83 ± 0.30	-8.04 ± 0.55	101.31 ± 0.63
87.89	266.20 ± 0.19	-63.53 ± 0.20	-62.40 ± 0.56	283.03 ± 0.30	119.13 ± 0.19	-9.57 ± 0.13	-16.78 ± 1.34	129.01 ± 0.96
97.66	270.79 ± 0.29	-60.61 ± 0.19	-61.20 ± 0.78	276.78 ± 0.80	128.09 ± 0.29	-8.55 ± 0.16	-20.43 ± 2.82	128.94 ± 1.25
107.42	273.82 ± 0.13	-59.02 ± 0.28	-65.58 ± 0.31	285.87 ± 0.37	138.66 ± 0.26	-9.58 ± 0.30	-16.33 ± 0.42	147.77 ± 0.50
117.19	280.13 ± 0.23	-56.23 ± 0.14	-64.95 ± 0.77	294.96 ± 1.18	147.56 ± 0.24	-10.40 ± 0.16	-24.02 ± 1.10	155.30 ± 0.67
126.95	284.25 ± 0.34	-53.87 ± 0.23	-61.65 ± 0.93	291.20 ± 1.02	158.21 ± 0.25	-10.39 ± 0.11	-20.13 ± 1.48	164.78 ± 0.57
136.72	287.49 ± 0.52	-49.50 ± 0.14	-60.25 ± 1.79	299.54 ± 0.53	169.93 ± 0.24	-10.15 ± 0.27	-28.52 ± 0.57	169.71 ± 0.47
146.48	289.32 ± 1.40	-43.87 ± 0.92	-50.94 ± 1.97	298.98 ± 0.83	179.45 ± 0.26	-12.11 ± 0.47	-18.05 ± 1.70	172.29 ± 1.80
156.25	294.26 ± 1.35	-33.70 ± 0.41	-46.66 ± 3.87	275.45 ± 1.61	189.11 ± 0.70	-10.25 ± 0.69	-19.04 ± 1.13	171.39 ± 0.76
166.02	297.56 ± 0.42	-40.06 ± 0.24	-47.70 ± 1.70	318.15 ± 0.56	200.43 ± 0.63	-16.08 ± 0.39	-30.79 ± 3.18	210.56 ± 1.59
175.78	297.67 ± 0.38	-34.43 ± 0.17	-54.14 ± 1.74	320.20 ± 0.89	212.38 ± 0.55	-17.09 ± 0.16	-27.55 ± 2.00	212.23 ± 0.85
185.55	301.45 ± 0.37	-30.24 ± 0.16	-51.03 ± 1.52	324.30 ± 0.44	223.72 ± 0.53	-15.09 ± 0.23	-23.05 ± 1.05	215.81 ± 0.81
195.31	303.86 ± 0.15	-22.34 ± 0.16	-48.69 ± 1.95	316.48 ± 0.39	239.14 ± 0.34	-14.75 ± 0.18	-30.18 ± 1.56	232.11 ± 0.80
205.08	304.99 ± 0.48	-17.73 ± 0.15	-51.47 ± 1.23	327.76 ± 0.93	248.17 ± 0.43	-14.36 ± 0.21	-19.22 ± 0.44	251.41 ± 0.86
214.84	311.15 ± 0.19	-7.84 ± 0.07	-44.88 ± 1.89	327.36 ± 0.50	269.68 ± 0.43	-11.21 ± 0.23	-24.66 ± 2.15	249.09 ± 0.96
224.61	317.35 ± 0.32	28.08 ± 0.22	-54.77 ± 2.29	229.02 ± 1.02	286.16 ± 0.40	-4.03 ± 0.25	-24.88 ± 2.47	300.41 ± 0.58
234.38	326.39 ± 0.37	0.64 ± 0.20	-54.55 ± 2.70	353.25 ± 1.07	297.58 ± 0.33	-24.89 ± 0.14	-31.44 ± 0.81	288.40 ± 0.61
244.14	324.45 ± 0.41	6.69 ± 0.16	-47.31 ± 3.34	353.78 ± 1.11	318.76 ± 0.17	-23.98 ± 0.18	-22.50 ± 1.43	298.44 ± 1.31

Table F. 10. Dynamic-stiffness 9,000 rpm 726 kPa (modified bearing)

Frequency [Hz]	Re (H_{xx}) [MN/m]	Re (H_{xy}) [MN/m]	Re (H_{yx}) [MN/m]	Re (H_{yy}) [MN/m]	Im (H_{xx}) [MN/m]	Im (H_{xy}) [MN/m]	Im (H_{yx}) [MN/m]	Im (H_{yy}) [MN/m]
9.77	219.92 ± 0.58	-60.65 ± 1.05	-63.28 ± 0.83	205.44 ± 0.96	11.86 ± 0.63	-3.03 ± 1.39	0.66 ± 0.67	8.00 ± 1.64
19.53	220.53 ± 0.41	-62.10 ± 0.65	-64.12 ± 0.61	207.67 ± 1.11	23.52 ± 0.66	-8.72 ± 1.17	-5.76 ± 0.68	22.31 ± 1.94
29.30	221.24 ± 0.78	-63.41 ± 0.99	-65.03 ± 0.60	209.88 ± 1.20	35.10 ± 0.85	-12.55 ± 1.29	-8.10 ± 0.53	32.55 ± 2.01
39.06	224.34 ± 0.97	-61.87 ± 1.04	-65.62 ± 0.62	211.61 ± 1.31	42.07 ± 1.60	-11.49 ± 0.92	-16.23 ± 0.71	46.83 ± 1.53
48.83	225.47 ± 1.47	-63.66 ± 1.10	-62.29 ± 1.11	203.79 ± 1.50	52.55 ± 1.00	-14.16 ± 0.95	-15.95 ± 0.33	53.24 ± 1.72
58.59	231.60 ± 6.42	-65.74 ± 2.17	-64.17 ± 2.53	213.73 ± 1.34	66.93 ± 3.90	-15.94 ± 1.47	-5.50 ± 5.53	55.56 ± 2.79
68.36	234.95 ± 0.99	-82.78 ± 0.92	-55.71 ± 0.92	184.58 ± 2.87	71.42 ± 1.13	-18.08 ± 1.28	-11.28 ± 1.42	58.73 ± 2.34
78.13	230.71 ± 0.74	-67.67 ± 0.69	-60.32 ± 0.40	205.88 ± 1.17	78.84 ± 0.74	-12.18 ± 0.92	-15.88 ± 0.74	73.87 ± 2.08
87.89	235.21 ± 0.68	-68.54 ± 0.73	-71.88 ± 0.42	224.68 ± 0.86	88.56 ± 0.98	-17.97 ± 1.05	-19.12 ± 0.61	84.28 ± 1.92
97.66	236.83 ± 1.16	-62.67 ± 1.73	-78.66 ± 1.09	247.32 ± 2.77	99.89 ± 0.65	-35.07 ± 2.64	-18.70 ± 0.64	94.91 ± 2.81
107.42	238.54 ± 0.55	-67.96 ± 0.80	-72.57 ± 0.75	229.90 ± 1.12	102.71 ± 1.32	-14.51 ± 0.78	-17.47 ± 1.33	94.96 ± 1.99
117.19	240.58 ± 4.78	-70.65 ± 1.63	-60.73 ± 3.91	227.65 ± 1.76	111.67 ± 4.70	-18.11 ± 1.89	-9.23 ± 1.47	102.98 ± 2.10
126.95	238.85 ± 2.37	-65.36 ± 1.38	-68.40 ± 0.68	237.75 ± 0.96	116.96 ± 0.60	-13.98 ± 0.61	-18.43 ± 1.50	112.35 ± 1.87
136.72	239.62 ± 0.86	-64.29 ± 0.76	-71.73 ± 1.52	244.47 ± 0.92	124.51 ± 1.70	-12.02 ± 0.88	-20.97 ± 1.14	121.01 ± 1.63
146.48	237.02 ± 2.09	-63.84 ± 3.31	-59.70 ± 2.62	227.54 ± 1.51	136.94 ± 3.49	-13.62 ± 1.68	-25.56 ± 2.02	140.61 ± 2.94
156.25	238.54 ± 2.43	-60.01 ± 3.64	-52.48 ± 1.51	208.55 ± 4.60	147.29 ± 1.87	-13.67 ± 4.33	-30.35 ± 3.10	130.81 ± 5.15
166.02	238.61 ± 0.39	-58.20 ± 1.43	-59.09 ± 0.48	231.01 ± 0.94	153.83 ± 0.57	-9.94 ± 0.86	-21.54 ± 0.46	135.44 ± 1.98
175.78	234.40 ± 0.27	-56.39 ± 0.77	-57.36 ± 0.45	241.34 ± 1.14	167.23 ± 0.25	-12.27 ± 0.91	-24.38 ± 0.38	152.15 ± 1.73
185.55	234.13 ± 1.23	-54.43 ± 0.73	-61.53 ± 0.37	254.28 ± 1.08	176.11 ± 0.34	-12.90 ± 0.82	-24.55 ± 0.37	158.16 ± 1.50
195.31	228.33 ± 0.42	-49.86 ± 1.27	-46.81 ± 0.74	234.09 ± 1.28	192.39 ± 0.42	-14.92 ± 1.41	-21.22 ± 1.22	171.39 ± 1.70
205.08	229.49 ± 1.04	-36.70 ± 2.37	-54.66 ± 0.98	239.76 ± 3.20	203.27 ± 1.14	-9.22 ± 1.37	-18.19 ± 0.63	183.53 ± 1.78
214.84	225.20 ± 1.45	-20.27 ± 1.08	-40.07 ± 0.85	248.20 ± 1.15	227.45 ± 0.87	-5.50 ± 0.87	1.55 ± 0.83	159.97 ± 1.69
224.61	225.35 ± 1.03	-23.25 ± 1.38	-46.80 ± 0.54	208.04 ± 1.25	261.61 ± 0.79	-4.27 ± 2.23	-9.82 ± 0.53	193.19 ± 1.78
234.38	164.96 ± 3.43	-22.55 ± 1.33	-84.77 ± 1.53	273.11 ± 2.73	268.29 ± 1.49	-18.50 ± 2.06	44.23 ± 1.97	221.29 ± 2.28
244.14	178.43 ± 2.63	-6.65 ± 2.52	-12.43 ± 2.48	252.18 ± 1.87	380.49 ± 2.17	-20.43 ± 1.43	90.39 ± 1.60	178.04 ± 2.23

Table F. 11. Dynamic-stiffness 9,000 rpm 1,452 kPa (original bearing)

Frequency [Hz]	Re (H_{xx}) [MN/m]	Re (H_{xy}) [MN/m]	Re (H_{yx}) [MN/m]	Re (H_{yy}) [MN/m]	Im (H_{xx}) [MN/m]	Im (H_{xy}) [MN/m]	Im (H_{yx}) [MN/m]	Im (H_{yy}) [MN/m]
9.77	274.36 ± 0.48	-65.04 ± 2.10	-72.24 ± 0.78	317.66 ± 1.00	13.51 ± 0.34	-5.40 ± 1.08	-10.07 ± 2.79	34.02 ± 3.14
19.53	276.09 ± 0.44	-71.91 ± 1.51	-62.32 ± 4.28	286.27 ± 2.22	25.33 ± 0.40	-6.48 ± 0.64	10.77 ± 4.47	8.76 ± 5.91
29.30	278.86 ± 0.30	-68.41 ± 0.78	-75.69 ± 1.84	336.24 ± 4.49	38.93 ± 0.39	-10.53 ± 0.50	-13.13 ± 0.99	18.58 ± 2.51
39.06	282.51 ± 0.34	-68.61 ± 0.51	-72.07 ± 3.60	322.37 ± 1.77	50.16 ± 0.15	-11.40 ± 0.09	-17.31 ± 3.03	41.22 ± 1.50
48.83	286.80 ± 0.22	-68.21 ± 0.29	-65.19 ± 0.39	313.29 ± 0.60	63.12 ± 0.23	-12.92 ± 0.20	-13.47 ± 1.23	60.00 ± 0.58
58.59	289.16 ± 0.47	-68.81 ± 0.36	-71.69 ± 1.30	323.09 ± 0.92	73.52 ± 0.20	-12.54 ± 0.19	-22.97 ± 1.02	70.68 ± 1.06
68.36	289.08 ± 0.39	-69.58 ± 0.46	-68.57 ± 0.48	318.62 ± 0.77	84.05 ± 0.28	-13.72 ± 0.21	-19.83 ± 1.00	64.68 ± 0.85
78.13	296.79 ± 0.19	-66.06 ± 0.19	-64.46 ± 0.68	311.52 ± 0.48	97.91 ± 0.22	-13.47 ± 0.09	-20.79 ± 0.64	76.78 ± 0.80
87.89	298.49 ± 0.21	-68.74 ± 0.20	-73.64 ± 0.27	336.24 ± 0.48	105.43 ± 0.28	-15.14 ± 0.17	-24.04 ± 0.66	103.58 ± 0.87
97.66	301.58 ± 0.32	-66.16 ± 0.33	-70.87 ± 0.49	325.14 ± 0.42	112.92 ± 0.12	-15.04 ± 0.20	-18.65 ± 0.97	105.54 ± 0.41
107.42	304.96 ± 0.15	-64.74 ± 0.10	-70.87 ± 0.57	335.95 ± 0.88	122.80 ± 0.19	-16.56 ± 0.25	-22.96 ± 0.66	121.62 ± 0.78
117.19	310.16 ± 0.16	-62.95 ± 0.12	-73.78 ± 0.65	339.30 ± 0.32	130.77 ± 0.45	-16.90 ± 0.15	-35.33 ± 0.59	129.15 ± 0.59
126.95	312.32 ± 0.27	-59.57 ± 0.28	-69.27 ± 0.80	334.62 ± 0.66	140.63 ± 0.21	-17.05 ± 0.18	-28.61 ± 0.55	142.15 ± 0.43
136.72	315.20 ± 0.43	-54.57 ± 0.37	-73.84 ± 0.66	340.14 ± 0.62	149.72 ± 0.32	-17.12 ± 0.59	-30.66 ± 0.37	149.39 ± 0.86
146.48	317.28 ± 1.18	-50.63 ± 1.13	-59.86 ± 0.86	341.30 ± 1.56	159.54 ± 0.39	-20.19 ± 1.02	-28.40 ± 1.30	152.15 ± 1.14
156.25	317.20 ± 0.72	-43.10 ± 1.09	-59.51 ± 1.92	325.49 ± 1.88	168.70 ± 0.39	-20.07 ± 0.91	-25.40 ± 0.64	142.63 ± 1.49
166.02	321.47 ± 0.29	-48.55 ± 0.26	-64.72 ± 0.53	360.81 ± 1.74	177.86 ± 0.57	-23.96 ± 0.43	-33.54 ± 1.43	183.75 ± 0.72
175.78	320.52 ± 0.29	-41.80 ± 0.29	-65.52 ± 0.35	359.05 ± 0.81	186.84 ± 0.35	-25.57 ± 0.33	-38.60 ± 1.09	187.60 ± 0.61
185.55	324.12 ± 0.20	-38.12 ± 0.23	-56.91 ± 0.17	362.39 ± 0.65	199.89 ± 0.25	-25.35 ± 0.19	-36.11 ± 0.67	193.07 ± 0.55
195.31	325.45 ± 0.16	-31.27 ± 0.11	-61.39 ± 1.20	356.47 ± 1.16	213.04 ± 0.21	-26.15 ± 0.29	-32.40 ± 0.95	203.60 ± 0.58
205.08	325.32 ± 0.36	-27.73 ± 0.13	-57.80 ± 0.96	373.93 ± 0.76	221.68 ± 0.29	-30.10 ± 0.13	-37.54 ± 0.90	227.11 ± 0.63
214.84	332.91 ± 0.18	-19.16 ± 0.23	-51.18 ± 1.65	375.51 ± 1.33	235.50 ± 0.33	-29.36 ± 0.34	-41.30 ± 0.74	219.03 ± 1.02
224.61	335.93 ± 0.14	-8.82 ± 0.18	-55.23 ± 1.13	322.12 ± 1.15	246.89 ± 0.41	-30.02 ± 0.42	-34.54 ± 0.36	232.50 ± 0.44
234.38	342.87 ± 0.26	-16.07 ± 0.20	-62.30 ± 1.35	390.06 ± 0.91	260.54 ± 0.22	-43.21 ± 0.11	-37.63 ± 0.79	257.20 ± 0.57
244.14	344.00 ± 0.30	-10.08 ± 0.13	-51.49 ± 0.90	387.70 ± 1.31	275.61 ± 0.22	-43.61 ± 0.09	-39.61 ± 0.60	266.78 ± 0.66

Table F. 12. Dynamic-stiffness 9,000 rpm 1,452 kPa (modified bearing)

Frequency [Hz]	Re (H_{xx}) [MN/m]	Re (H_{xy}) [MN/m]	Re (H_{yx}) [MN/m]	Re (H_{yy}) [MN/m]	Im (H_{xx}) [MN/m]	Im (H_{xy}) [MN/m]	Im (H_{yx}) [MN/m]	Im (H_{yy}) [MN/m]
9.77	247.00 ± 0.96	-65.51 ± 1.87	-62.26 ± 0.62	261.19 ± 1.77	12.01 ± 1.36	-2.22 ± 1.15	0.70 ± 1.07	4.06 ± 2.17
19.53	246.04 ± 1.05	-63.93 ± 2.40	-62.40 ± 0.51	262.39 ± 1.44	24.28 ± 1.25	-5.21 ± 1.20	-4.79 ± 0.64	17.05 ± 2.09
29.30	250.87 ± 0.61	-67.17 ± 1.64	-62.00 ± 0.76	263.21 ± 1.16	30.43 ± 1.01	-8.05 ± 0.88	-11.69 ± 0.60	25.71 ± 1.55
39.06	253.60 ± 0.59	-65.90 ± 0.79	-60.34 ± 0.83	260.34 ± 1.10	41.94 ± 0.91	-9.47 ± 1.20	-14.80 ± 0.42	35.70 ± 2.26
48.83	254.56 ± 1.49	-66.30 ± 1.77	-60.45 ± 1.04	249.53 ± 1.11	49.52 ± 1.46	-10.42 ± 1.79	-13.10 ± 0.77	36.72 ± 1.77
58.59	264.01 ± 4.87	-65.98 ± 1.70	-63.31 ± 3.22	263.19 ± 1.39	53.02 ± 2.42	-9.10 ± 1.12	-4.18 ± 1.54	36.10 ± 1.90
68.36	263.05 ± 1.16	-73.60 ± 1.69	-64.23 ± 0.54	258.24 ± 1.78	71.55 ± 1.11	-38.06 ± 0.89	7.75 ± 1.53	-43.22 ± 1.93
78.13	261.91 ± 0.60	-70.90 ± 1.40	-58.99 ± 0.73	252.04 ± 1.77	74.57 ± 0.40	-9.32 ± 0.87	-16.92 ± 0.54	55.35 ± 1.77
87.89	261.99 ± 1.19	-66.97 ± 0.91	-70.10 ± 0.80	263.78 ± 1.01	79.33 ± 0.89	-15.40 ± 0.86	-22.39 ± 0.82	63.49 ± 1.81
97.66	264.70 ± 1.22	-63.54 ± 1.33	-76.61 ± 0.50	285.72 ± 1.73	91.62 ± 1.07	-33.61 ± 3.03	-24.52 ± 0.68	76.96 ± 3.43
107.42	268.95 ± 0.56	-67.24 ± 1.02	-68.93 ± 0.41	266.28 ± 1.05	91.21 ± 0.57	-12.46 ± 1.13	-19.38 ± 0.65	69.08 ± 1.52
117.19	263.27 ± 1.23	-63.24 ± 1.02	-63.56 ± 0.92	261.41 ± 0.86	98.54 ± 2.90	-14.70 ± 1.50	-23.63 ± 0.53	90.80 ± 2.49
126.95	268.42 ± 0.55	-60.33 ± 1.05	-69.95 ± 1.41	274.78 ± 1.17	103.60 ± 0.92	-15.43 ± 0.90	-26.82 ± 1.44	90.26 ± 1.61
136.72	270.47 ± 2.32	-57.10 ± 1.12	-69.86 ± 1.40	277.05 ± 1.29	109.29 ± 1.21	-15.05 ± 0.98	-32.56 ± 1.23	99.60 ± 1.68
146.48	267.18 ± 2.78	-59.33 ± 3.98	-56.98 ± 2.43	255.34 ± 2.23	115.41 ± 1.64	-12.59 ± 4.46	-30.90 ± 3.10	116.65 ± 4.67
156.25	266.25 ± 2.31	-53.61 ± 6.74	-51.86 ± 2.24	241.71 ± 4.48	125.53 ± 1.79	-24.06 ± 3.32	-27.49 ± 2.25	98.79 ± 4.15
166.02	270.37 ± 0.72	-53.88 ± 1.83	-59.47 ± 0.76	265.47 ± 1.45	133.35 ± 0.96	-13.40 ± 1.42	-23.97 ± 0.73	106.97 ± 1.51
175.78	264.81 ± 0.43	-49.90 ± 0.80	-57.74 ± 0.34	272.84 ± 1.07	143.87 ± 0.54	-18.72 ± 0.66	-29.00 ± 0.45	125.93 ± 1.46
185.55	265.02 ± 0.50	-49.69 ± 0.78	-62.25 ± 0.61	282.44 ± 1.16	149.77 ± 0.43	-18.94 ± 0.62	-32.99 ± 0.14	133.60 ± 1.54
195.31	262.64 ± 0.84	-44.54 ± 1.21	-46.10 ± 0.94	257.61 ± 1.14	161.11 ± 0.87	-24.27 ± 1.08	-35.42 ± 1.04	145.47 ± 1.62
205.08	263.53 ± 0.68	-35.64 ± 2.10	-48.40 ± 1.39	266.58 ± 2.41	173.94 ± 0.79	-31.83 ± 2.35	-33.85 ± 0.81	164.40 ± 3.81
214.84	250.83 ± 0.49	-9.72 ± 1.04	-54.31 ± 0.70	285.83 ± 1.05	174.29 ± 0.55	-17.30 ± 1.09	-20.50 ± 0.60	132.27 ± 1.42
224.61	254.18 ± 0.57	-16.78 ± 1.22	-53.10 ± 0.60	268.70 ± 1.88	187.61 ± 0.51	-23.67 ± 0.71	-26.09 ± 0.95	157.09 ± 2.52
234.38	260.27 ± 0.89	-28.69 ± 0.70	-44.15 ± 1.72	296.70 ± 2.34	205.24 ± 2.66	-29.30 ± 1.74	-37.85 ± 2.78	201.22 ± 3.62
244.14	246.42 ± 0.62	-18.07 ± 1.75	-56.50 ± 0.59	266.81 ± 1.65	220.95 ± 0.63	-27.24 ± 1.62	-15.31 ± 0.43	176.22 ± 2.20

Table F. 13. Dynamic-stiffness 9,000 rpm 2,177 kPa (original bearing)

Frequency [Hz]	Re (H_{xx}) [MN/m]	Re (H_{xy}) [MN/m]	Re (H_{yx}) [MN/m]	Re (H_{yy}) [MN/m]	Im (H_{xx}) [MN/m]	Im (H_{xy}) [MN/m]	Im (H_{yx}) [MN/m]	Im (H_{yy}) [MN/m]
9.77	306.94 ± 1.16	-71.41 ± 0.92	-85.49 ± 5.33	412.73 ± 3.95	11.61 ± 0.68	-5.37 ± 2.09	-16.22 ± 5.54	4.19 ± 15.07
19.53	305.16 ± 0.45	-73.02 ± 1.32	-69.10 ± 7.28	254.43 ± 19.16	24.72 ± 0.49	-9.99 ± 1.01	-20.86 ± 17.64	55.97 ± 11.40
29.30	308.71 ± 0.62	-70.48 ± 0.83	-76.84 ± 9.52	405.35 ± 4.79	34.77 ± 0.22	-10.07 ± 0.41	-10.34 ± 3.87	-9.47 ± 7.70
39.06	311.91 ± 0.35	-71.38 ± 0.63	-61.24 ± 6.77	361.04 ± 2.25	45.78 ± 0.35	-10.90 ± 0.66	-8.91 ± 11.64	31.95 ± 3.64
48.83	315.89 ± 0.30	-71.94 ± 0.61	-70.83 ± 1.56	356.61 ± 1.82	57.87 ± 0.14	-13.24 ± 0.34	-8.42 ± 0.83	52.09 ± 1.46
58.59	317.82 ± 0.66	-71.72 ± 0.32	-72.81 ± 8.76	374.82 ± 2.50	67.85 ± 0.53	-12.93 ± 0.32	-23.82 ± 1.15	59.59 ± 1.80
68.36	318.67 ± 0.38	-71.77 ± 0.30	-77.79 ± 2.52	363.68 ± 1.33	77.37 ± 0.27	-15.28 ± 0.22	-16.70 ± 5.43	46.59 ± 2.26
78.13	326.20 ± 0.13	-67.97 ± 0.20	-68.85 ± 1.75	355.45 ± 1.19	92.81 ± 0.17	-14.46 ± 0.15	-14.80 ± 1.92	62.94 ± 1.38
87.89	326.47 ± 0.09	-71.83 ± 0.09	-78.44 ± 0.27	378.67 ± 0.61	96.36 ± 0.15	-18.11 ± 0.23	-27.55 ± 2.12	91.56 ± 0.91
97.66	329.34 ± 0.33	-69.70 ± 0.22	-74.08 ± 2.42	366.23 ± 1.65	103.16 ± 0.29	-18.42 ± 0.18	-27.42 ± 1.10	94.46 ± 1.22
107.42	332.30 ± 0.15	-68.44 ± 0.18	-79.30 ± 2.07	380.43 ± 1.69	111.75 ± 0.34	-19.51 ± 0.11	-29.66 ± 2.86	107.60 ± 1.05
117.19	336.45 ± 0.11	-66.41 ± 0.10	-78.65 ± 4.18	375.33 ± 1.78	119.13 ± 0.27	-20.59 ± 0.16	-35.37 ± 1.53	120.16 ± 1.20
126.95	339.24 ± 0.32	-63.04 ± 0.27	-73.97 ± 1.37	373.16 ± 1.28	127.70 ± 0.41	-20.55 ± 0.37	-34.77 ± 2.55	125.25 ± 1.04
136.72	341.03 ± 0.41	-58.49 ± 0.36	-74.98 ± 1.58	385.49 ± 2.35	136.72 ± 0.59	-23.06 ± 0.26	-33.29 ± 2.25	129.79 ± 1.35
146.48	342.72 ± 1.13	-53.35 ± 0.90	-67.92 ± 1.33	393.17 ± 2.22	143.18 ± 1.39	-25.02 ± 1.26	-30.23 ± 2.08	132.32 ± 1.36
156.25	342.71 ± 1.06	-48.95 ± 0.74	-59.96 ± 4.14	371.00 ± 1.40	153.29 ± 0.99	-26.19 ± 0.63	-32.69 ± 3.14	132.28 ± 2.55
166.02	346.46 ± 0.55	-53.57 ± 0.35	-75.67 ± 2.70	402.46 ± 0.88	160.49 ± 0.58	-30.29 ± 0.22	-35.35 ± 1.54	162.17 ± 1.87
175.78	346.41 ± 0.42	-48.23 ± 0.12	-78.27 ± 2.78	403.86 ± 2.06	168.41 ± 0.46	-32.64 ± 0.29	-40.97 ± 4.64	169.26 ± 1.61
185.55	347.66 ± 0.19	-44.46 ± 0.23	-69.26 ± 3.39	403.07 ± 1.61	180.28 ± 0.33	-33.18 ± 0.15	-32.27 ± 0.62	174.11 ± 0.98
195.31	348.45 ± 0.17	-38.96 ± 0.28	-62.59 ± 4.43	388.65 ± 1.65	191.61 ± 0.25	-35.74 ± 0.14	-37.09 ± 5.25	185.02 ± 1.44
205.08	348.23 ± 0.38	-33.70 ± 0.16	-61.93 ± 2.50	400.78 ± 1.57	199.37 ± 0.22	-37.81 ± 0.12	-37.69 ± 2.51	211.89 ± 2.12
214.84	355.71 ± 0.14	-27.86 ± 0.16	-56.82 ± 5.04	412.33 ± 1.96	212.15 ± 0.34	-40.00 ± 0.25	-50.58 ± 5.63	210.88 ± 1.91
224.61	356.03 ± 0.29	-16.47 ± 0.19	-55.15 ± 2.14	359.33 ± 2.40	222.27 ± 0.42	-44.72 ± 0.17	-45.23 ± 2.56	221.15 ± 2.84
234.38	363.11 ± 0.36	-27.93 ± 0.12	-57.01 ± 1.93	420.55 ± 1.53	233.71 ± 0.18	-54.80 ± 0.25	-47.37 ± 1.39	240.29 ± 0.61
244.14	362.78 ± 0.21	-22.74 ± 0.15	-53.01 ± 3.51	422.60 ± 2.04	246.64 ± 0.31	-55.17 ± 0.11	-41.38 ± 3.01	249.12 ± 2.10

Table F. 14. Dynamic-stiffness 9,000 rpm 2,177 kPa (modified bearing)

Frequency [Hz]	Re (H_{xx}) [MN/m]	Re (H_{xy}) [MN/m]	Re (H_{yx}) [MN/m]	Re (H_{yy}) [MN/m]	Im (H_{xx}) [MN/m]	Im (H_{xy}) [MN/m]	Im (H_{yx}) [MN/m]	Im (H_{yy}) [MN/m]
9.77	272.25 ± 1.43	-71.01 ± 2.20	-67.34 ± 1.21	310.49 ± 1.30	10.10 ± 1.79	1.55 ± 1.16	0.75 ± 1.81	5.42 ± 2.07
19.53	274.94 ± 1.80	-71.01 ± 0.93	-66.78 ± 0.76	312.58 ± 1.01	21.91 ± 1.48	-4.95 ± 1.33	-4.56 ± 1.25	13.49 ± 2.16
29.30	277.12 ± 1.00	-77.23 ± 2.75	-65.95 ± 0.84	310.69 ± 2.24	28.09 ± 1.33	-6.45 ± 1.57	-9.32 ± 1.61	19.38 ± 2.00
39.06	280.08 ± 1.25	-69.95 ± 2.80	-63.77 ± 0.76	309.67 ± 2.11	35.87 ± 0.84	-7.37 ± 0.79	-12.89 ± 0.66	27.66 ± 1.80
48.83	280.25 ± 1.69	-65.86 ± 2.02	-63.22 ± 0.87	298.00 ± 1.50	40.36 ± 0.94	-5.71 ± 2.10	-16.22 ± 1.56	29.83 ± 2.30
58.59	286.58 ± 2.55	-70.58 ± 1.56	-65.24 ± 1.60	308.80 ± 1.44	59.07 ± 2.11	-8.67 ± 2.25	-2.90 ± 1.56	25.56 ± 2.28
68.36	284.14 ± 2.51	-63.68 ± 2.92	-73.44 ± 1.87	337.40 ± 2.81	59.70 ± 0.80	-11.09 ± 1.41	-6.97 ± 0.81	7.69 ± 1.90
78.13	286.69 ± 1.43	-74.79 ± 1.33	-60.43 ± 0.88	289.73 ± 1.09	63.21 ± 1.11	-5.49 ± 1.41	-18.63 ± 0.52	41.47 ± 2.06
87.89	289.63 ± 0.73	-69.39 ± 0.96	-68.73 ± 0.49	306.07 ± 1.03	71.29 ± 0.89	-14.94 ± 2.03	-21.30 ± 0.62	44.87 ± 2.10
97.66	289.38 ± 1.09	-67.38 ± 2.59	-75.62 ± 1.33	323.06 ± 1.73	82.62 ± 1.13	-41.19 ± 4.18	-22.17 ± 1.19	51.94 ± 3.68
107.42	294.18 ± 1.97	-68.69 ± 1.83	-70.62 ± 1.48	304.70 ± 1.62	79.50 ± 2.21	-10.05 ± 0.96	-21.19 ± 1.37	54.46 ± 1.84
117.19	291.20 ± 4.95	-57.49 ± 1.91	-63.15 ± 2.59	302.81 ± 1.54	81.94 ± 1.15	-12.32 ± 1.29	-27.53 ± 1.42	72.12 ± 2.40
126.95	292.37 ± 0.86	-59.92 ± 1.21	-68.50 ± 0.69	312.97 ± 0.85	93.77 ± 0.67	-14.92 ± 0.95	-26.13 ± 1.14	71.30 ± 2.02
136.72	294.70 ± 1.84	-58.64 ± 1.61	-68.96 ± 0.80	314.24 ± 0.86	95.16 ± 1.85	-13.88 ± 0.89	-32.64 ± 1.34	81.04 ± 1.90
146.48	292.86 ± 2.58	-52.36 ± 5.35	-54.52 ± 2.41	287.77 ± 3.14	101.54 ± 2.42	-12.78 ± 2.99	-32.98 ± 1.92	97.16 ± 6.31
156.25	289.79 ± 1.43	-53.47 ± 5.36	-52.72 ± 1.63	277.88 ± 6.43	109.30 ± 0.73	-27.02 ± 2.68	-28.55 ± 2.05	78.61 ± 4.39
166.02	290.27 ± 1.46	-51.37 ± 1.36	-59.66 ± 0.99	302.32 ± 1.88	115.82 ± 0.97	-10.66 ± 1.11	-26.08 ± 1.19	89.59 ± 2.53
175.78	286.09 ± 0.72	-47.74 ± 0.81	-57.07 ± 0.62	307.79 ± 1.01	126.27 ± 0.66	-21.34 ± 0.79	-31.56 ± 0.50	104.68 ± 1.74
185.55	287.05 ± 0.94	-48.82 ± 1.04	-60.23 ± 0.75	314.24 ± 1.15	132.61 ± 0.58	-22.83 ± 0.91	-34.60 ± 0.45	110.98 ± 1.67
195.31	284.70 ± 1.70	-39.51 ± 1.47	-43.17 ± 1.17	291.94 ± 1.60	139.09 ± 1.74	-30.09 ± 1.41	-38.30 ± 1.42	123.33 ± 2.31
205.08	284.96 ± 0.90	-34.65 ± 2.78	-45.06 ± 0.79	298.01 ± 2.48	151.32 ± 1.24	-38.86 ± 2.01	-37.39 ± 0.71	138.59 ± 3.41
214.84	272.48 ± 0.70	-8.82 ± 1.61	-51.10 ± 0.72	317.71 ± 1.47	150.40 ± 0.55	-23.36 ± 1.68	-27.70 ± 0.51	109.62 ± 2.49
224.61	276.30 ± 0.79	-17.33 ± 1.74	-51.51 ± 0.62	305.07 ± 1.97	162.70 ± 0.85	-29.15 ± 2.55	-33.72 ± 0.88	131.73 ± 2.55
234.38	275.51 ± 2.12	-29.22 ± 1.79	-43.65 ± 1.74	329.32 ± 2.26	172.91 ± 2.28	-33.97 ± 1.88	-54.54 ± 1.52	180.08 ± 2.94
244.14	270.89 ± 0.57	-22.11 ± 1.86	-49.36 ± 0.68	297.59 ± 1.82	188.73 ± 0.77	-33.77 ± 1.63	-32.55 ± 0.79	145.83 ± 2.12

Table F. 15. Dynamic-stiffness 9,000 rpm 2,903 kPa (original bearing)

Frequency [Hz]	Re (H_{xx}) [MN/m]	Re (H_{xy}) [MN/m]	Re (H_{yx}) [MN/m]	Re (H_{yy}) [MN/m]	Im (H_{xx}) [MN/m]	Im (H_{xy}) [MN/m]	Im (H_{yx}) [MN/m]	Im (H_{yy}) [MN/m]
9.77	331.54 ± 1.62	-75.30 ± 1.21	-96.00 ± 3.20	461.82 ± 5.51	11.15 ± 1.57	-5.94 ± 4.06	-41.01 ± 7.91	76.91 ± 9.66
19.53	327.77 ± 0.47	-73.98 ± 0.49	-120.89 ± 4.18	402.29 ± 3.83	21.14 ± 0.38	-10.30 ± 1.46	-39.55 ± 4.60	40.47 ± 5.23
29.30	332.64 ± 0.72	-74.06 ± 0.81	-66.97 ± 1.78	420.24 ± 1.28	29.96 ± 0.45	-8.65 ± 0.61	-8.66 ± 1.29	21.96 ± 1.78
39.06	335.31 ± 0.47	-75.92 ± 0.75	-75.09 ± 2.39	411.61 ± 1.63	42.79 ± 0.57	-11.61 ± 0.54	22.71 ± 5.56	18.56 ± 1.99
48.83	338.63 ± 0.19	-74.85 ± 0.47	-87.90 ± 2.56	409.40 ± 1.02	53.63 ± 0.31	-13.64 ± 0.69	-9.19 ± 1.37	39.56 ± 1.08
58.59	342.98 ± 0.32	-75.11 ± 0.27	-77.79 ± 2.33	414.86 ± 0.90	61.57 ± 0.30	-14.53 ± 0.65	-25.62 ± 1.55	52.77 ± 1.06
68.36	339.87 ± 0.30	-74.40 ± 0.27	-84.53 ± 1.42	410.40 ± 0.47	70.35 ± 0.18	-17.82 ± 0.20	-15.74 ± 0.77	46.49 ± 0.58
78.13	339.58 ± 0.24	-72.54 ± 0.27	-93.33 ± 1.94	398.94 ± 0.85	90.40 ± 0.09	-15.34 ± 0.28	-2.90 ± 1.83	58.81 ± 0.68
87.89	348.45 ± 0.27	-75.27 ± 0.31	-80.72 ± 0.30	421.20 ± 0.56	87.95 ± 0.30	-20.87 ± 0.09	-26.48 ± 1.74	84.55 ± 0.60
97.66	352.12 ± 0.22	-73.06 ± 0.21	-74.60 ± 0.44	409.12 ± 0.85	95.81 ± 0.10	-21.64 ± 0.13	-21.36 ± 2.71	78.62 ± 0.68
107.42	353.34 ± 0.18	-72.00 ± 0.15	-75.74 ± 1.30	417.94 ± 0.68	103.20 ± 0.23	-22.72 ± 0.17	-30.19 ± 2.09	96.82 ± 0.63
117.19	357.61 ± 0.41	-70.65 ± 0.12	-82.60 ± 0.84	421.10 ± 0.80	108.16 ± 0.32	-23.84 ± 0.22	-39.41 ± 1.87	101.33 ± 0.63
126.95	360.15 ± 0.42	-67.27 ± 0.40	-77.00 ± 1.58	416.27 ± 0.77	116.95 ± 0.28	-24.43 ± 0.15	-44.10 ± 1.50	116.87 ± 0.67
136.72	361.72 ± 0.61	-62.44 ± 0.27	-72.61 ± 1.14	422.87 ± 0.69	126.14 ± 0.20	-27.17 ± 0.31	-37.68 ± 1.14	121.45 ± 0.44
146.48	361.85 ± 1.44	-55.11 ± 1.24	-59.35 ± 1.23	416.29 ± 1.03	132.89 ± 0.64	-28.89 ± 1.14	-35.91 ± 0.62	124.34 ± 1.91
156.25	362.57 ± 1.06	-56.21 ± 1.03	-60.11 ± 2.18	417.22 ± 1.35	140.74 ± 1.02	-31.88 ± 0.79	-40.05 ± 0.76	110.36 ± 1.50
166.02	365.61 ± 0.23	-59.94 ± 0.32	-77.69 ± 0.98	434.14 ± 1.44	147.38 ± 0.60	-35.05 ± 0.56	-50.58 ± 0.84	152.75 ± 1.70
175.78	365.40 ± 0.37	-54.92 ± 0.26	-68.69 ± 1.65	436.79 ± 0.45	155.76 ± 0.57	-38.23 ± 0.27	-52.39 ± 1.80	158.85 ± 0.97
185.55	367.46 ± 0.16	-51.36 ± 0.33	-72.06 ± 0.90	442.20 ± 0.58	166.44 ± 0.45	-38.62 ± 0.29	-47.15 ± 1.77	156.32 ± 0.50
195.31	367.50 ± 0.16	-46.05 ± 0.19	-66.34 ± 2.47	432.47 ± 0.63	176.87 ± 0.40	-41.30 ± 0.26	-44.49 ± 0.67	167.54 ± 0.82
205.08	366.44 ± 0.49	-42.91 ± 0.18	-63.77 ± 0.90	447.32 ± 0.62	183.82 ± 0.31	-44.67 ± 0.19	-41.61 ± 2.58	186.97 ± 0.62
214.84	374.06 ± 0.24	-35.59 ± 0.13	-55.63 ± 0.88	450.64 ± 0.50	194.21 ± 0.47	-44.69 ± 0.22	-59.28 ± 4.99	185.99 ± 0.87
224.61	373.85 ± 0.25	-34.07 ± 0.13	-55.46 ± 2.20	417.39 ± 1.11	203.14 ± 0.41	-49.67 ± 0.12	-44.75 ± 2.94	183.32 ± 0.71
234.38	379.86 ± 0.45	-41.04 ± 0.12	-55.74 ± 1.70	475.51 ± 1.17	213.77 ± 0.19	-59.40 ± 0.22	-45.62 ± 2.32	213.46 ± 0.55
244.14	379.28 ± 0.21	-33.88 ± 0.05	-53.10 ± 0.45	472.69 ± 0.76	226.23 ± 0.13	-60.35 ± 0.26	-45.61 ± 2.23	221.09 ± 0.62

Table F. 16. Dynamic-stiffness 9,000 rpm 2,903 kPa (modified bearing)

Frequency [Hz]	Re (H_{xx}) [MN/m]	Re (H_{xy}) [MN/m]	Re (H_{yx}) [MN/m]	Re (H_{yy}) [MN/m]	Im (H_{xx}) [MN/m]	Im (H_{xy}) [MN/m]	Im (H_{yx}) [MN/m]	Im (H_{yy}) [MN/m]
9.77	302.14 ± 1.73	-80.87 ± 1.13	-69.61 ± 1.23	349.88 ± 1.10	9.30 ± 1.51	1.70 ± 1.50	1.47 ± 1.41	6.31 ± 2.57
19.53	298.75 ± 1.37	-73.19 ± 1.35	-72.74 ± 1.28	358.46 ± 1.53	15.87 ± 2.00	-0.65 ± 1.55	-6.65 ± 1.00	16.21 ± 2.09
29.30	301.56 ± 1.27	-77.04 ± 1.71	-70.99 ± 0.73	358.25 ± 1.82	23.74 ± 1.93	-6.97 ± 2.49	-9.26 ± 1.55	18.49 ± 2.77
39.06	304.88 ± 0.34	-74.97 ± 0.80	-69.86 ± 0.30	353.53 ± 1.18	32.77 ± 1.09	-7.55 ± 1.26	-11.74 ± 0.89	23.91 ± 1.65
48.83	305.54 ± 2.04	-72.37 ± 1.09	-65.29 ± 1.06	332.13 ± 1.45	36.75 ± 0.95	-4.58 ± 1.07	-14.31 ± 0.88	24.22 ± 2.45
58.59	307.22 ± 1.25	-70.62 ± 1.51	-69.93 ± 1.53	354.10 ± 1.47	48.22 ± 3.47	-5.49 ± 1.20	-3.80 ± 1.23	17.07 ± 1.77
68.36	310.01 ± 0.95	-78.01 ± 2.20	-73.64 ± 0.47	363.46 ± 1.60	53.22 ± 1.23	-9.66 ± 2.69	-7.73 ± 0.75	10.96 ± 2.26
78.13	311.64 ± 0.92	-80.37 ± 1.38	-60.49 ± 0.67	325.24 ± 1.28	58.63 ± 0.93	-4.93 ± 1.30	-13.94 ± 0.63	28.96 ± 1.74
87.89	311.41 ± 0.47	-73.94 ± 1.34	-70.20 ± 0.63	345.79 ± 1.41	61.61 ± 1.99	-13.09 ± 0.95	-22.17 ± 0.78	34.52 ± 1.54
97.66	315.73 ± 1.86	-79.28 ± 2.20	-77.32 ± 0.93	362.99 ± 1.22	69.21 ± 2.38	-27.98 ± 1.96	-25.29 ± 1.23	48.01 ± 3.12
107.42	314.13 ± 0.63	-69.48 ± 0.84	-71.63 ± 0.69	345.83 ± 0.93	71.90 ± 1.15	-10.22 ± 1.60	-19.66 ± 0.55	38.54 ± 2.10
117.19	311.35 ± 1.76	-64.11 ± 3.83	-64.07 ± 0.69	329.14 ± 2.92	73.38 ± 1.30	-14.19 ± 2.91	-22.64 ± 0.61	52.56 ± 2.68
126.95	311.86 ± 1.58	-60.62 ± 0.98	-70.26 ± 1.52	349.68 ± 1.19	83.51 ± 1.11	-13.63 ± 1.01	-24.00 ± 0.89	56.76 ± 1.82
136.72	312.17 ± 1.77	-58.94 ± 0.95	-68.56 ± 1.15	347.74 ± 1.08	88.57 ± 0.89	-14.64 ± 1.05	-30.01 ± 0.69	65.50 ± 1.55
146.48	307.42 ± 2.69	-54.48 ± 2.49	-56.26 ± 2.15	323.16 ± 2.55	90.51 ± 1.34	-12.62 ± 3.78	-29.03 ± 3.36	86.38 ± 4.37
156.25	306.65 ± 1.58	-50.45 ± 5.15	-51.65 ± 1.12	306.92 ± 2.67	101.94 ± 1.19	-38.00 ± 4.45	-23.00 ± 1.54	50.03 ± 8.08
166.02	309.37 ± 1.38	-50.90 ± 1.94	-63.07 ± 1.14	338.58 ± 1.55	104.94 ± 0.84	-11.03 ± 1.53	-25.80 ± 0.49	68.18 ± 2.05
175.78	304.20 ± 0.54	-49.41 ± 0.97	-56.52 ± 0.41	339.11 ± 0.67	115.17 ± 0.54	-21.85 ± 1.00	-29.94 ± 0.62	88.13 ± 1.93
185.55	305.51 ± 0.53	-49.04 ± 0.65	-59.10 ± 0.56	344.18 ± 0.86	118.40 ± 0.28	-23.45 ± 0.98	-37.04 ± 0.19	93.95 ± 1.75
195.31	299.92 ± 0.46	-43.18 ± 1.40	-43.55 ± 0.64	314.97 ± 1.43	126.04 ± 0.93	-31.93 ± 2.12	-37.37 ± 0.61	106.36 ± 2.40
205.08	303.21 ± 1.04	-43.27 ± 2.25	-38.91 ± 0.47	304.14 ± 1.34	137.99 ± 0.96	-34.91 ± 4.34	-38.60 ± 0.92	115.37 ± 3.74
214.84	288.18 ± 0.62	-7.54 ± 1.56	-49.36 ± 0.74	343.57 ± 1.84	137.40 ± 0.59	-30.12 ± 0.97	-30.37 ± 0.86	94.41 ± 1.75
224.61	291.30 ± 0.63	-15.50 ± 1.87	-50.15 ± 0.40	336.39 ± 1.29	148.50 ± 0.60	-36.57 ± 1.71	-36.67 ± 0.73	108.87 ± 2.70
234.38	292.30 ± 1.21	-35.60 ± 2.04	-41.48 ± 1.02	366.60 ± 2.32	159.86 ± 2.03	-34.43 ± 3.29	-59.59 ± 2.16	171.97 ± 3.49
244.14	287.64 ± 1.18	-26.30 ± 1.91	-46.41 ± 0.82	322.78 ± 2.33	172.97 ± 0.80	-39.69 ± 0.75	-37.58 ± 0.77	130.02 ± 2.46

Table F. 17. Dynamic-stiffness 10,800 rpm 726 kPa (original bearing)

Frequency [Hz]	Re (H_{xx}) [MN/m]	Re (H_{xy}) [MN/m]	Re (H_{yx}) [MN/m]	Re (H_{yy}) [MN/m]	Im (H_{xx}) [MN/m]	Im (H_{xy}) [MN/m]	Im (H_{yx}) [MN/m]	Im (H_{yy}) [MN/m]
9.77	263.87 ± 1.03	-67.22 ± 2.26	-69.57 ± 3.70	272.91 ± 6.07	14.31 ± 1.23	-0.98 ± 1.73	-19.48 ± 1.45	62.03 ± 4.19
19.53	267.36 ± 0.55	-66.86 ± 1.57	-61.95 ± 6.00	249.95 ± 6.04	31.42 ± 1.03	-5.28 ± 1.55	23.19 ± 3.76	8.88 ± 1.59
29.30	268.12 ± 1.03	-69.85 ± 0.80	-83.10 ± 2.83	281.40 ± 2.09	43.73 ± 0.76	-9.82 ± 0.91	-7.18 ± 2.44	37.13 ± 2.63
39.06	271.59 ± 0.70	-70.66 ± 0.94	-75.87 ± 2.39	268.59 ± 1.71	54.05 ± 0.27	-8.14 ± 0.29	-12.27 ± 2.55	67.11 ± 1.49
48.83	277.86 ± 0.40	-70.84 ± 0.34	-68.71 ± 0.81	270.95 ± 0.95	68.33 ± 0.55	-10.83 ± 0.49	-3.84 ± 1.22	77.39 ± 1.10
58.59	279.87 ± 0.32	-69.82 ± 0.10	-81.83 ± 1.93	281.77 ± 0.89	81.28 ± 0.49	-9.15 ± 0.94	-6.47 ± 1.59	89.26 ± 0.99
68.36	284.44 ± 0.58	-71.64 ± 0.98	-75.30 ± 0.56	280.70 ± 0.70	100.68 ± 0.46	-8.22 ± 0.78	-0.85 ± 0.96	93.32 ± 1.53
78.13	291.45 ± 0.39	-67.14 ± 0.48	-68.60 ± 0.53	279.76 ± 0.69	106.22 ± 0.38	-10.48 ± 0.31	-8.54 ± 1.32	98.83 ± 0.68
87.89	293.92 ± 0.30	-68.96 ± 0.51	-71.13 ± 1.29	306.72 ± 0.43	117.09 ± 0.28	-12.03 ± 0.24	-9.87 ± 0.80	125.77 ± 0.64
97.66	299.58 ± 0.50	-67.00 ± 0.54	-66.83 ± 1.30	301.68 ± 0.59	126.54 ± 0.25	-12.48 ± 0.13	-13.44 ± 1.71	128.95 ± 0.81
107.42	302.32 ± 0.28	-65.06 ± 0.32	-75.30 ± 1.14	311.63 ± 0.43	136.52 ± 0.48	-12.76 ± 0.14	-13.64 ± 1.20	146.21 ± 0.61
117.19	308.64 ± 0.36	-62.71 ± 0.32	-72.68 ± 1.61	320.03 ± 1.25	144.57 ± 0.41	-13.31 ± 0.23	-18.03 ± 2.43	151.02 ± 1.10
126.95	314.71 ± 0.28	-59.34 ± 0.32	-66.11 ± 0.79	317.05 ± 0.77	154.76 ± 0.21	-13.13 ± 0.08	-19.08 ± 1.60	163.60 ± 0.70
136.72	318.26 ± 0.19	-55.52 ± 0.33	-60.65 ± 1.99	331.11 ± 0.77	166.46 ± 0.32	-14.79 ± 0.36	-18.48 ± 1.00	166.43 ± 0.82
146.48	321.27 ± 0.29	-50.50 ± 0.19	-59.49 ± 0.62	329.81 ± 1.16	174.44 ± 0.17	-15.69 ± 0.46	-13.69 ± 1.57	167.00 ± 0.96
156.25	326.39 ± 0.14	-41.24 ± 0.33	-50.68 ± 2.62	305.73 ± 0.63	181.01 ± 0.39	-15.22 ± 0.21	-21.91 ± 1.56	165.50 ± 0.54
166.02	329.95 ± 0.49	-49.01 ± 0.46	-56.70 ± 0.61	346.40 ± 0.94	193.38 ± 0.65	-21.07 ± 0.53	-20.89 ± 2.31	199.36 ± 0.83
175.78	330.56 ± 0.78	-43.53 ± 0.56	-52.88 ± 1.94	346.18 ± 1.59	203.69 ± 0.98	-23.04 ± 1.93	-13.81 ± 1.75	199.48 ± 1.52
185.55	332.92 ± 0.88	-40.69 ± 2.83	-44.75 ± 2.51	354.50 ± 0.95	214.08 ± 1.19	-19.18 ± 0.98	-15.09 ± 2.41	207.10 ± 3.51
195.31	337.26 ± 0.48	-35.50 ± 0.59	-42.67 ± 1.39	344.75 ± 1.50	228.13 ± 0.47	-18.51 ± 0.76	-13.98 ± 1.22	219.09 ± 0.44
205.08	338.32 ± 0.44	-32.24 ± 0.13	-44.54 ± 1.07	355.97 ± 0.54	235.90 ± 0.42	-17.80 ± 0.36	-19.88 ± 1.22	237.75 ± 0.86
214.84	347.49 ± 0.44	-22.09 ± 0.52	-40.78 ± 2.83	357.00 ± 0.60	259.54 ± 0.37	-10.73 ± 0.20	-20.14 ± 1.76	232.13 ± 0.65
224.61	353.51 ± 0.20	9.17 ± 0.22	-44.35 ± 2.79	269.11 ± 0.93	273.24 ± 0.54	-5.26 ± 0.26	-18.16 ± 1.94	276.15 ± 0.56
234.38	357.52 ± 0.36	-15.46 ± 0.15	-41.76 ± 2.54	379.60 ± 0.70	283.95 ± 0.46	-19.24 ± 0.47	-20.71 ± 1.23	269.37 ± 0.99
244.14	354.44 ± 0.29	-9.28 ± 0.23	-40.05 ± 2.28	381.69 ± 0.66	307.51 ± 0.40	-16.87 ± 0.22	-19.74 ± 2.53	282.38 ± 1.29

Table F. 18. Dynamic-stiffness 10,800 rpm 726 kPa (modified bearing)

Frequency [Hz]	Re (H_{xx}) [MN/m]	Re (H_{xy}) [MN/m]	Re (H_{yx}) [MN/m]	Re (H_{yy}) [MN/m]	Im (H_{xx}) [MN/m]	Im (H_{xy}) [MN/m]	Im (H_{yx}) [MN/m]	Im (H_{yy}) [MN/m]
9.77	247.85 ± 0.67	-70.67 ± 1.76	-77.01 ± 0.63	233.32 ± 0.94	12.81 ± 1.28	-2.33 ± 0.86	-1.60 ± 1.07	10.37 ± 1.95
19.53	252.15 ± 0.95	-70.99 ± 0.73	-77.97 ± 0.87	236.33 ± 1.28	23.87 ± 0.49	-9.13 ± 1.32	-5.58 ± 0.39	23.09 ± 1.43
29.30	252.48 ± 0.89	-71.84 ± 1.13	-79.58 ± 0.48	239.53 ± 0.98	33.45 ± 1.51	-11.11 ± 0.94	-10.10 ± 1.37	34.34 ± 1.79
39.06	254.41 ± 1.43	-71.23 ± 0.96	-78.14 ± 0.76	239.59 ± 0.84	45.45 ± 1.16	-13.65 ± 1.63	-13.46 ± 0.51	45.09 ± 2.19
48.83	256.32 ± 1.87	-71.75 ± 1.15	-75.88 ± 1.40	232.67 ± 1.13	54.21 ± 1.46	-15.48 ± 2.12	-16.61 ± 1.00	54.95 ± 2.40
58.59	259.34 ± 0.95	-72.67 ± 0.72	-81.18 ± 1.77	242.96 ± 1.07	69.43 ± 2.76	-17.40 ± 1.69	-1.53 ± 2.52	55.18 ± 2.15
68.36	271.59 ± 1.15	-94.70 ± 1.17	-65.25 ± 0.83	209.07 ± 1.34	72.97 ± 1.27	-20.73 ± 1.44	-10.79 ± 0.93	59.25 ± 3.18
78.13	264.65 ± 1.19	-78.16 ± 0.98	-72.27 ± 0.56	233.54 ± 0.81	84.20 ± 1.17	-16.14 ± 1.38	-17.45 ± 0.63	76.67 ± 1.83
87.89	269.03 ± 0.79	-78.36 ± 0.97	-85.14 ± 0.96	253.44 ± 1.01	90.80 ± 1.30	-21.80 ± 0.96	-18.76 ± 0.73	85.94 ± 1.62
97.66	272.41 ± 1.63	-74.60 ± 2.94	-91.44 ± 1.33	273.52 ± 1.90	102.85 ± 1.59	-39.61 ± 0.91	-18.27 ± 0.57	92.38 ± 2.40
107.42	273.70 ± 1.53	-77.20 ± 1.27	-84.56 ± 1.08	260.20 ± 1.19	106.76 ± 1.67	-21.67 ± 1.35	-17.62 ± 0.53	98.69 ± 1.44
117.19	269.44 ± 2.93	-71.82 ± 2.12	-83.56 ± 2.08	272.35 ± 1.67	110.23 ± 0.46	-23.26 ± 1.54	-25.37 ± 2.83	117.99 ± 2.16
126.95	276.34 ± 1.49	-78.57 ± 1.09	-83.47 ± 2.00	267.08 ± 1.13	120.00 ± 1.22	-20.97 ± 0.96	-18.00 ± 1.04	113.10 ± 1.81
136.72	279.17 ± 0.76	-78.15 ± 0.91	-81.94 ± 0.65	274.86 ± 0.87	127.34 ± 1.02	-17.79 ± 0.65	-18.17 ± 0.85	121.10 ± 1.70
146.48	278.81 ± 1.04	-75.32 ± 1.20	-73.53 ± 1.50	260.44 ± 1.51	136.27 ± 1.27	-19.60 ± 1.37	-25.55 ± 0.45	143.40 ± 2.07
156.25	276.58 ± 1.48	-66.68 ± 2.63	-67.66 ± 1.69	243.54 ± 3.30	145.78 ± 1.48	-27.08 ± 1.13	-20.48 ± 1.69	126.35 ± 2.37
166.02	281.18 ± 0.98	-72.60 ± 1.84	-71.26 ± 1.10	266.19 ± 1.54	155.90 ± 0.83	-17.26 ± 1.44	-16.66 ± 1.06	134.83 ± 2.64
175.78	276.27 ± 1.14	-70.48 ± 1.37	-70.32 ± 0.39	275.43 ± 1.39	163.90 ± 2.06	-19.51 ± 1.39	-18.15 ± 0.95	148.95 ± 2.02
185.55	277.55 ± 2.22	-69.51 ± 1.99	-71.52 ± 1.40	289.21 ± 1.15	174.78 ± 1.54	-20.88 ± 1.16	-17.71 ± 1.95	155.46 ± 2.87
195.31	274.11 ± 0.72	-64.93 ± 0.96	-57.05 ± 1.31	270.78 ± 1.87	189.36 ± 1.91	-23.11 ± 1.75	-15.45 ± 1.04	168.87 ± 2.48
205.08	272.05 ± 1.65	-55.81 ± 4.03	-61.74 ± 1.03	275.94 ± 3.04	197.09 ± 0.98	-18.35 ± 2.26	-13.24 ± 1.58	179.58 ± 2.88
214.84	273.83 ± 1.20	-36.92 ± 1.35	-42.19 ± 1.42	281.08 ± 0.89	213.41 ± 1.05	-11.48 ± 0.59	4.56 ± 1.10	153.80 ± 2.03
224.61	273.77 ± 0.55	-38.94 ± 2.30	-43.55 ± 1.32	237.47 ± 3.04	245.11 ± 0.96	-5.88 ± 3.81	-9.29 ± 1.47	188.84 ± 3.46
234.38	212.47 ± 2.93	-41.05 ± 3.69	-64.86 ± 3.28	311.34 ± 1.86	279.63 ± 2.24	-29.95 ± 0.96	74.51 ± 1.84	202.59 ± 3.93
244.14	284.81 ± 4.61	-40.24 ± 2.16	14.24 ± 3.05	273.25 ± 3.32	328.37 ± 3.88	-26.87 ± 1.79	52.75 ± 3.61	168.58 ± 4.17

Table F. 19. Dynamic-stiffness 10,800 rpm 1,452 kPa (original bearing)

Frequency [Hz]	Re (H_{xx}) [MN/m]	Re (H_{xy}) [MN/m]	Re (H_{yx}) [MN/m]	Re (H_{yy}) [MN/m]	Im (H_{xx}) [MN/m]	Im (H_{xy}) [MN/m]	Im (H_{yx}) [MN/m]	Im (H_{yy}) [MN/m]
9.77	293.76 ± 1.42	-69.68 ± 1.65	-83.37 ± 3.19	330.92 ± 5.73	12.73 ± 0.70	-1.64 ± 1.74	-26.27 ± 2.43	72.94 ± 2.95
19.53	293.64 ± 0.88	-68.88 ± 2.69	-108.57 ± 5.84	343.88 ± 7.09	24.95 ± 0.87	-6.61 ± 0.74	-4.13 ± 4.31	18.20 ± 4.70
29.30	298.37 ± 0.68	-71.41 ± 1.72	-73.51 ± 1.63	337.83 ± 4.48	38.58 ± 0.32	-11.93 ± 1.23	-12.71 ± 1.05	31.64 ± 0.95
39.06	301.46 ± 1.07	-73.45 ± 1.04	-61.57 ± 2.61	326.83 ± 3.30	47.95 ± 0.25	-12.07 ± 0.50	-5.34 ± 2.60	45.68 ± 1.74
48.83	305.89 ± 0.46	-72.98 ± 0.55	-71.79 ± 0.60	324.58 ± 0.95	61.88 ± 0.30	-15.23 ± 0.25	-9.82 ± 1.00	61.36 ± 1.70
58.59	307.54 ± 0.63	-73.03 ± 0.79	-78.43 ± 2.41	330.52 ± 0.72	72.75 ± 0.42	-13.01 ± 0.45	-16.22 ± 0.93	65.68 ± 0.81
68.36	308.60 ± 0.40	-73.96 ± 0.66	-78.07 ± 1.18	331.94 ± 0.60	83.82 ± 0.49	-16.04 ± 0.36	-21.89 ± 0.93	67.99 ± 0.88
78.13	317.00 ± 0.32	-71.27 ± 0.34	-68.24 ± 0.77	323.80 ± 0.73	97.64 ± 0.36	-15.53 ± 0.43	-12.33 ± 1.33	73.35 ± 0.52
87.89	318.65 ± 0.22	-74.61 ± 0.32	-75.80 ± 1.41	345.60 ± 0.48	105.45 ± 0.32	-17.29 ± 0.24	-19.10 ± 0.55	105.35 ± 0.67
97.66	321.56 ± 0.28	-73.39 ± 0.41	-74.60 ± 1.56	339.34 ± 0.51	112.16 ± 0.32	-17.61 ± 0.20	-18.23 ± 0.71	102.25 ± 0.63
107.42	324.78 ± 0.26	-71.94 ± 0.35	-75.42 ± 0.62	347.48 ± 0.49	121.91 ± 0.44	-18.57 ± 0.21	-20.46 ± 0.79	123.08 ± 0.67
117.19	330.81 ± 0.33	-70.35 ± 0.12	-73.66 ± 1.33	353.05 ± 0.81	130.01 ± 0.25	-18.26 ± 0.17	-30.28 ± 0.70	125.68 ± 0.34
126.95	334.10 ± 0.33	-66.96 ± 0.33	-70.29 ± 0.53	348.83 ± 0.35	139.40 ± 0.47	-17.80 ± 0.10	-30.03 ± 0.21	142.98 ± 0.55
136.72	336.79 ± 0.40	-62.59 ± 0.34	-67.66 ± 0.74	352.03 ± 0.49	149.28 ± 0.42	-18.54 ± 0.38	-28.64 ± 0.70	146.35 ± 0.41
146.48	340.32 ± 0.32	-57.51 ± 0.23	-57.83 ± 0.79	356.32 ± 0.98	156.76 ± 0.09	-20.47 ± 0.10	-27.25 ± 1.03	150.80 ± 0.59
156.25	341.61 ± 0.26	-50.86 ± 0.23	-51.53 ± 2.81	339.82 ± 0.64	165.87 ± 0.59	-21.48 ± 0.24	-30.13 ± 1.57	140.32 ± 0.40
166.02	345.47 ± 0.29	-56.95 ± 0.23	-68.68 ± 1.80	375.72 ± 1.08	174.15 ± 0.60	-24.98 ± 0.34	-39.50 ± 2.21	180.86 ± 0.86
175.78	344.23 ± 0.86	-50.39 ± 1.07	-66.67 ± 1.93	375.63 ± 0.76	181.62 ± 1.23	-27.25 ± 0.39	-36.91 ± 1.31	180.34 ± 1.53
185.55	347.79 ± 0.50	-48.39 ± 1.03	-57.90 ± 2.25	377.71 ± 1.98	192.45 ± 1.54	-25.22 ± 1.28	-29.55 ± 1.40	186.50 ± 1.01
195.31	350.19 ± 0.34	-43.21 ± 0.48	-57.92 ± 2.59	373.06 ± 0.57	206.58 ± 0.60	-28.23 ± 0.37	-25.81 ± 2.08	195.52 ± 0.77
205.08	349.57 ± 0.49	-41.04 ± 0.39	-57.77 ± 1.01	386.26 ± 0.42	212.72 ± 0.30	-26.86 ± 0.23	-29.94 ± 2.62	209.28 ± 0.61
214.84	356.59 ± 0.39	-34.13 ± 0.21	-45.00 ± 0.95	389.94 ± 0.48	227.97 ± 0.33	-26.28 ± 0.26	-34.87 ± 1.55	203.20 ± 0.74
224.61	359.43 ± 0.25	-22.99 ± 0.18	-40.13 ± 3.11	334.23 ± 0.73	236.21 ± 0.38	-24.70 ± 0.11	-29.16 ± 2.07	212.93 ± 0.63
234.38	364.53 ± 0.30	-29.99 ± 0.28	-47.69 ± 2.19	403.88 ± 0.60	250.14 ± 0.16	-35.49 ± 0.11	-36.78 ± 1.80	237.17 ± 0.62
244.14	363.67 ± 0.28	-17.69 ± 0.25	-35.89 ± 2.69	387.69 ± 0.42	264.64 ± 0.40	-32.25 ± 0.19	-34.35 ± 1.67	253.66 ± 0.58

Table F. 20. Dynamic-stiffness 10,800 rpm 1,452 kPa (modified bearing)

Frequency [Hz]	Re (H_{xx}) [MN/m]	Re (H_{xy}) [MN/m]	Re (H_{yx}) [MN/m]	Re (H_{yy}) [MN/m]	Im (H_{xx}) [MN/m]	Im (H_{xy}) [MN/m]	Im (H_{yx}) [MN/m]	Im (H_{yy}) [MN/m]
9.77	269.65 ± 1.29	-73.35 ± 1.21	-71.43 ± 1.38	277.30 ± 1.42	13.51 ± 1.88	-1.32 ± 1.61	2.62 ± 1.34	5.73 ± 2.12
19.53	268.24 ± 1.58	-72.30 ± 1.32	-73.74 ± 1.47	279.69 ± 1.67	23.81 ± 2.51	-6.82 ± 1.41	-4.96 ± 1.37	17.37 ± 2.03
29.30	272.45 ± 2.59	-73.90 ± 1.72	-73.21 ± 1.53	282.38 ± 1.16	32.52 ± 1.38	-9.47 ± 2.62	-9.63 ± 0.58	26.19 ± 2.38
39.06	271.86 ± 1.40	-69.28 ± 1.62	-75.10 ± 1.26	282.76 ± 1.11	41.99 ± 2.54	-10.62 ± 1.81	-14.48 ± 1.85	36.57 ± 2.00
48.83	277.18 ± 1.69	-73.90 ± 1.94	-69.26 ± 1.89	268.42 ± 1.95	44.72 ± 1.69	-10.04 ± 2.08	-16.95 ± 1.27	40.54 ± 2.69
58.59	278.61 ± 1.31	-74.07 ± 1.56	-75.23 ± 1.41	282.18 ± 1.30	62.50 ± 2.01	-13.89 ± 2.07	-5.13 ± 2.18	37.76 ± 2.31
68.36	282.38 ± 2.17	-81.41 ± 2.87	-77.69 ± 1.92	287.16 ± 2.62	76.68 ± 2.19	-42.67 ± 1.56	10.37 ± 1.84	-37.75 ± 2.29
78.13	284.62 ± 0.66	-78.29 ± 2.30	-68.31 ± 0.82	271.66 ± 1.96	74.60 ± 2.12	-10.52 ± 1.09	-17.51 ± 1.49	58.97 ± 1.88
87.89	284.40 ± 1.15	-75.88 ± 1.89	-80.81 ± 0.61	283.96 ± 1.34	82.32 ± 1.13	-19.99 ± 1.03	-20.42 ± 0.86	62.23 ± 2.14
97.66	291.13 ± 1.53	-76.66 ± 4.01	-87.27 ± 1.08	304.60 ± 3.81	93.22 ± 2.10	-31.77 ± 2.22	-25.68 ± 1.28	80.00 ± 3.21
107.42	293.97 ± 1.54	-77.01 ± 1.28	-75.71 ± 1.41	285.95 ± 1.44	97.22 ± 1.68	-18.53 ± 1.13	-19.20 ± 1.68	70.53 ± 2.27
117.19	281.28 ± 2.94	-68.77 ± 2.50	-80.54 ± 2.44	284.82 ± 1.92	104.01 ± 3.21	-19.88 ± 1.86	-23.96 ± 1.69	90.60 ± 2.87
126.95	295.67 ± 2.85	-72.50 ± 1.02	-77.92 ± 2.41	295.46 ± 1.13	109.20 ± 1.83	-19.82 ± 1.11	-23.17 ± 1.23	90.57 ± 1.67
136.72	296.37 ± 0.87	-68.29 ± 0.89	-81.36 ± 0.91	302.60 ± 1.08	115.13 ± 0.92	-17.84 ± 1.34	-28.48 ± 0.81	100.06 ± 1.65
146.48	299.06 ± 1.42	-70.08 ± 2.04	-64.69 ± 1.80	274.71 ± 3.01	120.69 ± 1.17	-16.76 ± 1.71	-31.38 ± 1.00	119.43 ± 2.47
156.25	295.31 ± 1.66	-67.46 ± 3.90	-62.55 ± 1.19	261.61 ± 4.38	131.83 ± 1.94	-33.24 ± 3.24	-24.91 ± 1.22	94.80 ± 4.31
166.02	300.19 ± 0.86	-65.39 ± 1.68	-69.94 ± 1.35	291.93 ± 2.45	134.29 ± 1.42	-13.67 ± 1.96	-21.87 ± 0.94	106.37 ± 2.33
175.78	297.89 ± 1.09	-65.50 ± 1.31	-67.35 ± 0.96	296.48 ± 1.57	146.69 ± 1.61	-21.26 ± 2.10	-25.12 ± 0.83	122.28 ± 3.15
185.55	300.31 ± 1.00	-65.61 ± 2.37	-71.44 ± 0.89	306.36 ± 1.26	152.07 ± 1.06	-20.57 ± 2.40	-28.29 ± 1.16	129.56 ± 3.74
195.31	294.72 ± 1.71	-58.63 ± 2.35	-58.34 ± 0.69	283.86 ± 2.69	159.80 ± 1.60	-23.20 ± 3.51	-31.44 ± 1.16	146.04 ± 1.98
205.08	300.65 ± 2.76	-61.28 ± 1.93	-55.12 ± 2.51	290.97 ± 4.54	169.90 ± 2.41	-29.83 ± 5.69	-32.02 ± 1.78	160.40 ± 2.70
214.84	287.23 ± 0.67	-25.92 ± 0.54	-59.35 ± 0.66	307.33 ± 1.07	173.07 ± 1.19	-16.57 ± 1.27	-12.38 ± 0.89	125.76 ± 1.73
224.61	291.36 ± 0.67	-34.36 ± 1.05	-57.45 ± 0.95	289.59 ± 1.33	183.67 ± 0.79	-24.43 ± 2.11	-18.67 ± 0.86	145.19 ± 3.50
234.38	290.41 ± 0.97	-49.90 ± 3.04	-56.92 ± 1.51	321.31 ± 2.63	192.38 ± 0.39	-21.48 ± 0.98	-40.44 ± 0.98	197.00 ± 3.23
244.14	285.22 ± 0.88	-38.64 ± 1.29	-53.51 ± 0.49	282.81 ± 1.66	216.50 ± 0.76	-19.44 ± 2.24	-4.59 ± 0.71	156.83 ± 2.72

Table F. 21. Dynamic-stiffness 10,800 rpm 2,177 kPa (original bearing)

Frequency [Hz]	Re (H_{xx}) [MN/m]	Re (H_{xy}) [MN/m]	Re (H_{yx}) [MN/m]	Re (H_{yy}) [MN/m]	Im (H_{xx}) [MN/m]	Im (H_{xy}) [MN/m]	Im (H_{yx}) [MN/m]	Im (H_{yy}) [MN/m]
9.77	321.17 ± 1.44	-73.60 ± 1.02	-92.65 ± 2.15	406.13 ± 3.39	12.23 ± 1.64	-6.09 ± 3.70	-33.86 ± 5.29	69.48 ± 2.90
19.53	320.11 ± 1.54	-77.87 ± 1.11	-111.38 ± 6.67	364.00 ± 3.68	21.74 ± 0.85	-4.21 ± 2.66	-8.42 ± 11.31	13.41 ± 3.00
29.30	325.71 ± 0.90	-76.63 ± 1.35	-80.48 ± 3.20	390.94 ± 2.23	32.57 ± 0.83	-7.74 ± 1.08	-18.50 ± 2.17	30.51 ± 2.42
39.06	327.28 ± 0.55	-76.64 ± 1.41	-71.50 ± 1.14	373.66 ± 1.80	44.76 ± 1.10	-10.10 ± 0.69	3.59 ± 8.34	35.62 ± 2.59
48.83	331.14 ± 0.60	-76.18 ± 0.66	-83.16 ± 1.89	370.59 ± 0.99	56.34 ± 0.70	-14.05 ± 1.05	-9.21 ± 0.96	55.75 ± 1.35
58.59	333.94 ± 0.29	-76.57 ± 0.56	-80.92 ± 3.86	378.14 ± 0.99	65.66 ± 0.66	-14.32 ± 0.59	-18.40 ± 2.12	51.41 ± 1.29
68.36	332.03 ± 0.39	-76.94 ± 0.39	-81.63 ± 2.48	379.13 ± 0.70	76.86 ± 0.39	-18.35 ± 0.63	-14.89 ± 1.99	53.37 ± 0.86
78.13	341.72 ± 0.24	-72.86 ± 0.34	-73.90 ± 1.40	367.03 ± 0.43	91.61 ± 0.16	-17.37 ± 0.19	-7.41 ± 0.74	61.01 ± 0.81
87.89	341.84 ± 0.37	-78.14 ± 0.39	-84.04 ± 1.12	388.07 ± 0.44	94.99 ± 0.44	-20.20 ± 0.52	-21.68 ± 2.52	92.05 ± 0.67
97.66	346.13 ± 0.38	-77.39 ± 0.31	-73.93 ± 1.45	377.48 ± 0.59	102.49 ± 0.35	-20.72 ± 0.59	-20.51 ± 1.15	86.87 ± 0.49
107.42	347.67 ± 0.25	-75.64 ± 0.13	-84.60 ± 2.22	390.44 ± 0.72	110.44 ± 0.31	-21.31 ± 0.30	-25.98 ± 1.20	105.51 ± 0.52
117.19	352.26 ± 0.22	-74.58 ± 0.20	-79.66 ± 1.55	388.61 ± 0.53	118.00 ± 0.31	-22.32 ± 0.35	-34.30 ± 1.00	112.70 ± 0.48
126.95	356.02 ± 0.18	-72.23 ± 0.47	-80.99 ± 0.79	387.03 ± 0.52	127.98 ± 0.18	-23.22 ± 0.32	-38.01 ± 1.71	126.27 ± 0.46
136.72	358.38 ± 0.34	-67.58 ± 0.12	-76.56 ± 0.38	390.37 ± 0.26	136.06 ± 0.28	-23.47 ± 0.37	-38.50 ± 2.20	129.42 ± 0.52
146.48	360.95 ± 0.29	-63.86 ± 0.41	-69.52 ± 1.01	394.15 ± 0.44	143.82 ± 0.26	-26.57 ± 0.36	-31.98 ± 1.26	133.84 ± 0.47
156.25	361.44 ± 0.49	-58.01 ± 0.23	-69.77 ± 0.84	380.93 ± 0.37	151.35 ± 0.29	-27.06 ± 0.20	-26.64 ± 1.60	120.30 ± 0.37
166.02	365.07 ± 0.42	-63.54 ± 0.15	-77.29 ± 0.81	408.68 ± 0.34	157.92 ± 0.43	-30.14 ± 0.39	-35.98 ± 1.06	163.14 ± 0.84
175.78	364.73 ± 0.87	-58.30 ± 0.82	-79.22 ± 2.87	411.04 ± 0.77	164.93 ± 1.48	-32.46 ± 0.56	-37.31 ± 2.83	165.65 ± 1.30
185.55	366.81 ± 0.91	-55.98 ± 1.31	-66.68 ± 2.50	412.25 ± 1.49	176.86 ± 1.72	-32.52 ± 1.29	-34.13 ± 1.39	167.32 ± 0.95
195.31	369.02 ± 0.39	-51.93 ± 0.38	-66.50 ± 1.67	409.38 ± 0.69	188.14 ± 0.49	-33.45 ± 0.55	-28.66 ± 2.67	172.23 ± 0.76
205.08	368.08 ± 0.55	-47.26 ± 0.31	-68.06 ± 1.31	418.26 ± 0.47	194.01 ± 0.53	-35.30 ± 0.18	-32.55 ± 1.66	194.12 ± 0.60
214.84	375.16 ± 0.58	-41.40 ± 0.15	-62.36 ± 3.11	427.35 ± 0.77	206.22 ± 0.35	-35.38 ± 0.25	-44.91 ± 4.50	188.58 ± 0.81
224.61	375.27 ± 0.30	-31.79 ± 0.29	-63.33 ± 1.53	374.49 ± 0.79	215.38 ± 0.54	-38.68 ± 0.13	-39.86 ± 2.05	200.59 ± 0.76
234.38	380.45 ± 0.53	-40.24 ± 0.18	-61.15 ± 1.24	437.30 ± 0.70	226.04 ± 0.28	-44.91 ± 0.33	-43.62 ± 3.30	216.49 ± 1.08
244.14	379.94 ± 0.27	-33.82 ± 0.18	-60.32 ± 1.82	434.52 ± 0.55	239.96 ± 0.40	-44.43 ± 0.08	-42.93 ± 0.79	225.47 ± 0.53

Table F. 22. Dynamic-stiffness 10,800 rpm 2,177 kPa (modified bearing)

Frequency [Hz]	Re (H_{xx}) [MN/m]	Re (H_{xy}) [MN/m]	Re (H_{yx}) [MN/m]	Re (H_{yy}) [MN/m]	Im (H_{xx}) [MN/m]	Im (H_{xy}) [MN/m]	Im (H_{yx}) [MN/m]	Im (H_{yy}) [MN/m]
9.77	288.09 ± 1.58	-76.85 ± 1.94	-74.12 ± 0.40	320.08 ± 1.12	11.71 ± 1.92	-2.49 ± 1.52	3.73 ± 1.04	3.28 ± 1.89
19.53	290.46 ± 1.12	-76.60 ± 2.16	-74.99 ± 0.92	325.70 ± 1.86	19.69 ± 1.18	-4.06 ± 1.76	-5.32 ± 0.62	16.76 ± 2.70
29.30	293.17 ± 1.50	-78.35 ± 3.47	-73.61 ± 1.09	325.83 ± 2.59	28.15 ± 1.31	-3.78 ± 2.91	-10.46 ± 1.24	25.63 ± 3.48
39.06	297.17 ± 1.53	-75.57 ± 1.88	-73.79 ± 1.10	325.90 ± 2.07	36.38 ± 1.29	-9.58 ± 1.99	-12.93 ± 1.44	29.02 ± 2.17
48.83	296.67 ± 1.39	-73.98 ± 2.88	-70.76 ± 1.45	306.59 ± 2.53	42.89 ± 2.55	-9.83 ± 3.52	-13.26 ± 1.72	28.64 ± 4.06
58.59	295.93 ± 0.91	-74.78 ± 3.08	-76.37 ± 1.06	324.58 ± 2.53	51.30 ± 3.20	-9.07 ± 1.49	-8.34 ± 1.88	27.45 ± 2.19
68.36	303.41 ± 0.51	-76.27 ± 1.46	-77.30 ± 0.37	345.72 ± 1.75	61.19 ± 1.58	-15.64 ± 1.40	-5.78 ± 1.04	9.24 ± 2.29
78.13	303.47 ± 1.66	-81.40 ± 1.59	-67.83 ± 0.74	306.73 ± 1.29	69.25 ± 0.50	-9.99 ± 1.89	-13.35 ± 0.78	39.17 ± 2.80
87.89	306.38 ± 1.01	-79.45 ± 1.31	-76.87 ± 0.78	320.63 ± 0.91	71.30 ± 1.72	-15.39 ± 1.67	-21.87 ± 1.65	46.63 ± 2.16
97.66	308.02 ± 1.71	-84.01 ± 3.58	-84.69 ± 1.48	338.94 ± 4.18	84.11 ± 1.99	-34.99 ± 5.48	-23.92 ± 1.36	58.43 ± 4.78
107.42	313.19 ± 2.31	-78.20 ± 1.57	-76.67 ± 1.32	321.54 ± 1.04	82.99 ± 0.61	-14.22 ± 1.85	-19.93 ± 0.53	52.68 ± 3.03
117.19	305.57 ± 2.61	-72.75 ± 4.23	-73.14 ± 1.98	312.28 ± 3.35	88.12 ± 1.34	-14.51 ± 1.22	-24.94 ± 0.53	70.40 ± 2.49
126.95	312.22 ± 0.70	-69.04 ± 1.14	-78.34 ± 0.41	330.40 ± 1.40	95.44 ± 0.89	-14.78 ± 0.96	-25.90 ± 0.38	70.68 ± 1.70
136.72	314.37 ± 0.57	-69.90 ± 1.03	-78.01 ± 0.45	330.00 ± 1.09	100.31 ± 1.19	-15.26 ± 1.19	-29.89 ± 0.42	79.35 ± 1.92
146.48	310.73 ± 1.13	-61.36 ± 1.75	-62.54 ± 0.68	303.41 ± 1.05	105.02 ± 1.10	-16.52 ± 4.53	-33.45 ± 0.62	99.63 ± 3.03
156.25	310.00 ± 1.51	-60.61 ± 5.21	-60.51 ± 1.58	289.90 ± 7.19	116.60 ± 1.85	-35.72 ± 5.89	-22.84 ± 0.80	66.80 ± 4.23
166.02	314.32 ± 1.60	-61.74 ± 3.37	-70.87 ± 0.97	319.86 ± 3.01	118.93 ± 0.96	-10.91 ± 1.58	-22.79 ± 1.12	82.57 ± 1.65
175.78	310.43 ± 0.50	-59.80 ± 1.01	-64.89 ± 1.22	324.88 ± 1.61	128.93 ± 1.38	-20.45 ± 0.96	-25.80 ± 1.49	99.92 ± 1.88
185.55	312.84 ± 0.59	-62.09 ± 1.64	-68.53 ± 1.48	331.15 ± 2.41	133.97 ± 1.11	-20.87 ± 2.96	-29.93 ± 0.92	106.30 ± 2.29
195.31	310.12 ± 0.76	-56.64 ± 2.64	-52.16 ± 1.18	305.22 ± 3.22	139.40 ± 0.88	-26.23 ± 2.85	-34.65 ± 0.99	118.34 ± 2.63
205.08	314.25 ± 1.41	-57.08 ± 5.13	-52.14 ± 1.37	312.62 ± 7.31	148.05 ± 0.73	-25.51 ± 3.36	-37.13 ± 0.91	141.83 ± 4.85
214.84	302.03 ± 0.87	-22.97 ± 1.22	-57.64 ± 0.75	334.47 ± 1.23	149.79 ± 0.97	-22.22 ± 1.12	-19.69 ± 0.68	99.95 ± 2.08
224.61	306.33 ± 1.17	-34.00 ± 2.41	-56.76 ± 0.77	316.18 ± 2.36	159.38 ± 0.99	-27.36 ± 3.39	-28.57 ± 0.82	121.73 ± 3.51
234.38	301.38 ± 2.14	-44.06 ± 4.81	-75.07 ± 2.79	357.16 ± 4.58	156.90 ± 5.81	-24.64 ± 1.77	-56.67 ± 10.23	166.61 ± 3.43
244.14	299.01 ± 0.75	-33.54 ± 3.40	-52.59 ± 1.35	313.49 ± 3.18	184.15 ± 0.61	-23.79 ± 1.58	-22.75 ± 0.72	134.10 ± 3.33

Table F. 23. Dynamic-stiffness 10,800 rpm 2,903 kPa (original bearing)

Frequency [Hz]	Re (H_{xx}) [MN/m]	Re (H_{xy}) [MN/m]	Re (H_{yx}) [MN/m]	Re (H_{yy}) [MN/m]	Im (H_{xx}) [MN/m]	Im (H_{xy}) [MN/m]	Im (H_{yx}) [MN/m]	Im (H_{yy}) [MN/m]
9.77	343.85 ± 1.77	-85.70 ± 4.67	-94.88 ± 1.29	440.75 ± 4.32	9.70 ± 1.97	-1.89 ± 6.28	-34.94 ± 3.36	64.96 ± 4.13
19.53	343.91 ± 1.31	-78.96 ± 3.43	-106.51 ± 2.44	418.32 ± 6.09	21.12 ± 1.82	-12.20 ± 3.29	-16.86 ± 3.99	32.66 ± 4.17
29.30	345.16 ± 0.42	-81.72 ± 0.82	-82.46 ± 2.44	425.47 ± 3.91	28.94 ± 0.88	-6.27 ± 0.62	-14.38 ± 3.78	26.98 ± 1.51
39.06	349.49 ± 0.43	-80.36 ± 0.68	-83.42 ± 2.34	422.43 ± 1.29	42.70 ± 1.35	-11.61 ± 0.59	1.96 ± 3.58	31.72 ± 1.02
48.83	352.65 ± 0.25	-81.99 ± 0.44	-90.70 ± 1.02	427.89 ± 1.00	53.41 ± 0.72	-14.93 ± 0.31	-10.58 ± 1.02	42.44 ± 1.42
58.59	355.19 ± 1.17	-82.18 ± 0.48	-85.23 ± 2.78	427.34 ± 1.61	60.50 ± 0.65	-14.63 ± 0.56	-19.60 ± 1.48	46.02 ± 0.75
68.36	354.12 ± 0.50	-80.80 ± 0.27	-86.87 ± 1.43	427.20 ± 1.57	70.72 ± 0.63	-17.22 ± 0.26	-15.28 ± 0.54	45.60 ± 0.53
78.13	355.72 ± 0.44	-80.88 ± 0.33	-89.82 ± 0.89	410.01 ± 1.01	91.68 ± 0.45	-18.18 ± 0.32	-4.31 ± 0.89	55.42 ± 0.93
87.89	362.59 ± 0.25	-82.69 ± 0.18	-86.76 ± 0.48	433.68 ± 0.82	88.18 ± 0.45	-21.57 ± 0.32	-24.05 ± 1.26	82.57 ± 0.92
97.66	366.96 ± 0.36	-81.41 ± 0.44	-81.52 ± 0.83	422.62 ± 1.03	95.43 ± 0.54	-22.21 ± 0.30	-22.25 ± 0.38	72.65 ± 0.52
107.42	367.52 ± 0.15	-80.08 ± 0.17	-86.05 ± 1.96	434.06 ± 1.49	104.05 ± 0.33	-23.61 ± 0.27	-28.11 ± 0.62	93.18 ± 0.56
117.19	371.67 ± 0.54	-78.71 ± 0.21	-85.73 ± 0.87	433.91 ± 0.72	110.11 ± 0.39	-24.29 ± 0.20	-33.56 ± 1.77	96.04 ± 0.52
126.95	374.69 ± 0.44	-75.95 ± 0.45	-86.02 ± 0.55	428.24 ± 0.88	117.93 ± 0.46	-24.60 ± 0.16	-34.22 ± 1.06	112.60 ± 0.84
136.72	377.46 ± 0.21	-71.65 ± 0.29	-80.97 ± 1.22	432.33 ± 1.41	128.13 ± 0.25	-27.86 ± 0.18	-39.37 ± 0.73	118.86 ± 0.43
146.48	380.03 ± 0.29	-65.68 ± 0.33	-73.27 ± 1.16	425.67 ± 1.76	133.62 ± 0.25	-28.81 ± 0.25	-33.90 ± 0.54	123.02 ± 1.91
156.25	379.81 ± 0.48	-64.77 ± 0.38	-76.60 ± 1.91	428.32 ± 1.33	141.78 ± 0.40	-31.92 ± 0.18	-30.93 ± 1.31	104.57 ± 0.77
166.02	382.97 ± 0.43	-68.73 ± 0.21	-81.67 ± 0.67	448.85 ± 1.11	147.45 ± 0.71	-33.81 ± 0.62	-40.85 ± 0.84	150.50 ± 0.82
175.78	382.85 ± 1.73	-62.86 ± 2.57	-83.05 ± 1.53	454.15 ± 1.73	154.22 ± 1.13	-35.18 ± 1.97	-42.13 ± 2.89	148.83 ± 4.49
185.55	383.72 ± 1.18	-61.05 ± 0.70	-74.27 ± 2.31	452.62 ± 1.52	165.82 ± 1.18	-38.43 ± 0.48	-36.43 ± 1.81	152.32 ± 0.49
195.31	385.51 ± 0.50	-56.36 ± 0.28	-69.16 ± 0.90	446.10 ± 0.81	175.42 ± 0.44	-38.73 ± 0.66	-38.41 ± 2.51	155.65 ± 0.71
205.08	384.96 ± 0.55	-53.41 ± 0.30	-71.76 ± 1.66	458.76 ± 1.18	182.03 ± 0.45	-42.27 ± 0.32	-37.32 ± 1.90	175.57 ± 0.50
214.84	392.77 ± 0.34	-47.41 ± 0.37	-64.27 ± 1.66	463.01 ± 1.16	191.40 ± 0.78	-40.65 ± 0.41	-50.56 ± 2.68	169.03 ± 0.65
224.61	392.40 ± 0.53	-45.97 ± 0.42	-66.27 ± 2.75	430.97 ± 1.76	200.48 ± 0.41	-44.91 ± 0.39	-44.15 ± 1.09	168.79 ± 0.41
234.38	396.66 ± 0.45	-49.63 ± 0.43	-65.21 ± 1.64	482.36 ± 1.33	210.29 ± 0.25	-53.49 ± 0.51	-49.19 ± 0.50	202.37 ± 0.52
244.14	394.98 ± 0.63	-40.68 ± 0.17	-62.56 ± 1.31	474.76 ± 1.14	222.74 ± 0.22	-53.79 ± 0.39	-46.81 ± 1.70	212.02 ± 0.44

Table F. 24. Dynamic-stiffness 10,800 rpm 2,903 kPa (modified bearing)

Frequency [Hz]	Re (H_{xx}) [MN/m]	Re (H_{xy}) [MN/m]	Re (H_{yx}) [MN/m]	Re (H_{yy}) [MN/m]	Im (H_{xx}) [MN/m]	Im (H_{xy}) [MN/m]	Im (H_{yx}) [MN/m]	Im (H_{yy}) [MN/m]
9.77	317.66 ± 1.43	-84.88 ± 1.14	-74.64 ± 1.14	360.01 ± 1.36	9.16 ± 0.92	3.97 ± 1.93	2.56 ± 0.99	9.28 ± 2.04
19.53	314.81 ± 2.28	-83.24 ± 3.77	-77.96 ± 1.29	363.79 ± 2.98	16.62 ± 1.79	-4.04 ± 2.00	-6.36 ± 0.90	15.36 ± 2.24
29.30	318.71 ± 1.33	-79.64 ± 2.15	-75.93 ± 1.00	370.83 ± 1.88	27.21 ± 2.33	-3.03 ± 2.18	-6.28 ± 1.74	21.66 ± 2.67
39.06	327.32 ± 2.65	-86.00 ± 1.32	-70.35 ± 1.93	360.86 ± 1.50	35.54 ± 1.35	-8.37 ± 1.55	-9.55 ± 0.58	23.08 ± 1.66
48.83	321.33 ± 0.65	-77.57 ± 2.34	-72.05 ± 0.67	347.11 ± 2.00	40.66 ± 2.30	-7.27 ± 2.51	-11.40 ± 1.33	21.77 ± 2.80
58.59	318.76 ± 3.40	-77.41 ± 1.96	-77.01 ± 2.00	363.71 ± 1.45	44.74 ± 3.27	-5.20 ± 1.90	-7.68 ± 2.04	18.34 ± 2.19
68.36	325.21 ± 0.75	-84.75 ± 3.00	-78.30 ± 1.12	374.09 ± 2.28	50.87 ± 0.68	-0.63 ± 2.56	-7.18 ± 0.52	14.51 ± 2.85
78.13	325.10 ± 0.80	-89.21 ± 1.10	-67.22 ± 0.62	334.63 ± 1.30	60.29 ± 2.41	-10.55 ± 2.11	-12.26 ± 1.99	25.28 ± 2.58
87.89	329.37 ± 2.56	-80.89 ± 1.68	-74.95 ± 1.49	357.25 ± 1.18	64.17 ± 1.57	-13.57 ± 1.98	-20.58 ± 0.88	32.15 ± 2.53
97.66	329.49 ± 1.95	-89.60 ± 1.94	-82.29 ± 1.17	370.25 ± 1.39	75.55 ± 1.24	-30.38 ± 3.38	-21.40 ± 0.57	44.01 ± 3.61
107.42	331.16 ± 0.71	-78.14 ± 1.05	-76.69 ± 0.49	356.88 ± 1.26	74.81 ± 0.74	-8.80 ± 2.81	-19.20 ± 0.72	38.14 ± 3.33
117.19	329.08 ± 1.98	-73.35 ± 4.17	-70.76 ± 1.67	343.65 ± 2.70	81.39 ± 2.06	-14.29 ± 4.67	-19.47 ± 1.69	48.93 ± 3.83
126.95	333.37 ± 0.59	-72.25 ± 1.18	-74.53 ± 0.61	360.05 ± 1.30	87.70 ± 2.03	-14.31 ± 1.93	-22.60 ± 1.32	53.20 ± 2.69
136.72	329.42 ± 0.92	-68.71 ± 0.75	-78.03 ± 0.48	360.64 ± 1.00	90.39 ± 0.87	-13.17 ± 1.10	-28.04 ± 0.51	61.01 ± 2.04
146.48	329.92 ± 0.93	-65.68 ± 3.61	-61.69 ± 0.65	330.45 ± 3.59	92.61 ± 0.85	-8.88 ± 1.05	-31.04 ± 0.48	84.37 ± 2.62
156.25	328.39 ± 1.41	-67.43 ± 5.88	-58.41 ± 0.54	316.61 ± 1.25	104.91 ± 2.45	-37.98 ± 12.42	-20.92 ± 1.02	40.90 ± 5.53
166.02	333.50 ± 1.89	-60.31 ± 1.45	-69.51 ± 0.62	352.64 ± 1.55	105.20 ± 0.96	-4.93 ± 2.04	-25.01 ± 0.51	66.62 ± 2.66
175.78	327.26 ± 0.71	-60.78 ± 2.33	-63.83 ± 0.69	351.24 ± 2.14	117.44 ± 1.42	-19.74 ± 0.81	-25.69 ± 0.76	82.07 ± 2.69
185.55	328.83 ± 1.67	-61.11 ± 1.45	-66.84 ± 0.70	357.20 ± 2.11	121.97 ± 0.90	-20.66 ± 1.98	-31.28 ± 1.06	86.01 ± 2.51
195.31	325.62 ± 1.61	-55.30 ± 4.27	-50.10 ± 1.07	326.84 ± 3.67	125.81 ± 0.58	-24.47 ± 2.53	-33.32 ± 1.05	97.85 ± 3.80
205.08	326.09 ± 1.12	-48.81 ± 2.18	-49.58 ± 0.80	325.60 ± 2.52	138.75 ± 0.88	-37.43 ± 2.83	-33.31 ± 0.90	106.00 ± 5.96
214.84	317.03 ± 0.65	-17.99 ± 1.31	-54.98 ± 0.64	354.48 ± 1.67	135.16 ± 0.83	-23.36 ± 0.83	-23.46 ± 1.16	81.72 ± 1.71
224.61	320.16 ± 0.94	-27.46 ± 3.66	-55.89 ± 0.51	348.16 ± 2.37	145.29 ± 0.80	-29.92 ± 2.07	-29.06 ± 0.51	93.26 ± 2.53
234.38	323.57 ± 4.99	-47.76 ± 3.74	-56.94 ± 3.83	376.44 ± 4.98	152.07 ± 4.63	-23.00 ± 5.60	-62.15 ± 2.78	162.05 ± 3.53
244.14	316.11 ± 1.09	-37.73 ± 1.25	-49.33 ± 0.75	325.64 ± 1.88	165.20 ± 0.59	-26.99 ± 2.84	-30.31 ± 0.62	116.08 ± 3.20

Table F. 25. Dynamic-stiffness 13,200 rpm 726 kPa (original bearing)

Frequency [Hz]	Re (H_{xx}) [MN/m]	Re (H_{xy}) [MN/m]	Re (H_{yx}) [MN/m]	Re (H_{yy}) [MN/m]	Im (H_{xx}) [MN/m]	Im (H_{xy}) [MN/m]	Im (H_{yx}) [MN/m]	Im (H_{yy}) [MN/m]
9.77	305.05 ± 3.22	-65.70 ± 2.17	-95.61 ± 3.86	301.96 ± 2.87	13.03 ± 1.91	-15.02 ± 2.41	-7.64 ± 3.42	36.71 ± 1.45
19.53	303.25 ± 1.81	-70.82 ± 1.10	-95.71 ± 4.13	302.78 ± 1.74	25.24 ± 1.16	-13.29 ± 1.72	1.40 ± 3.17	12.70 ± 2.24
29.30	306.51 ± 3.76	-75.84 ± 1.44	-98.46 ± 2.31	314.88 ± 2.41	30.49 ± 2.39	-8.22 ± 3.43	-7.12 ± 1.60	31.89 ± 2.71
39.06	306.07 ± 0.93	-71.97 ± 1.60	-93.41 ± 2.03	304.64 ± 1.83	42.96 ± 1.70	-13.32 ± 0.75	-12.78 ± 3.36	45.49 ± 1.31
48.83	306.34 ± 0.76	-69.86 ± 1.30	-96.70 ± 0.43	306.00 ± 0.52	55.39 ± 0.68	-20.98 ± 0.86	-9.39 ± 1.53	61.16 ± 0.80
58.59	309.77 ± 1.09	-71.08 ± 0.43	-95.77 ± 1.38	314.08 ± 0.68	66.80 ± 1.46	-19.95 ± 0.99	-14.35 ± 0.89	71.52 ± 0.76
68.36	316.90 ± 0.51	-73.39 ± 1.07	-83.65 ± 1.95	316.78 ± 1.32	82.18 ± 0.68	-23.95 ± 0.66	-3.91 ± 0.82	72.36 ± 0.81
78.13	317.56 ± 0.37	-70.37 ± 0.58	-89.56 ± 2.32	305.50 ± 0.92	88.95 ± 0.51	-27.77 ± 0.41	-11.74 ± 1.65	80.78 ± 0.50
87.89	320.19 ± 0.72	-74.45 ± 0.45	-98.69 ± 1.16	329.68 ± 0.72	97.18 ± 1.07	-30.49 ± 1.06	-14.40 ± 2.94	108.84 ± 1.00
97.66	324.92 ± 0.34	-74.41 ± 0.37	-94.59 ± 2.85	321.12 ± 0.71	105.87 ± 0.53	-33.61 ± 0.34	-16.61 ± 2.63	112.12 ± 0.85
107.42	324.48 ± 0.97	-75.42 ± 0.41	-98.82 ± 0.88	330.71 ± 1.10	114.62 ± 0.68	-34.38 ± 0.45	-12.44 ± 1.47	126.73 ± 0.59
117.19	329.36 ± 0.37	-77.48 ± 0.46	-97.02 ± 0.96	335.02 ± 0.70	123.77 ± 0.48	-36.57 ± 0.19	-18.60 ± 1.30	133.72 ± 0.85
126.95	332.01 ± 0.60	-77.12 ± 0.66	-92.93 ± 0.97	330.94 ± 0.57	131.26 ± 0.54	-38.20 ± 0.52	-19.37 ± 2.06	150.81 ± 0.76
136.72	335.65 ± 0.47	-74.99 ± 0.65	-90.93 ± 1.17	342.74 ± 0.60	143.98 ± 0.55	-39.82 ± 0.37	-18.03 ± 1.52	154.32 ± 1.03
146.48	338.42 ± 0.78	-73.23 ± 0.42	-90.51 ± 1.41	346.86 ± 0.52	151.24 ± 0.53	-42.28 ± 0.55	-20.99 ± 1.85	158.50 ± 0.96
156.25	338.76 ± 0.40	-68.73 ± 0.74	-83.20 ± 2.08	325.00 ± 0.73	159.21 ± 0.90	-43.80 ± 0.27	-24.12 ± 1.52	164.91 ± 1.05
166.02	344.46 ± 0.88	-80.04 ± 0.31	-87.99 ± 0.40	362.91 ± 0.66	167.60 ± 0.58	-42.56 ± 0.51	-18.95 ± 1.90	189.70 ± 0.68
175.78	343.99 ± 0.43	-76.95 ± 0.27	-86.97 ± 1.00	370.10 ± 0.54	178.33 ± 0.64	-45.31 ± 0.38	-20.03 ± 1.16	190.16 ± 0.77
185.55	345.03 ± 0.63	-74.99 ± 0.24	-81.41 ± 0.61	369.82 ± 0.40	186.36 ± 0.67	-42.03 ± 0.30	-17.09 ± 1.13	189.72 ± 1.09
195.31	348.05 ± 0.77	-70.62 ± 0.67	-71.83 ± 1.39	358.99 ± 0.60	197.64 ± 0.57	-41.19 ± 0.31	-14.62 ± 3.30	196.84 ± 1.00
205.08	349.40 ± 1.01	-71.90 ± 0.44	-72.36 ± 0.80	369.54 ± 0.75	204.43 ± 0.96	-38.11 ± 0.27	-17.05 ± 2.17	216.94 ± 0.66
214.84	355.97 ± 0.96	-66.87 ± 0.70	-67.61 ± 1.08	373.93 ± 1.21	218.03 ± 1.13	-36.30 ± 0.30	-23.83 ± 2.72	210.49 ± 1.17
224.61	358.73 ± 2.35	-42.82 ± 0.51	-56.20 ± 3.53	286.12 ± 1.19	229.97 ± 2.77	-36.76 ± 1.01	-35.46 ± 1.12	266.94 ± 1.27
234.38	367.20 ± 0.55	-68.74 ± 0.38	-68.84 ± 1.37	391.51 ± 0.56	238.60 ± 1.08	-39.57 ± 0.23	-32.84 ± 3.05	244.44 ± 1.26
244.14	364.06 ± 0.60	-64.28 ± 0.33	-65.72 ± 1.93	394.11 ± 0.77	252.32 ± 0.26	-35.45 ± 0.16	-24.89 ± 2.49	251.41 ± 0.81

Table F. 26. Dynamic-stiffness 13,200 rpm 726 kPa (modified bearing)

Frequency [Hz]	Re (H_{xx}) [MN/m]	Re (H_{xy}) [MN/m]	Re (H_{yx}) [MN/m]	Re (H_{yy}) [MN/m]	Im (H_{xx}) [MN/m]	Im (H_{xy}) [MN/m]	Im (H_{yx}) [MN/m]	Im (H_{yy}) [MN/m]
9.77	276.75 ± 1.79	-71.88 ± 1.52	-88.15 ± 3.67	263.86 ± 1.98	7.28 ± 2.16	0.96 ± 1.77	-3.35 ± 1.14	10.82 ± 2.34
19.53	280.33 ± 1.57	-71.77 ± 1.77	-84.86 ± 2.09	264.90 ± 1.74	21.45 ± 2.07	-6.28 ± 1.45	-8.88 ± 3.84	20.63 ± 2.81
29.30	282.32 ± 2.90	-73.26 ± 1.51	-85.74 ± 1.70	268.24 ± 1.34	30.46 ± 3.20	-9.76 ± 1.87	-8.24 ± 2.42	29.10 ± 2.23
39.06	278.37 ± 2.03	-70.20 ± 1.92	-91.60 ± 2.14	270.37 ± 1.78	42.86 ± 0.76	-12.85 ± 1.39	-10.01 ± 1.42	37.82 ± 1.99
48.83	277.45 ± 3.01	-67.25 ± 5.28	-83.19 ± 1.40	250.28 ± 3.02	46.53 ± 1.17	-16.16 ± 2.99	-10.07 ± 1.48	43.07 ± 3.72
58.59	281.69 ± 2.59	-71.57 ± 1.46	-85.27 ± 1.30	266.27 ± 1.11	58.26 ± 3.07	-18.30 ± 1.37	-8.56 ± 1.64	43.14 ± 1.80
68.36	284.38 ± 3.27	-82.62 ± 1.29	-79.67 ± 2.08	242.56 ± 2.20	65.48 ± 2.13	-19.67 ± 1.54	-4.42 ± 1.51	48.20 ± 2.76
78.13	284.92 ± 2.08	-70.34 ± 1.38	-79.21 ± 1.96	257.53 ± 1.21	74.70 ± 1.88	-17.82 ± 1.08	-9.69 ± 2.99	60.19 ± 2.56
87.89	283.97 ± 1.22	-71.63 ± 1.52	-91.04 ± 1.44	272.61 ± 2.07	83.97 ± 1.66	-27.94 ± 1.18	-8.89 ± 1.05	64.65 ± 2.39
97.66	295.19 ± 2.19	-87.65 ± 3.16	-87.66 ± 1.72	275.51 ± 4.84	94.82 ± 2.21	-41.93 ± 2.99	-7.75 ± 1.52	64.26 ± 2.34
107.42	289.62 ± 2.18	-72.50 ± 1.59	-87.84 ± 2.14	274.37 ± 1.94	95.99 ± 1.30	-24.65 ± 1.42	-10.94 ± 1.08	80.11 ± 2.58
117.19	289.65 ± 1.55	-70.24 ± 5.08	-83.30 ± 1.67	275.85 ± 5.13	100.52 ± 2.41	-19.61 ± 3.29	-13.70 ± 1.62	89.96 ± 4.76
126.95	293.90 ± 2.30	-72.85 ± 1.49	-88.23 ± 0.71	285.44 ± 1.07	114.48 ± 1.39	-28.91 ± 1.00	-13.07 ± 1.68	99.50 ± 2.13
136.72	293.02 ± 2.91	-72.16 ± 1.38	-86.04 ± 2.65	288.33 ± 1.45	126.24 ± 1.39	-33.01 ± 1.29	-11.96 ± 0.99	107.95 ± 2.01
146.48	292.61 ± 2.70	-70.26 ± 2.85	-74.68 ± 3.00	263.98 ± 2.10	134.69 ± 2.48	-40.15 ± 5.07	-21.49 ± 2.16	134.37 ± 6.32
156.25	290.13 ± 1.70	-51.02 ± 5.14	-73.45 ± 2.77	269.47 ± 9.64	138.37 ± 2.77	-30.16 ± 7.53	-3.90 ± 2.76	68.12 ± 8.64
166.02	300.25 ± 1.15	-74.58 ± 1.18	-77.73 ± 0.91	280.27 ± 1.08	145.91 ± 1.38	-23.88 ± 0.86	-15.62 ± 1.34	120.43 ± 2.49
175.78	300.65 ± 0.48	-72.74 ± 1.51	-73.13 ± 0.46	286.30 ± 1.34	160.35 ± 1.22	-33.10 ± 1.22	-13.88 ± 0.96	135.16 ± 2.14
185.55	301.98 ± 1.40	-73.42 ± 1.69	-70.41 ± 0.95	301.01 ± 1.76	170.06 ± 1.05	-32.40 ± 1.07	-9.11 ± 2.54	137.08 ± 3.07
195.31	300.60 ± 1.43	-71.71 ± 1.87	-56.51 ± 1.08	277.69 ± 4.94	187.67 ± 1.11	-40.92 ± 2.11	-3.11 ± 1.19	149.60 ± 3.05
205.08	313.95 ± 1.77	-85.98 ± 4.00	-47.91 ± 1.25	272.00 ± 6.62	207.56 ± 1.60	-45.33 ± 6.74	-3.62 ± 2.01	183.62 ± 9.14
214.84	314.33 ± 1.94	-38.32 ± 3.09	-37.65 ± 3.41	292.42 ± 2.92	199.54 ± 3.73	-28.83 ± 3.85	6.58 ± 2.34	130.45 ± 4.03
224.61	340.41 ± 7.11	-45.48 ± 7.18	-18.89 ± 10.19	259.82 ± 5.87	235.32 ± 17.90	-28.94 ± 6.26	-25.72 ± 7.92	184.30 ± 8.68
234.38	332.44 ± 5.05	-67.02 ± 2.74	-43.64 ± 4.00	326.37 ± 4.51	218.19 ± 3.44	-35.73 ± 2.72	-2.18 ± 4.37	190.18 ± 4.90
244.14	327.86 ± 2.73	-66.81 ± 3.72	-24.95 ± 4.12	284.39 ± 3.33	240.15 ± 1.57	-29.15 ± 2.65	-3.63 ± 1.41	150.30 ± 4.00

Table F. 27. Dynamic-stiffness 13,200 rpm 1,452 kPa (original bearing)

Frequency [Hz]	Re (H_{xx}) [MN/m]	Re (H_{xy}) [MN/m]	Re (H_{yx}) [MN/m]	Re (H_{yy}) [MN/m]	Im (H_{xx}) [MN/m]	Im (H_{xy}) [MN/m]	Im (H_{yx}) [MN/m]	Im (H_{yy}) [MN/m]
9.77	331.63 ± 6.02	-83.40 ± 5.22	-91.25 ± 5.48	351.30 ± 4.70	22.54 ± 5.02	-19.50 ± 2.57	3.34 ± 5.26	41.54 ± 4.28
19.53	330.70 ± 1.30	-85.35 ± 3.92	-96.44 ± 1.95	353.24 ± 5.95	23.67 ± 1.33	-14.76 ± 3.53	-3.72 ± 1.28	26.70 ± 4.06
29.30	336.10 ± 2.12	-83.83 ± 3.17	-109.59 ± 1.75	359.89 ± 1.24	29.65 ± 2.35	-14.14 ± 1.90	-12.54 ± 3.71	23.31 ± 2.33
39.06	334.70 ± 1.24	-84.87 ± 1.74	-96.40 ± 1.99	345.17 ± 1.80	39.29 ± 1.51	-12.76 ± 1.37	-20.90 ± 2.92	43.40 ± 1.22
48.83	335.17 ± 1.40	-81.65 ± 1.28	-98.11 ± 1.82	344.38 ± 0.74	52.58 ± 0.55	-19.38 ± 0.51	-12.53 ± 1.22	57.99 ± 0.62
58.59	334.24 ± 1.02	-82.32 ± 0.69	-100.05 ± 2.16	353.65 ± 0.98	59.92 ± 1.19	-20.70 ± 0.66	-18.82 ± 1.98	59.94 ± 1.17
68.36	332.82 ± 0.71	-81.45 ± 0.93	-102.60 ± 0.92	356.37 ± 0.53	71.28 ± 0.94	-22.06 ± 0.74	-20.56 ± 1.01	62.53 ± 1.58
78.13	344.10 ± 0.77	-83.27 ± 0.33	-94.11 ± 0.71	345.89 ± 0.75	83.74 ± 0.87	-25.11 ± 0.63	-7.81 ± 1.09	65.67 ± 0.64
87.89	346.06 ± 0.98	-86.86 ± 0.48	-100.35 ± 1.40	364.55 ± 0.48	90.08 ± 0.50	-27.77 ± 0.40	-16.35 ± 2.28	95.09 ± 0.96
97.66	347.61 ± 0.65	-86.65 ± 0.48	-93.98 ± 1.03	355.46 ± 0.43	98.06 ± 1.25	-30.33 ± 0.60	-20.30 ± 1.15	94.67 ± 0.65
107.42	348.52 ± 0.67	-87.52 ± 0.89	-103.86 ± 1.48	365.31 ± 0.91	105.46 ± 0.32	-30.80 ± 0.53	-20.91 ± 1.47	114.60 ± 0.64
117.19	352.54 ± 0.53	-87.35 ± 0.49	-103.32 ± 0.87	369.53 ± 0.54	112.92 ± 0.43	-31.68 ± 0.50	-20.70 ± 0.64	118.10 ± 0.90
126.95	355.18 ± 0.20	-86.24 ± 0.27	-96.68 ± 0.90	363.86 ± 0.69	122.28 ± 0.54	-33.13 ± 0.57	-22.44 ± 0.53	133.78 ± 1.05
136.72	355.94 ± 0.37	-83.80 ± 0.56	-94.56 ± 0.74	368.42 ± 1.12	132.05 ± 0.43	-33.88 ± 0.46	-23.92 ± 1.12	141.61 ± 0.80
146.48	360.15 ± 0.48	-83.43 ± 0.35	-92.37 ± 0.73	372.91 ± 0.50	137.91 ± 0.48	-34.21 ± 0.30	-23.43 ± 2.25	144.51 ± 0.72
156.25	360.29 ± 0.95	-77.94 ± 0.39	-86.01 ± 1.48	357.51 ± 0.57	146.38 ± 0.64	-34.43 ± 0.43	-26.73 ± 1.91	134.90 ± 0.88
166.02	363.03 ± 0.45	-86.07 ± 0.29	-95.04 ± 0.76	392.60 ± 0.90	153.31 ± 0.68	-37.99 ± 0.75	-22.15 ± 0.84	175.40 ± 0.60
175.78	363.64 ± 0.70	-83.23 ± 0.22	-92.40 ± 1.26	390.52 ± 1.00	163.55 ± 0.47	-39.06 ± 0.68	-28.42 ± 0.65	177.41 ± 0.91
185.55	366.87 ± 0.84	-82.57 ± 0.25	-93.57 ± 0.78	397.18 ± 0.92	172.38 ± 0.80	-37.44 ± 0.30	-19.83 ± 1.36	175.36 ± 1.50
195.31	368.29 ± 0.75	-78.68 ± 0.34	-86.55 ± 0.72	390.51 ± 0.73	180.78 ± 0.87	-36.05 ± 0.55	-17.22 ± 1.98	183.61 ± 1.01
205.08	367.61 ± 1.04	-76.30 ± 0.83	-84.86 ± 1.34	403.37 ± 0.50	187.72 ± 0.75	-34.58 ± 0.39	-20.52 ± 2.14	199.54 ± 0.97
214.84	373.14 ± 1.34	-71.18 ± 0.85	-77.89 ± 2.59	408.84 ± 1.73	199.07 ± 1.03	-32.50 ± 1.65	-25.15 ± 1.27	191.71 ± 0.76
224.61	376.99 ± 4.32	-63.80 ± 1.55	-72.29 ± 4.68	346.23 ± 1.52	208.29 ± 4.08	-31.12 ± 1.24	-32.71 ± 3.79	201.90 ± 1.91
234.38	380.71 ± 0.69	-73.41 ± 0.34	-75.32 ± 1.60	422.14 ± 1.21	220.46 ± 1.20	-39.84 ± 0.36	-37.36 ± 2.47	225.79 ± 0.81
244.14	378.96 ± 0.31	-62.24 ± 0.21	-74.77 ± 1.15	409.99 ± 1.16	231.61 ± 0.49	-36.32 ± 0.34	-27.83 ± 1.67	240.51 ± 1.14

Table F. 28. Dynamic-stiffness 13,200 rpm 1,452 kPa (modified bearing)

Frequency [Hz]	Re (H_{xx}) [MN/m]	Re (H_{xy}) [MN/m]	Re (H_{yx}) [MN/m]	Re (H_{yy}) [MN/m]	Im (H_{xx}) [MN/m]	Im (H_{xy}) [MN/m]	Im (H_{yx}) [MN/m]	Im (H_{yy}) [MN/m]
9.77	291.51 ± 2.72	-79.22 ± 1.47	-86.20 ± 0.77	297.45 ± 1.91	7.64 ± 1.13	0.16 ± 1.82	-2.89 ± 2.25	8.48 ± 2.33
19.53	289.81 ± 2.48	-77.07 ± 1.25	-83.74 ± 1.97	298.79 ± 1.28	15.09 ± 1.55	-3.55 ± 1.54	-8.79 ± 0.95	18.66 ± 2.44
29.30	293.42 ± 0.96	-79.61 ± 2.48	-84.69 ± 1.38	300.81 ± 3.39	32.34 ± 1.97	-11.18 ± 1.24	-6.59 ± 1.61	22.75 ± 2.48
39.06	290.12 ± 2.71	-73.59 ± 1.35	-88.33 ± 2.06	305.22 ± 1.77	43.19 ± 2.53	-12.12 ± 1.95	-8.99 ± 1.42	32.04 ± 2.15
48.83	296.64 ± 3.02	-72.84 ± 2.96	-78.19 ± 1.50	281.26 ± 1.83	45.51 ± 2.11	-10.84 ± 3.64	-9.82 ± 2.14	32.08 ± 2.80
58.59	290.73 ± 6.10	-75.70 ± 2.22	-90.57 ± 3.71	301.21 ± 1.89	48.33 ± 4.70	-10.66 ± 1.98	-7.32 ± 5.18	33.46 ± 2.91
68.36	295.42 ± 2.79	-81.23 ± 1.79	-87.34 ± 1.42	303.11 ± 1.77	66.98 ± 2.77	-31.76 ± 1.71	10.07 ± 3.50	-23.05 ± 3.46
78.13	300.92 ± 1.49	-81.12 ± 0.99	-77.83 ± 1.98	288.55 ± 1.48	65.61 ± 0.95	-13.02 ± 1.37	-14.61 ± 2.16	47.66 ± 2.41
87.89	299.93 ± 2.51	-78.77 ± 1.18	-87.84 ± 2.14	301.12 ± 1.51	78.52 ± 0.97	-21.46 ± 0.96	-13.04 ± 1.61	51.91 ± 2.70
97.66	312.39 ± 3.16	-98.99 ± 2.92	-89.13 ± 2.16	304.86 ± 3.59	92.93 ± 1.92	-42.82 ± 4.26	-13.64 ± 1.36	54.69 ± 3.94
107.42	311.58 ± 1.52	-84.12 ± 1.64	-85.12 ± 1.29	299.83 ± 1.22	86.75 ± 1.97	-18.43 ± 1.07	-16.40 ± 2.19	64.44 ± 2.75
117.19	313.74 ± 3.24	-75.30 ± 7.84	-78.45 ± 3.03	287.96 ± 3.23	96.76 ± 2.48	-18.40 ± 3.70	-17.90 ± 2.51	72.53 ± 5.34
126.95	309.63 ± 1.06	-77.28 ± 1.73	-85.49 ± 1.04	307.33 ± 1.25	106.56 ± 2.74	-23.09 ± 1.36	-19.53 ± 3.66	82.97 ± 2.28
136.72	308.59 ± 2.46	-73.37 ± 1.12	-91.61 ± 3.05	314.75 ± 1.74	115.13 ± 2.46	-24.54 ± 1.41	-17.09 ± 2.19	88.66 ± 2.23
146.48	311.73 ± 1.70	-78.43 ± 4.36	-77.21 ± 1.67	283.30 ± 3.69	120.42 ± 0.75	-26.32 ± 1.98	-31.17 ± 1.70	125.28 ± 2.67
156.25	308.84 ± 2.08	-53.21 ± 6.21	-77.19 ± 2.99	309.28 ± 6.86	135.97 ± 3.34	-50.83 ± 11.15	-2.66 ± 3.47	17.96 ± 7.48
166.02	316.95 ± 0.93	-73.85 ± 2.38	-79.37 ± 1.10	304.29 ± 1.41	134.78 ± 0.89	-19.63 ± 1.42	-16.51 ± 0.78	96.13 ± 2.98
175.78	313.55 ± 0.83	-72.90 ± 1.11	-76.17 ± 0.83	308.94 ± 1.46	144.51 ± 0.89	-23.22 ± 1.15	-18.72 ± 0.51	114.18 ± 2.55
185.55	315.32 ± 1.51	-73.64 ± 1.23	-79.21 ± 0.38	320.18 ± 1.35	150.57 ± 1.51	-27.40 ± 1.18	-19.08 ± 1.02	120.10 ± 2.38
195.31	313.04 ± 1.59	-71.21 ± 2.82	-65.98 ± 1.04	292.46 ± 3.59	159.65 ± 1.78	-36.19 ± 1.61	-18.94 ± 0.95	127.90 ± 2.58
205.08	323.14 ± 3.03	-103.78 ± 13.20	-69.33 ± 2.45	291.32 ± 9.69	165.27 ± 2.25	-38.94 ± 9.20	-23.19 ± 1.58	174.84 ± 7.16
214.84	304.67 ± 2.72	-32.39 ± 3.94	-64.97 ± 2.06	321.06 ± 1.55	173.93 ± 2.46	-25.98 ± 3.61	3.09 ± 0.98	105.56 ± 3.38
224.61	308.62 ± 2.19	-40.85 ± 4.86	-62.60 ± 2.03	306.79 ± 5.24	184.42 ± 2.87	-24.13 ± 5.89	-4.35 ± 3.32	140.14 ± 5.65
234.38	325.77 ± 9.65	-61.15 ± 3.91	-54.90 ± 9.22	340.91 ± 5.99	200.29 ± 8.16	-26.36 ± 4.81	4.40 ± 8.97	179.79 ± 6.23
244.14	306.23 ± 1.77	-53.64 ± 3.53	-52.06 ± 0.98	295.28 ± 3.62	215.99 ± 1.70	-30.89 ± 2.15	13.64 ± 1.57	132.26 ± 3.84

Table F. 29. Dynamic-stiffness 13,200 rpm 2,177 kPa (modified bearing)

Frequency [Hz]	Re (H_{xx}) [MN/m]	Re (H_{xy}) [MN/m]	Re (H_{yx}) [MN/m]	Re (H_{yy}) [MN/m]	Im (H_{xx}) [MN/m]	Im (H_{xy}) [MN/m]	Im (H_{yx}) [MN/m]	Im (H_{yy}) [MN/m]
9.77	308.09 ± 0.88	-86.18 ± 1.85	-87.24 ± 0.53	333.18 ± 1.99	9.00 ± 1.96	-0.25 ± 2.72	0.24 ± 2.97	6.76 ± 3.68
19.53	311.57 ± 0.97	-84.53 ± 1.54	-88.35 ± 0.57	339.08 ± 1.92	16.71 ± 2.45	-3.04 ± 1.43	-6.61 ± 2.11	18.09 ± 2.05
29.30	309.19 ± 3.39	-84.62 ± 2.13	-90.79 ± 3.00	342.14 ± 1.57	29.16 ± 3.31	-8.10 ± 1.51	-6.66 ± 1.74	19.69 ± 2.23
39.06	311.46 ± 3.04	-83.43 ± 2.83	-90.98 ± 1.74	341.05 ± 2.58	34.95 ± 3.00	-8.64 ± 2.12	-11.71 ± 2.00	28.45 ± 2.87
48.83	313.27 ± 2.38	-72.66 ± 3.84	-81.21 ± 0.80	321.82 ± 3.50	37.26 ± 1.63	1.53 ± 6.69	-12.75 ± 1.69	36.22 ± 4.52
58.59	318.10 ± 3.50	-82.08 ± 2.78	-88.58 ± 2.08	338.71 ± 2.03	45.69 ± 3.77	-7.90 ± 2.49	-6.05 ± 2.71	25.11 ± 3.19
68.36	321.59 ± 1.51	-87.22 ± 1.00	-89.24 ± 1.00	354.06 ± 1.62	58.15 ± 1.83	-13.72 ± 1.97	-5.64 ± 1.38	19.46 ± 3.27
78.13	323.08 ± 1.54	-89.08 ± 1.77	-79.13 ± 1.64	320.90 ± 1.61	61.19 ± 1.91	-10.10 ± 1.83	-13.84 ± 1.42	36.09 ± 2.40
87.89	324.21 ± 2.20	-86.35 ± 2.34	-89.36 ± 1.81	336.26 ± 1.29	70.58 ± 1.99	-19.22 ± 1.54	-13.00 ± 2.19	38.96 ± 2.35
97.66	328.98 ± 1.33	-100.96 ± 2.98	-91.68 ± 1.24	344.10 ± 4.46	80.27 ± 2.16	-24.83 ± 3.36	-15.42 ± 1.44	51.16 ± 2.78
107.42	327.39 ± 2.04	-85.77 ± 1.11	-88.61 ± 2.22	335.00 ± 1.33	80.58 ± 1.85	-12.63 ± 1.04	-18.23 ± 1.18	51.60 ± 2.31
117.19	320.90 ± 4.22	-70.91 ± 7.74	-84.03 ± 3.45	328.44 ± 6.45	89.22 ± 4.54	-19.64 ± 6.29	-17.39 ± 2.94	52.64 ± 5.26
126.95	327.10 ± 1.45	-79.56 ± 2.33	-89.52 ± 1.79	340.20 ± 2.18	95.81 ± 3.34	-16.72 ± 1.22	-18.35 ± 2.38	67.77 ± 2.67
136.72	333.86 ± 1.88	-80.74 ± 2.94	-86.47 ± 1.81	342.64 ± 1.95	103.20 ± 2.47	-18.89 ± 1.91	-21.10 ± 0.88	74.57 ± 2.37
146.48	327.00 ± 1.61	-66.09 ± 2.98	-73.85 ± 1.62	313.79 ± 5.63	107.20 ± 1.68	-18.45 ± 1.93	-26.43 ± 0.52	106.56 ± 2.75
156.25	323.60 ± 4.48	-58.91 ± 16.80	-80.50 ± 3.27	349.30 ± 9.82	111.65 ± 4.52	-17.94 ± 15.95	-6.44 ± 4.31	16.62 ± 16.21
166.02	335.15 ± 1.37	-77.25 ± 2.95	-78.42 ± 1.04	330.50 ± 2.12	116.94 ± 0.72	-10.89 ± 1.72	-16.90 ± 0.94	80.50 ± 2.75
175.78	333.48 ± 0.73	-74.24 ± 1.59	-74.96 ± 0.77	337.22 ± 1.39	127.61 ± 0.99	-17.40 ± 1.16	-22.41 ± 0.77	97.84 ± 2.23
185.55	334.14 ± 1.30	-74.50 ± 1.93	-78.51 ± 1.26	344.89 ± 1.99	136.22 ± 0.81	-22.45 ± 1.79	-20.78 ± 0.31	101.65 ± 1.97
195.31	328.34 ± 1.26	-68.94 ± 3.62	-64.96 ± 1.20	313.85 ± 4.05	138.48 ± 1.45	-30.98 ± 1.98	-25.75 ± 1.21	111.66 ± 4.46
205.08	336.37 ± 1.52	-73.19 ± 5.47	-66.80 ± 1.80	320.94 ± 8.37	153.12 ± 2.37	-43.19 ± 9.21	-26.30 ± 1.41	143.85 ± 6.64
214.84	322.67 ± 2.59	-32.30 ± 2.22	-64.18 ± 2.96	349.19 ± 3.52	153.61 ± 1.84	-26.41 ± 6.87	-4.13 ± 1.36	87.93 ± 2.79
224.61	327.30 ± 3.22	-38.68 ± 10.45	-63.30 ± 2.20	341.05 ± 7.45	162.56 ± 2.06	-26.72 ± 6.15	-13.75 ± 1.69	111.66 ± 6.00
234.38	317.38 ± 8.54	-52.33 ± 2.96	-70.19 ± 12.49	371.87 ± 4.49	167.79 ± 8.80	-20.32 ± 3.50	-47.99 ± 11.82	166.42 ± 4.75
244.14	328.04 ± 1.72	-57.80 ± 3.22	-56.50 ± 1.09	320.15 ± 3.44	185.25 ± 1.14	-26.14 ± 5.11	-6.53 ± 0.74	115.38 ± 3.98

Table F. 30. Dynamic-stiffness 13,200 rpm 2,903 kPa (modified bearing)

Frequency [Hz]	Re (H_{xx}) [MN/m]	Re (H_{xy}) [MN/m]	Re (H_{yx}) [MN/m]	Re (H_{yy}) [MN/m]	Im (H_{xx}) [MN/m]	Im (H_{xy}) [MN/m]	Im (H_{yx}) [MN/m]	Im (H_{yy}) [MN/m]
9.77	333.93 ± 3.24	-95.11 ± 1.92	-87.46 ± 1.16	369.75 ± 2.10	10.91 ± 3.14	1.11 ± 1.83	2.26 ± 2.23	7.77 ± 3.89
19.53	331.18 ± 2.38	-92.52 ± 3.40	-92.29 ± 2.21	375.45 ± 2.63	16.20 ± 1.28	-5.83 ± 1.64	-5.19 ± 0.94	15.26 ± 1.69
29.30	334.77 ± 1.72	-93.32 ± 3.68	-92.01 ± 1.36	378.10 ± 3.13	18.13 ± 2.01	1.23 ± 2.24	-11.13 ± 1.98	24.72 ± 2.39
39.06	335.86 ± 3.04	-88.24 ± 2.96	-89.15 ± 3.28	378.49 ± 3.11	33.34 ± 4.03	-6.49 ± 2.50	-8.64 ± 3.32	26.29 ± 2.86
48.83	336.22 ± 2.60	-89.57 ± 5.74	-85.69 ± 1.57	349.11 ± 3.86	39.10 ± 2.41	-10.20 ± 4.05	-8.73 ± 1.40	20.05 ± 4.08
58.59	348.96 ± 2.69	-90.97 ± 1.78	-83.84 ± 2.15	374.79 ± 1.43	42.80 ± 2.29	-4.84 ± 2.19	-6.06 ± 2.64	20.94 ± 2.95
68.36	339.53 ± 1.25	-95.04 ± 1.51	-93.24 ± 1.01	387.09 ± 1.47	56.94 ± 2.67	-12.30 ± 1.57	-3.92 ± 2.53	16.91 ± 3.26
78.13	343.10 ± 1.41	-96.24 ± 1.28	-79.11 ± 1.14	350.15 ± 1.40	58.70 ± 0.47	-6.21 ± 1.44	-11.73 ± 0.97	27.97 ± 2.18
87.89	344.64 ± 1.73	-91.07 ± 2.19	-88.11 ± 1.26	372.95 ± 1.52	62.80 ± 1.38	-15.26 ± 1.17	-17.02 ± 1.97	30.31 ± 1.82
97.66	351.87 ± 4.85	-108.93 ± 4.65	-90.24 ± 3.72	375.37 ± 3.53	76.25 ± 1.13	-31.65 ± 4.08	-13.24 ± 1.69	32.39 ± 5.12
107.42	353.04 ± 1.51	-89.63 ± 2.46	-86.39 ± 1.48	370.13 ± 1.72	76.47 ± 2.24	-11.34 ± 3.30	-16.01 ± 1.35	38.24 ± 2.53
117.19	347.51 ± 2.84	-92.85 ± 8.44	-81.62 ± 1.36	352.34 ± 3.11	72.62 ± 3.98	-17.91 ± 9.19	-20.26 ± 2.29	40.68 ± 5.51
126.95	352.08 ± 1.02	-85.36 ± 2.81	-86.04 ± 1.29	373.39 ± 2.28	89.13 ± 3.04	-13.26 ± 1.83	-21.45 ± 1.70	54.00 ± 2.59
136.72	351.58 ± 1.67	-80.97 ± 2.01	-86.60 ± 1.07	375.86 ± 1.36	88.30 ± 1.56	-11.04 ± 1.32	-25.94 ± 1.88	61.23 ± 1.82
146.48	351.14 ± 1.40	-85.19 ± 3.37	-73.54 ± 0.91	343.89 ± 3.98	95.78 ± 3.01	-10.62 ± 3.91	-28.04 ± 2.26	92.26 ± 3.80
156.25	333.57 ± 3.32	-5.76 ± 12.40	-91.88 ± 3.09	431.24 ± 11.83	93.40 ± 6.52	14.40 ± 28.42	-1.48 ± 5.34	-33.28 ± 25.00
166.02	356.36 ± 2.42	-75.42 ± 2.92	-80.41 ± 2.35	368.67 ± 2.68	108.44 ± 1.79	-8.44 ± 3.06	-17.96 ± 1.87	63.11 ± 2.12
175.78	351.14 ± 0.82	-74.95 ± 0.79	-73.65 ± 0.74	366.41 ± 1.34	118.12 ± 0.69	-15.32 ± 1.47	-21.81 ± 1.37	80.48 ± 2.63
185.55	350.44 ± 0.61	-73.89 ± 1.87	-77.61 ± 1.26	373.59 ± 1.55	121.43 ± 0.95	-17.19 ± 1.40	-24.52 ± 0.72	86.35 ± 1.96
195.31	348.26 ± 1.58	-67.44 ± 3.64	-61.66 ± 1.44	339.45 ± 4.61	128.55 ± 1.00	-24.31 ± 2.07	-27.78 ± 1.57	97.78 ± 3.86
205.08	357.12 ± 2.13	-101.30 ± 5.42	-53.00 ± 2.14	300.09 ± 7.76	139.79 ± 2.57	-31.21 ± 11.20	-29.52 ± 1.28	124.95 ± 5.63
214.84	338.28 ± 1.26	-29.93 ± 2.59	-68.43 ± 1.62	378.67 ± 3.51	133.27 ± 1.28	-21.65 ± 2.03	-14.30 ± 2.07	73.34 ± 2.76
224.61	340.63 ± 2.52	-33.85 ± 4.42	-67.83 ± 1.73	376.82 ± 3.19	147.32 ± 0.85	-27.83 ± 3.81	-15.60 ± 1.41	82.37 ± 2.75
234.38	345.47 ± 5.68	-58.56 ± 5.24	-54.78 ± 3.87	406.36 ± 5.24	145.16 ± 4.27	-19.16 ± 3.33	-53.19 ± 4.97	151.82 ± 2.90
244.14	341.88 ± 1.09	-44.45 ± 4.84	-55.62 ± 0.98	348.79 ± 3.00	165.59 ± 0.78	-21.19 ± 2.99	-17.56 ± 0.94	105.79 ± 4.79

APPENDIX G: R-SQUARED VALUES

The accuracy of the dynamic coefficients was determined using uncertainties of the least-squares regression at a 95% confidence interval. These uncertainties provided only limited insight into whether or not the dynamic-stiffness was fitted correctly as linear functions of Ω (imaginary part) and Ω^2 (real part). To further answer this question, this appendix presents R^2 values for each curve fit.

The R^2 statistic is calculated from the residual sum of squares (SS_{res}) and the total sum of squares (SS_{tot}),

$$R^2 = 1 - \frac{SS_{res}}{SS_{tot}} = 1 - \frac{\sum (y_i - q_i)^2}{\sum (y_i - \tilde{y})^2} \tag{40}$$

where y_i is the dynamic-stiffness at an individual excitation frequency $\Omega(i)$, $\tilde{y}$ is the mean dynamic-stiffness, and q_i is the estimated value at $\Omega(i)$. A value of R^2=1 indicates that the data is perfectly fitted as a linear function. Table G. 1 provides the R^2 values of Im($\boldsymbol{H}_{ij}$) for the original and modified bearing.

Table G. 1. R-squared values for Im(H_{ij}) curve fits

Speed [RPM]	Unit Load [kPa]	Original Bearing				Modified Bearing			
		Im Hxx	Im Hxy	Im Hyx	Im Hyy	Im Hxx	Im Hxy	Im Hyx	Im Hyy
6,800	725	1.00	0.82	0.58	0.98	0.95	-0.17	-0.09	0.98
	1,452	1.00	0.91	-0.01	0.98	0.99	0.52	0.35	0.87
	2,178	1.00	0.97	0.43	0.94	0.99	0.79	0.81	0.94
	2,903	0.99	0.98	0.52	0.92	0.97	0.78	0.92	0.91
9,000	725	0.99	0.21	0.51	0.98	0.90	-1.19	-0.10	0.96
	1452	0.99	0.85	0.65	0.98	0.98	0.17	0.45	0.87
	2178	0.99	0.92	0.63	0.96	0.98	0.61	0.78	0.93
	2903	0.99	0.96	0.37	0.92	0.99	0.76	0.83	0.87
10,800	725	0.99	0.01	0.36	0.95	0.94	-0.70	-0.11	0.94
	1452	0.99	0.71	0.38	0.94	0.98	-0.24	0.22	0.86
	2178	0.99	0.94	0.45	0.94	0.98	0.43	0.60	0.91
	2903	0.99	0.96	0.56	0.93	0.98	0.56	0.73	0.84
13,200	725	1.00	0.16	0.61	0.97	0.99	0.39	-0.52	0.90
	1452	0.99	-0.21	0.39	0.97	0.99	0.25	-0.27	0.76
	2178	---	---	---	---	0.99	0.61	0.18	0.78
	2903	---	---	---	---	0.98	0.30	0.43	0.61

The R^2 values for the real part of dynamic-stiffness Re($\boldsymbol{H}_{ij}$) were not included because Re($\boldsymbol{H}_{ij}$) is nearly constant (virtual-mass is near zero). The R^2 statistic is not valid for a constant because the mean $\tilde{y}$ and estimated value q_i are nearly identical, making R^2 nearly zero.

Figure G. 1 and Figure G. 2 show Im($\boldsymbol{H}_{xx}$) and Im($\boldsymbol{H}_{yy}$), respectively, along with the linear curve fit at the shaft speed 10,800 rpm with 1.452 MPa (210.5 psi).

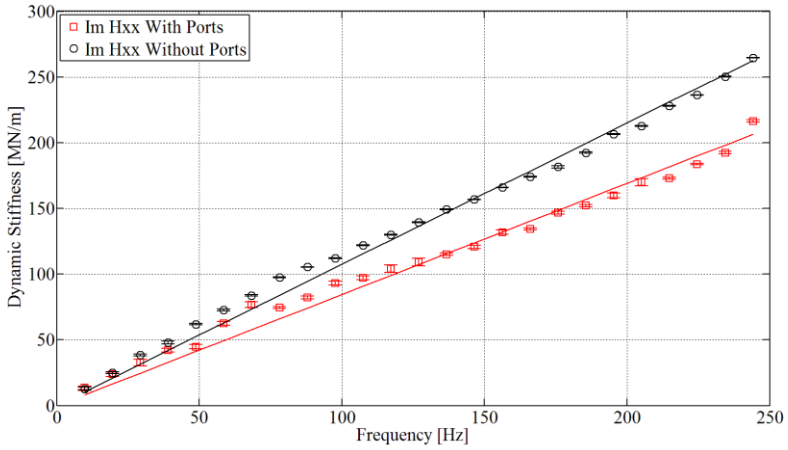

Figure G. 1. Dynamic-stiffness Im(H_{xx}) at 10,800 rpm and 1.452 MPa (210.5 psi)

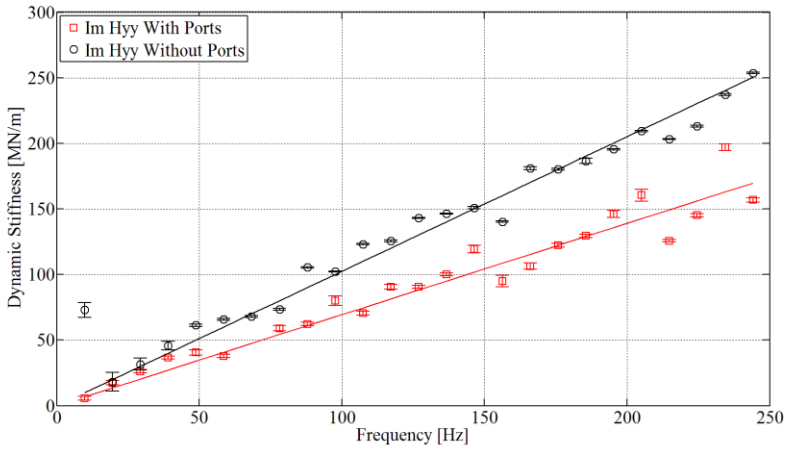

Figure G. 2. Dynamic-stiffness Im(H_{yy}) at 10,800 rpm and 1.452 MPa (210.5 psi)

For both the original and modified bearings, the dynamic-stiffness Im($\boldsymbol{H}_{xx}$) was fit very well with a constant slope and zero intercept (Figure G. 1). Dynamic-stiffness in the load direction, Im($\boldsymbol{H}_{yy}$), had consistently had lower R^2 values due to random variations, but still showed a clearly linear relation between Im($\boldsymbol{H}_{yy}$) and Ω (Figure G. 2).

Figure G. 3 and Figure G. 4 show Im($\boldsymbol{H}_{xy}$) and Im($\boldsymbol{H}_{yx}$), respectively, along with the linear curve fit at the shaft speed 10,800 rpm with 1.452 MPa (210.5 psi).

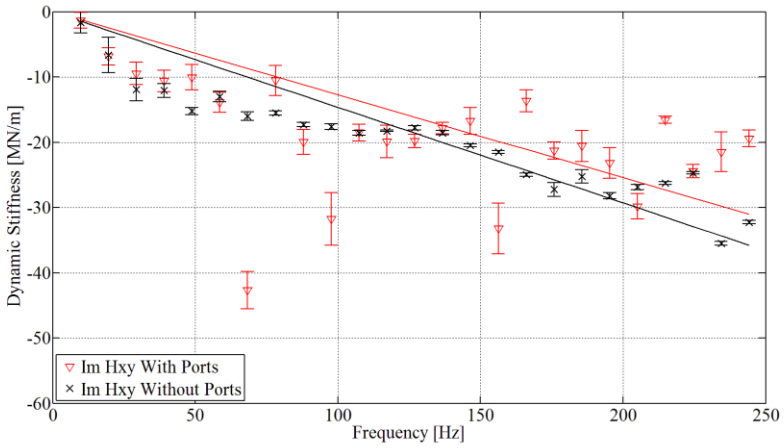

Figure G. 3. Dynamic-stiffness Im(H_{xy}) at 10,800 rpm and 1.452 MPa (210.5 psi)

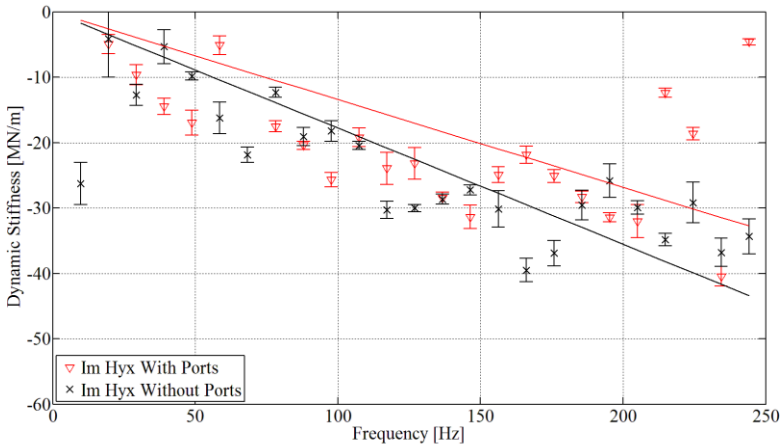

Figure G. 4. Dynamic-stiffness Im(H_{yx}) at 10,800 rpm and 1.452 MPa (210.5 psi)

The cross-coupled data generally had very low R^2 values indicating that Im($\boldsymbol{H}_{xy}$) and Im($\boldsymbol{H}_{yx}$) were not fit well as a line. For these data, the random error in the measurement system is of similar magnitude to the actual measurement. Consequently, the cross-coupled damping cannot be predicted with much certainty. For a given excitation frequency, the linear curve fit can only provide a rough estimate of Im($\boldsymbol{H}_{xy}$) or Im($\boldsymbol{H}_{yx}$).